AN EXPERIMENTAL INVESTIGATION OF A TURBULENT JUNCTION VORTEX

by

Martin D. Harsh III

Dissertation submitted to the Graduate Faculty of the

Virginia Polytechnic Institute and State University

in partial fulfillment of the requirements for the degree of

DOCTOR OF PHILOSOPHY

in

Mechanical Engineering

APPROVED:

F. J. Pierce, Chairman

E. F. Brown

B. Vick

L. W. Johnson

W. C. Thomas

January, 1985

Blacksburg, Virginia

AN EXPERIMENTAL INVESTIGATION OF A TURBULENT JUNCTION VORTEX

by

Martin D. Harsh III

Committee Chairman: F. J. Pierce
Mechanical Engineering

(ABSTRACT)

An experimental study of the incompressible, three-dimensional, turbulent flow separation around the base of a bluff obstacle on a flat surface is described. The bluff obstacle is a streamlined, right circular cylinder mounted with its axis normal to the flat surface. The flow environment is characterized by a body Reynolds number of 183,000, based on the diameter of the circular cylinder. The study includes surface flow visualizations, surface pressure measurements, and mean flow measurements. The mean flow measurements consist of total pressure, static pressure, and velocity distributions in three planes around the base of the streamlined cylinder.

The results show the presence of a large, dominant vortex in the junction between the cylinder and the flat surface. This vortex was found to consist of low total pressure fluid from the boundary layer flow upstream of the junction.

In addition to the three-dimensional flow measurements, extensive measurements in the two-dimensional turbulent boundary layer on the flat surface are reported. These results show the existence of small, but statistically significant, spanwise variations in the nominally two-

dimensional turbulent boundary layer. A systematic approach for estimating the wall shear stress from velocity profile data in a two-dimensional turbulent boundary layer based on the method of least squares is presented.

TABLE OF CONTENTS

TABLE OF CONTENTS (continued)

LIST OF FIGURES

LIST OF FIGURES (continued)

LIST OF FIGURES (continued)

LIST OF FIGURES (continued)

LIST OF TABLES

LIST OF TABLES (continued)

LIST OF TABLES (continued)

LIST OF TABLES (continued)

LIST OF TABLES (continued)

LIST OF TABLES (continued)

LIST OF TABLES (continued)

LIST OF SYMBOLS

$B_1, B_2, \ldots B_{11}$	Eleven calibration coefficients estimated using the method of least squares
$\bar{B}$	Matrix of coefficients estimated using the method of nonlinear least squares
$\bar{B}_{(j)}$	Matrix of estimated coefficients at the jth iteration in the solution of the nonlinear least squares problem
C	Wall-law constant, assumed to be 5.0
C_f	Skin friction coefficient, $2\tau_w/(\rho U_e^2)$
C_P	Pressure coefficient
$C_{P,S}$	Static pressure coefficient
$C_{P,T}$	Total pressure coefficient
D_P	Diameter of the probe
e	Estimated standard error in the nonlinear least squares problem
f_1	Total pressure coefficient for the three-tube Conrad probe, $(P_1 - P_T)/Q$
f_2	Yaw pressure coefficient for the three-tube Conrad Probe, $(P_2 - P_3)/Q$
f_3	Pitch pressure coefficient for the five-hole probe, $(P_4 - P_5)/(P_1 - P_2)$
f_4	Dynamic pressure coefficient for the five-hole probe, $Q/(P_1 - P_2)$
f_5	Total pressure coefficient for the five-hole probe, $(P_1 - P_T)/Q$
H	Shape factor, δ^*/θ
i,j	Indices denoting the ith and jth elements in an ordered sequence
L	Length

n	An index corresponding to the largest i or the total number of observations
P	Pressure
P_K	Pressure indicated by the Kiel probe
P_S	Static pressure
P_T	Total pressure, $P_S + \rho\bar{V}^2/2$
$P_{T,*}$	Total pressure at the throat
P_∞	Barometric pressure
$P_1, P_2, \ldots P_5$	Pressures indicated at the various ports on the three-tube and five-hole pressure probes
p	The number of estimated parameters in a least squares analysis
Q	Dynamic pressure, $\rho\bar{V}^2/2$
Q_*	Dynamic pressure at the throat
R	(1) The gas constant for air, or (2) a general result calculated from k experimental observations
$\bar{R}$	Matrix of residual errors estimated using the method of least squares
$\bar{R}_{(j)}$	Matrix of estimated residual errors at the jth iteration in the solution of the nonlinear least squares problem
Re	Reynolds number, $\rho\bar{V}L/\mu$
Re_p	Reynolds number based on the probe diameter, $\rho\bar{V}D_p/\mu$
r_i	The ith residual error after least squares optimization of the parameters
$r_{x_i x_j}$	Estimated correlation coefficient between the ith and jth observations
SS_I	Sum of squares function for model I
SS_{II}	Sum of squares function for model II
T_∞	Ambient temperature
U	Streamwise component of the mean velocity vector

U_e	Streamwise velocity at the edge of a two-dimensional boundary layer
U_i	The experimentally observed streamwise velocity at the ith vertical (y) position in a two-dimensional boundary layer
$\hat{U}_{j,i}$	The estimated streamwise velocity in a two-dimensional boundary layer at the jth iteration in the solution of the nonlinear least squares problem and at the ith vertical (y) position in the boundary layer
u^+	Wall-law velocity coordinate
u_τ	Friction velocity, $(\tau_w/\rho)^{1/2}$
$u_{\tau,(j)}$	Friction velocity at the jth iteration in the solution of the nonlinear least squares problem
V	Vertical component of the mean velocity vector
$\bar{V}$	Speed
$\bar{V}_*$	Speed at the throat
W	Spanwise component of the mean velocity vector
w	Uncertainty
w_R	Uncertainty in the result R
$\bar{\bar{X}}$	Matrix of partial derivatives in the nonlinear least squares problem
$\bar{\bar{X}}_{(j)}$	Matrix of partial derivatives at the jth iteration in the solution of the nonlinear least squares problem
$\bar{\bar{X}}^T_{(j)}$	Transpose of the aforementioned matrix
x	The streamwise coordinate
x_i	A general experimental observation
y	The vertical coordinate
y_i	The ith vertical position
y^+	Wall-law position coordinate
z	The spanwise coordinate

Greek Symbols

α	Pitch angle
α_o	Pitch angle with respect to the five-hole probe at the null position
β	Yaw angle
β_o	Yaw angle relative to the traversing mechanism at the null position
$\beta_o(y_i)$	Yaw angle relative to the traversing mechanism at the null position and at the ith y location in a traverse
β_{Ref}	Reference yaw angle indicated on the traversing mechanism
δ	Boundary layer thickness
$\delta_{(j)}$	Boundary layer thickness at the jth iteration in the solution of the nonlinear least squares problem
δ^*	Boundary layer displacement thickness
ε_i	Random deviation at the ith observation
θ	Boundary layer momentum thickness
κ	von Karman's constant, assumed to be 0.41
ϕ	Viscosity
ν	Kinematic viscosity, μ/ρ
Π	Pressure gradient parameter
$\Pi_{(j)}$	Pressure gradient parameter at the jth iteration in the solution of the nonlinear least squares problem
π	3.1415926...
ρ	Density
τ_w	Wall shear stress
$\bar{\Phi}$	Diagonal weight matrix in the weighted least squares problem

ϕ_i	Least squares weight parameter at the ith observation, the ith diagonal component of $\bar{\Phi}$
Ω	Streamwise component of mean vorticity

1. INTRODUCTION

The objective of this experimental study is to describe the incompressible, three-dimensional separated flow around the base of an obstacle protruding through a turbulent boundary layer. This type of flow is illustrated in Fig. 1.1. The prominent feature of this flow is the horseshoe-shaped vortex (or system of vortices) formed in the corner between the obstacle and the surface. The physical mechanism responsible for the formation of this vortex is the total pressure gradient near the leading edge of the obstacle resulting from the upstream boundary layer flow. This type of flow occurs around bridge piers in rivers, around buildings and structures in the presence of the atmospheric boundary layer, at wing-fuselage junctions, and at the leading edge junction between turbomachine blades and endwalls.

This study is an extension of the work reported by Menna [1].[1] He investigated the pressure-driven, three-dimensional, turbulent boundary layer upstream and around a junction vortex. His objective was to provide a benchmark experimental study to guide three-dimensional turbulence modelling and computational methods. To meet this objective, he measured the mean velocity field, the Reynolds stress tensor field, the wall shear stress, and the static pressure field in the boundary layer flow around the obstacle. He did not provide any explicit information about the three-dimensional separation and junction vortex. This study extends Menna's database into the separated region.

[1] Numbers in brackets indicate references listed at the end of the dissertation.

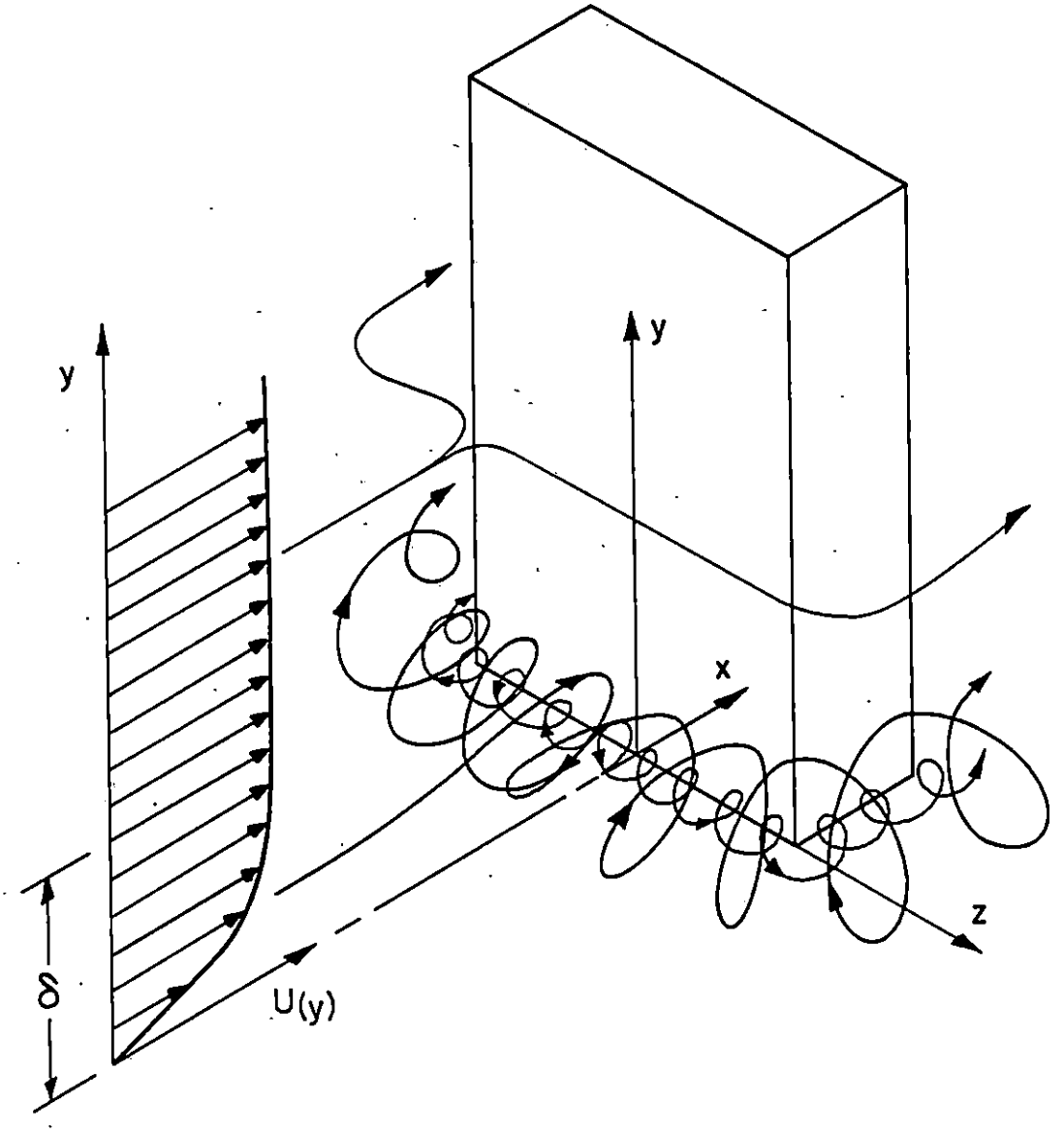

Fig. 1.1 The Junction Vortex

Other experimental studies of the low-speed, three-dimensional separated flow around the base of a bluff obstacle have been reported [2-23]. These studies are briefly summarized in Table 1.1. Both laminar and turbulent flow studies are included. A large number of these experiments consist of flow visualization studies only. Most of them contain only sparse quantitative information about the three-dimensional separated flow.

It was determined that a significant contribution could be made by documenting the mean flow structure of the junction vortex. There are three measurement techniques capable of providing this information, including optical, heat meter, and pressure probe methods. The optical method, namely laser-doppler velocimetry, is the subject of a separate investigation [24] and was not considered. The heat meter methods, including single element [25-36] and multiple element [37-50] arrays of hot wires and films, and the pulsed-wire anemometer [51-58] have been widely used, as have the multiple-tube pressure probes [59-70]. It is difficult to assign a figure of merit to these measurement techniques. Such a figure should include factors reflecting cost, availability, dependability, and accuracy. Simpson [71] and Lakshminarayana [72] have cited some of the problems associated with these measurement techniques. Their comments are summarized in Table 1.2 and Table 1.3. Based on these comments, the general acceptance of three-dimensional pressure probe techniques in the literature [35,73], low cost, and commercial availability, a pressure probe method was chosen to document the mean flow field. The method used yielded the three-dimensional mean velocity, the total pressure, and the static pressure.

Table 1.1 Low-Speed, Three-Dimensional Flow Experiments Involving a Junction Vortex

Author	Type of Flow	Comment
Schwind, 1962 [2]	Laminar	Smoke flow visualization study of flow separation at the intersection of a 60° wedge with a flat plate.
Peake & Galway, 1965 [3]	Laminar	Water tunnel flow visualization study study of limiting stream lines near the intersection of a circular cylinder with a flat plate.
Peake, et al., 1965 [4]	Laminar	Water tunnel flow visualization study of limiting streamlines near the intersection of a Rankine oval with a flat plate.
Steinheuer, 1965 [5]	Laminar	Surface pressure distribution and mean velocity profiles near the intersection of a circular cylinder with a flat plate.
Shen & Jones, 1967 [6]	Laminar	Water tunnel flow visualization study of limiting streamlines near the intersection of a half-delta wing with a flat plate.
Shen & Jones, 1967 [7]	Laminar	Water tunnel flow visualization study of limiting streamlines near the intersection of a half-cone with a flat a flat plate.
Roper, 1967 [8]	Turbulent	Smoke flow visualization study of flow separation at the intersection of a circular cylinder with a flat plate.
Belik, 1973 [9]	Laminar & Turbulent	Investigated the distance between the leading edge of a circular cylinder and the point of primary separation on a flat plate.

Table 1.1, continued

Dechow, 1977 [10,11]	Turbulent	Mean velocity, Reynolds stress tensor, surface pressure, and wall shear stress measurements along a freestream streamline produced by a streamlined circular cylinder standing on a flat plate.
Barber, 1978 [12]	Turbulent	Surface flow visualization and wake total pressure profiles for the intersection loses associated with the junction between a symmetric, zero-camber airfoil and a flat plate.
Baker, 1979 [13,14]	Laminar & Turbulent	Surface pressure distributions, smoke flow visualization, and surface flow visualization near the intersection of a circular cylinder with a flat plate.
Shabaka, 1979 [15,16]	Turbulent	Mean velocity, Reynolds stress tensor, surface pressure, and wall shear stress measurements in the junction between an idealized wing (with elliptic leading edge, zero camber, and constant thickness) and a flat plate.
McMahon, et al., 1982-1984 [17-19]	Turbulent	Mean velocity, Reynolds stress tensor, surface pressure, and wall shear stress measurements in the junction between an idealized wing (with elliptic leading edge, zero camber, and constant thickness) and a flat plate.
Dickinson, 1984 [20]	Turbulent	Surface flow visualization and plane-of-symmetry laser-doppler velocimetry measurements in the junction between a hybrid strut (elliptic leading edge and NACA 0020 tail) and a flat plate.
Hsing, 1984 [21]	Turbulent	Mean velocity, Reynolds stress tensor, surface pressure, and wall shear stress measurements in the junction between a streamlined circular cylinder and a flat plate.

Table 1.1, continued

Moore & Forlini, 1984 [22]	Turbulent	Mean velocity, surface flow visualization, and total and static pressure distributions near the junction between a Rankine half-body and a flat plate.
Rood, 1984 [23]	Turbulent	Mean velocity, turbulence intensity, surface pressure, and spectral analysis near the junction between an idealized wing (elliptic leading edge, zero camber, and circular arc trailing edge) and a flat plate.

Table 1.2 Simpson's Comparison of Separated-Flow Measurement Techniques [71]

Pitot-Static

- Not directionally sensitive in presence of flow reversal; can be used in most types of three-dimensional flow with proper alignment.
- Difficult to interpret in zones of high local turbulence intensity.
- Can cause interference with flow and/or itself, especially near a wall.
- Cannot measure turbulence.
- More reliable at high velocities.
- Large probe volume.

Hot-Wire or Hot-Film Arrays

- Not directionally sensitive in presence of flow reversal; can be used in most types of three-dimensional flow with proper alignment.
- Difficult to interpret in zones of high local turbulence intensity.
- Can cause interference with flow and/or itself, especially near a wall.
- Large probe volume.
- Problems with measurement very close to solid surfaces.
- Requires clean fluid for stable, long-time calibration.
- Requires careful management of fluid temperature.

Laser Anemometer

- Very expensive to implement.
- In air flow turbulence, data obtained by sampling individual particle speeds rather than as continuous time series.
- Problems with measurement very close to solid surfaces.
- Measuring system and flow field must be closely integrated and require expensive, custom design of traversing equipment.
- Requires seeding with particles.

Pulsed-Wire Anemometer

- Can cause interference with flow and/or itself, especially near a wall.
- In air flow turbulence, data obtained by sampling individual particle speeds rather than as continuous time series.
- Large probe volume.
- Problems with measurement very close to solid surfaces.
- Basic limit on maximum velocity measurable with presently known configurations.

Table 1.3 Lakshminarayana's Comparison of Three-Dimensional Flow Measurement Techniques [72]

Errors in Three-Sensor Hot-Wire Measurements

- Inclination of the wire to the flow streamlines.
- Geometry of prongs and probe body.
- Finite distances between wires.
- Finite dimensions of individual wires.
- Temporal resolution or thermal inertia of the wires.
- Aging, oxidation, and contamination of the wires.
- Ambient temperature drift.
- Proximity of wire to the wall.
- Probe body vibration due to rotation and flow induced excitation.
- Spurious signals from the power line.
- Finite sampling time.
- Measurement of wire angles with respect to the reference coordinate system.
- Mis-alignment of the probe with respect to the reference axis.

Errors in Pressure Probe Measurements

- Effects of Reynolds number and Mach number.
- Effects of velocity and pressure gradients.
- Effect of turbulence.
- Effects of probe interference, blockage and size.
- Effects of yaw and pitch angles.
- Effects of wall interference and nose shape.

The experimental program was divided into five parts. The first part was an investigation of the nominally two-dimensional turbulent boundary layer on the flat floor of the wind tunnel. There was no obstacle in the flow field during this part of the investigation. The objective was to confirm previously documented, small nonuniformities in the two-dimensional turbulent boundary layer. The objective of the remaining four parts, including flow visualization, surface pressure measurements, total pressure measurements, and three-dimensional mean flow measurements, was to describe the mean flow structure of the turbulent junction vortex.

The following chapters describe this experimental study of an incompresssible, turbulent junction vortex. Chapter 2 contains descriptions of the obstacle, the coordinate system used to describe the measurements, the wind tunnel, and some supporting equipment used during the experimental study. The probes, procedures, and data reduction are described in Chapter 3. Chapter 4 presents the experimental observations and some discussion of the results. The sections within Chapters 3 and 4 reflect the five parts of the experimental study. A brief chapter summarizing the study is included at the end.

2. FACILITIES

2.1 Bluff Body and Coordinate System

The interaction between the faired cylinder shown in Fig. 2.1 and the turbulent boundary layer on the floor of the wind tunnel produced the junction vortex flow. The flat sides of the cylinder terminate in a sharp trailing edge and are tangent to the circular leading edge of the body. The cylinder has a leading edge diameter (maximum thickness) of 127 mm, an overall length (chord) of 298 mm, and a height of 229 mm.

The righthand coordinate system used to describe this flow is also shown in Fig. 2.1. The origin of the coordinate system is at the intersection of the floor centerline with the leading edge of the faired cylinder. The y axis ideally defines the stagnation line on the body while the x-z plane defines the flat floor of the wind tunnel. Probes were traversed across the flow field in the y direction. For convenience, the x and z directions will be referred to as the streamwise and spanwise directions, respectively.

A typical mean velocity vector is shown in Fig. 2.2. Yaw and pitch angles are defined as angles of rotation about the y and z axes. In terms of the components of the mean velocity vector, these angles are given by:

$$\beta = \begin{matrix} + \\ - \end{matrix} \tan^{-1}\left(\frac{W}{U}\right) , \tag{2.1}$$

$$\alpha = \tan^{-1}\left(\frac{V}{U}\right) . \tag{2.2}$$

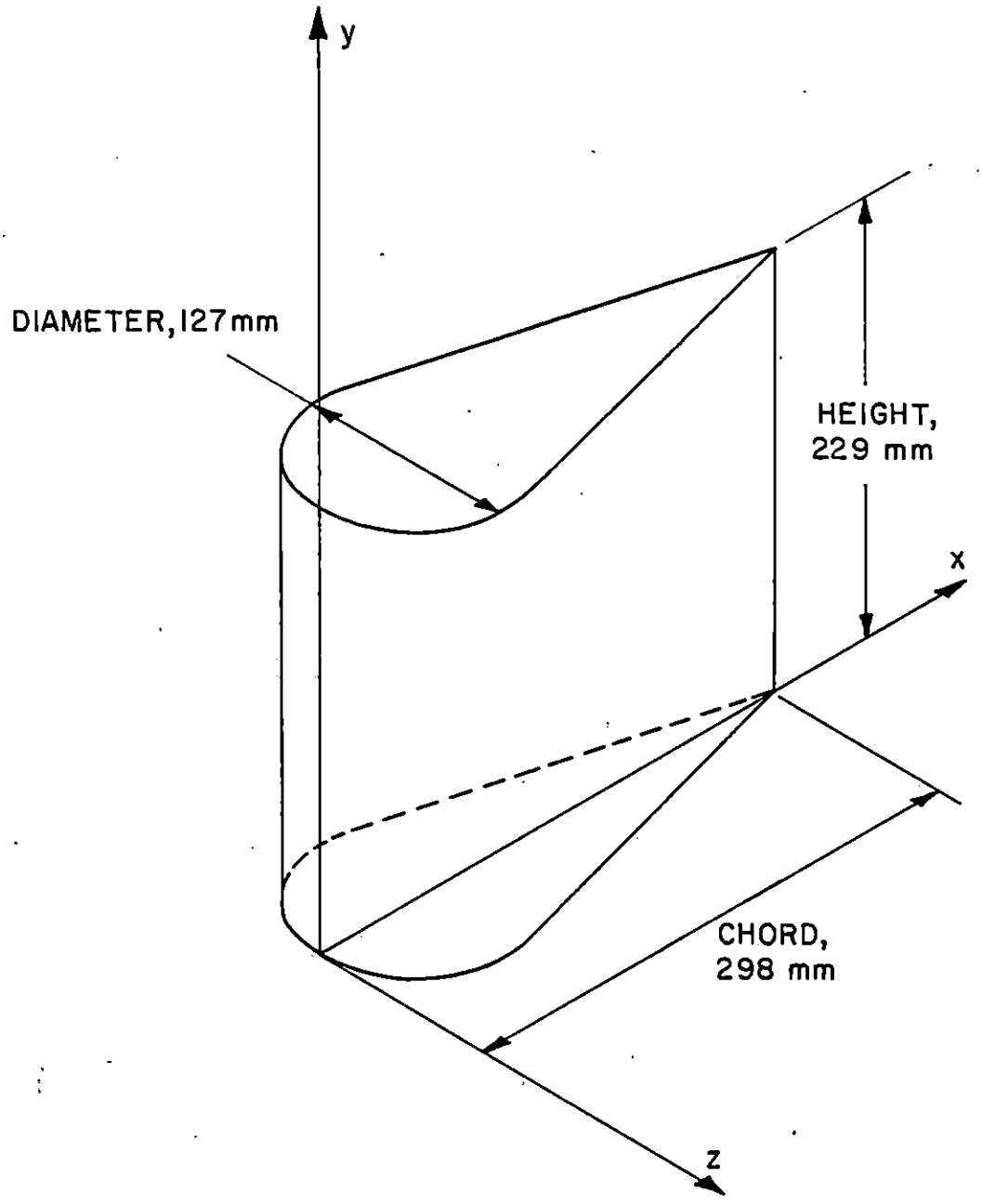

Fig. 2.1 The Bluff Body

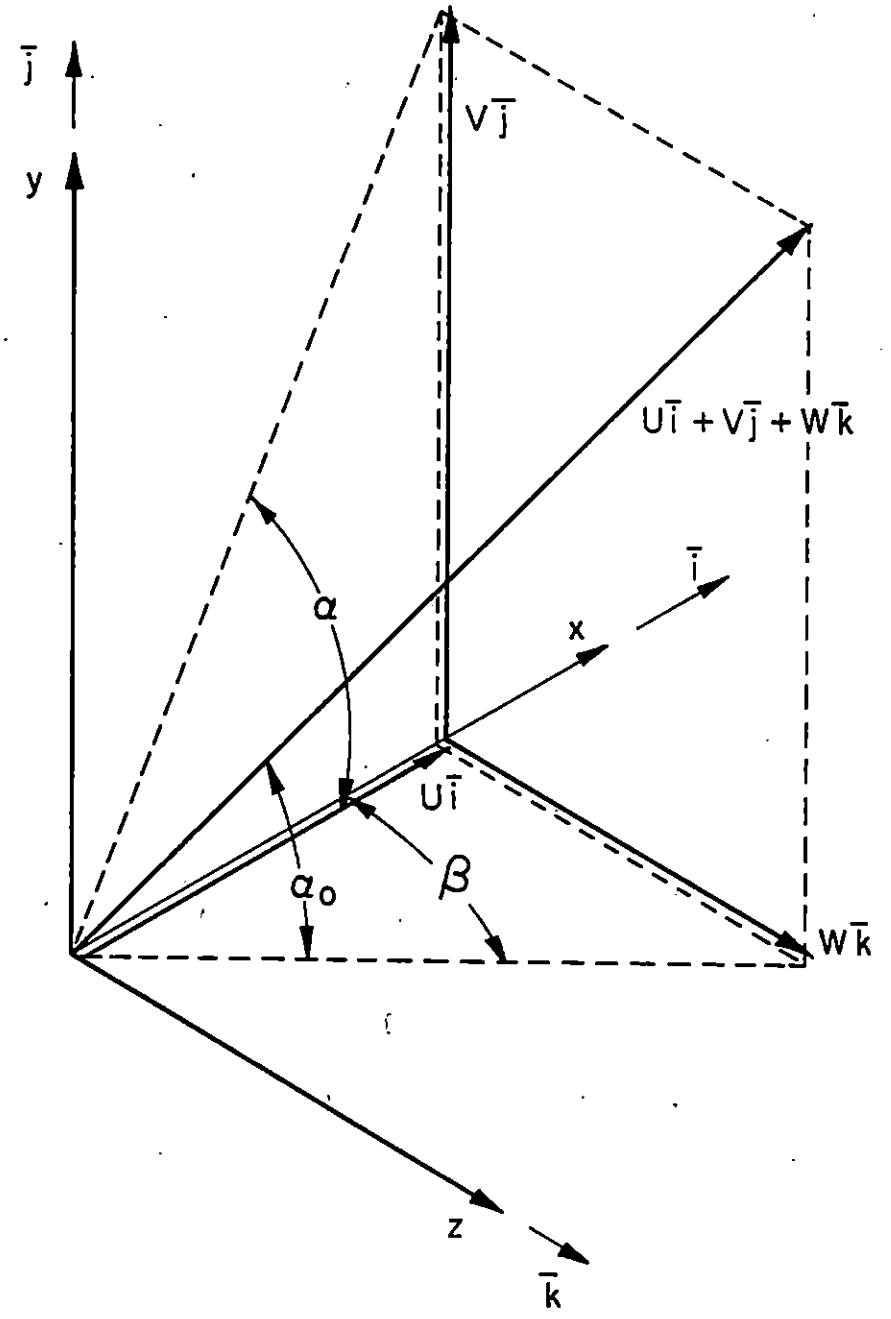

Fig. 2.2 Typical Mean Velocity Vector and Flow Angles

2.2 Large Scale Wind Tunnel

The separated flow experiments were conducted in the open circuit, subsonic wind tunnel designed by Tennant [74] and shown in Fig. 2.3. This section describes the major components of the wind tunnel from inlet to discharge.

Air is drawn into the wind tunnel through a rectangular inlet 3.66 m wide and 2.44 m high (flow area equal to 8.92 m^2). In this section, the air consecutively passes through:

(1) a 6 mm thick polyester filter cloth,

(2) one fiberglass screen with an open area ratio (flow area per unit cross section) of 0.71,

(3) a matrix of flow straighteners consisting of 25 mm outside diameter, closely packed cardboard tubes with a length-to-diameter ratio of 6.0 and wall thickness of 2 mm, and

(4) three fiberglass screens identical to the screen described as item (2).

Menna [1] conducted an extensive experimental investigation of this inlet section and chose the present arrangement to minimize flow nonuniformities far downstream of the inlet.

A 16:1 area ratio contraction follows the inlet. Tennant [74] designed this section to produce a uniform, non-accelerating flow at the exit (hereafter referred to as the throat) by choosing wall profiles corresponding to sine functions with periods of 4.9 m. The boundary

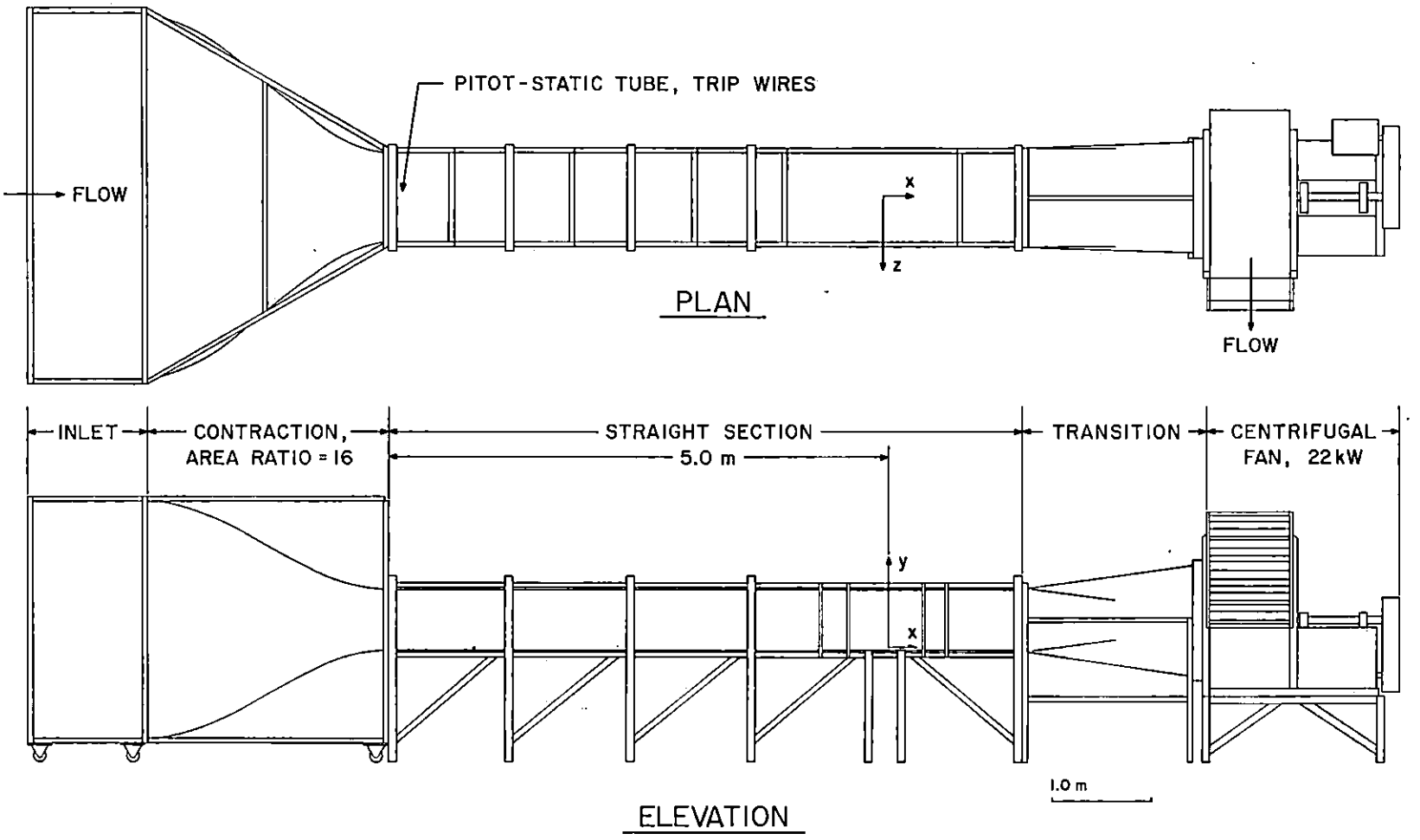

Fig. 2.3 Open Circuit, Subsonic Wind Tunnel Used in the Experimental Investigation

layer is tripped on all four sides of the wind tunnel throat with 2.8 mm diameter rods. A 1.6 mm diameter pitot tube is positioned in the center of the throat to monitor the air speed.

Connected to the contraction at the throat is a straight, constant cross section channel 6.35 m long, 0.91 m wide, and 0.61 m high (flow area equal to 0.56 m^2, aspect ratio equal to 1.5). The bluff body is positioned 5.0 m downstream of the throat and in the center of a 254 mm wide, removable plate built into the wind tunnel floor. A 1.22 m long, 0.51 m wide section of the roof immediately above the bluff body is also removable and can be replaced by sections configured to accommodate various probes and traversing equipment.

A rectangular to circular transition couples the straight channel to a 22 kW, Twin City Fan and Blower Company model BC-402 centrifugal fan. Two rows of 50 mm outside diameter, closely packed cardboard flow straighteners with a length-to-diameter ratio of 3 and wall thickness of 2 mm are located in the downstream end of the transition to eliminate fan induced whirl from propagating upstream. The fan is isolated from the transition by a flexible foam seal and has louvers at the discharge to control the tunnel Reynolds number. Air speeds up to approximately 25 m/s at the throat are possible by adjusting these louvers. The fan discharges into a 280 m^2, temperature controlled laboratory.

Dynamic similarity for the low speed, three-dimensional flow study was achieved by maintaining a constant Reynolds number at the wind tunnel throat. The Reynolds number per unit length,

$$\frac{Re}{L} = \frac{\rho \bar{V}_*}{\mu} , \qquad (2.3)$$

was equal to 1,340,000 per meter. Table 2.1 summarizes the nominal laboratory and tunnel conditions for this study.

2.3 Data Acquisition System

The two degree-of-freedom, multi-channel, data acquisition system designed by Herwig [75] was used to acquire the pressure probe data. A block diagram of the system is shown in Fig. 2.4. The center of this system is a TRS-80 model III microcomputer manufactured by Radio Shack, Incorporated, and built around the 8-bit Z-80 microprocessor. The system is capable of addressing 256 input/output ports, limited by the 8-bit address bus of the Z-80 microprocessor. Five input/output ports were used, including four ports for digital manometers and one port for traverse stepper-motor control. Manufacturer's specifications for the digital manometers are given in Table 2.2.

The two degree-of-freedom traversing mechanism used in the automated system is shown in Fig. 2.5. Probe motion is effected by two Bodine Electric Company type 23T1BEHH stepper motors. The microcomputer controls the number of steps taken by the motors which, in turn, defines the vertical and yaw positions (y and β, respectively) of the probe. The physical limitations on the vertical movement include a minimum displacement of 5 μm and a range of 180 mm. The minimum angular displacement is 0.036^{o}.

Table 2.1 Nominal Laboratory and Wind Tunnel Conditions for the Low Speed, Three-Dimensional, Separated Flow Experiment

Ambient Temperature	25 C
Barometric Pressure	94.5 kPa
Dynamic Pressure at Wind Tunnel Throat	0.274 kPa
Reynolds Number at Throat[1]	9.80×10^5
Pressure Drop Through Inlet Section	45 Pa
Flow Parameters at Test Section[2]	
Freestream Turbulence Intensity	0.5% - 0.6%
Freestream Speed/Speed at Throat	1.077
Boundary Layer Thickness	81.6 mm
Displacement Thickness	10.5 mm
Momentum Thickness	8.09 mm
Skin Friction Coefficient	2.56×10^{-3}

[1]Based on the hydraulic diameter.

[2]"Test section" refers to a streamwise position 5.0 m downstream of the wind tunnel throat. These boundary layer parameters are an average of 9 observations made across the test section with no test article in the wind tunnel.

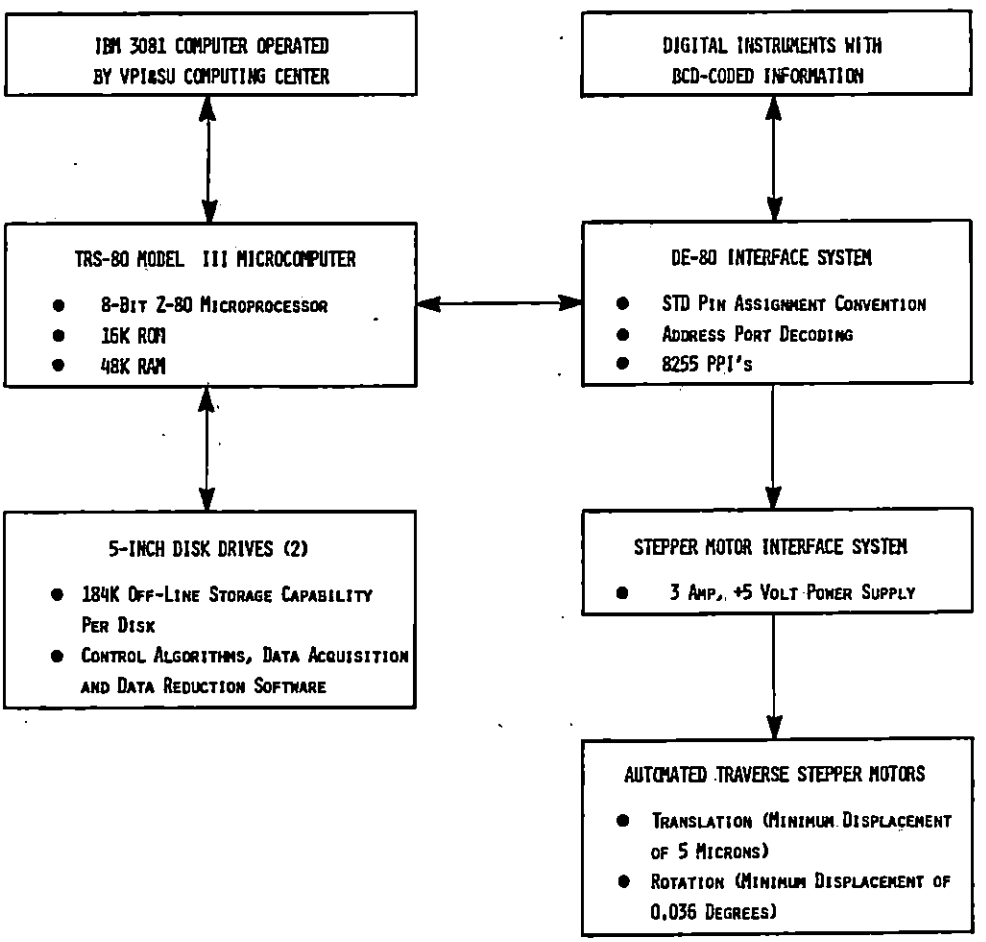

Fig. 2.4 Block Diagram of the Data Acquisition System (75)

Table 2.2 Manufacturer's Specifications for the Digital Manometers

Manufacturer	Datametrics Dresser Industries, Inc. 340 Fordham Road Willimgton, Massachusetts 01887
Specifications	
Model	1400-9AX (readout) 590D-10W-1P1-V1X-4D (pressure sensor)
Range	± 2.5 kPa
Accuracy	0.15% reading + 0.001% full scale

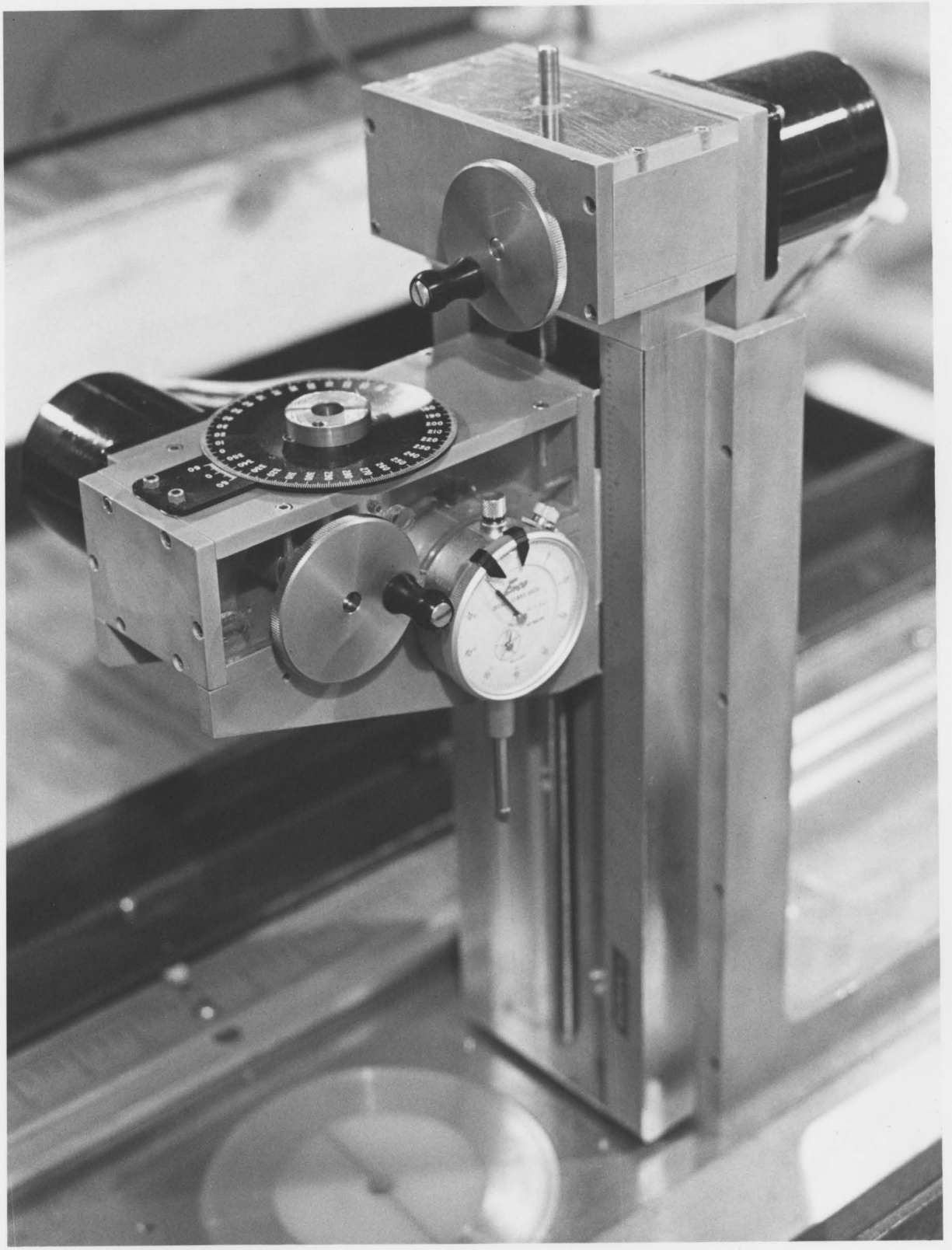

Fig. 2.5 Two Degree-of-Freedom Traversing Mechanism (75)

2.4 Calibration Wind Tunnel

The open circuit, subsonic wind tunnel shown in Fig. 2.6 was used to calibrate the pressure probes. This wind tunnel consists of seven components:

(1) an inlet plenum chamber covered on four sides by 6 mm thick, polyester filter cloth,

(2) louvers used to control the air speed,

(3) a 7.5 kW, ILG Electric Ventilating Company model BC-300 centrifugal fan,

(4) a 2.6:1 area ratio diffuser,

(5) a settling chamber with six screens upstream and five screens downstream of 50 mm outside diameter, cardboard flow straighteners with a length-to-diameter ratio of 10.5 and wall thickness of 2 mm (the screens here are identical to those used in the inlet of the large scale wind tunnel),

(6) a 15:1 area ratio nozzle,

(7) and a 1.22 m long, straight, constant cross section duct 356 mm wide, 254 mm high (flow area equal to 904 cm^2, aspect ratio equal to 1.4).

Probe calibrations were performed in the center of the large free jet leaving the straight section of duct. Air speeds in the core of this large jet ranging from 5 to 40 m/s at a turbulence intensity level less than 1 percent were possible by adjusting the louvers upstream of the centrifugal fan.

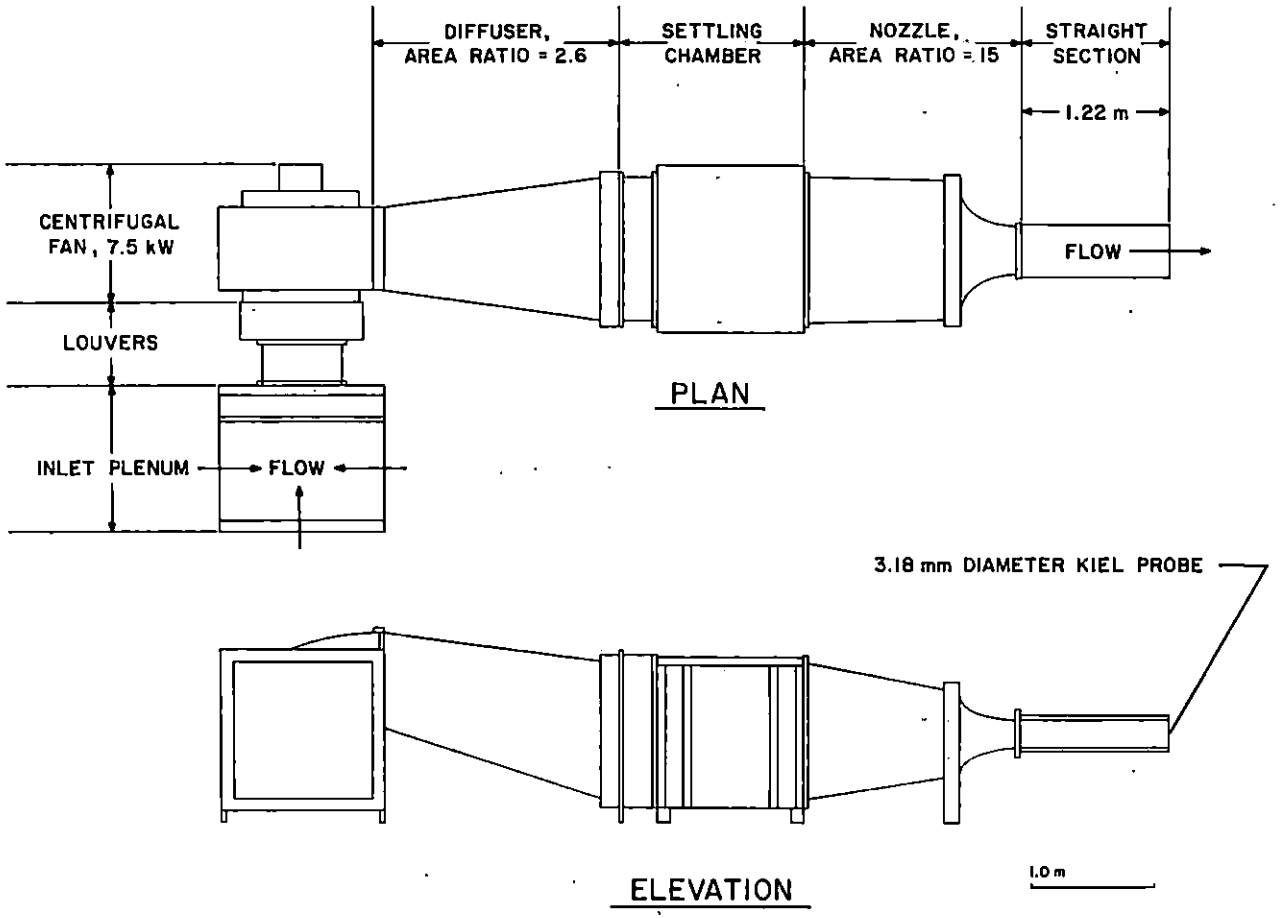

Fig. 2.6 Open Circuit, Subsonic, Calibration Wind Tunnel

The air speed for the probe calibrations was obtained by assuming that the dynamic pressure, Q, in the core of the jet was equal to the pressure difference:

$$Q = P_K - P_\infty \,, \tag{2.4}$$

where P_K is the total pressure indicated by a 3.18 mm diameter, United Sensor Corporation Kiel probe positioned near, but not too near, the probe to be calibrated. Thus, the speed was given by:

$$\bar{V} = \sqrt{\frac{2RT_\infty Q}{P_\infty}} \,. \tag{2.5}$$

The pressure difference in Eq. 2.4 was measured with a Datametrics model 1400-9AX digital manometer described in Table 2.2.

The probes were mounted in a calibration stand which straddled the straight section of duct. The estimated accuracy of the pitch and yaw positioning of the probes is 0.2^o.

3. METHODS

3.1 Two-Dimensional Boundary Layer Measurements

The two-dimensional turbulent boundary layer flow on the flat floor of the wind tunnel was measured to confirm previously documented, small spanwise nonuniformities in the flow field. Menna [1] measured the displacement thickness, the momentum thickness, and the skin friction coefficient in this boundary layer at seven spanwise positions 5.0 m downstream of the tunnel throat. His results indicate deviations from the spanwise average of seven observations as large as 13 percent in the displacement thickness, 12 percent in the momentum thickness, and -5 percent in the skin friction coefficient.

A three-tube Conrad probe was used to indicate flow speed and direction. Possible probe-head configurations for two- and three-tube Conrad probes are shown in Fig. 3.1. Bryer and Pankhurst [59] review the use of these probes in flows where the flow direction varies mainly in one plane. The three-tube version offers a direct indication of total pressure and, consequently, a simpler method of data reduction. The probe stem, configured for boundary layer measurements, is shown in Fig. 3.2. This is the same probe used by Menna [1] in some of his two-dimensional flow studies and referred to as a "gooseneck cobra probe".

The two-dimensional turbulent boundary layer was surveyed at nine spanwise positions 5.0 m downstream of the tunnel throat as shown in Fig. 3.3. Pressure taps, 0.38 mm in diameter and 25 mm upstream of each spanwise position in the removable floor test plate provided static pressure information.

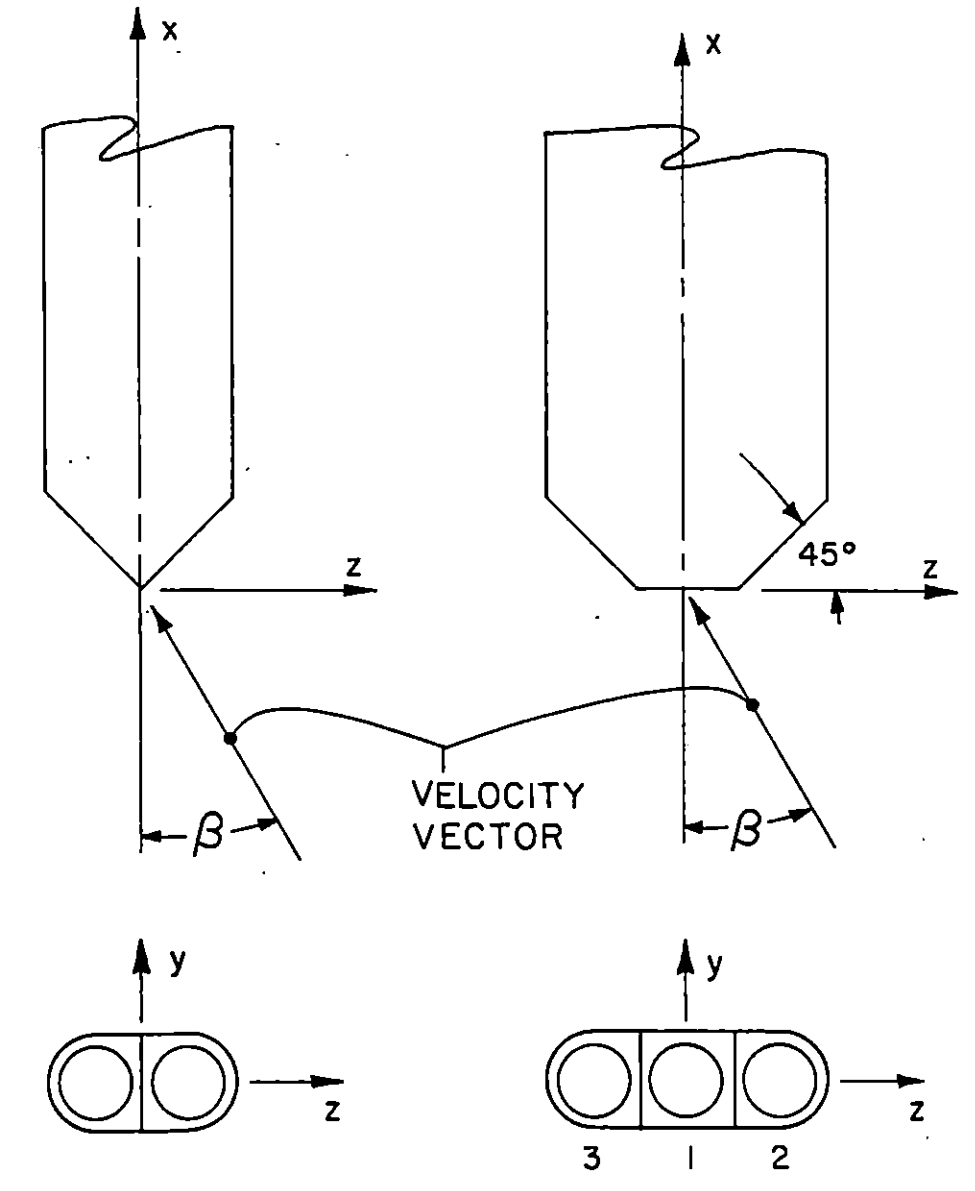

Fig. 3.1 Typical Conrad Probe Configurations

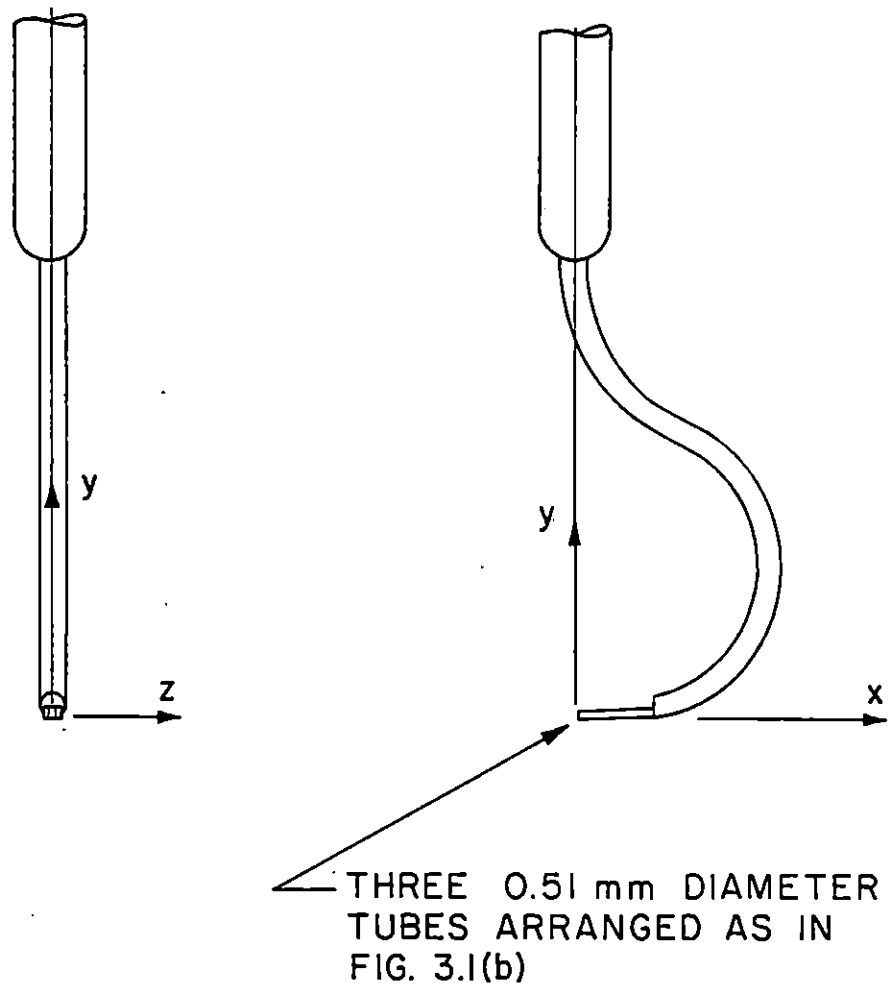

Fig. 3.2 Conrad Probe Configured for Boundary Layer Measurements

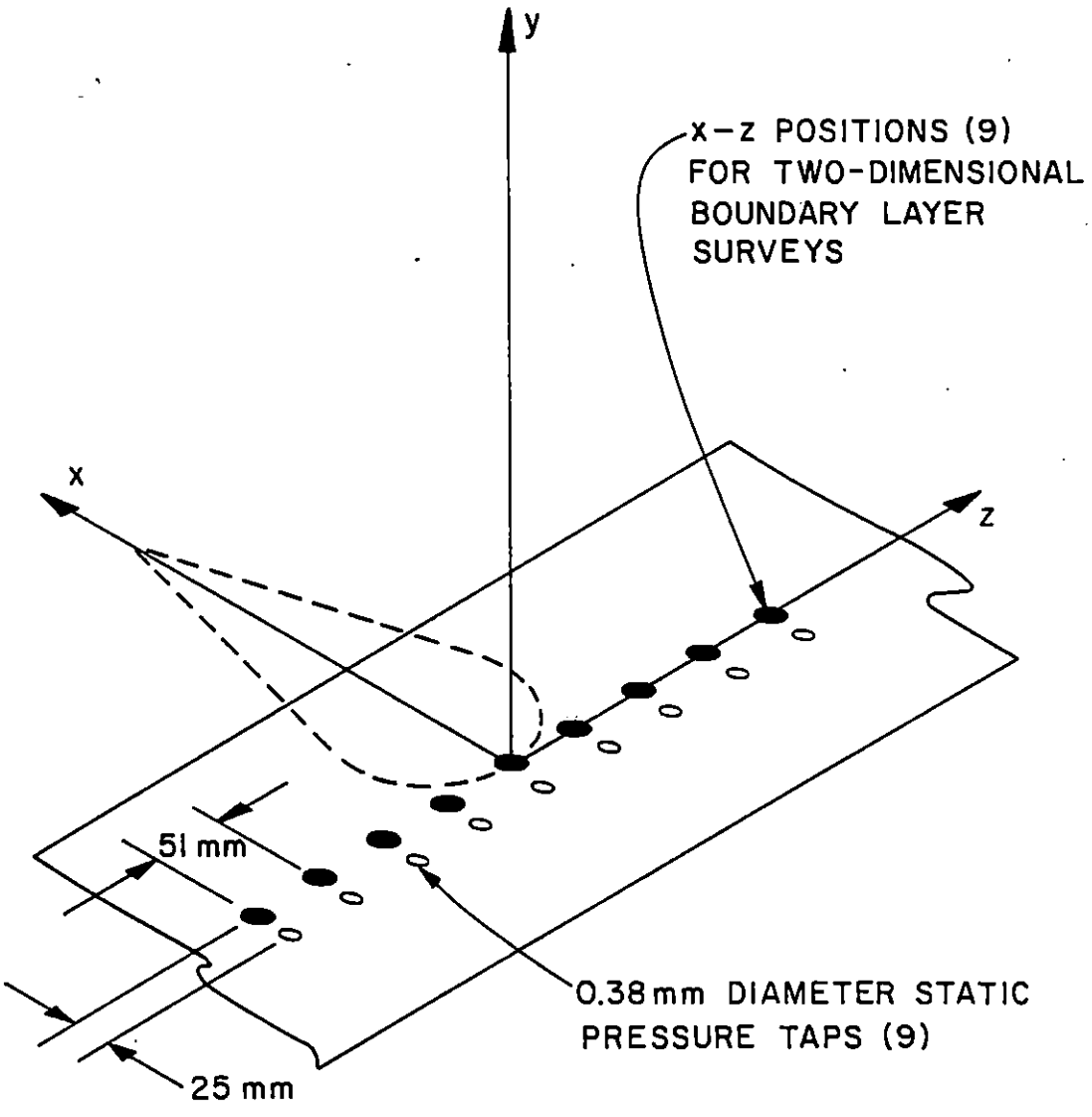

Fig. 3.3 Spanwise Positions of the Two-Dimensional Turbulent Boundary Layer Measurements

The remainder of this section describes the three-tube Conrad probe calibration and the two-dimensional boundary layer parameters used in assessing the nonuniformities present in the nominally two-dimensional flow field.

3.1.1 Three-Tube Conrad Probe Calibration

The three-tube Conrad probe shown in Fig. 3.2 was calibrated for yaw angle in the free jet of the calibration tunnel described in Section 2.4. Two calibration functions were considered, including a total pressure coefficient,

$$f_1(\beta,Re_p) = \frac{P_1 - P_T}{Q} \quad , \tag{3.1}$$

and a yaw pressure coefficient,

$$f_2(\beta,Re_p) = \frac{P_2 - P_3}{Q} \quad , \tag{3.2}$$

where the probe Reynolds number is given by:

$$Re_p = \frac{\rho \bar{V} D_p}{\mu} \quad . \tag{3.3}$$

Data required to evaluate these functions was acquired over a range of yaw angles and Reynolds numbers greater than those anticipated in the nominally two-dimensional flow measurements. The calibration data is shown in Fig. 3.4. Neither function exhibits a significant Reynolds

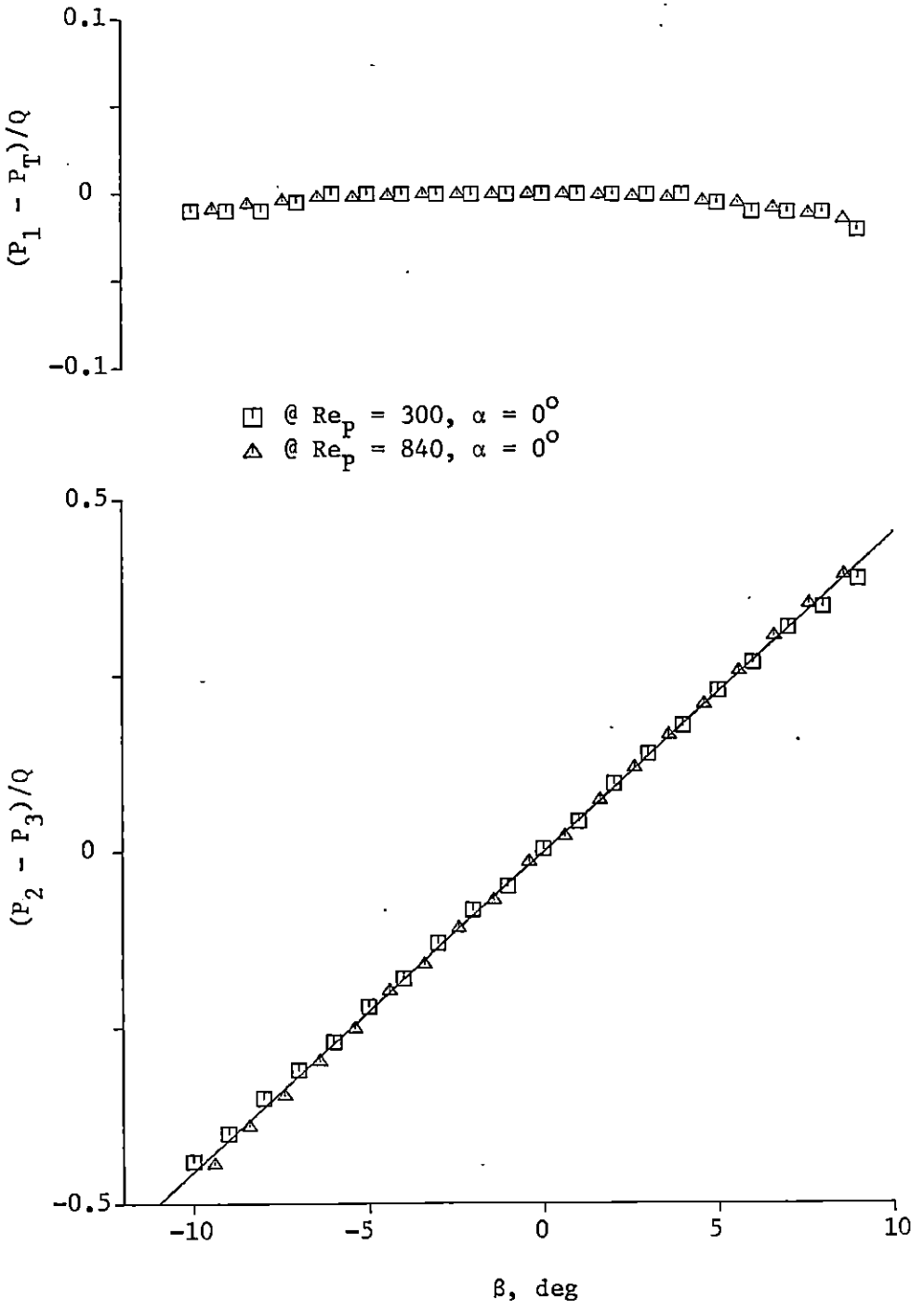

Fig. 3.4 Calibration Data for the Three-Tube Conrad Probe

number dependency. Based on the observed data, it was concluded that the center tube indicated the true total pressure over the range of yaw angles:

$$-5^{o} \leq \beta \leq +5^{o} \ , \tag{3.4}$$

and that the yaw pressure coefficient was adequately described by:

$$\begin{aligned} f_2(\beta) &= B_1\beta \quad , \\ &= 0.0455\ \beta \ . \end{aligned} \tag{3.5}$$

The parameter B_1 was evaluated using the method of least squares [76-80].

The probe was traversed across the nominally two-dimensional turbulent boundary layer at a fixed yaw orientation. This orientation was obtained by rotating the probe into the freestream flow on the tunnel centerline until the pressure difference, $P_2 - P_3$, was zero.

Two pressure differences, $P_1 - P_S$ and $P_2 - P_3$, were recorded using the data acquisition system as the probe was traversed in the y direction. Using the above calibration functions, the local dynamic pressure, Q, was equated to the pressure difference between the center tube of the probe and the 0.38 mm diameter wall pressure tap located 25 mm upstream of the probe,

$$Q = P_1 - P_S \ . \tag{3.6}$$

The flow yaw angle and speed were calculated by:

$$\beta = \frac{P_2 - P_3}{B_1 Q} , \tag{3.7}$$

and the Bernoulli relation, Eq. 2.5, respectively.

3.1.2 Two-Dimensional Boundary Layer Integral Parameters

Two integral parameters were used to compare the measured velocity distributions in the two-dimensional flow studies. The displacement thickness,

$$\delta^* = \int_0^\infty \left(1 - \frac{U}{U_e}\right) dy , \tag{3.8}$$

and the momentum thickness,

$$\theta = \int_0^\infty \frac{U}{U_e}\left(1 - \frac{U}{U_e}\right) dy, \tag{3.9}$$

were approximated as finite sums using the trapezoidal integration rule. With the no-slip condition at the wall:

$$\delta^* = y_n - \frac{y_1 U_1}{2U_e} - \sum_{i=2}^{n} \left[\frac{(y_i - y_{i-1})(U_{i-1} + U_i)}{2U_e}\right] , \tag{3.10}$$

$$\theta = \frac{y_1 U_1}{2U_e}\left(1 - \frac{U_1}{U_e}\right) \tag{3.11}$$

$$+ \sum_{i=2}^{n} \left\{\frac{(y_i - y_{i-1})}{2}\left[\frac{U_{i-1}}{U_e}\left(1 - \frac{U_{i-1}}{U_e}\right) + \frac{U_i}{U_e}\left(1 - \frac{U_i}{U_e}\right)\right]\right\}.$$

The velocity at the edge of the boundary layer, U_e, was determined by averaging the nine uppermost observations in the velocity profile, all essentially outside the boundary layer.

$$U_e = \frac{1}{9} \sum_{i=n-8}^{n} (U_i) \tag{3.12}$$

3.1.3 Skin Friction Coefficient

In addition to the two integral parameters above, the skin friction coefficient,

$$C_f = \frac{2\tau_w}{\rho U_e^2} , \tag{3.13}$$

was used to assess the spanwise uniformity of the nominally two-dimensional flow. Winter [81,82] and Rechenberg [83] review the techniques available for obtaining the wall shear stress, τ_w, in the above definition. One approach is to infer the skin friction coefficient, the wall shear stress, or the friction velocity, u_τ, related to the wall shear stress via:

$$u_\tau = \sqrt{\frac{\tau_w}{\rho}} , \tag{3.14}$$

from the velocity profile data. Many ways have been proposed to implement this approach, including those by:

(1) Clauser, 1956 [84],

(2) Bradshaw, 1959 [85],

(3) Dickinson, 1965 [in 81],

(4) Schraub and Kline, 1965 [86],

(5) Ozarapoglu, 1967 [in 81],

(6) Rajaratnam and Froelich, 1967 [87],

(7) Coles, 1968 [88], and

(8) Pierce and Zimmerman, 1973 [89].

These techniques rely on the existence of a similarity relationship that is applicable over some portion of the two-dimensional turbulent boundary layer velocity profile. Coles [88], in the 1968 AFOSR-IFP-Stanford Conference, considered two relationships:

Model I

$$U_i = u_\tau\left[\frac{1}{\kappa} \ln \left(\frac{y_i u_\tau}{\nu}\right) + C \right] + \varepsilon_i \ , \tag{3.15}$$

Model II

$$U_i = u_\tau\left[\frac{1}{\kappa} \ln \left(\frac{y_i u_\tau}{\nu}\right) + C + \frac{2\Pi}{\kappa} \sin^2 \left(\frac{\pi y_i}{2\delta}\right)\right] + \varepsilon_i . \tag{3.16}$$

where an additive error term has been inserted. A somewhat ideal situation results when this error is normally distributed with zero mean and small variance. Model II, evaluated at the edge of the boundary layer, yields:

$$U_e = u_\tau\left[\frac{1}{\kappa}\ln\left(\frac{\delta u_\tau}{\nu}\right) + C + \frac{2\Pi}{\kappa}\right] . \tag{3.17}$$

For specified values of κ, C, ν and U_e, Eq. 3.17 is a constraint among u_τ, δ, and Π. Coles [88] selected values of u_τ and δ to minimize the sum of the squared differences between model II and the data--the method of least squares. Equation 3.17 served as a constraint from which he determined the pressure gradient parameter, Π.

The method of least squares [76-80] was used to obtain the wall shear stress using the two models considered by Coles [88]. For model I, the least squares estimate of the friction velocity, u_τ, is that value which minimizes the sum of squares function:

$$SS_I(u_\tau) = \sum_i \left(\phi_i\left\{U_i - u_\tau\left[\frac{1}{\kappa}\ln\left(\frac{y_i u_\tau}{\nu}\right) + C\right]\right\}^2\right), \tag{3.18}$$

for fixed values of κ, C, and ν. Similarly for model II, the least squares estimates of the three parameters, u_τ, δ, and Π, are those values which minimize the sum of squares function:

$$SS_{II}(u_\tau,\delta,\Pi) = \sum_i \left(\phi_i\left\{U_i - u_\tau\left[\frac{1}{\kappa}\ln\left(\frac{y_i u_\tau}{\nu}\right) + C + \frac{2\Pi}{\kappa}\sin^2\left(\frac{\pi y_i}{2\delta}\right)\right]\right\}^2\right) , \tag{3.19}$$

also for fixed values of κ, C, and ν. Ordinary least squares estimates were obtained by setting the weight parameters, ϕ_i, equal to one. Weighted least squares estimates were obtained by setting the weight

parameter equal to the inverse of the squared, estimated uncertainty in the observed velocity.

$$\phi_i = \frac{1}{w_{U_i}^2} \tag{3.20}$$

In this fashion, an observation with a small uncertainty had more impact (weight) on the estimated parameters than one with a large uncertainty.

An iterative approach is required to calculate the least squares parameter estimates because the two models are intrinsically nonlinear in the estimable parameters [78]. Gauss' least squares differential correction algorithm summarized by Junkins [80] was used. For a single parameter problem, such as estimating the friction velocity using model I, Gauss' algorithm simplifies to a recursion formula for the parameter. Thus, for model I:

$$u_{\tau,(j+1)} = u_{\tau,(j)} + \frac{\sum_i \left[\phi_i \left.\frac{\partial U}{\partial u_\tau}\right|_{j,i} (U_i - \hat{U}_{j,i})\right]}{\sum_i \left(\phi_i \left.\frac{\partial U}{\partial u_\tau}\right|_{j,i}^2\right)} \tag{3.21}$$

where:

$$\left.\frac{\partial U}{\partial u_\tau}\right|_{j,i} = \frac{\hat{U}_{j,i}}{u_{\tau,(j)}} + \frac{1}{\kappa} \quad , \tag{3.22}$$

$$\hat{U}_{j,i} = u_{\tau,(j)}\left[\frac{1}{\kappa} \ln \left(\frac{y_i u_{\tau,(j)}}{\nu}\right) + C\right] . \tag{3.23}$$

For the three-parameter problem resulting from model II, the matrix recursion formula is:

$$\bar{B}_{(j+1)} = \bar{B}_{(j)} + \left(\bar{X}^{T}_{(j)}\ \bar{\Phi}\ \bar{X}_{(j)}\right)^{-1}\ \bar{X}^{T}_{(j)}\ \bar{\Phi}\ \bar{R}_{(j)}, \tag{3.24}$$

where:

$$\bar{B}_{(j)} = \begin{bmatrix} u_{\tau,(j)} \\ \delta_{(j)} \\ \Pi_{(j)} \end{bmatrix}, \tag{3.25}$$

$$\bar{X}_{(j)} = \begin{bmatrix} \left.\frac{\partial U}{\partial u_\tau}\right|_{j,1} & \left.\frac{\partial U}{\partial \delta}\right|_{j,1} & \left.\frac{\partial U}{\partial \Pi}\right|_{j,1} \\ \left.\frac{\partial U}{\partial u_\tau}\right|_{j,2} & \left.\frac{\partial U}{\partial \delta}\right|_{j,2} & \left.\frac{\partial U}{\partial \Pi}\right|_{j,2} \\ \left.\frac{\partial U}{\partial u_\tau}\right|_{j,3} & \left.\frac{\partial U}{\partial \delta}\right|_{j,3} & \left.\frac{\partial U}{\partial \Pi}\right|_{j,3} \\ \vdots & \vdots & \vdots \\ \left.\frac{\partial U}{\partial u_\tau}\right|_{j,n} & \left.\frac{\partial U}{\partial \delta}\right|_{j,n} & \left.\frac{\partial U}{\partial \Pi}\right|_{j,n} \end{bmatrix}, \tag{3.26}$$

$$\left.\frac{\partial U}{\partial u_\tau}\right|_{j,i} = \frac{\hat{U}_{j,i}}{u_{\tau,(j)}} + \frac{1}{\kappa}, \tag{3.27}$$

$$\left.\frac{\partial U}{\partial \delta}\right|_{j,i} = \frac{-\pi y_i u_{\tau,(j)} \Pi_{(j)}}{\kappa \delta^2_{(j)}} \sin\left(\frac{\pi y_i}{\delta_{(j)}}\right), \tag{3.28}$$

$$\left.\frac{\partial U}{\partial \Pi}\right|_{j,i} = \frac{2u_{\tau,(j)}}{\kappa} \sin^2\left(\frac{\pi y_i}{2\delta_{(j)}}\right) , \tag{3.29}$$

$$\bar{\Phi} = \begin{bmatrix} \phi_1 & 0 & 0 & \cdots & 0 \\ 0 & \phi_2 & 0 & \cdots & 0 \\ 0 & 0 & \phi_3 & \cdots & 0 \\ \vdots & \vdots & \vdots & & \\ 0 & 0 & 0 & \cdots & \phi_n \end{bmatrix} , \tag{3.30}$$

$$\bar{R}_{(j)} = \begin{bmatrix} U_1 - \hat{U}_{j,1} \\ U_2 - \hat{U}_{j,2} \\ U_3 - \hat{U}_{j,3} \\ \vdots \\ U_n - \hat{U}_{j,n} \end{bmatrix} , \tag{3.31}$$

$$\hat{U}_{j,i} = u_{\tau,(j)}\left[\frac{1}{\kappa} \ln\left(\frac{y_i u_{\tau,(j)}}{\nu}\right) + C + \frac{2\Pi_{(j)}}{\kappa} \sin^2\left(\frac{\pi y_i}{2\delta_{(j)}}\right)\right] . \tag{3.32}$$

Initial values and convergence criteria are required to implement the iterative algorithm. The initial estimate for the friction velocity, $u_{\tau,(0)}$, was obtained using the integral parameters and the Ludwieg-Tillmann formula [90],

$$C_f = 0.246(10)^{-0.678H} \left(\frac{U_e \theta}{\nu}\right)^{-0.268} , \tag{3.33}$$

$$H = \frac{\delta^*}{\theta} . \tag{3.34}$$

For the boundary layer thickness and the pressure gradient parameter, visual inspection of the plotted velocity profile and a representative value for zero pressure gradient, two-dimensional turbulent boundary layer flow (0.50) provided adequate starting values. All iterations were continued until the following relative convergence criteria were met:

$$\left| \frac{u_{\tau,(j+1)} - u_{\tau,(j)}}{u_{\tau,(j)}} \right| \leq 1.0(10^{-6}) , \tag{3.35}$$

$$\left| \frac{\delta_{(j+1)} - \delta_{(j)}}{\delta_{(j)}} \right| \leq 1.0(10^{-6}) , \tag{3.36}$$

$$\left| \frac{\Pi_{(j+1)} - \Pi_{(j)}}{\Pi_{(j)}} \right| \leq 1.0(10^{-6}) . \tag{3.37}$$

There are at least two important differences between the models used to estimate the parameters. The first difference is the origin of the model. Model I results from dimensional analysis. Model II is simply an extension of model I to include the wake-like structure of a

typical, equilibrium, two-dimensional turbulent boundary layer. The functional form of the extension to model I incorporates some desirable boundary conditions on the wake-like structure but is otherwise arbitrary. In spite of this arbitrariness, much data has been accumulated in support of model II, which describes the typical, equilibrium, two-dimensional boundary layer velocity distribution over a much greater range of y values than model I. The range of applicability of the model is the second important difference. Because of this second difference, data in the range:

$$0.71 \text{ mm} \leq y \leq 6.60 \text{ mm} , \tag{3.38}$$

which corresponds approximately to:

$$35 \leq y^{+} \leq 350 , \tag{3.39}$$

was used with model I. For model II, data in the range:

$$0.71 \text{ mm} \leq y \leq 70.9 \text{ mm} , \tag{3.40}$$

was used where the upper limit corresponds to approximately 90 percent of the estimated boundary layer thickness. The validity of model II closer to the freestream edge of the boundary layer is questionable because of its non-zero velocity gradient there.

Three-parameter optimization, Gauss' algorithm, and the use of estimated uncertainties to calculate weights distinguish this approach from that of Coles [88]. In all of these calculations, values for κ and C were assumed to be 0.41 and 5, respectively [88]. It was not the objective of this study to challenge or to propose new values for these parameters.

The remainder of this chapter describes the methods used in the three dimensional flow investigation.

3.2 Flow Visualization

The surface flows on the flat floor of the wind tunnel and on the bluff body were made visible using an oil-film technique described by Squire, et al. [91]. This technique requires the application of a thin film of oil containing an indicator to the surfaces of the wind tunnel model. Shear forces at the oil film-air interface and pressure forces from the external flow break the thin film into filaments and carry them along the surface. The ideal situation is one in which shear forces are the dominant effect. In this case, the indicator is deposited on the surface along the limiting streamlines.

A mixture of 10.7 g of titanium dioxide (TiO_2), 30 mℓ of diesel fuel, and 2 drops of oleic acid was used for the oil film. Titanium dioxide is a nontoxic, white pigment used commercially in house paints and toothpaste. The best results were obtained when the titanium dioxide was first sifted through 60 mesh (250 μm square openings) screen to eliminate large agglomerations of particles. Diesel fuel was used for

the vehicle because of its vapor pressure, viscosity, and ease of application and clean-up. Oleic acid is a dispersing agent used to control the size of the streaks. The mixture was sprayed onto the model surfaces after all surfaces were uniformly wetted with a light coat of diesel fuel. Good streamline patterns were obtained after approximately two minutes of tunnel operation.

Both the flat wind tunnel floor and the bluff body were covered with removable coatings to preserve the limiting streamline patterns. The tunnel floor was covered with a 0.91 m wide, 1.22 m long, 0.81 mm thick piece of tempered aluminum sheet metal. The leading edge of this thin sheet was hand finished into a knife edge to minimize the roughness effect on the boundary layer. The bluff body was covered with a 50 μm - thick cellulose acetate sheet. The aluminum and cellulose acetate sheets were held in place with double-sided tape and painted flat black to enhance the visibility of the white titanium dioxide particles. After a test was completed, these sheets were removed from the model surfaces and painted with clear acrylic lacquer to preserve them for later consideration.

3.3 Surface Pressure Measurements

The surface pressure distributions on the flat floor in the vicinity of the leading edge and on the vertical sides of the bluff body were measured. Pressure taps, 0.51 mm in diameter, were distributed on both surfaces in anticipation of high pressure gradients. The two pressure differences required in the pressure coefficient,

$$C_P = \frac{P - P_{T,*}}{Q_*} , \qquad (3.41)$$

were measured using the digital manometers described in Table 2.2 and were recorded manually.

Three-hundred sixty-three pressure taps were machined into the removable aluminum test plate in the wind tunnel floor as shown in Fig. 3.5. Forty-three taps were included as shown in Fig. 3.6 to check the flow symmetry.

A hollow, cast, polyester resin body was made specifically for the body surface pressure measurements. A typical cross section is shown in Fig. 3.7 along with the details of the pressure tap installation. One side of the body was instrumented with six rows of thirteen pressure taps as shown in Fig. 3.8. An additional, symmetrically disposed row of twelve taps was included at approximately 120 mm from the floor to check for flow symmetry. Trip wires, 0.25 mm in diameter and spanning the height of the body, were mounted on both sides of the leading edge 85° from the attachment line.

3.4 Kiel Probe Measurements

The total pressure distribution was measured in two planes as shown in Fig. 3.9 using a 1.59 mm diameter, United Sensor Corporation Kiel probe. The directional characteristics of this probe were investigated in the free jet of the calibration tunnel described in Section 2.4. It was found that this probe indicated the true total pressure over the range of flow angles:

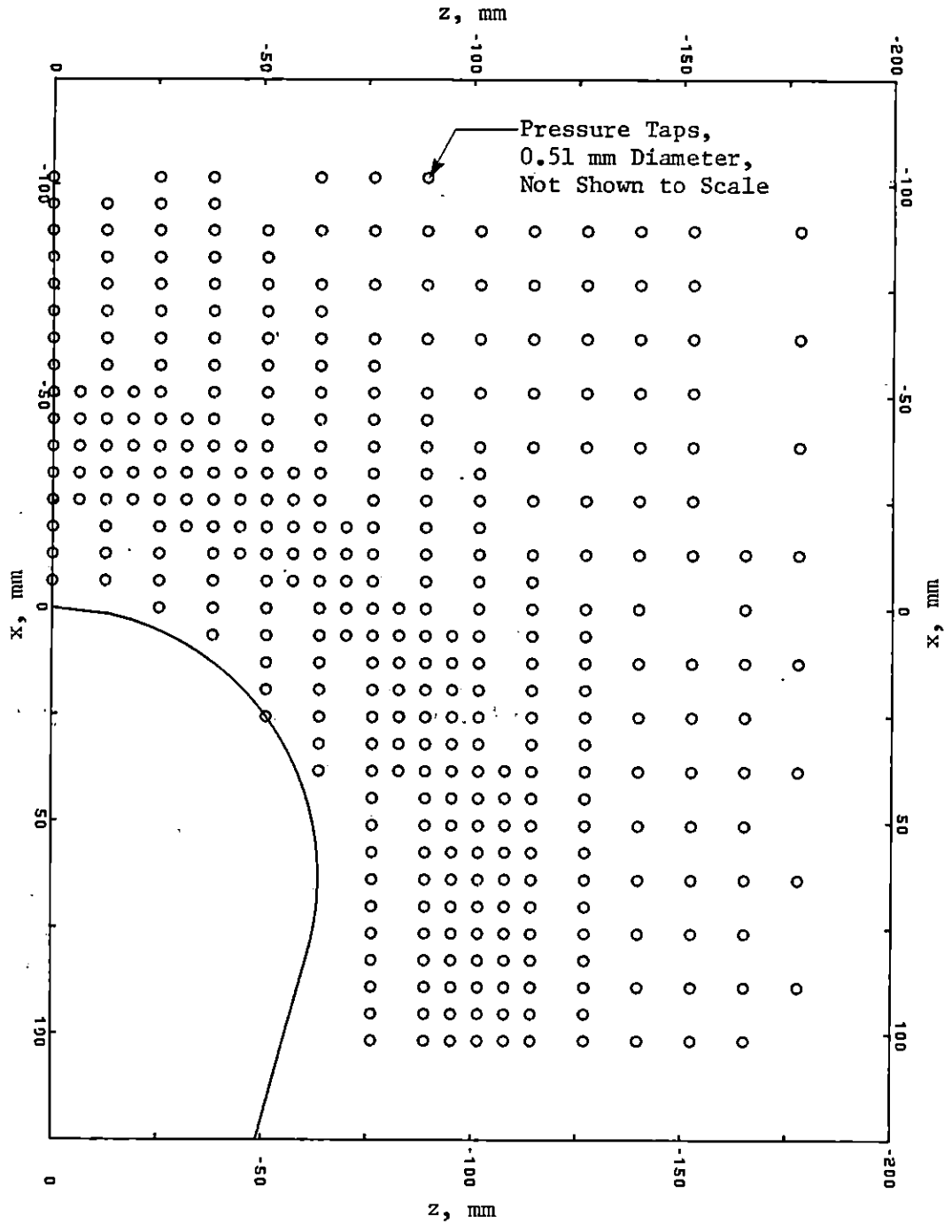

Fig. 3.5 Pressure Tap Distribution in the Wind Tunnel Floor

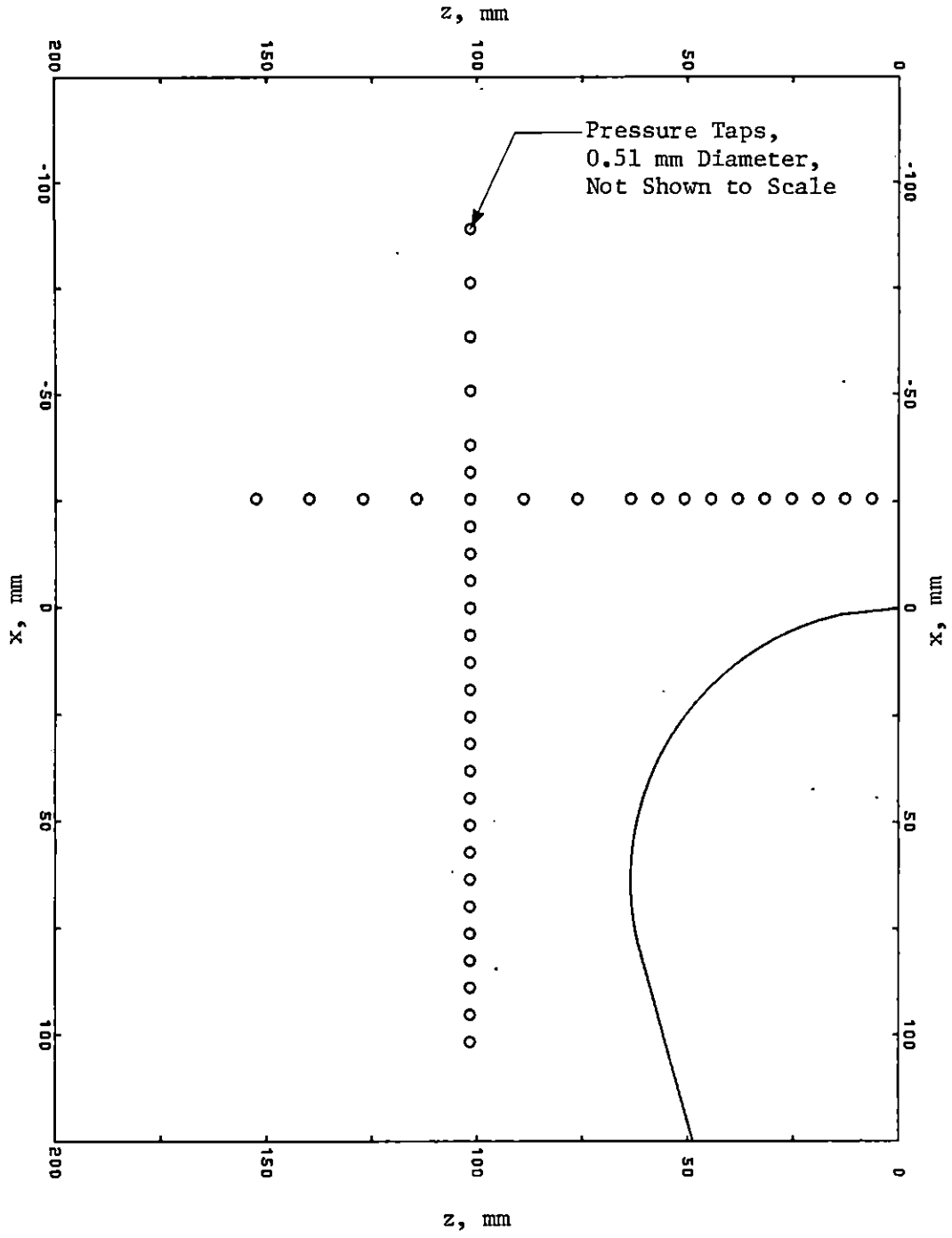

Fig. 3.6 Symmetrically Located Pressure Taps in the Wind Tunnel Floor

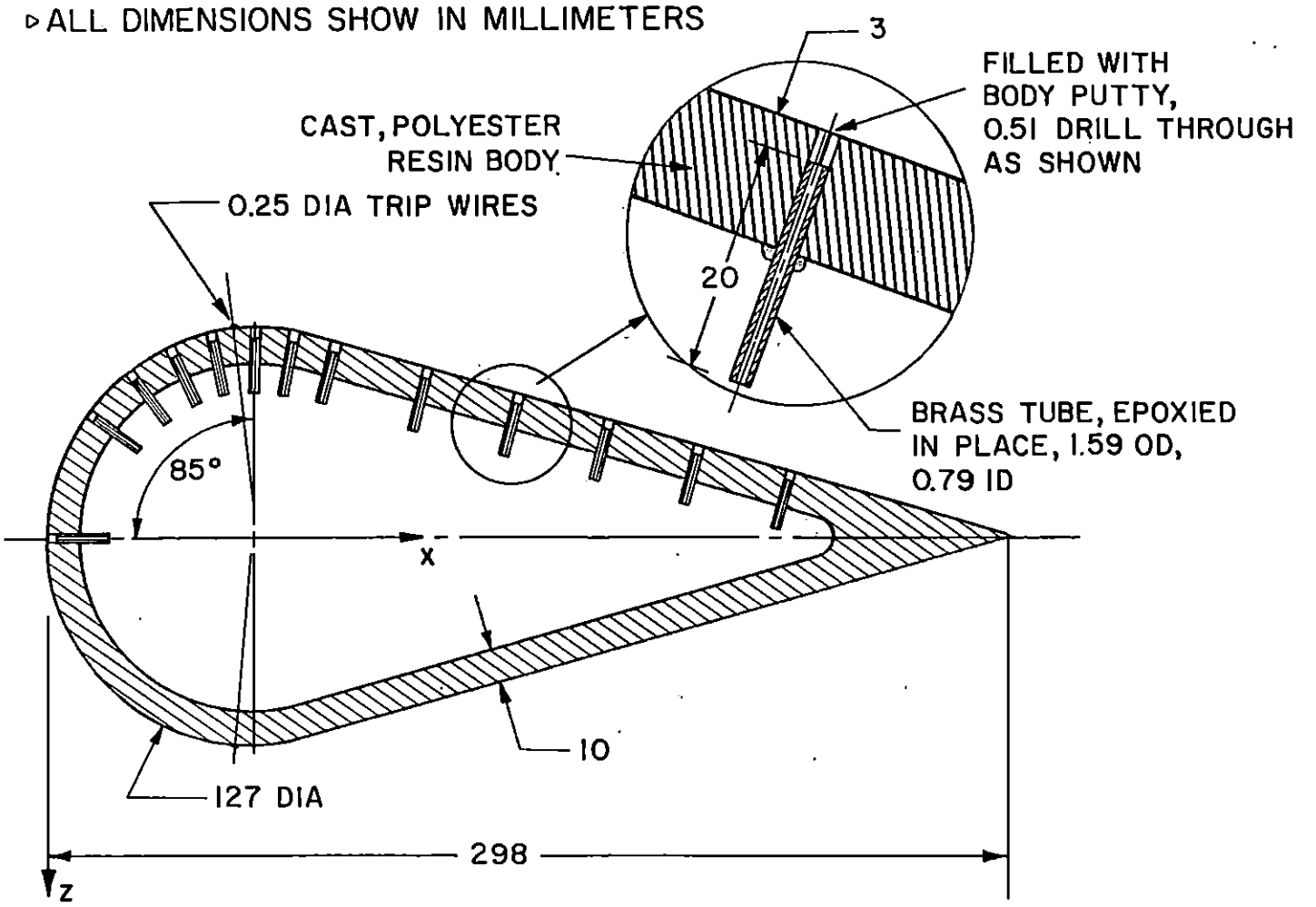

Fig. 3.7 Typical Cross Section of the Bluff Body with Surface Pressure Taps

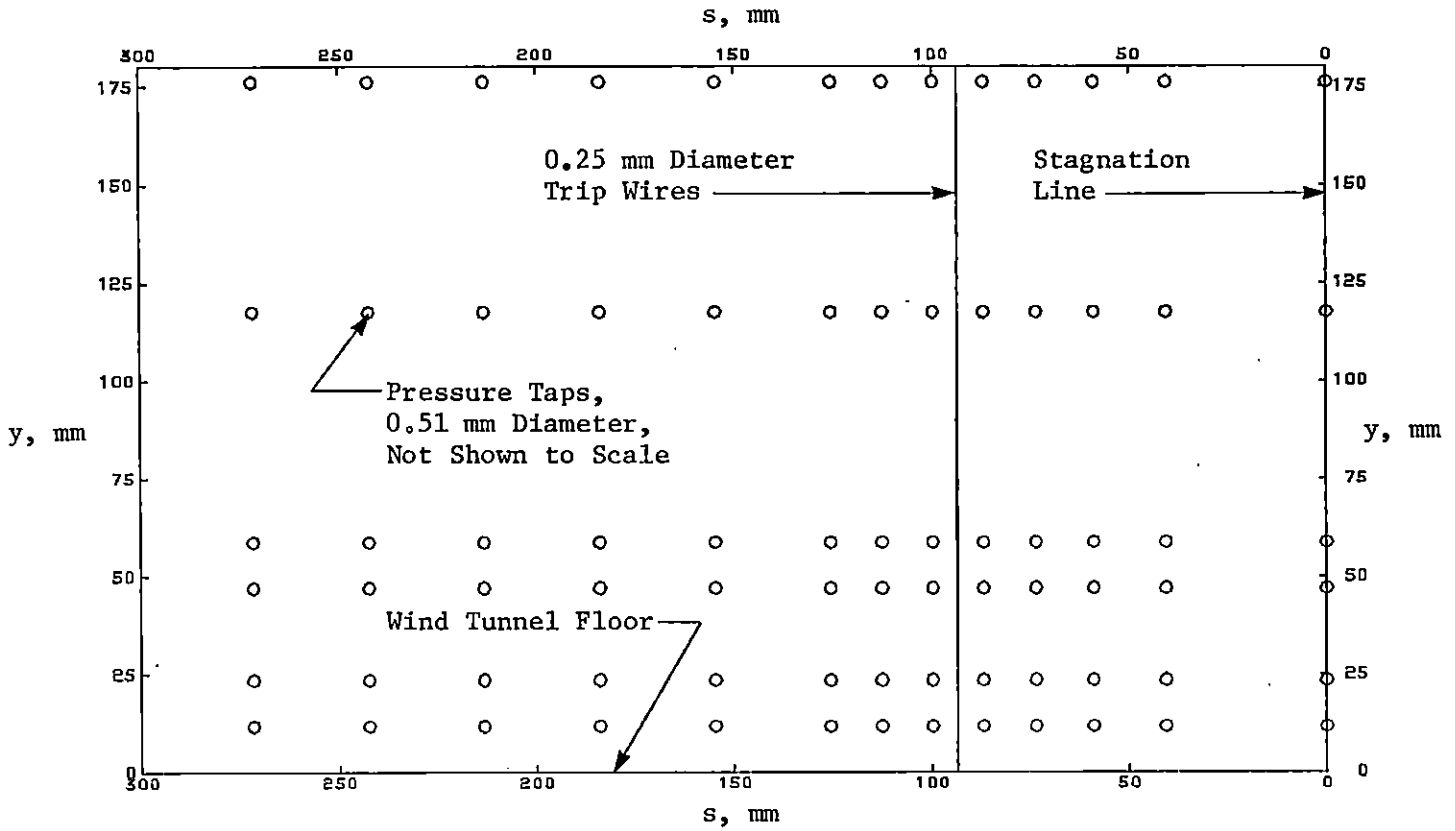

Fig. 3.8 Pressure Tap Distribution in the Surface of the Bluff Body

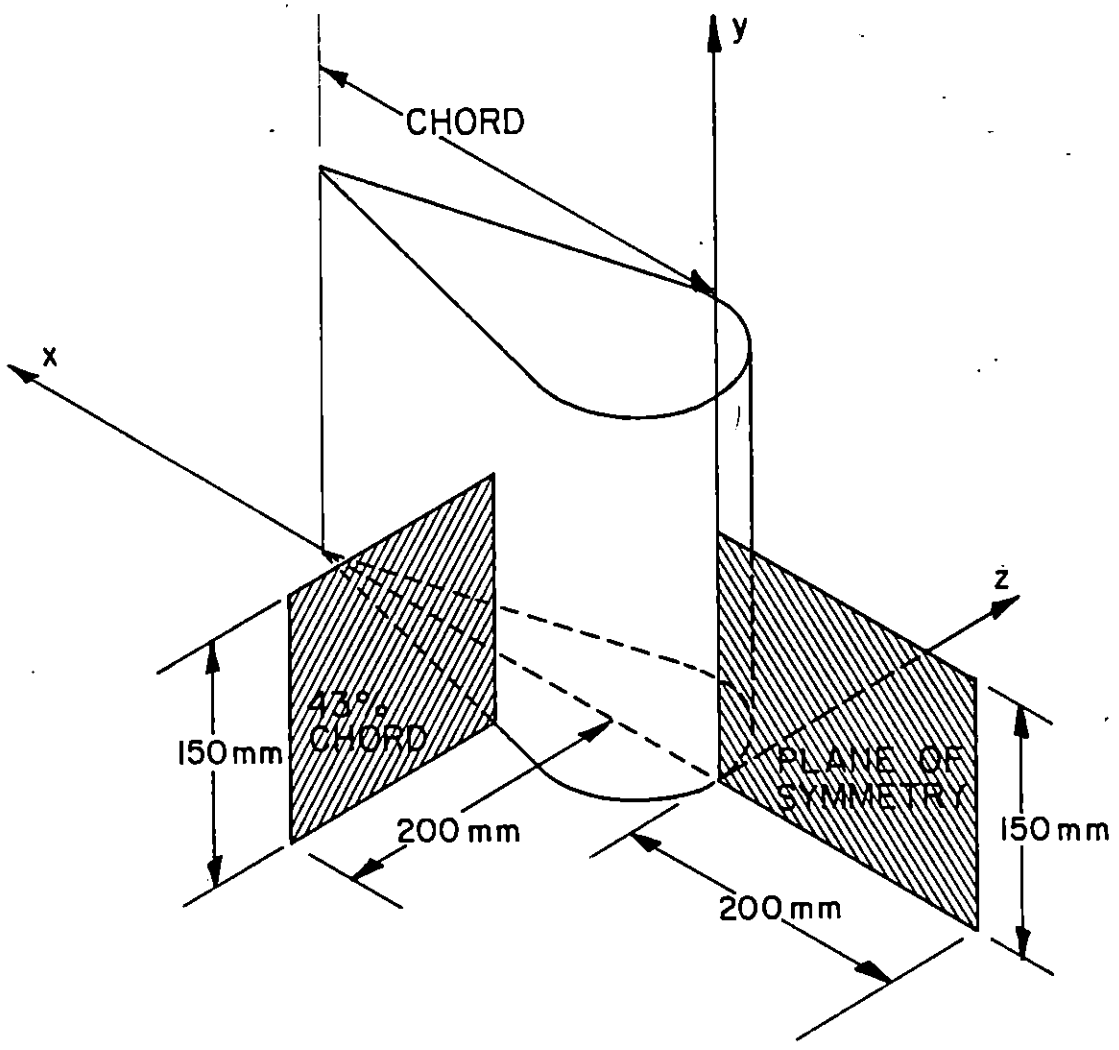

Fig. 3.9 Positions of Kiel Probe Total Pressure Measurements

$$-30^{\circ} \leq \alpha \leq +30^{\circ} ,$$
$$-30^{\circ} \leq \beta \leq +30^{\circ} . \qquad (3.42)$$

Since the probe was insensitive to modest yaw angles, it was aligned with the freestream centerline flow, without the body in the tunnel, once for each plane of data. The probe was then traversed across the three-dimensional flow field in the y direction at this yaw orientation. The pressure differences required to calculate the total pressure coefficient:

$$C_{P,T} = \frac{P_K - P_{T,*}}{Q_*} , \qquad (3.43)$$

were measured using the Datametrics digital manometers described in Table 2.2 and recorded using the data acquisition system.

Two observations of the total pressure coefficient were made at each x-y position of the probe in the plane of symmetry due to the anticipated flow reversal. These observations corresponded to two yaw orientations of the probe, one with the probe facing the freestream flow as described in the previous paragraph and one with the probe rotated 180° from this freestream orientation. The correct value of the total pressure coefficient was assumed to be given by:

$$C_{P,T} = \max \left(C_{P,T,\beta=0^{\circ}}, C_{P,T,\beta=180^{\circ}} \right) . \qquad (3.44)$$

This approach produced a crude indication of flow reversal in the plane of symmetry.

3.5 Five-Hole Probe Measurements

Distributions of three-dimensional velocity, total pressure, and static pressure were measured in three planes as shown in Fig. 3.10 using a 3.18 mm diameter, United Sensor Corporation, type DC, five-hole pressure probe. The geometry of the five-hole probe is shown in Fig. 3.11. For the data in the planes normal to the streamwise direction, the probe was pointed into the wind by rotating it in the yaw sense until the pressure difference, $P_2 - P_3$, was zero. The flow pitch angle with respect to the probe at this yaw orientation, the speed, the total pressure, and the static pressure were then determined from three measured pressure differences and three calibration curves. For the plane of symmetry data, the probe was traversed in the y direction at two fixed yaw orientations, one with the probe facing the freestream flow direction and one with the probe rotated 180° from this freestream orientation. The correct orientation of the probe was then obtained by maximizing the total pressure response (from hole 1 in Fig. 3.11) of the probe, identical to the procedure used with the Kiel probe and described in the preceding section.

The remainder of this section describes how the probe was pointed into the wind and the data reduction required to obtain the three-dimensional velocity vector, the total pressure, and the static pressure.

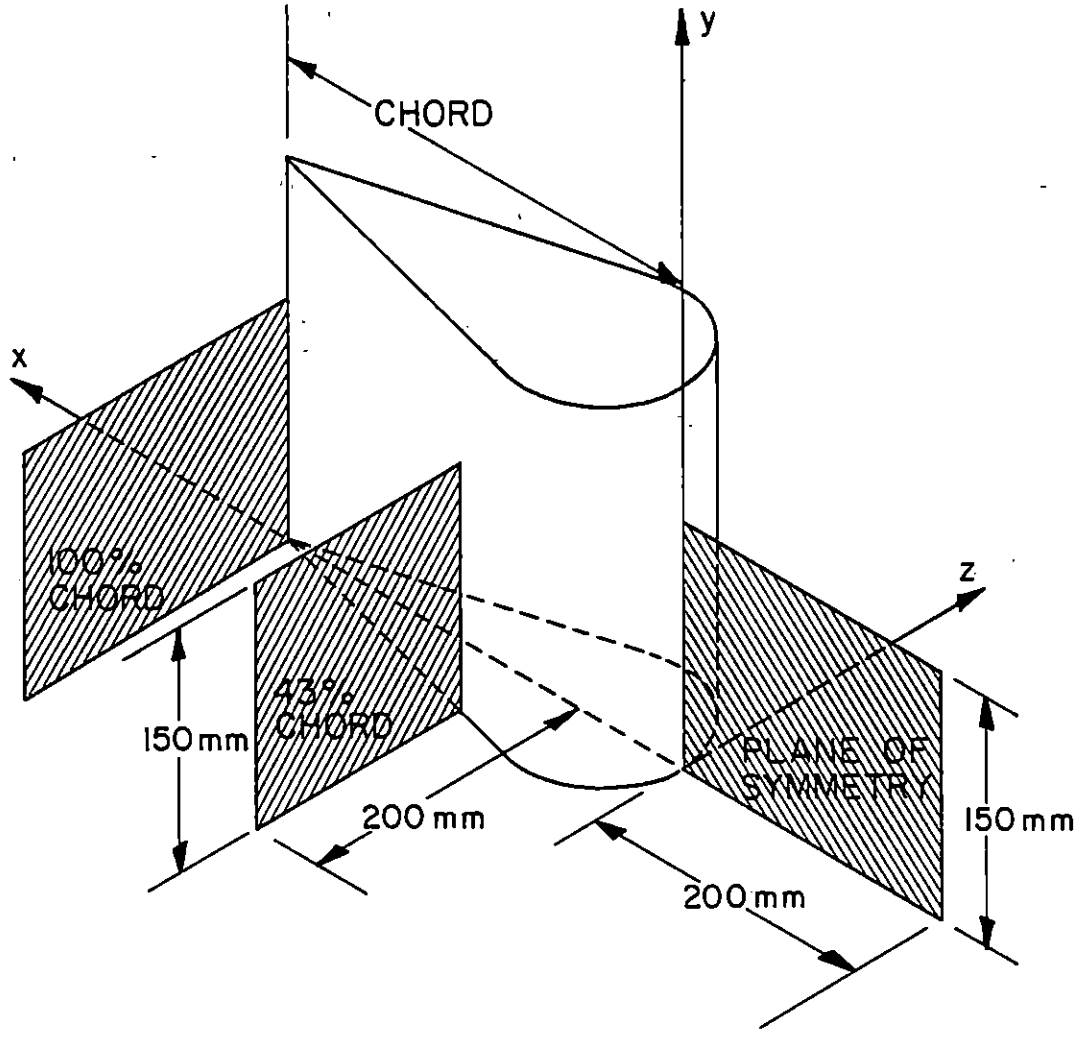

Fig. 3.10 Positions of Three-Dimensional Flow Measurements Using the Five-Hole Probe

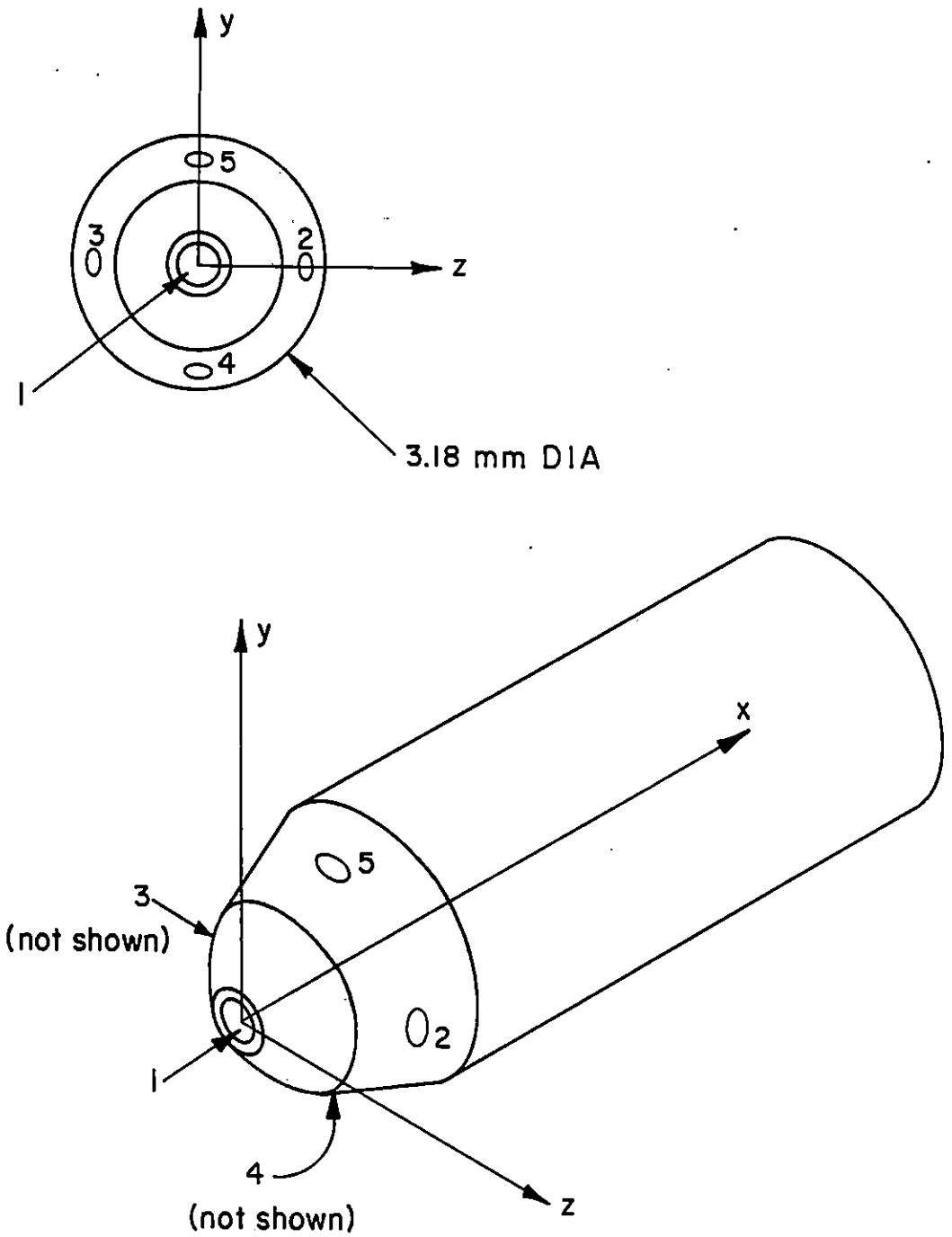

Fig. 3.11 Five-Hole Pressure Probe

3.5.1 Probe Nulling

The probe was rotated into the wind at each vertical position using a simple least squares control algorithm in the microcomputer. At the first vertical position in each traverse, the probe was nulled manually and the yaw orientation, $\beta_o(y_1)$, fed into the microcomputer. The probe was then moved a small increment in the y direction to the next vertical position, y_2, with a slightly different flow yaw angle, $\beta_o(y_2)$, as yet undetermined. To determine the new null position, the microcomputer observed the pressure difference, $P_2 - P_3$, at three yaw orientations, $\beta_o(y_1) - 3^o$, $\beta_o(y_1)$, and $\beta_o(y_1) + 3^o$. Simple linear regression [77-79] was then implemented by the microcomputer and the new null position, $\beta_o(y_2)$, predicted using the estimated regression coefficients. The increments of motion in the y direction were adjusted such that the change in the null position, $\beta_o(y_i) - \beta_o(y_{i-1})$, was never more than 3^o. This simple approach produced good results because of the linear behavior of the yaw pressure coefficient about the null point as shown in Fig. 3.12.

3.5.2 Five-Hole Probe Calibration

The five-hole probe shown in Fig. 3.11 was calibrated for pitch angle in the free jet of the calibration tunnel described in Section 2.4. Three calibration functions were considered, including a pitch pressure coefficient,

$$f_3(\alpha, Re_p) = \frac{P_4 - P_5}{P_1 - P_2}, \tag{3.45}$$

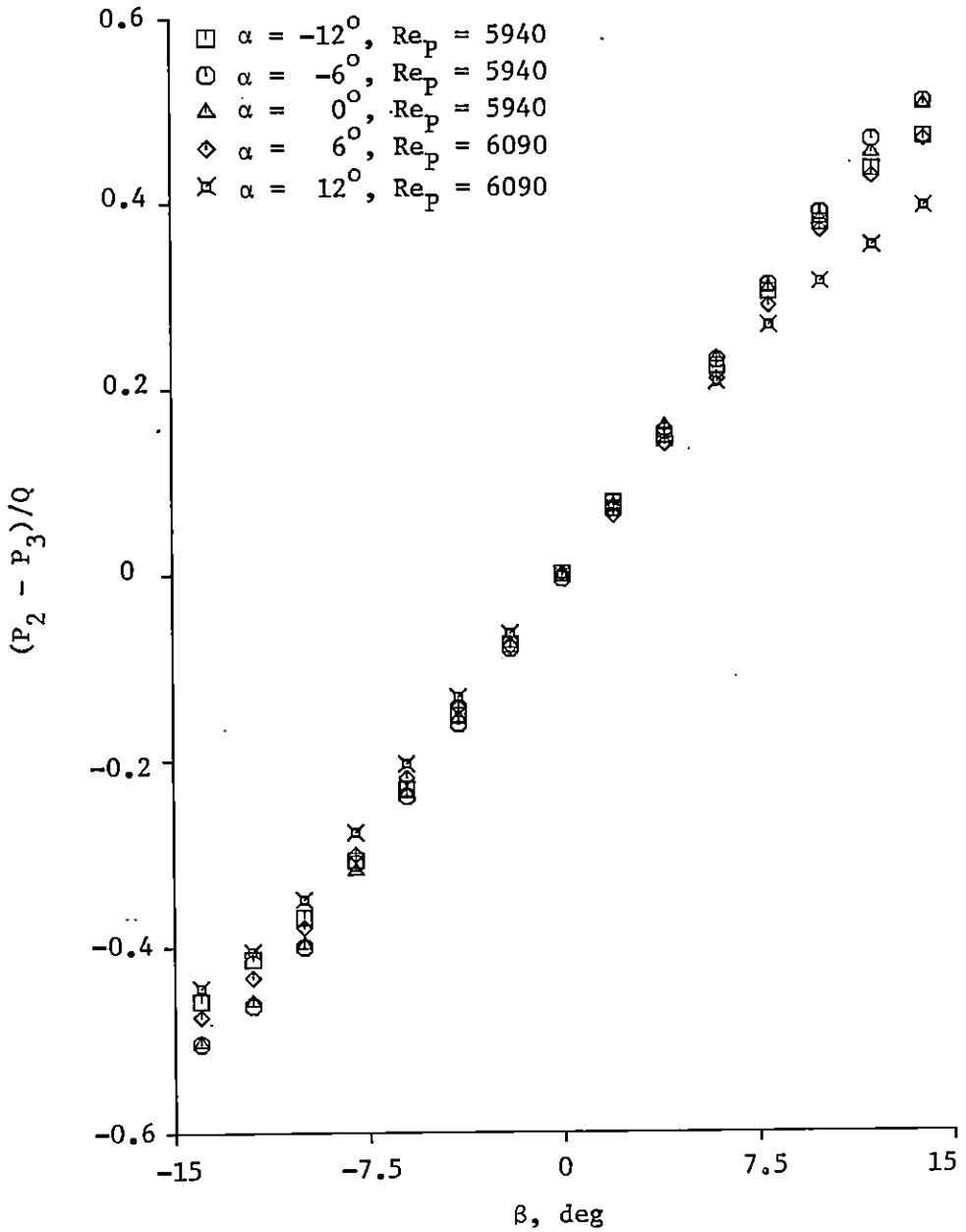

Fig. 3.12 Yaw Pressure Coefficient for the Five-Hole Probe

a dynamic pressure coefficient,

$$f_4(\alpha, Re_p) = \frac{Q}{P_1 - P_2} \quad , \tag{3.46}$$

and a total pressure coefficient,

$$f_5(\alpha, Re_p) = \frac{P_1 - P_T}{Q} \quad , \tag{3.47}$$

where the probe Reynolds number is given by Eq. 3.3. Data required to evaluate these functions was acquired over a large range of pitch angles (±15°) and a range of Reynolds numbers greater than those anticipated in the three-dimensional flow measurements. The calibration data are shown in Fig. 3.13 through Fig. 3.15. Thirty-two candidate models were considered for each calibration function, including all polynomial models through fourth-degree in pitch and first-degree in probe Reynolds number. Coefficients in the models for these data were evaluated using weighted least squares [76,78-80] with the weights equal to the inverse of the squared estimated uncertainties in the calibration data. The final choice for each of these models represents a trade-off between goodness of fit, predictive capability, and parsimony. Only the dynamic pressure coefficient was found to have a significant Reynolds number dependency. The optimized models for the calibration functions are given by:

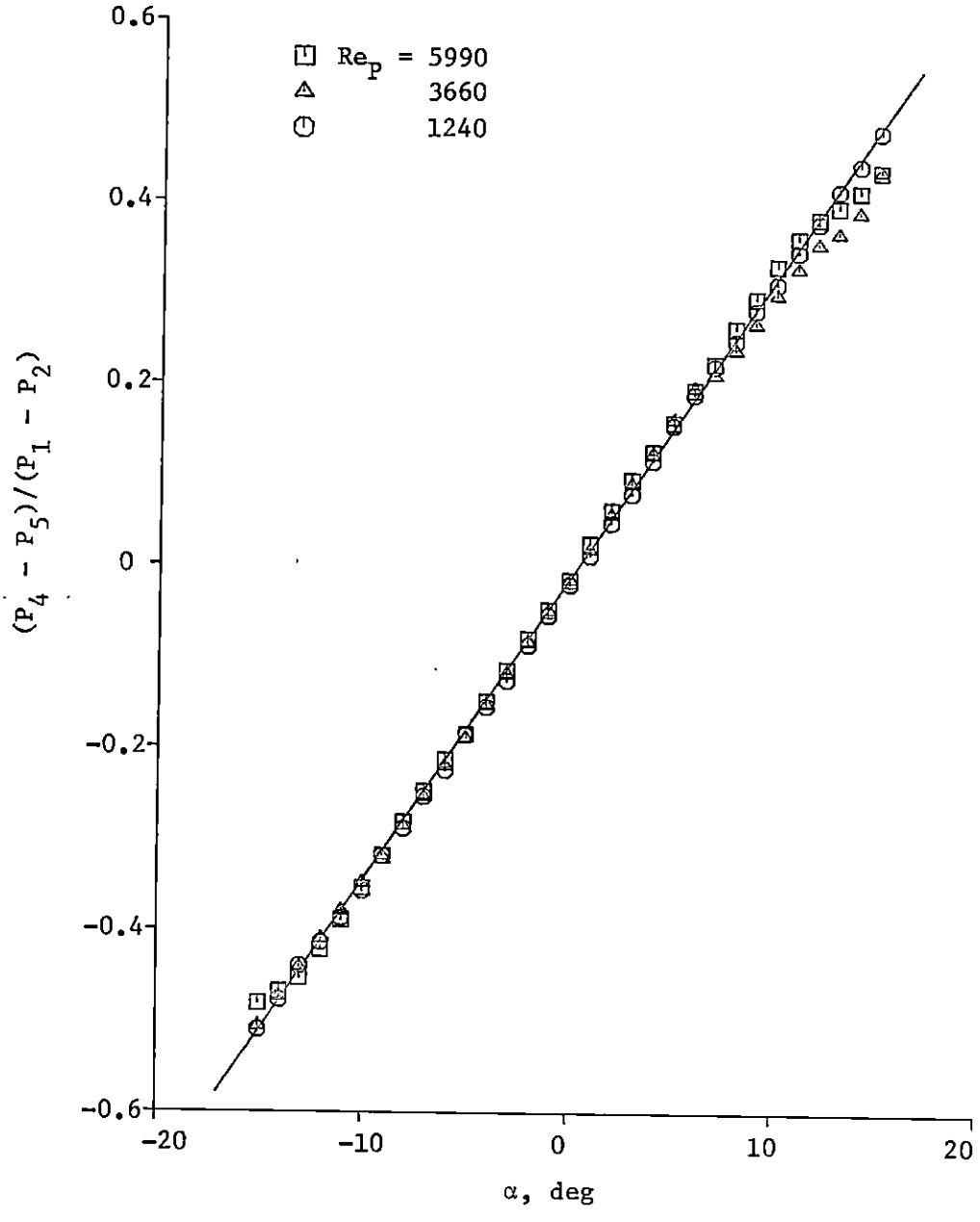

Fig. 3.13 Pitch Pressure Coefficient for the Five-Hole Probe

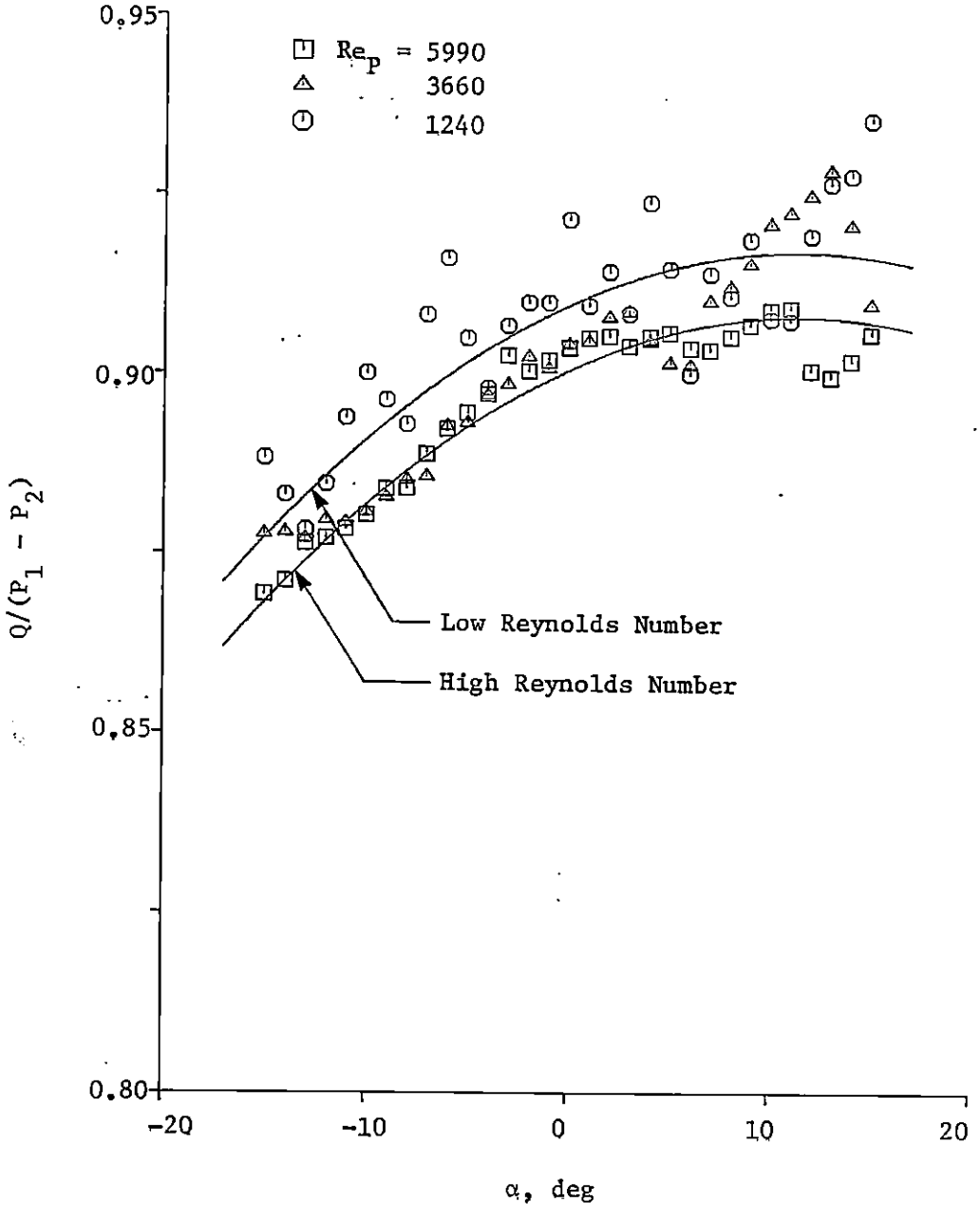

Fig. 3.14 Dynamic Pressure Coefficient for the Five-Hole Probe

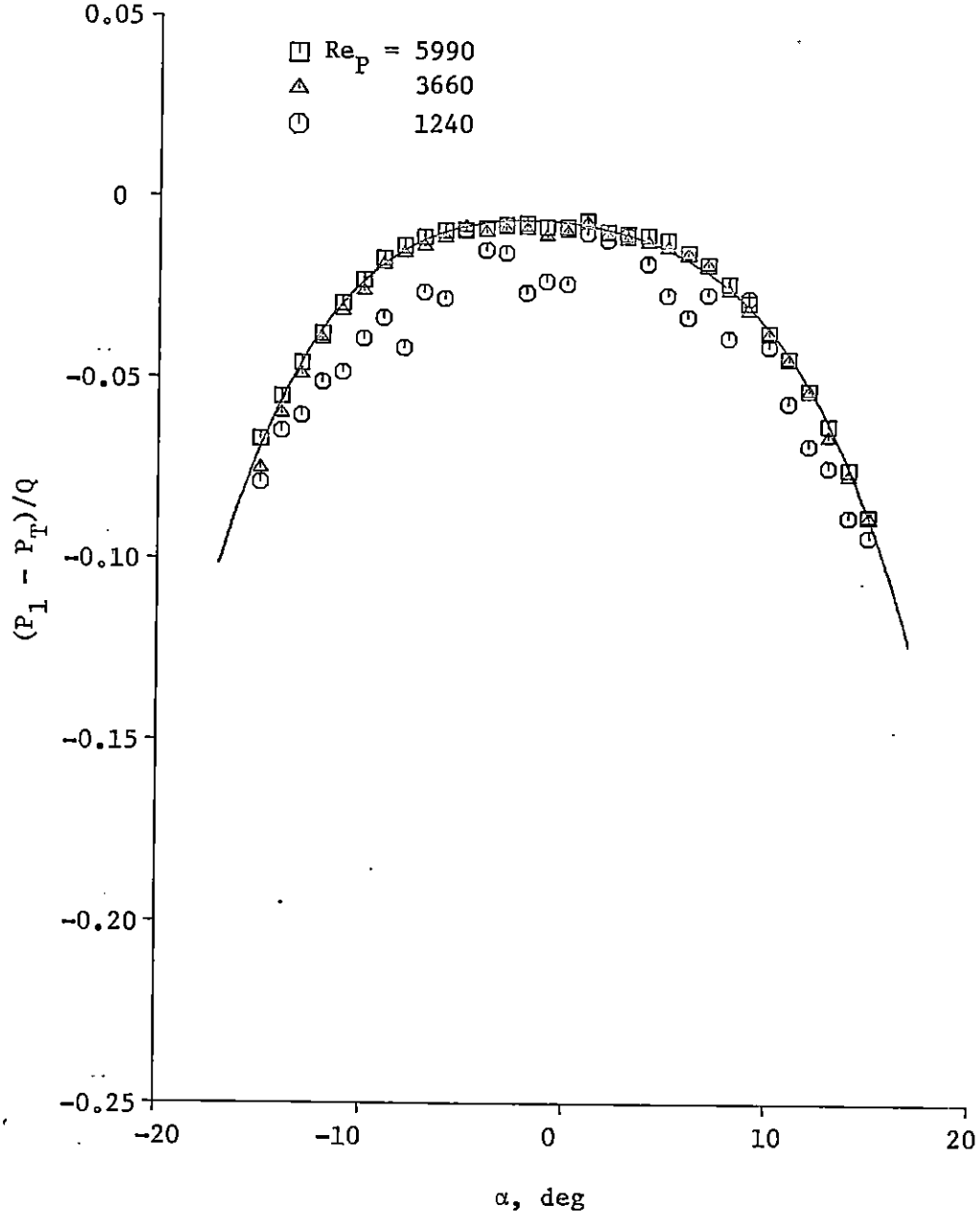

Fig. 3.15 Total Pressure Coefficient for the Five-Hole Probe

$$f_3(\alpha) = B_2 + B_3\alpha \ ,$$
$$= -0.0139 + 0.0332\alpha \ , \tag{3.48}$$

$$f_4(\alpha,Re_P) = B_4 + B_5\alpha + B_6\alpha^2 + B_7Re_P \ ,$$
$$= 0.912 + 0.00131\alpha$$
$$-5.7(10^{-5})\alpha^2 - 1.9(10^{-6})Re_P \ , \tag{3.49}$$

$$f_5(\alpha) = B_8 + B_9\alpha + B_{10}\alpha^2 + B_{11}\alpha^4,$$
$$= -0.0065 - 6.3(10^{-4})\alpha$$
$$-1.57(10^{-4})\alpha^2 - 7.2(10^{-7})\alpha^4 \ . \tag{3.50}$$

Three pressure differences, $P_4 - P_5$, $P_1 - P_2$, and $P_1 - P_{T,*}$, were recorded at each vertical position. Using these data and the aforementioned calibration functions, the pitch angle with respect to the probe was given by:

$$\alpha_o = \frac{1}{B_3}\left[\frac{(P_4 - P_5)}{(P_1 - P_2)} - B_2\right] . \tag{3.51}$$

Equation 3.49 was then used to determine the local dynamic pressure:

$$Q = (P_1 - P_2)\ f_4(\alpha_o,Re_P), \tag{3.52}$$

which yielded the speed using the Bernoulli relation, Eq. 2.5. The total pressure coefficient,

$$C_{P,T} = \frac{P_T - P_{T,*}}{Q_*} , \tag{3.53}$$

was given by:

$$C_{P,T} = \frac{(P_1 - P_{T,*}) - Qf_5(\alpha_o)}{Q_*} , \tag{3.54}$$

and the static pressure coefficient,

$$C_{P,S} = \frac{P_S - P_{T,*}}{Q_*} , \tag{3.55}$$

by:

$$C_{P,S} = C_{P,T} - \frac{Q}{Q_*} . \tag{3.56}$$

The flow pitch angle given by Eq. 3.51 is relative to the local flow yaw angle, as shown in Fig. 2.2. The reported data is relative to the tunnel coordinate system. Thus:

$$\beta = \beta_o - \beta_{Ref} , \tag{3.57}$$

$$\frac{U}{\bar{V}_*} = \frac{\bar{V}}{\bar{V}_*} \cos(\alpha_o) \cos(\beta) , \tag{3.58}$$

$$\frac{V}{\bar{V}_*} = \frac{\bar{V}}{\bar{V}_*} \sin(\alpha_o) \ , \tag{3.59}$$

$$\frac{W}{\bar{V}_*} = - \frac{\bar{V}}{\bar{V}_*} \cos(\alpha_o) \sin(\beta) \ , \tag{3.60}$$

$$\alpha = \tan^{-1} \left[\frac{\tan(\alpha_o)}{\cos(\beta)} \right] . \tag{3.61}$$

3.6 Uncertainty Estimates

The uncertainty estimates reported in the appendices were obtained by the Kline and McClintock method [92-95]. This method estimates the uncertainty in a result R, which is a function of k uncertain observations, x_i, i = 1,2,3,...k, by:

$$w_R = \left[\sum_{i=1}^{k} \sum_{j=1}^{k} \left(r_{x_i x_j} \, w_{x_i} \, w_{x_j} \, \frac{\partial R}{\partial x_i} \, \frac{\partial R}{\partial x_j} \right) \right]^{1/2} \ , \tag{3.62}$$

where the uncertainty estimates, w_R and w_{x_i} for all i, are at the same level of significance. A common situation is one in which the errors in the observations are independent. In this case, the estimated correlation coefficient, $r_{x_i x_j}$, is:

$$r_{x_i x_j} = \begin{cases} 0 \ , & i \neq j \\ 1 \ , & i = j \end{cases} \ , \tag{3.63}$$

and the estimated uncertainty becomes:

$$w_R = \left\{ \sum_{i=1}^{k} \left[\left(w_{x_i} \frac{\partial R}{\partial x_i} \right)^2 \right] \right\}^{1/2} \quad . \tag{3.64}$$

For the general case described by Eq. 3.62, $\frac{k}{2}(k + 3)$ pieces of information are required to estimate the uncertainty in a result. The required information includes k sensitivities (partial derivatives) of the result to the various observations, k estimated uncertainties in the observations, and $\frac{k}{2}(k - 1)$ estimated correlation coefficients. The k sensitivities can be evaluated explicitly using the data reduction equations or approximated with finite differences. Both approaches were used to obtain the reported results. For the k estimated uncertainties in the observations, at the 5 percent significance level (95 percent confidence interval, 19 to 1 odds), in general:

$$w_{T_\infty} = \pm 1 \text{ C} \quad , \tag{3.65}$$

$$w_{P_\infty} = \pm 170 \text{ Pa} \quad , \tag{3.66}$$

$$w_{Q_*} = \pm 1 \text{ Pa} \quad , \tag{3.67}$$

for the two-dimensional turbulent boundary layer data:

$$w_{P_2-P_3} = \pm \left[(0.5 + 0.0015 |P_2-P_3|)^2 + (2.5)^2 \right]^{1/2} \text{ Pa} \quad , \tag{3.68}$$

$$w_{P_1-P_S} = \pm \left[(0.5 + 0.0015 |P_1-P_s|)^2 + (2.5)^2 \right]^{1/2} \text{ Pa} \quad , \tag{3.69}$$

$$w_{B_1} = \pm 4 \times 10^{-4} \text{ deg}^{-1} \quad , \tag{3.70}$$

for the surface pressure data:

$$w_{P-P_{T,*}} = \pm \left[(0.5 + 0.0015|P-P_{T,*}|)^2 + (1.3)^2\right]^{1/2} \text{ Pa} \quad , \tag{3.71}$$

for the Kiel probe data:

$$w_{P_K-P_{T,*}} = \pm \left[(0.5 + 0.0015|P_K-P_{T,*}|)^2 + (1.3)^2\right]^{1/2} \text{ Pa}, \tag{3.72}$$

and for the five-hole probe data:

$$w_{P_4-P_5} = \pm \left[(0.5 + 0.0015|P_4-P_5|)^2 + (2.5)^2\right]^{1/2} \text{ Pa} \quad , \tag{3.73}$$

$$w_{P_1-P_2} = \pm \left[(0.5 + 0.0015|P_1-P_2|)^2 + (2.5)^2\right]^{1/2} \text{ Pa} \quad , \tag{3.74}$$

$$w_{P_1-P_{T,*}} = \pm \left[(0.5 + 0.0015|P_1-P_{T,*}|)^2 + (2.5)^2\right]^{1/2} \text{ Pa}, \tag{3.75}$$

$$w_{\beta_o} = \pm 0.2 \text{ deg} \quad , \tag{3.76}$$

$$w_{\beta_{Ref}} = \pm 0.2 \text{ deg} \quad , \tag{3.77}$$

$$w_{B_2} = \pm 2 \times 10^{-4} \quad , \tag{3.78}$$

$$w_{B_3} = \pm 3 \times 10^{-4} \text{ deg}^{-1} \quad , \tag{3.79}$$

$$w_{B_4} = \pm 4 \times 10^{-3} \quad , \tag{3.80}$$

$$w_{B_5} = \pm 1.0 \times 10^{-4} \text{ deg}^{-1} \quad , \tag{3.81}$$

$$w_{B_6} = \pm 1.3 \times 10^{-5} \text{ deg}^{-2} \quad , \tag{3.82}$$

$$w_{B_7} = \pm 7.6 \times 10^{-7} \quad , \tag{3.83}$$

$$w_{B_8} = \pm 6 \times 10^{-4} \quad , \tag{3.84}$$

$$w_{B_9} = \pm 3 \times 10^{-5} \text{ deg}^{-1} \quad , \tag{3.85}$$

$$w_{B_{10}} = \pm 2 \times 10^{-5} \text{ deg}^{-2} \quad , \tag{3.86}$$

$$w_{B_{11}} = \pm 7 \times 10^{-8} \text{ deg}^{-4} \quad , \tag{3.87}$$

The estimated uncertainties in the calibration coefficients were obtained from the least squares analysis of the calibration data [76-80]. Only the correlations between the calibration coefficients were recognized. The estimated correlation coefficients, from the least squares analysis, are:

$$r_{B_2B_3} = 0.368 \quad , \tag{3.88}$$

$$r_{B_4B_5} = 0.006 \quad , \tag{3.89}$$

$$r_{B_4B_6} = -0.247 \quad , \tag{3.90}$$

$$r_{B_4B_7} = -0.942 \quad , \tag{3.91}$$

$$r_{B_5B_6} = 0.026 \quad , \tag{3.92}$$

$$r_{B_5B_7} = -0.006 \quad , \tag{3.93}$$

$$r_{B_6B_7} = -0.005 \quad , \tag{3.94}$$

$$r_{B_8B_9} = 0.002 \quad , \tag{3.95}$$

$$r_{B_8B_{10}} = -0.753 \quad , \tag{3.96}$$

$$r_{B_8B_{11}} = 0.609 \quad , \tag{3.97}$$

$$r_{B_9B_{10}} = -0.011 \quad , \tag{3.98}$$

$$r_{B_9B_{11}} = 0.006 \quad , \tag{3.99}$$

$$r_{B_{10}B_{11}} = -0.961 \quad . \tag{3.100}$$

All other correlation coefficients were assumed to be zero.

4. RESULTS AND DISCUSSION

The experimental results are presented in this chapter. Many of these results are shown in contour plots. These contour plots were generated using the Surface II graphics package [96] and incorporate the estimation and smoothing capabilities of this software.

4.1 Two-Dimensional Flow Measurements

Measurements in the two-dimensional turbulent boundary layer on the flat floor of the wind tunnel confirm the small nonuniformities in the flow field found by Menna [1]. A three-tube Conrad probe was used to indicate flow speed and yaw angle at nine spanwise positions 5.0 m downstream of the tunnel throat. The measured spanwise variations agree well with those found by Menna.

The remainder of this section is divided into three parts, including a presentation of the spanwise variations found in the wind tunnel, the effects of two models used in the least squares estimation of some of the boundary layer characteristics, and the effects of two types of least squares estimators for these same boundary layer characteristics.

4.1.1 Spanwise Variations

Dimensionless speed and yaw angle data at nine spanwise positions are tabulated in Appendix A. These data are also shown in Fig. 4.1 and Fig. 4.2. Figure 4.1 shows the velocity profiles in law-of-the-wall coordinates where:

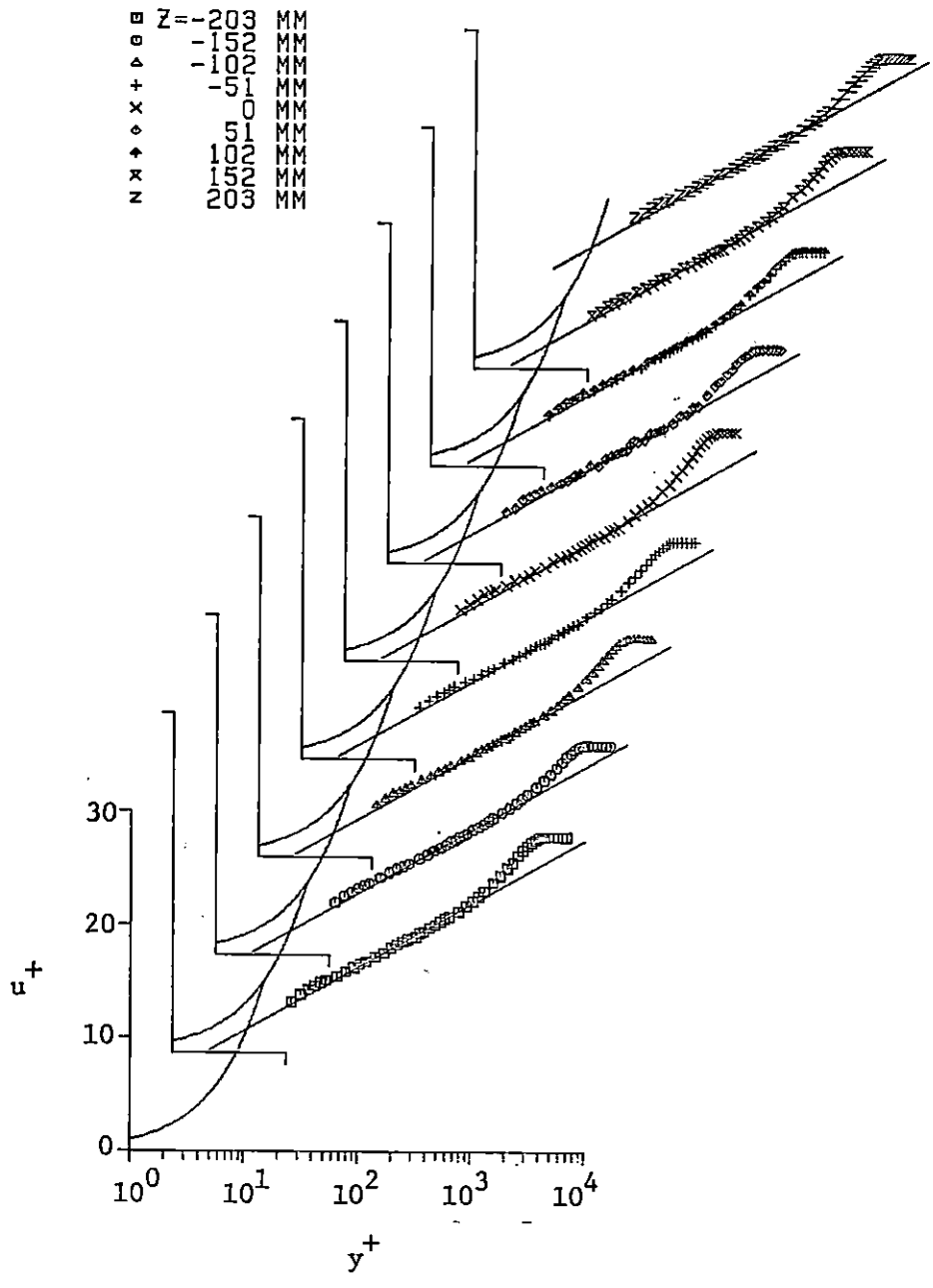

Fig. 4.1 Two-Dimensional Turbulent Boundary Layer Velocity Distributions

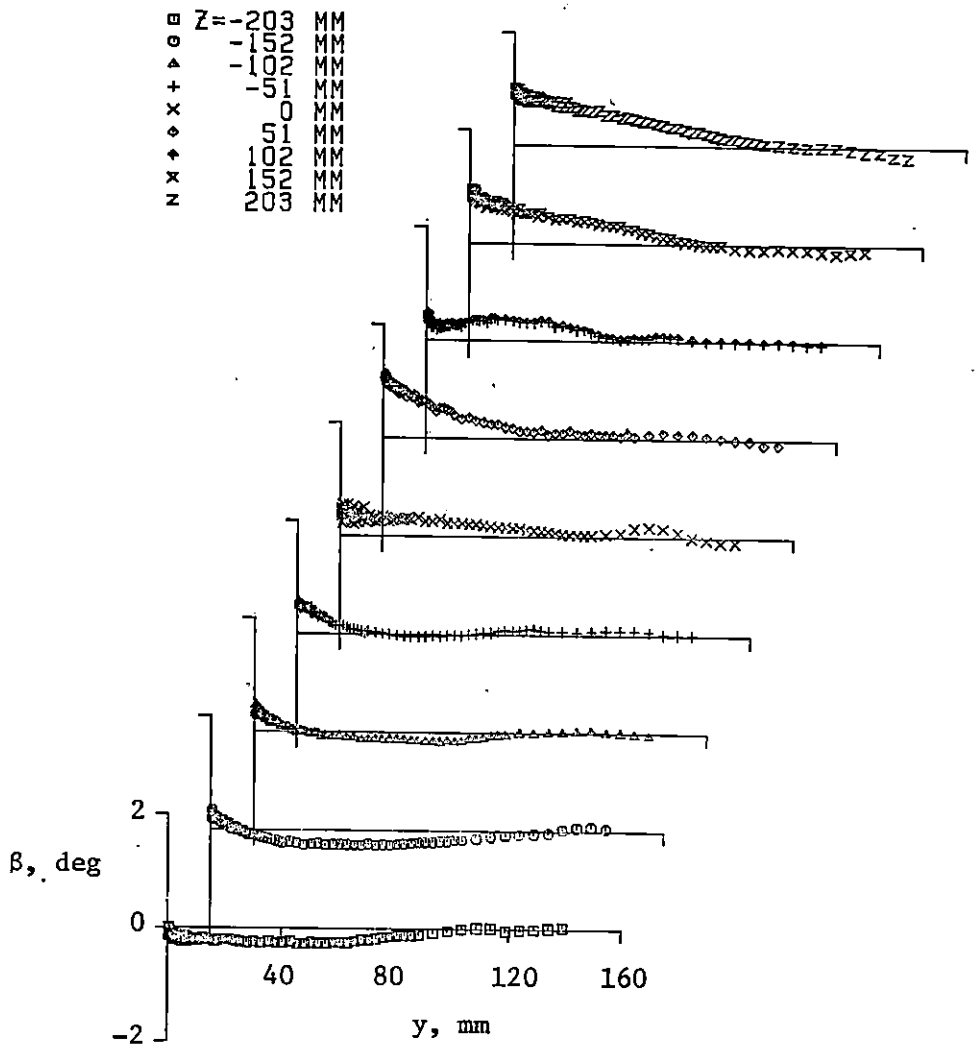

Fig. 4.2 Two-Dimensional Turbulent Boundary Layer Yaw Angle Distributions

$$y^+ = \frac{yu_\tau}{\nu} , \tag{4.1}$$

$$u^+ = \frac{U}{u_\tau} , \tag{4.2}$$

with the friction velocity, u_τ, inferred from the velocity data using the weighted least squares technique. The first data point in each distribution corresponds to the position where the probe tip was one tip diameter above the floor (measured from surface to tip center). The data in Fig. 4.1 appear well behaved with the small wake characteristic of turbulent boundary layer flows in the presence of a small negative pressure gradient, and follow the logarithmic line:

$$u^+ = \frac{1}{0.41} \ln (y^+) + 5 , \tag{4.3}$$

to a y^+ value of nearly 1000. The data outside the nominally two-dimensional turbulent boundary layer appear as constant u^+ points near the upper ends of the distributions. The yaw angle data in Fig. 4.2 shows a small amount of skewing in the flow with a maximum of 1.1°. The uncertainty estimates included in Appendix A for these yaw angle measurements range from nominally 0.8° near the wall to 0.2° near the freestream edge of the boundary layer. Based on these measurements and their estimated uncertainties, it is difficult to reject the hypothesis that the flow yaw angle in the floor boundary layer is zero. It is even more difficult to reject this hypothesis in light of the additional uncertainty associated with the possible effects of turbulence, the velocity gra-

dient, and the proximity of the probe to the wall.

Table 4.1 shows the boundary layer integral parameters and the three parameters estimated using the weighted least squares method. These parameters are also shown in Fig. 4.3 and Fig. 4.4 with the data reported by Menna [1]. There are two sources of variation evident in these results. One source of variation is due to the spanwise variation in a given parameter. The second source of variation is that due to experimental error at a given spanwise position. It is desirable to quantify these two sources of variation to determine if the measured spanwise variation in a given result is significant in light of the observed experimental error in that same result. An analysis of variance procedure, referred to by Walpole and Myers [77] as the one-way classification, was used to quantify these two sources of variation. Using this procedure, it was concluded that there is a statistically significant spanwise variation in the three boundary layer parameters, δ^*, θ, and C_f, and that the half-width of the 95 percent uncertainty intervals for these parameters are 0.85 mm, 0.63 mm, and 8.5 x 10^{-5}, respectively (based on seven pairs of 2 independent observations). These uncertainty intervals are shown in Fig. 4.3 and Fig. 4.4.

An interesting feature of the data shown in Fig. 4.3 and Fig. 4.4 is the anomalous behavior on the centerline. The data appears to indicate that a noticeable defect in momentum exists on the tunnel centerline. This streamwise defect appears in Fig. 4.5 where the dimensionless velocity distributions have been corrected for the spanwise average. The apparent momentum defect on the centerline corresponds to

Table 4.1 Spanwise Distributions of the Boundary Layer Parameters

z, mm	δ^*, mm	θ, mm	C_f x 1000	δ, mm	Π
-203	10.2	7.87	2.58	81.0	0.57
-152	9.47	7.42	2.69	83.6	0.46
-102	10.7	8.28	2.54	84.1	0.60
- 51	10.8	8.36	2.55	85.1	0.57
0	12.6	9.58	2.36	88.9	0.77
51	10.2	7.92	2.59	80.0	0.53
102	9.88	7.65	2.59	76.5	0.56
152	10.4	8.02	2.53	78.5	0.61
203	9.91	7.67	2.59	76.7	0.55

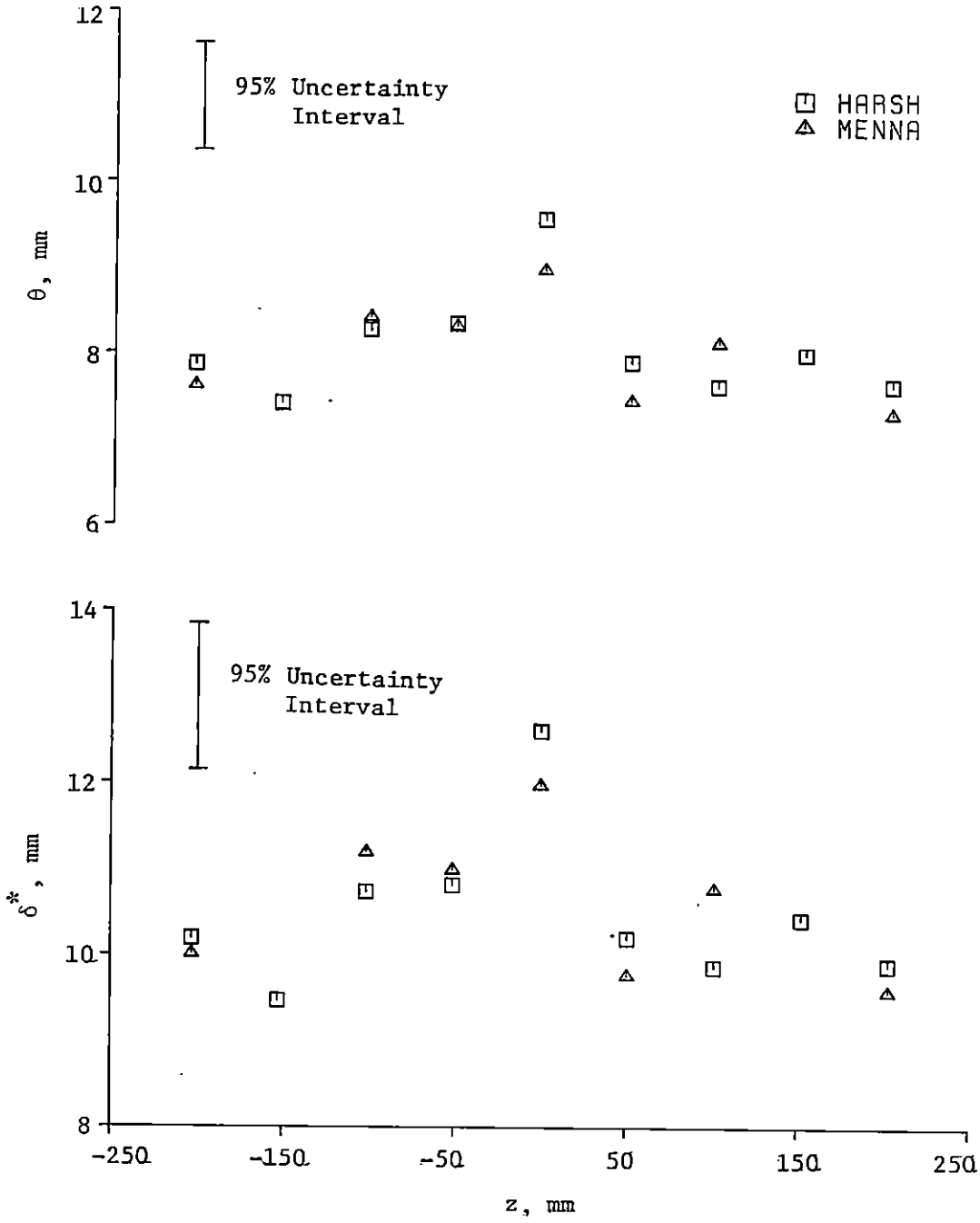

Fig. 4.3 Spanwise Distributions of the Two-Dimensional Boundary Layer Integral Parameters

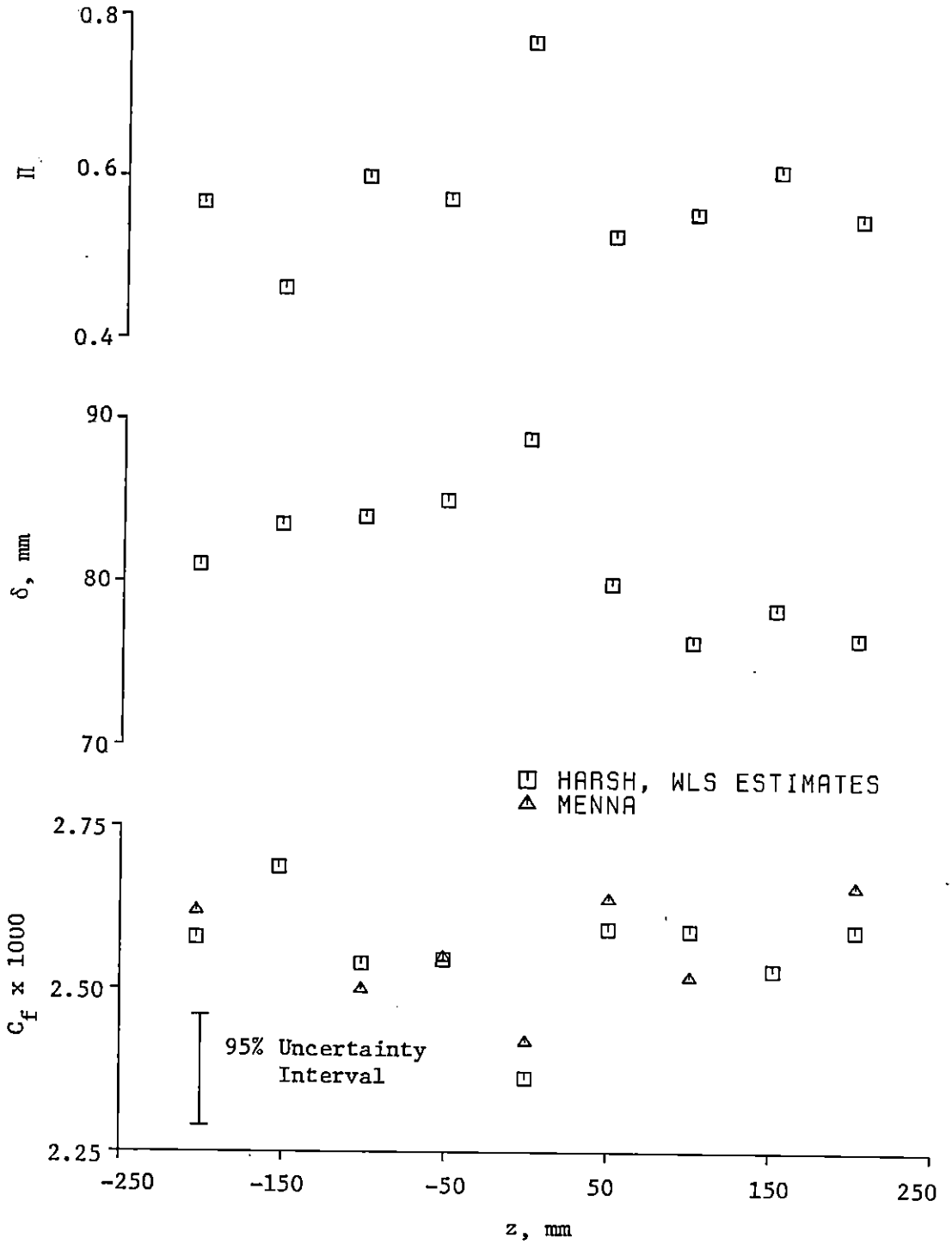

Fig. 4.4 Spanwise Distributions of the Two-Dimensional Boundary Layer Parameters Estimated by the Least Squares Method

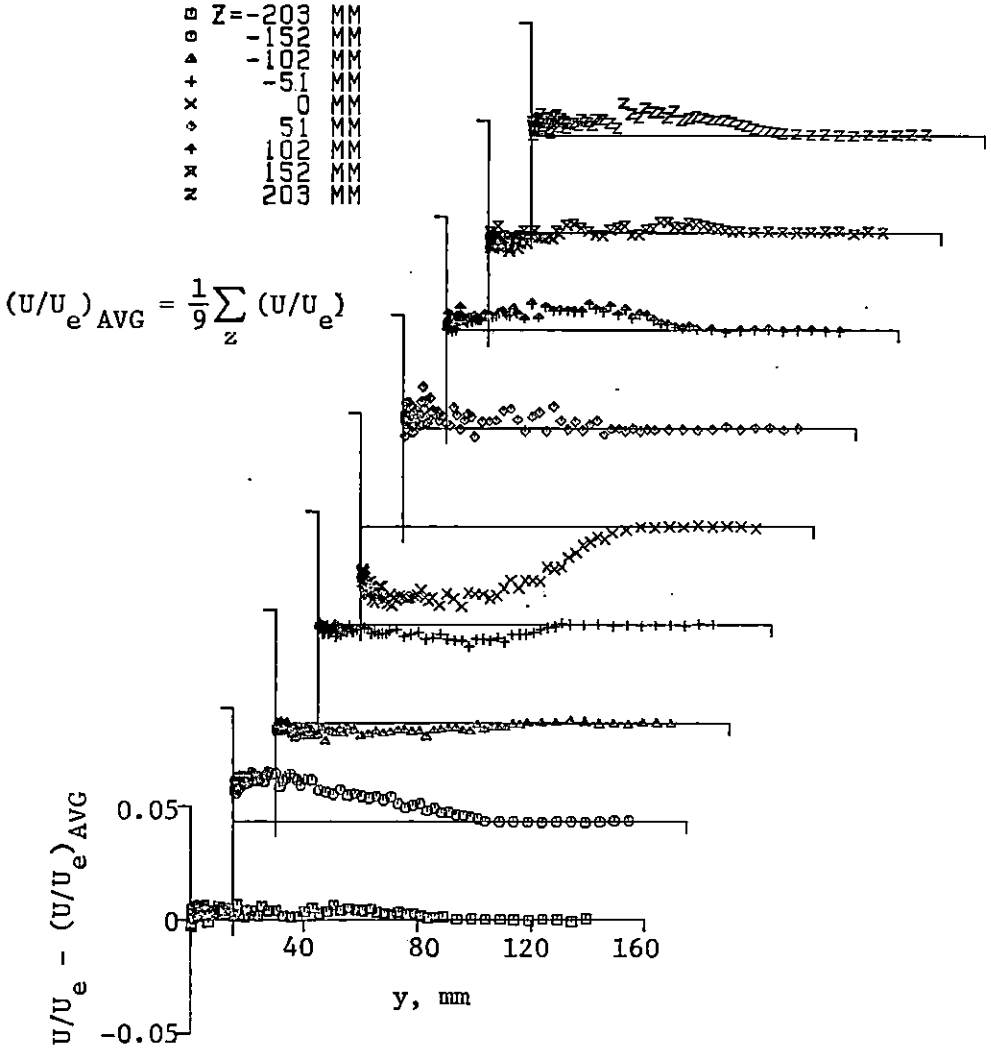

Fig. 4.5 Two-Dimensional Turbulent Boundary Layer Velocity Distributions Corrected for the Spanwise Average at Each Vertical Position

a velocity defect of less than 1 percent of the spanwise average at each vertical position. The cumulative effect of these small differences yields the anomalous behavior shown in Fig. 4.3 and Fig. 4.4.

Menna [1] discussed these spanwise nonuniformities. He noted that the spanwise variations are similar in magnitude with those reported by a number of other investigators and that the spanwise variations increased as the flow progressed to the test section. He cited the work by Fitts [97] who conducted a momentum integral study of this flow, and hypothesized that a small amount of flow convergency (3^{o} per meter in the spanwise direction) possibly resulting from the growth of tunnel side-wall boundary layers could explain the momentum defect on the centerline. There is not enough evidence here to reject Menna's hypothesis. Indeed, Fig. 4.2 lends some support to it by showing a small negative flow angle on the negative z side of the centerline and a small positive flow angle on the positive z side. The asymmetry about the centerline shown in Fig. 4.2 through Fig. 4.4 does not favor Menna's hypothesis.

Townsend [98] describes similar variations in the wall shear stress and attributes them to small spatial variations in the free stream caused by the instability of the flow through turbulence damping screens. He hypothesizes that these small spatial variations advance or retard the transition process in the boundary layer. This may be the case in this wind tunnel where a relatively long length of surface lies upstream of the 2.8 mm diameter trip rods in the throat.

4.1.2 Comparison of the Models Used for Estimating the Wall Shear Stress

Two models were used to estimate the wall shear stress using the method of least squares.

Model I

$$U_i = u_\tau\left[\frac{1}{\kappa}\ln\left(\frac{y_i u_\tau}{\nu}\right) + C\right] + \varepsilon_i \qquad (4.4)$$

Model II

$$U_i = u_\tau\left[\frac{1}{\kappa}\ln\left(\frac{y_i u_\tau}{\nu}\right) + C + \frac{2\Pi}{\kappa}\sin^2\left(\frac{\pi y_i}{2\delta}\right)\right] + \varepsilon_i \qquad (4.5)$$

In both models, κ and C were assumed to be known constants with values of 0.41 and 5, respectively. Model I was used to estimate u_τ only, related to the skin friction coefficient via:

$$C_f = 2\left(\frac{u_\tau}{U_e}\right)^2 , \qquad (4.6)$$

using data in the range:

$$0.71 \text{ mm} \leq y \leq 6.60 \text{ mm} , \qquad (4.7)$$

which corresponds approximately to:

$$35 \leq y^+ \leq 350 \ . \tag{4.8}$$

Model II was used to estimate u_τ, δ, and Π using data in the range:

$$0.71 \text{ mm} \leq y \leq 70.9 \text{ mm} \ , \tag{4.9}$$

which corresponds approximately to:

$$35 \leq y^+ \leq 3760 \ . \tag{4.10}$$

With the data in Appendix A, 34 data points were used with model I and 75 data points were used with model II.

Table 4.2 shows the least squares estimates using these models. The models can be compared with respect to their ability to estimate the wall shear stress and with respect to their ability to describe the data. One measure of performance of a model's ability to describe the data is the relative error, e/U_e, defined by:

$$\frac{e}{U_e} = \frac{1}{U_e} \sqrt{\frac{1}{n-p} \sum_i (r_i^2)} \ , \tag{4.11}$$

where n is the number of observations that were used in estimating the parameters, p is the number of estimated parameters, and r_i is the difference between the observed response (velocity) and the predicted response using the optimized parameters. For model I:

Table 4.2 Least Squares Estimates of the Boundary Layer Parameters

z,mm	Model I				Model II							
	e/U_e x 1000		C_f x 1000		e/U_e x 1000		C_f x 1000		δ, mm		Π	
	OLS	WLS	OLS	WLS	OLS	WLS	OLS	WLS	OLS	WLS	OLS	WLS
-203	7	7	2.62	2.61	7	7	2.59	2.58	86.1	81.0	0.58	0.57
-152	7	7	2.73	2.72	7	7	2.70	2.69	89.9	83.6	0.48	0.46
-102	7	7	2.59	2.58	7	7	2.55	2.54	89.9	84.1	0.63	0.60
- 51	7	7	2.59	2.58	7	7	2.56	2.55	90.7	85.1	0.60	0.57
0	8	8	2.40	2.40	7	7	2.38	2.36	94.5	88.9	0.81	0.77
51	9	9	2.63	2.62	8	8	2.61	2.59	85.1	80.0	0.54	0.53
102	7	7	2.63	2.63	7	7	2.60	2.59	79.8	76.5	0.56	0.56
152	7	7	2.57	2.56	6	6	2.54	2.53	81.3	78.5	0.62	0.61
203	7	7	2.64	2.63	7	7	2.60	2.59	80.3	76.7	0.56	0.55

OLS = ordinary least squares estimate, WLS = weighted least squares estimate

$$\left.\frac{e}{U_e}\right|_I = \frac{1}{U_e}\left(\frac{1}{33}\sum_{i=5}^{38}\left\{U_i - u_\tau\left[\frac{1}{\kappa}\ln\left(\frac{y_i u_\tau}{\nu}\right) + C\right]\right\}^2\right)^{1/2}, \quad (4.12)$$

and for model II:

$$\left.\frac{e}{U_e}\right|_{II} = \frac{1}{U_e}\left(\frac{1}{72}\sum_{i=5}^{79}\left\{U_i - u_\tau\left[\frac{1}{\kappa}\ln\left(\frac{y_i u_\tau}{\nu}\right) + C + \frac{2\Pi}{\kappa}\sin^2\left(\frac{\pi y_i}{2\delta}\right)\right]\right\}^2\right)^{1/2}. \quad (4.13)$$

It is important to recognize that the ordinary least squares parameter estimates are those values that minimize the relative error given by Eq. 4.12 and Eq. 4.13.

The model II least squares estimates for the skin friction coefficient are 1 percent to 2 percent lower than the model I results. This is the same trend observed by Coles [88].

Both models describe the data well. In no case is the relative error greater than nine parts per thousand (less than 1 percent) and is typically seven parts per thousand. Model II appears to describe the data as well as model I, but over a greater range in y. The residual errors (r_i) from both models at a representative spanwise position are shown in Fig. 4.6 and Fig. 4.7. Both figures show some structure remaining in the residuals after least squares optimization of the parameters. It is then reasonable to suspect that the estimated parameters are subject to specification bias--too high or too low because of a mis-specified model. There was no significant difference between the

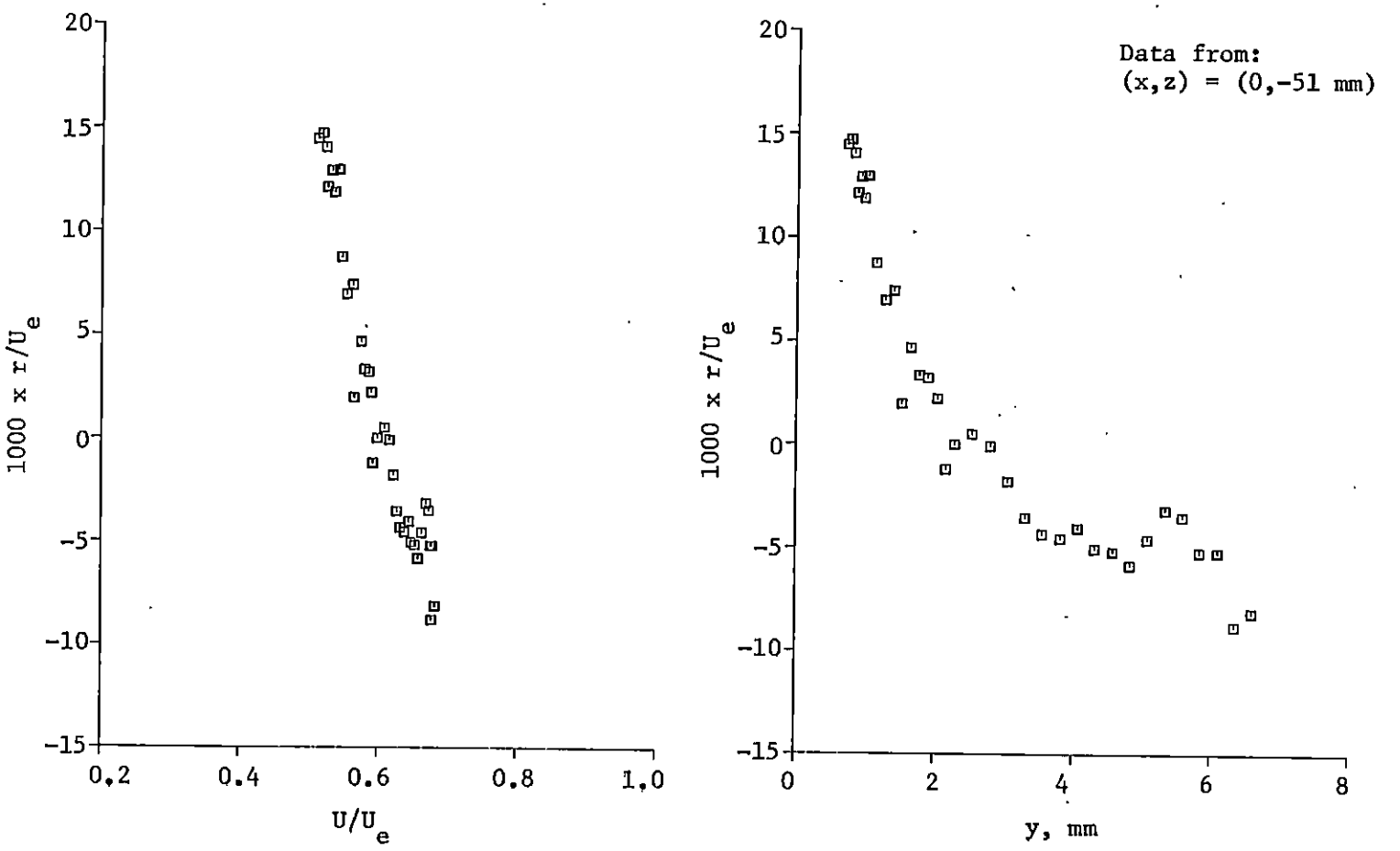

Fig. 4.6 Residual Errors after Weighted Least Squares Optimization Using Model I

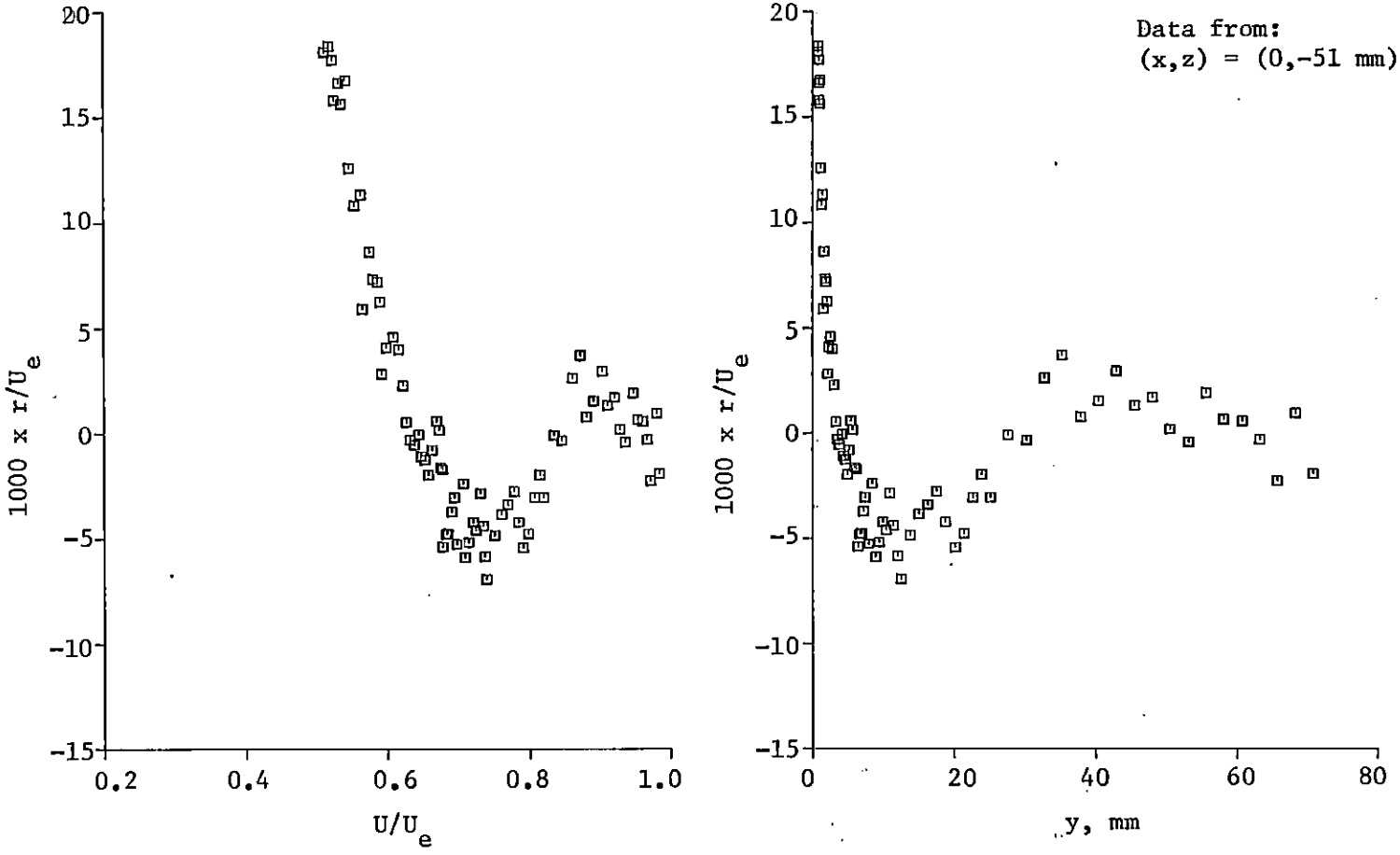

Fig. 4.7 Residual Errors after Weighted Least Squares Optimization Using Model II

residual error distributions resulting from ordinary least squares optimization and weighted least squares optimization of the parameters.

4.1.3 Comparison of Ordinary and Weighted Least Squares Estimates of the Parameters

Both ordinary least squares and weighted least squares estimates of the three boundary layer parameters, C_f, δ, and Π, were calculated. The weights for the weighted least squares estimates were equated to the inverse of the squared estimated uncertainties in the calculated velocities. For the uncertainty estimates in Appendix A, this weighting scheme places less emphasis on the low-velocity data near the wall and more emphasis on the higher-velocity data away from the wall.

The estimated characteristics are shown in Table 4.2. The skin friction coefficient appears to be insensitive to the weighting scheme with the weighted least squares estimates less than 1 percent smaller than the ordinary least squares estimates. The boundary layer thickness and the pressure gradient parameter are more sensitive to the weighting scheme. The weighted least squares estimates for the two parameters, δ and Π, are 6 percent and 3 percent smaller than the ordinary least squares estimates, respectively (based on the spanwise average of the nine weighted estimates).

4.2 Flow Visualization

The second part of the experimental program consisted of flow visualization studies. For these studies, the surface flows on the flat floor of the wind tunnel and on the vertical sides of the bluff body

were visualized using an oil-film technique. These studies were conducted at the standard test conditions described in Table 2.1. Based on the body diameter and the freestream speed at the test section without the body in place (5.0 m downstream of the tunnel throat), these standard conditions correspond to a body Reynolds number of 183,000.

The floor surface flow visualizations are shown in Fig. 4.8 through Fig. 4.10. Figure 4.8 shows all four quadrants of the floor plane (x-z) around the body. Qualitatively, the surface flow on this plane appears to be symmetric about the tunnel centerline. Figure 4.9 is an enlarged view of the floor, showing only the two quadrants over which the three-dimensional flow was measured. Figure 4.10 is a schematic of the photograph shown in Fig. 4.9, emphasizing the major features of the floor surface flow. Point A, 57 mm upstream of the leading edge, on the tunnel centerline, and difficult to locate in the photographs, is a singular separation point where the streamwise flow in the plane of symmetry meets with the reversed flow in the junction vortex. Emanating from point A are two rays, one on each side of the centerline and just as difficult to precisely locate as point A, corresponding to the loci of ordinary separation points around the junction. This line of ordinary separation divides the floor into an interior region and an exterior region. The interior region is not accessible to any limiting streamlines originating far upstream of the junction. Just downstream of point A and 38 mm upstream of the leading edge, a distinct line crosses the tunnel centerline in a near circular arc. Other investigators [5,9,13,14] have reported that this distinct line corresponds to the

Fig. 4.8 Surface Flow Visualization on the Flat Floor of the Wind Tunnel

Fig. 4.9 Enlarged View of the Surface Flow Visualization on the Flat Floor of the Wind Tunnel

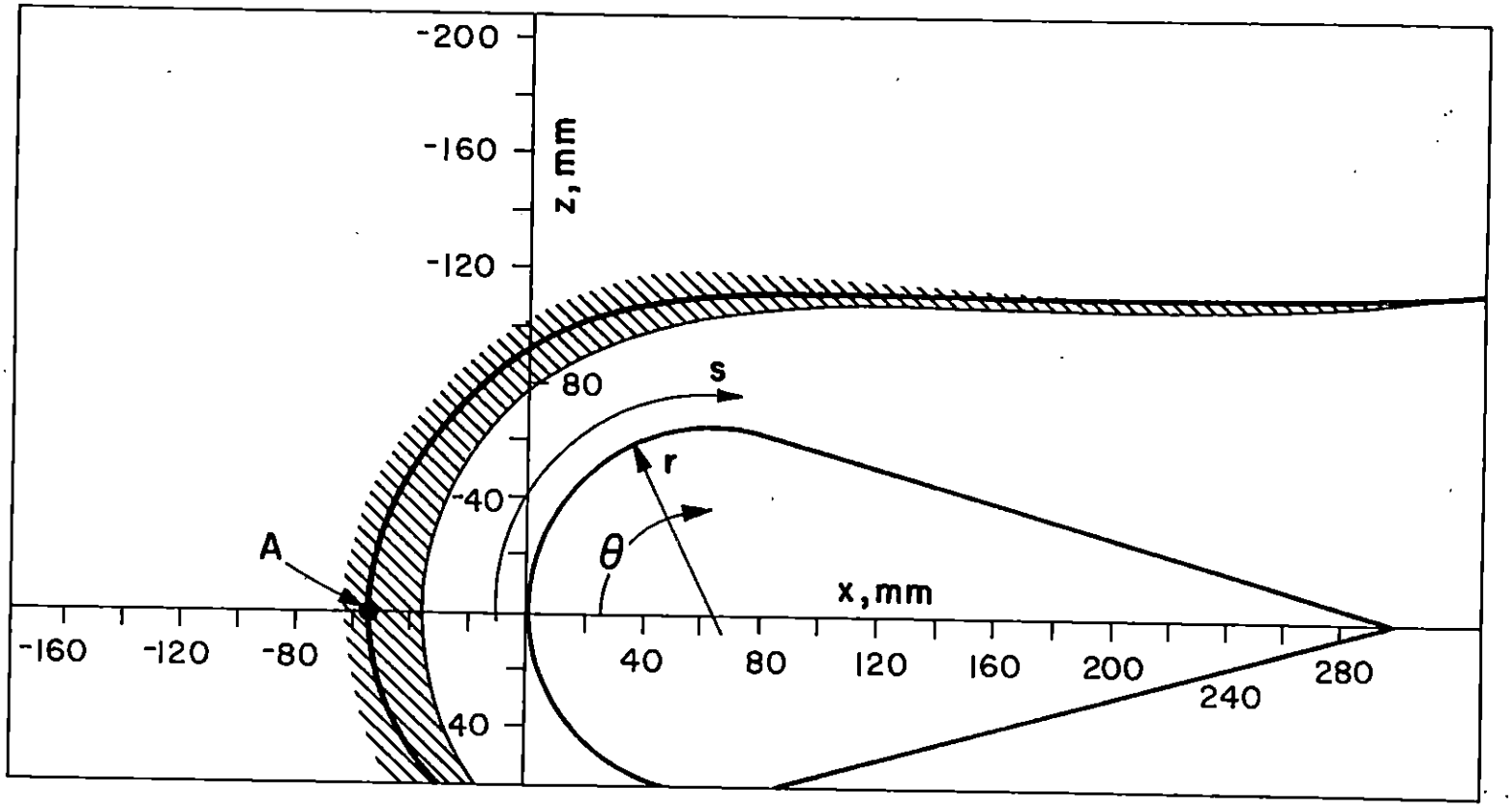

Fig. 4.10 Schematic Diagram of the Surface Flow Visualization on the Flat Floor of the Wind Tunnel

projection of the vortex center on the flat floor. Surface pressure measurements described in a subsequent section indicate that this line corresponds to a relative minimum in the wall pressure distribution. During the flow visualization studies it was observed that the portion of the floor between this distinct line and the body dried much more rapidly than the floor in the exterior region. The inference to be made from this observation is that the highest wall shear stresses on the floor occur in the interior region near the leading edge of the body. The lowest wall shear stress on the floor should occur at the singular separation point. The accumulation of white titanium dioxide particles in the vicinity of the singular separation point is a result of the low wall shear stresses and pressure gradients in the area. These hypotheses about the wall shear stress distribution on the floor are supported by direct-force wall shear measurements performed by McAllister [99].

The developed surface corresponding to the vertical sides of the bluff body is shown in Fig. 4.11 through Fig. 4.13. Figure 4.11 shows the entire developed surface with the attachment (stagnation) line in the center of the photograph. Qualitatively, this figure shows that the surface flow is the same on both sides of the body. Figure 4.12 is an enlarged view of the developed surface in the corner where the three-dimensional flow was measured. Figure 4.13 is a schematic of this later photograph, emphasizing the major features of the body-surface flow visualization. Three horizontal scales are shown in Fig. 4.13, one for the cylinder angle defined in Fig. 4.10, one for the distance along the

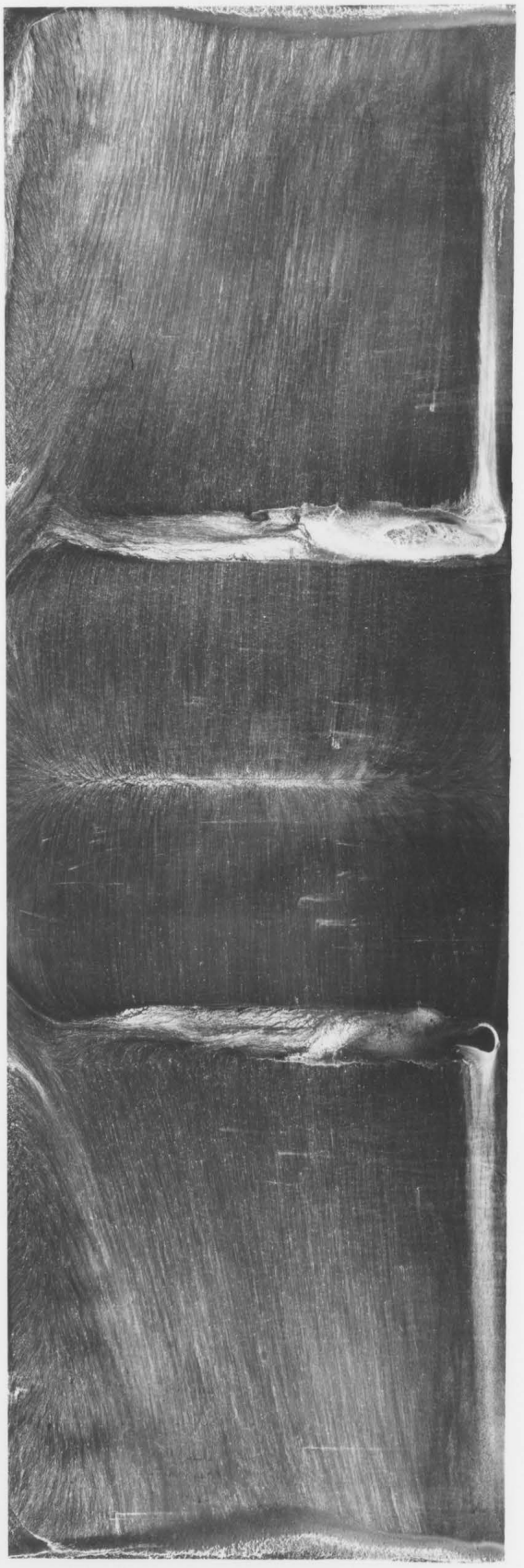

Fig. 4.11 Surface Flow Visualization on the Sides of the Bluff Body

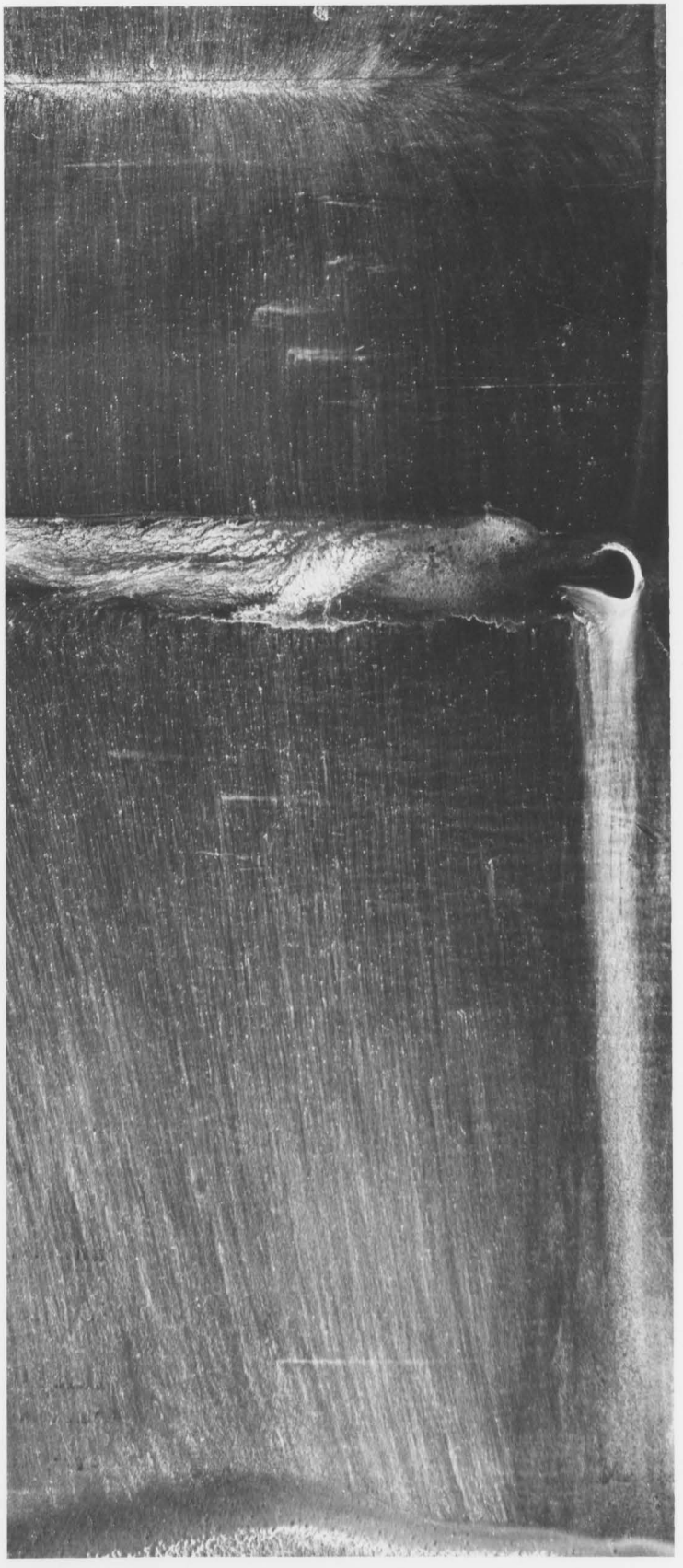

Fig. 4.12 Enlarged View of the Surface Flow Visualization on One Side of the Bluff Body

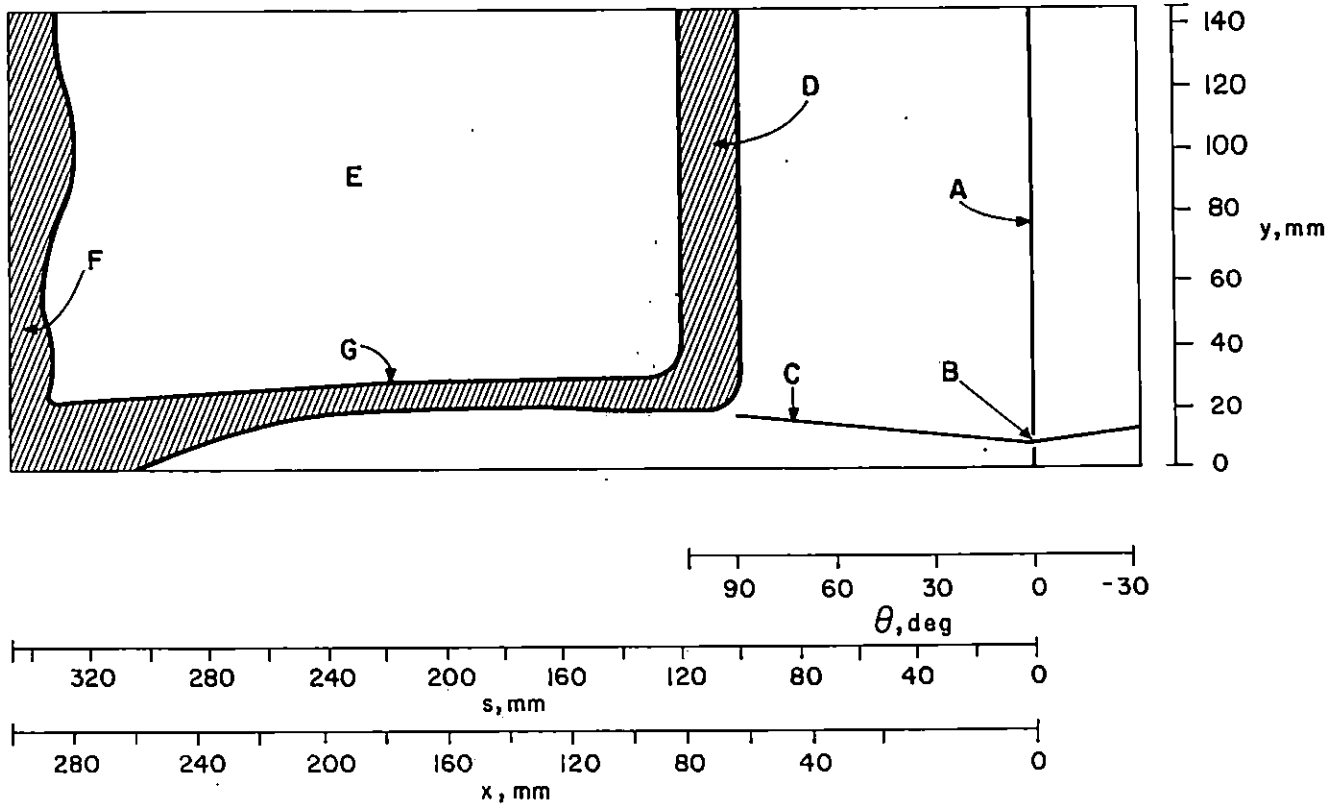

Fig. 4.13 Schematic Diagram of the Surface Flow Visualization on the Side of the Bluff Body

developed surface also shown in Fig. 4.10, and one nonlinear scale showing the streamwise distance. The leading edge attachment line is shown coincident with the origins of these axes. The total pressure gradient near the leading edge produces the downwash on the surface near the leading edge junction with the floor. This downwash meets with a small region of reversed flow at the singular separation point marked B. The ordinary separation line marked C divides the boundary layer like flow on the leading edge from a small junction vortex deep in the corner. The area marked D, beginning at approximately 90^{o} from the attachment line and extending for about 20 mm on the surface, is believed to be a laminar separation bubble. Early in the flow visualization process, a large amount of titanium dioxide-diesel fuel paint accumulated in this region and slowly sank to the floor under its own weight. Near the floor, the excess mixture exited the bubble and streamed back along the straight side of the body in the region marked G. A turbulent boundary layer reattached to the body surface downstream of the bubble and appears to have flowed markedly downward on the surface. This turbulent boundary layer was not able to overcome the adverse pressure gradient on the rearward portion of the body and separated near the trailing edge leaving the stalled region marked F.

A two-dimensional boundary layer analysis was performed for the idealized boundary layer flow over the sides of the bluff body. The Pohlhausen-Holstein-Bohlen, laminar, one-parameter integral method [100] and Moses' turbulent, two-parameter integral method [101] were used to perform the analysis. The freestream edge condition for these calcula-

tions was the surface pressure distribution resulting from a two-dimensional potential flow solution for the bluff body geometry. The laminar calculation was started at the stagnation point. Transition was assumed to occur at 85^{o} from the stagnation point. The calculation was continued from this point using Moses' turbulent integral method. The initial conditions required by Moses' calculation were obtained by equating the laminar momentum thickness to the turbulent momentum thickness at the point of transition and, somewhat arbitrarily, increasing the skin friction coefficient by a factor of two. This later assumption had little effect on the turbulent boundary layer calculations after a few millimeters downstream of the transition point. In fact, the skin friction coefficient was systematically varied from 95 percent to 300 percent of the laminar prediction at the transition point, and it was observed that the solutions converged to within 2 percent just 10 mm ($\approx 10^{0}$) downstream of the initial condition.

The predicted boundary layer parameters are shown in Fig. 4.14. The abscissa in this figure is distance measured along the surface of the body, as shown in Fig. 4.10. These results indicate separation of the thick turbulent boundary layer from the flat sides of the body 314 mm from the leading edge (90 percent chord), in fair agreement with the results of the flow visualization study.

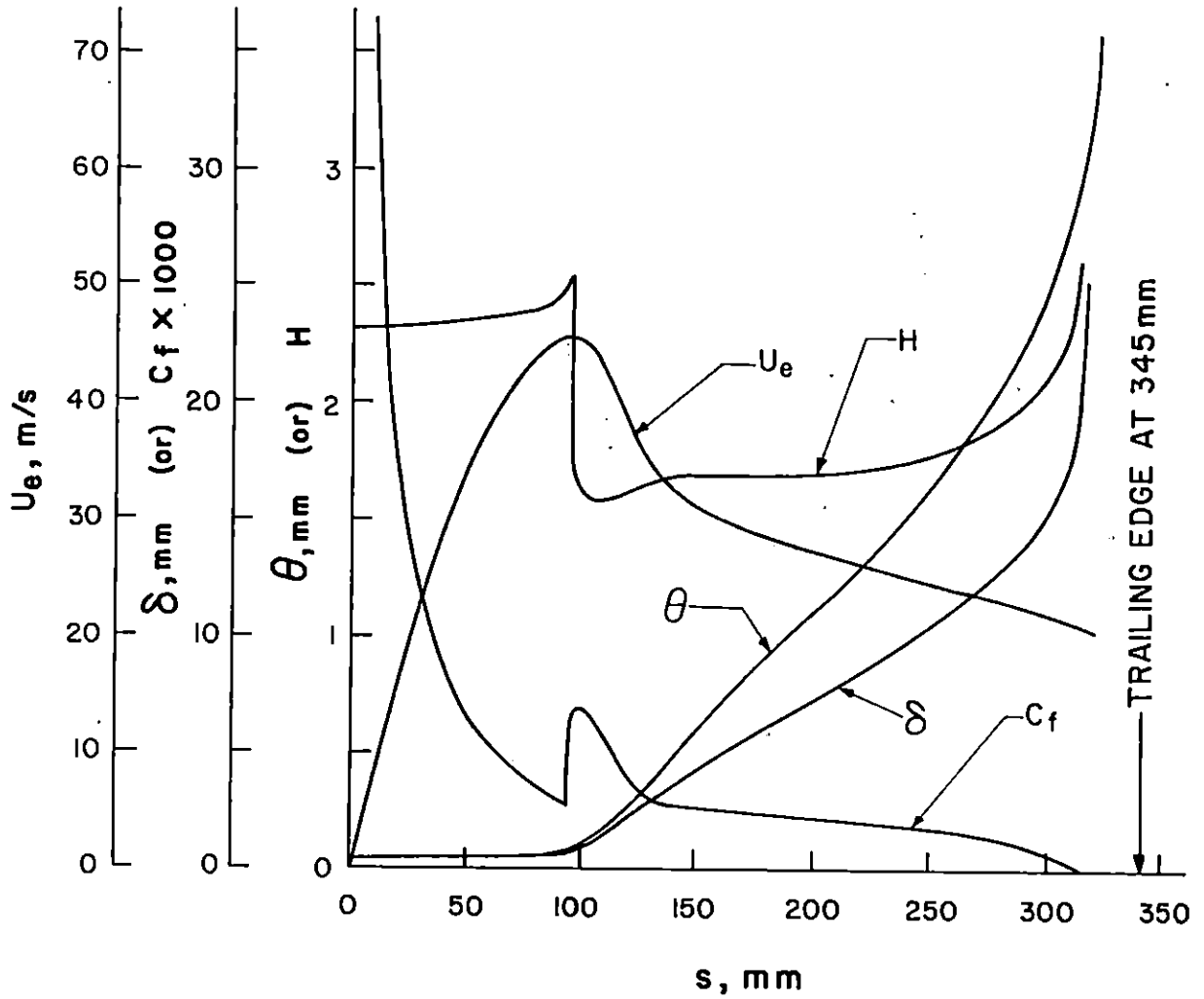

Fig. 4.14 Predicted Two-Dimensional Boundary Layer Parameters

4.3 Surface Pressure Measurements

Following the flow visualization studies, the pressure distributions on the flat floor near the leading edge and on the vertical side of the body were measured. These measurements are reported in Appendix B in terms of a pressure coefficient defined by:

$$C_P = \frac{P - P_{T,*}}{Q_*} \quad . \tag{4.14}$$

The measured pressure distribution on the floor near the leading edge of the body is shown in Fig. 4.15. The theoretical pressure distribution resulting from a potential flow analysis of the two-dimensional flow around a similar streamlined cylinder is shown in Fig. 4.16. Two notable differences between these figures are a result of the three-dimensional nature of the junction vortex. These three-dimensional effects are the relative maximum on the line of symmetry 60 mm upstream of the stagnation point and the locus of relative minima crossing the line of symmetry in a near circular arc 38 mm upstream of the stagnation point. These extreme points coincide with the singular separation point and the distinct line bounding the relatively high wall shear stress area shown in Fig. 4.8 through Fig. 4.10.

The pressure distribution on the surface of the body, plotted in s-y coordinates so that it corresponds to the developed surface, is shown in Fig. 4.17. The isobars shown are nearly one-dimensional over a large portion of the body surface. Near the point of maximum body thickness (90^o from the stagnation line or 100 mm downstream of the stagnation

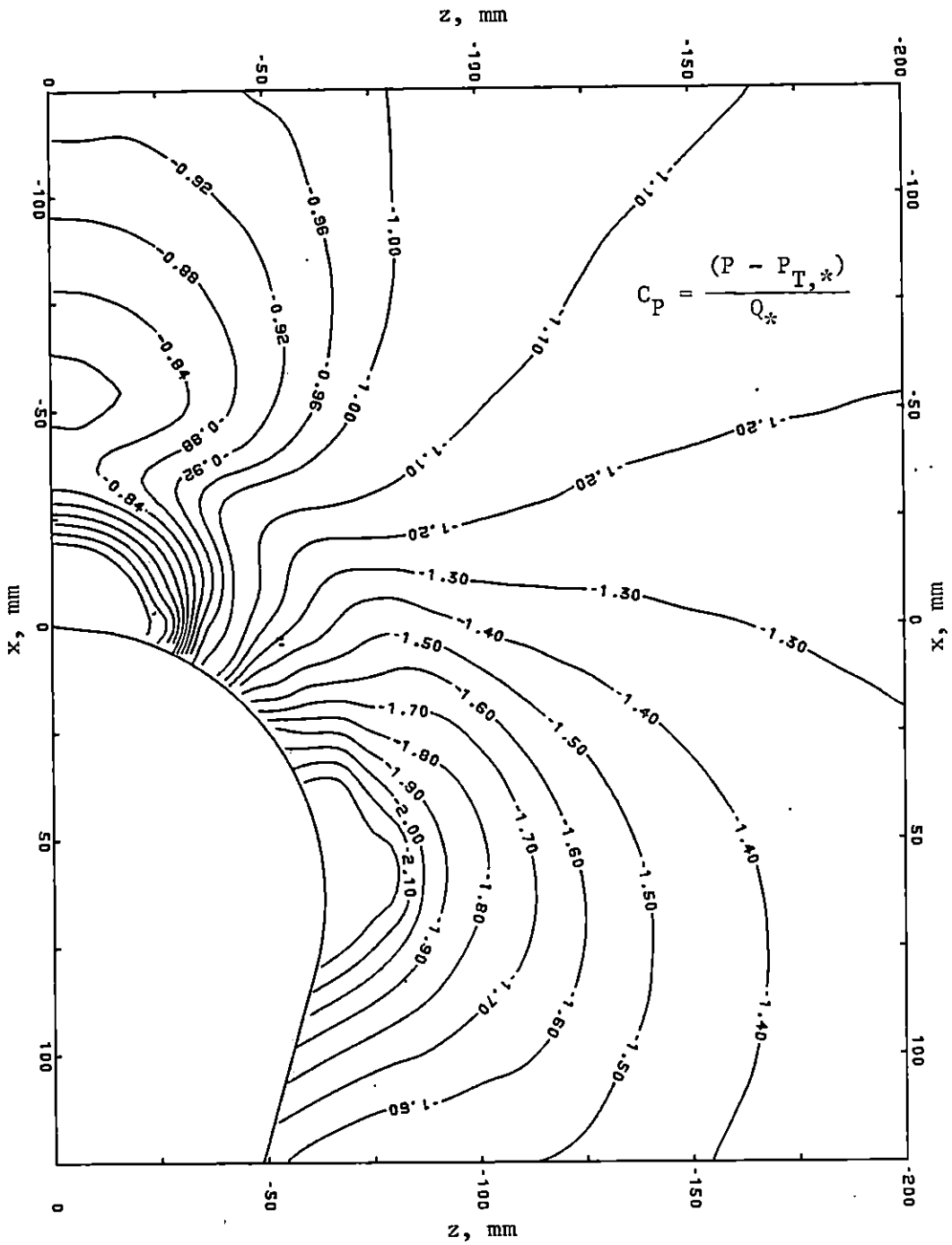

Fig. 4.15 Measured Pressure Distribution on the Flat Floor Near the Leading Edge of the Bluff Body

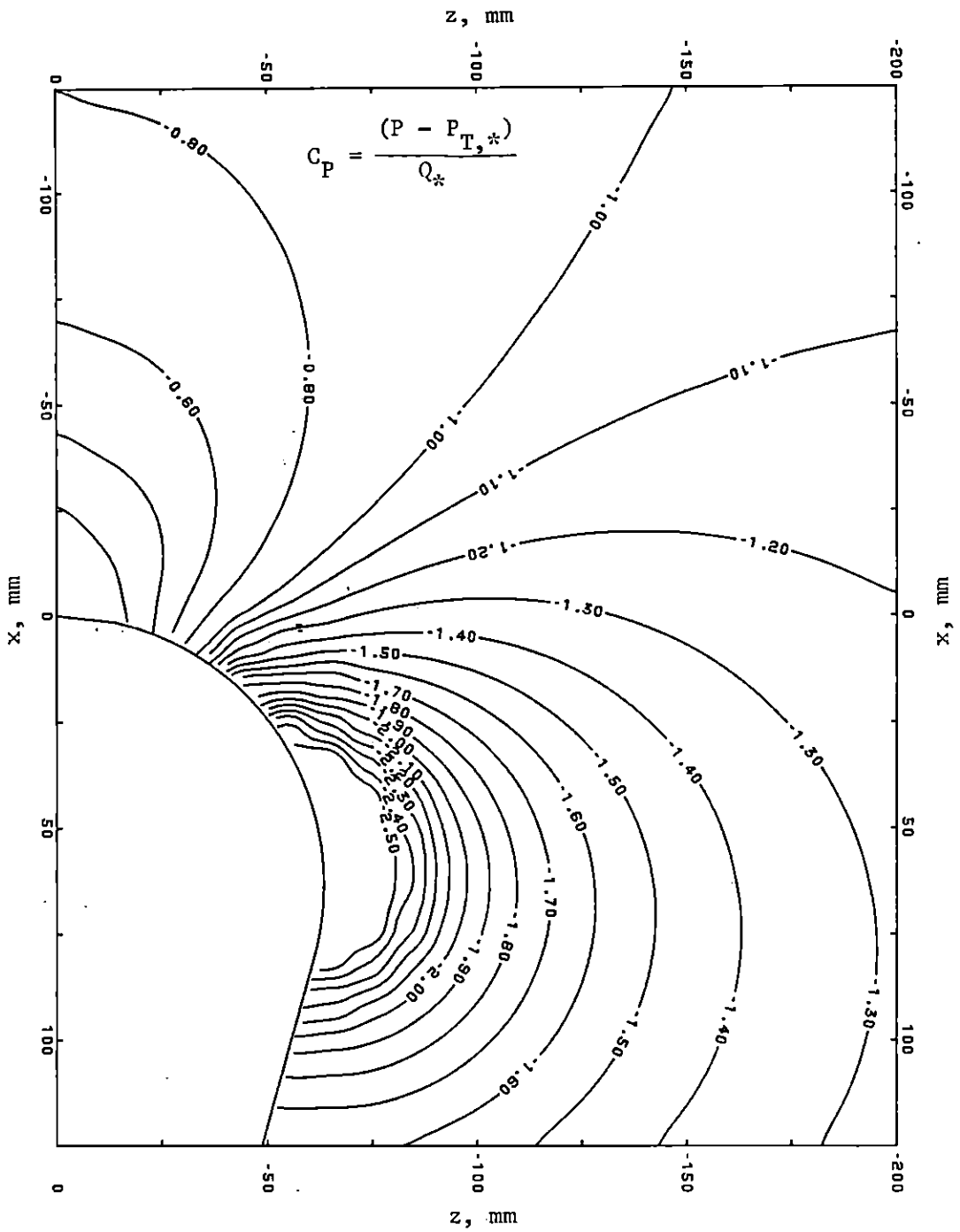

Fig. 4.16 Theoretical, Inviscid Pressure Distribution Near the Leading Edge of a Streamlined Cylinder

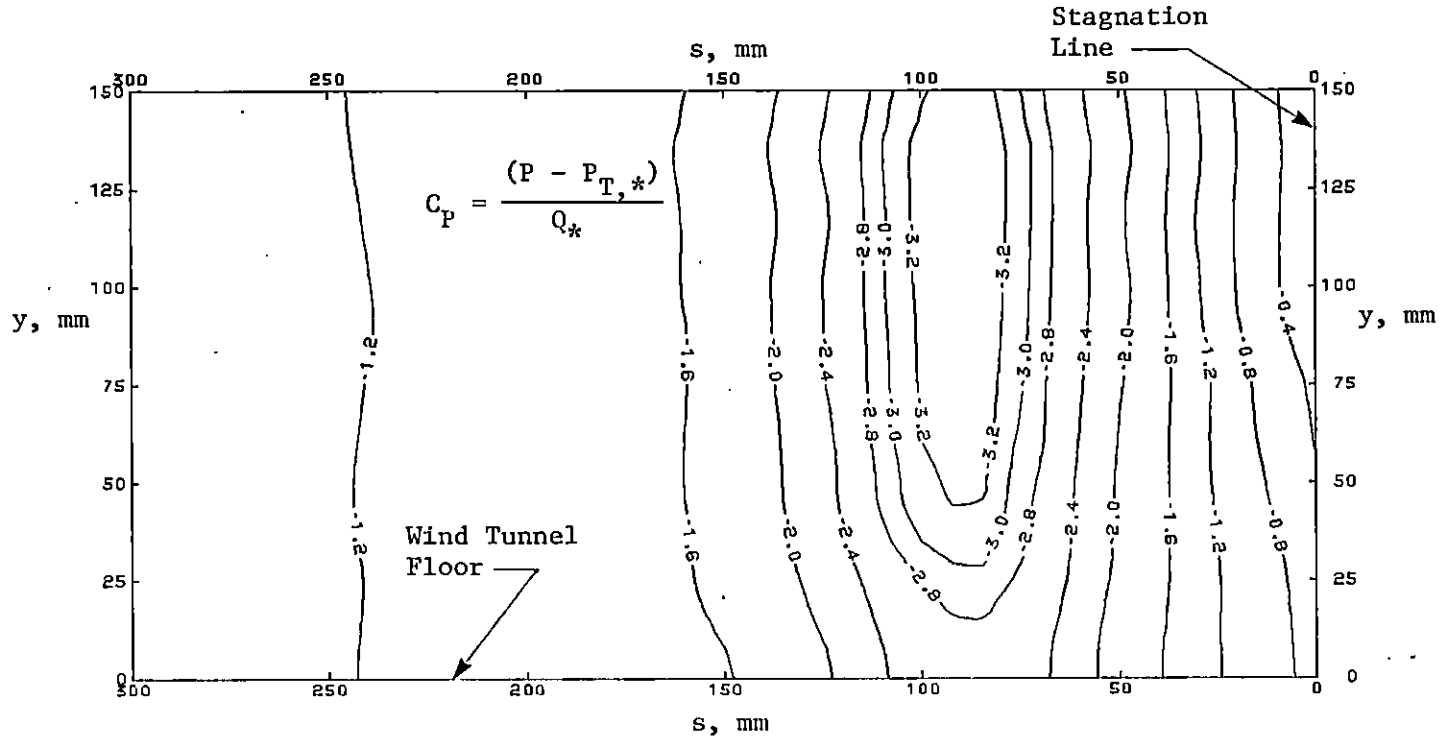

Fig. 4.17 Measured Pressure Distribution on the Vertical Side of the Bluff Body

line measured along the surface), the isobars are strongly two-dimensional in the body-floor junction region and indicate that the surface pressure increases in the negative y direction.

Some additional surface pressure measurements were made to assess the flow symmetry. Three rows of pressure taps were added for this purpose, two in the floor and one in the body. All of these taps were symmetrically disposed from taps on the opposite side of the tunnel centerline. The results are shown in Fig. 4.18 and Fig. 4.19. Each of these figures shows the results from two tests, reflecting sources of variation due to body positioning, body geometry, and repeatability of the experimental environment. In the legends of these figures, Body 1 rerers to the solid wood body used by Menna [1] and in all other phases of this experimental study. Body 2 and Body 3 refer to cast, polyester resin bodies made specifically for the body surface pressure measurements and described in Section 3.3. The significant difference in these bodies was their surface roughness. The wood body exhibited a somewhat uniform roughness as a result of the wood grain. The polyester resin bodies were smooth. In an attempt to make these bodies aerodynamically similar, 0.25 mm diameter trip wires were added to the polyester resin bodies 85° from the stagnation line.

The differences shown in the floor pressure coefficient data are at most 4 percent of the average at a given position. Similar differences are shown in the body surface pressure data except over the circular leading edge where the pressure coefficient is consistently larger on the righthand side of the body. A small positive flow yaw angle on the

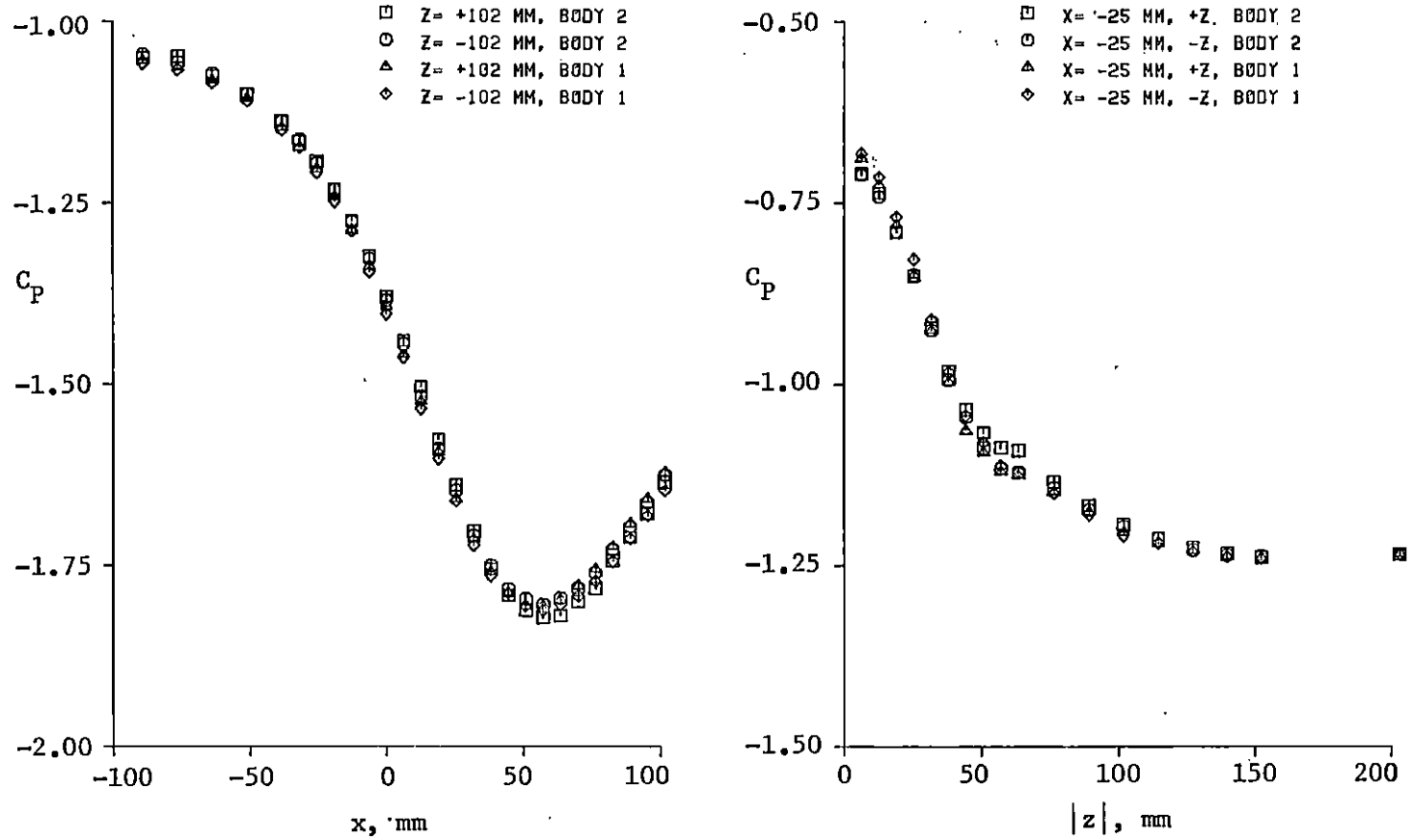

Fig. 4.18 Measured Pressure Distributions on the Flat Floor Showing the Symmetry of the Flow

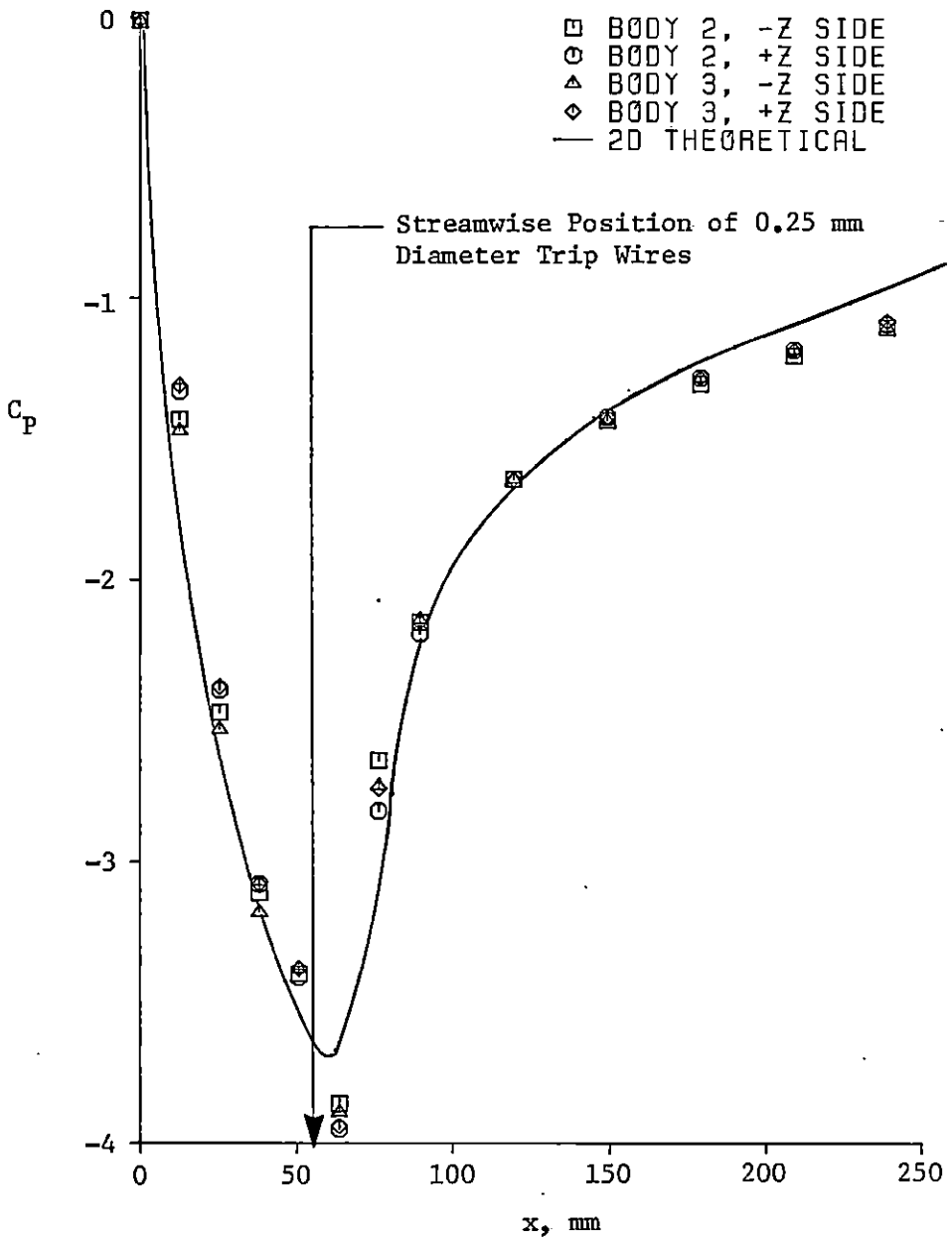

Fig. 4.19 Measured Pressure Distributions on the Vertical Sides of the Body Showing the Symmetry of the Flow

tunnel centerline, such as that shown near the free stream in Fig. 4.2, could cause this consistent difference. The two-dimensional boundary layer on the flat floor was measured at three additional positions along the centerline to verify that the small positive yaw angle shown in Fig. 4.2 was a significant feature of the flow. The three-tube Conrad probe described in Section 3.1.1 was used for these measurements. The yaw angle distributions are shown in Fig. 4.20. These results show that there was a positive yaw angle, less than 0.5^{o}, near the vertical position of the pressure taps used for the symmetry check.

4.4 Kiel Probe Measurements

Part four of the experimental investigation consisted of total pressure measurements using a miniature Kiel probe. The purpose of this part of the program was twofold. The primary objective was to obtain some preliminary, relatively inexpensive (in terms of test time) information about the three-dimensional flow field. The miniature Kiel probe proved to be ideal for this purpose since it was small, insensitive to the unknown flow angle, and required that only two pressure differences be observed at each probe position to determine the total pressure coefficient,

$$C_{P,T} = \frac{P_K - P_{T,*}}{Q_*} \quad . \tag{4.15}$$

The secondary objective was to acquire some independent data to verify the five-hole probe measurements to be performed later. These measure-

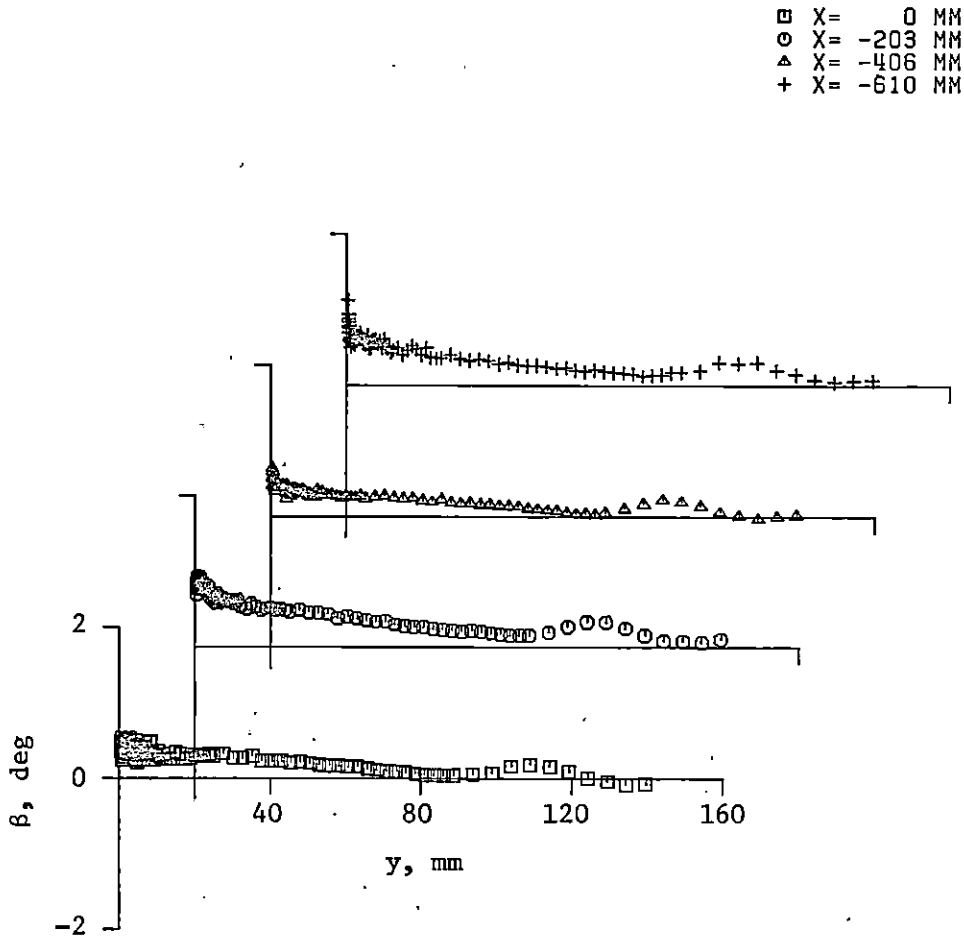

Fig. 4.20 Yaw Angle Distributions in the Two-Dimensional Turbulent Boundary Layer on the Wind Tunnel Centerline

ments were made in two planes as shown in Fig. 3.9. These data are included in Appendix C.

The total pressure distribution in the plane normal to the streamwise direction at 43 percent chord is shown in Fig. 4.21. This contour plot was constructed from 1378 data points. The data point nearest to the floor at each spanwise position corresponds to the position where the Kiel probe was lying on the floor. The center of a large total pressure defect is shown at approximately 125 mm from the centerline and 10 mm above the floor. This total pressure defect will be identified with the center of the junction vortex in the next section. The total pressure contours also indicate that high total pressure fluid fills the corner between the flat floor and the vertical side of the body.

The plane of symmetry data is shown in Fig. 4.22. This contour plot was constructed from 1944 data points where, as in the previous figure, the first data point at each streamwise position corresponds to the position where the Kiel probe was lying on the floor. In this case, the data near the floor and deep in the corner between the floor and the leading edge were acquired by maximizing the Kiel probe response with respect to yaw orientation. Figure 4.23 shows a small corner of the plane of symmetry, 25 mm high and 80 mm long, at the junction between the leading edge of the body and the flat floor. The arrowheads in this figure indicate the streamwise flow direction obtained by maximizing the Kiel probe response with respect to yaw orientation. The region of flow reversal obtained in this fashion is shown to extend no further than 60 mm upstream of the leading edge and 10 mm above the flat floor. Some of

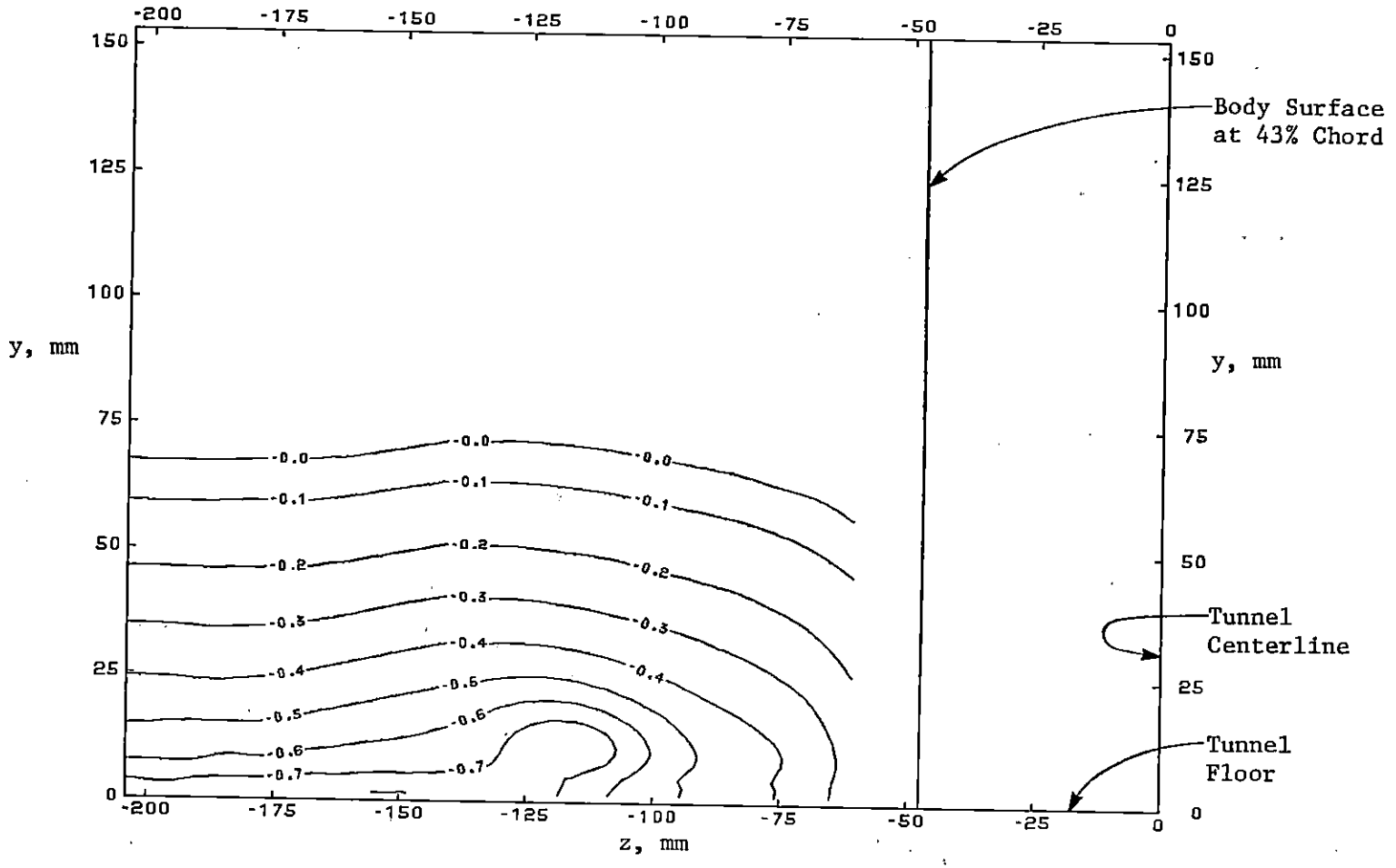

Fig. 4.21 Measured Total Pressure Distribution from Kiel Probe Surveys at 43 Percent Chord

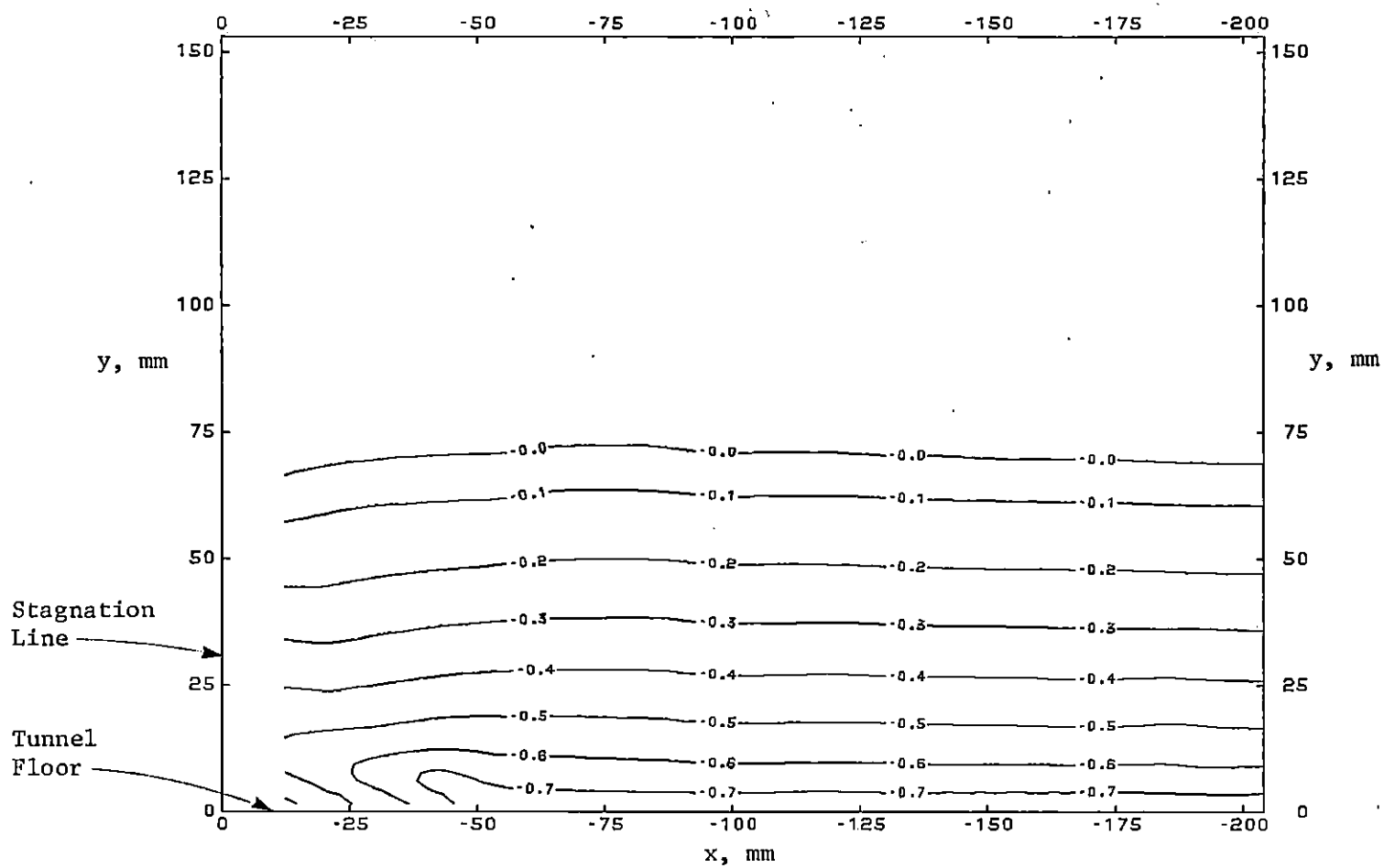

Fig. 4.22 Measured Total Pressure Distribution from Kiel Probe Surveys on the Plane of Symmetry

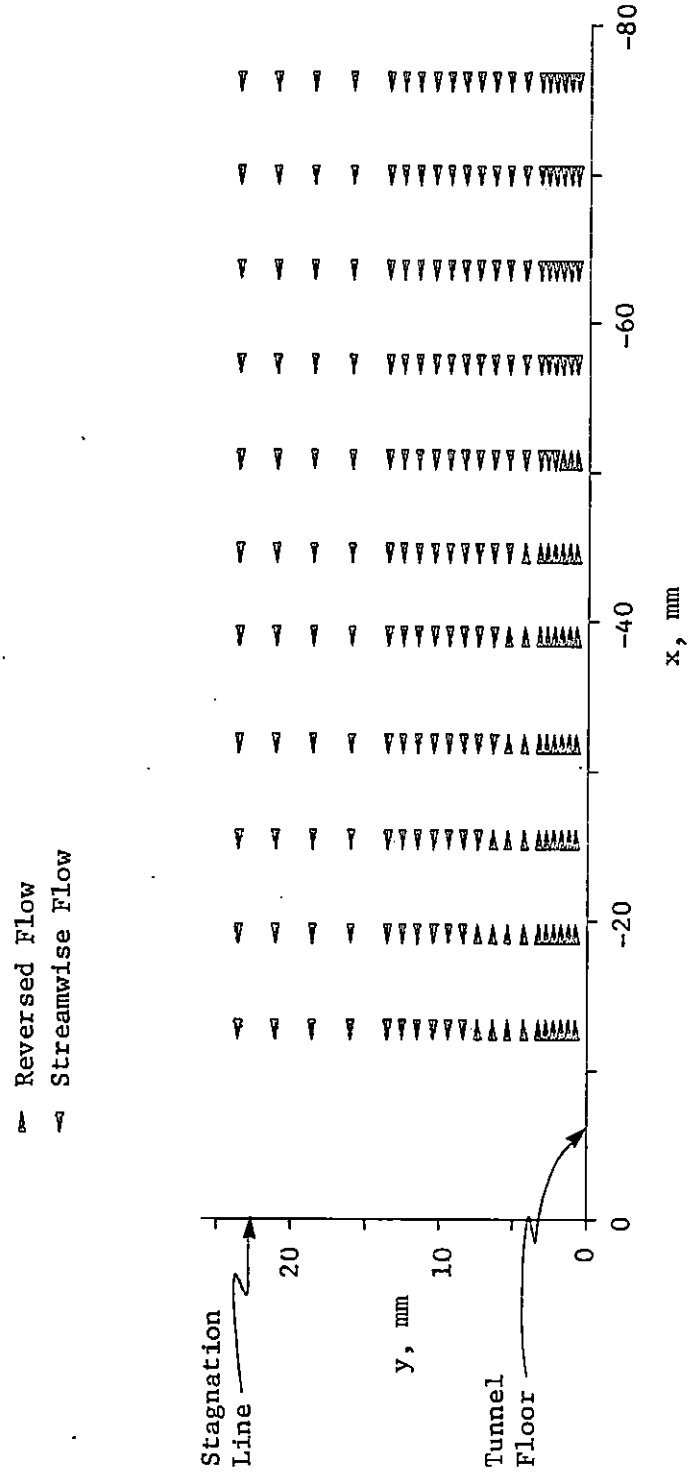

Fig. 4.23 Measured Streamwise Flow Direction Obtained by Maximizing the Kiel Probe Response on the Plane of Symmetry

the total pressure data deep in this corner may be biased low because of the Kiel probe sensitivity at pitch angles greater than 30^{o}.

4.5 Five-Hole Probe Measurements

The final phase of the experimental program consisted of three-dimensional flow measurements using a five-hole pressure probe. The flow was surveyed in three planes as shown in Fig. 3.10. The five-hole probe yielded the three-dimensional velocity field, the total pressure field, and the static pressure field in these planes. Five x-z positions, coincident with positions considered by Menna [1], were investigated to ensure consistency between this study and Menna's. In addition to the comparisons with Menna's data, a comparison was made between the three-tube Conrad probe and the five-hole probe. The remainder of this section describes these results. The five-hole probe data is included in Appendix D.

4.5.1 The Three-Dimensional Flow Field

The three-dimensional velocity distributions in the planes at 100 percent chord and at 43 percent chord are shown in Fig. 4.24 through Fig. 4.27. Figure 4.24 and Fig. 4.26 are identically scaled and show the y-z, or secondary component of the mean velocity vector.

A number of observations are worthy of recognition. These figures show only one vortex. Other vortices may be present but were not resolved by the data grid. Figure 4.25 and Fig. 4.27 show that the vortex consists of low streamwise momentum fluid. The corner between the flat

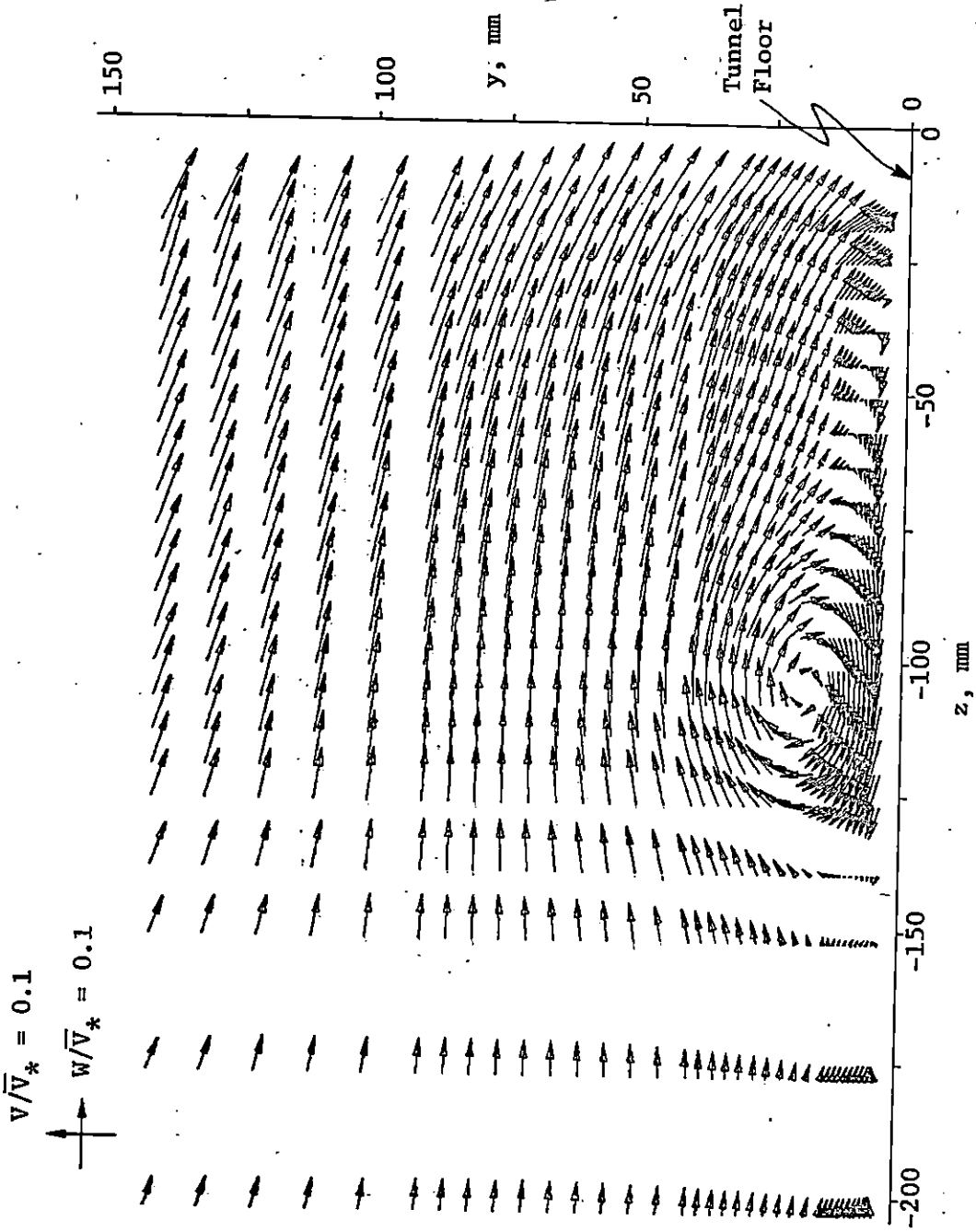

Fig. 4.24 Secondary Velocity Distribution at 100 Percent Chord

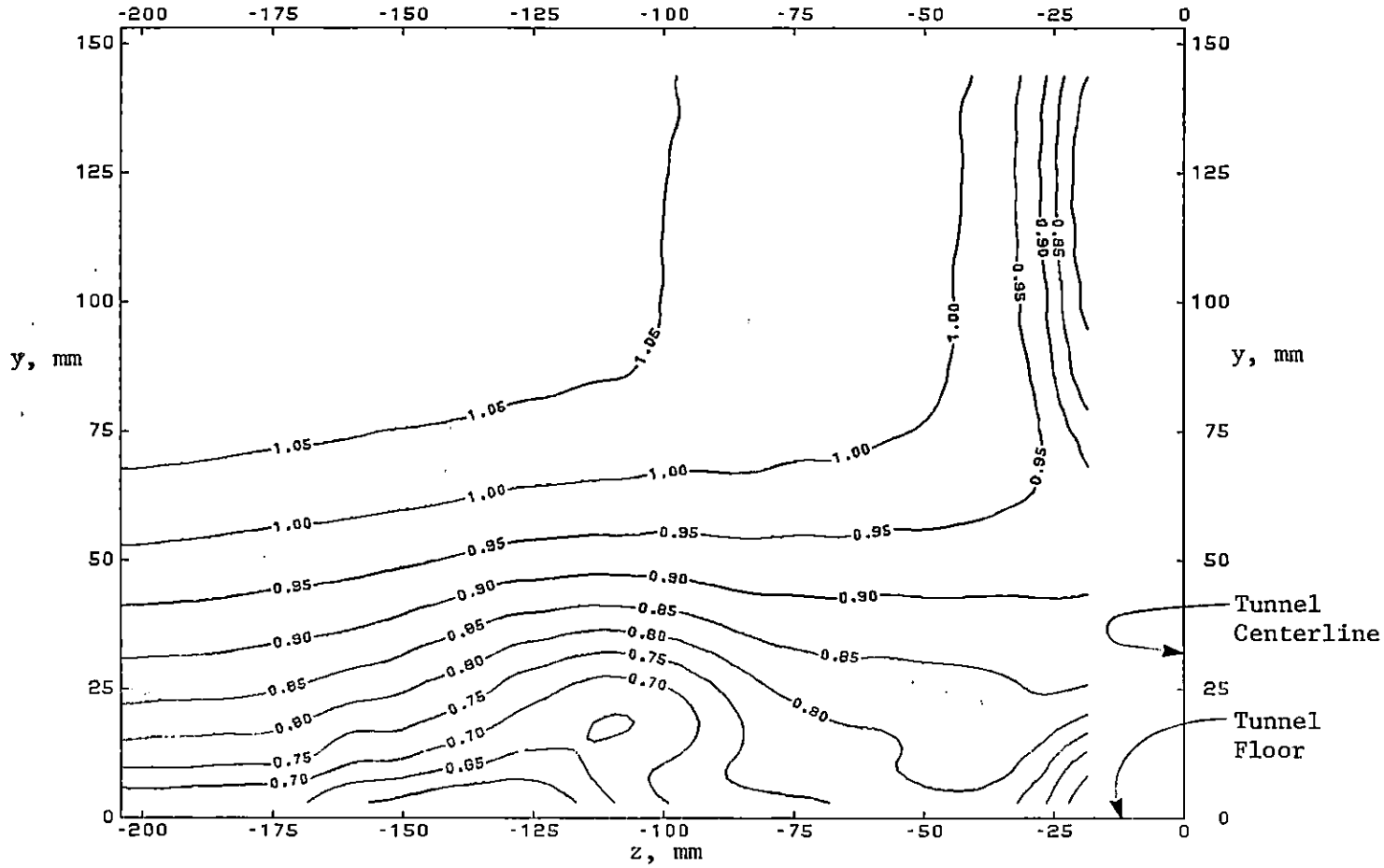

Fig. 4.25 Streamwise Velocity Distribution at 100 Percent Chord

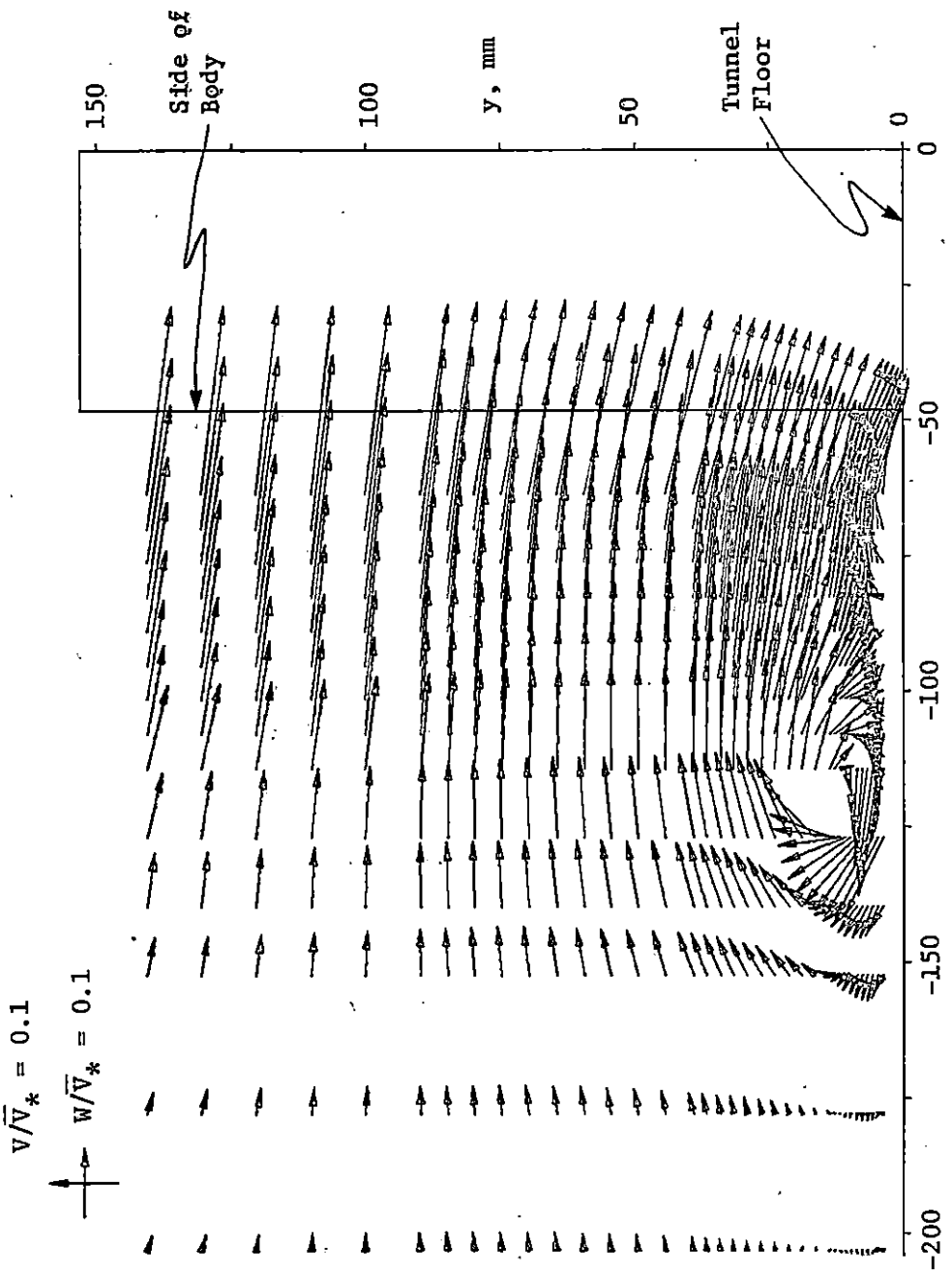

Fig. 4.26 Secondary Velocity Distribution at 43 Percent Chord

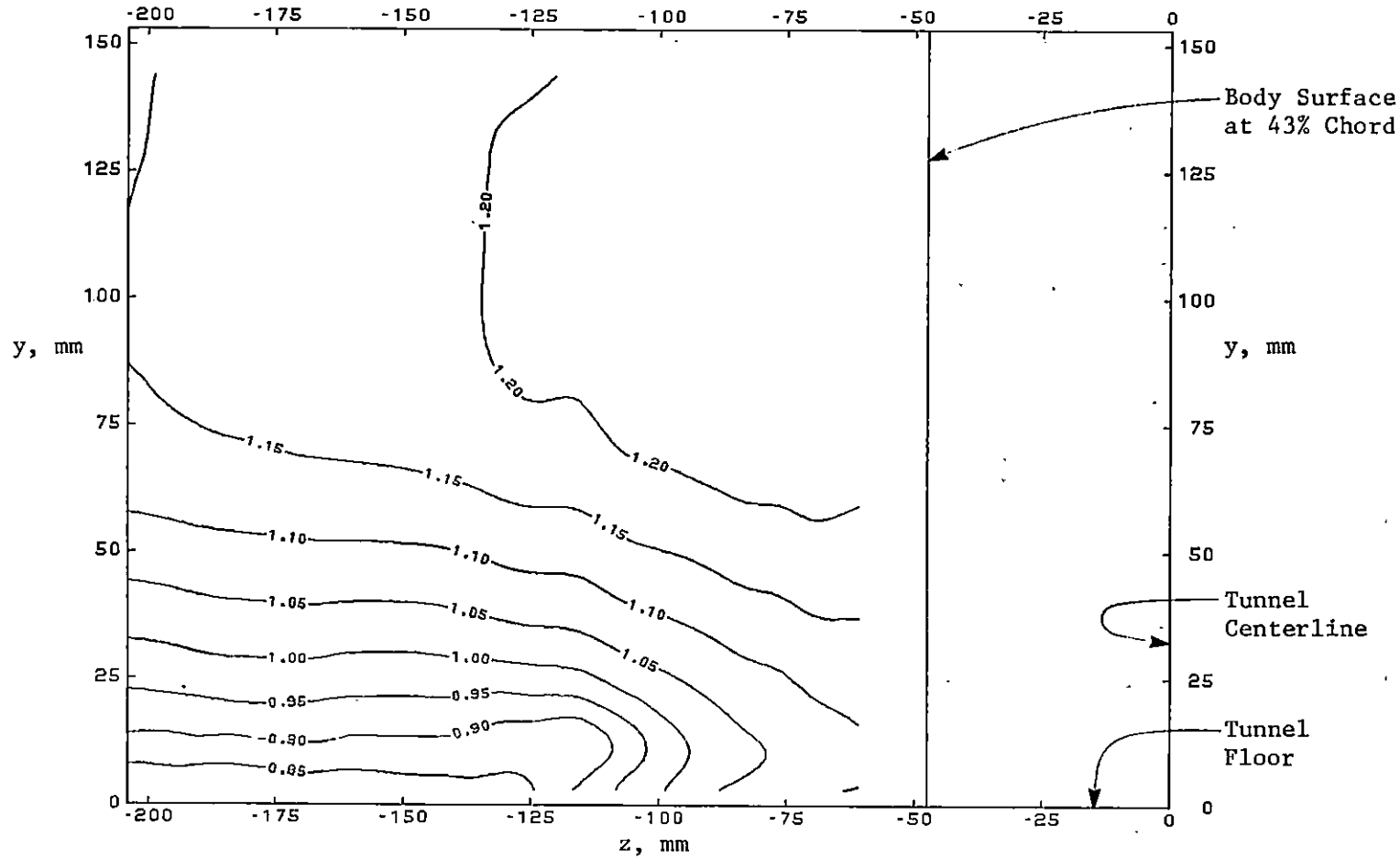

Fig. 4.27 Streamwise Velocity Distribution at 43 Percent Chord

floor and the vertical side of the body is filled with relatively high streamwise momentum fluid, possibly induced into the corner by the vortex. The negative y component of velocity near the side of the body in Fig. 4.24 and Fig. 4.26 is consistent with the flow visualization shown in Fig. 4.12. It was recognized in Section 4.2 that the surface flow on the side of the body was markedly downward.

An attempt was made to quanitify the streamwise vorticity,

$$\Omega = \frac{\partial W}{\partial y} - \frac{\partial V}{\partial z} , \tag{4.16}$$

apparent in Fig. 4.24 and Fig. 4.26 using finite difference approximations for the required partial derivatives and the experimental data. For the grid shown in Fig. 4.28, the average of forward and backward difference approximations was used.

$$\frac{\partial(W/\bar{V}_*)}{\partial y} = \frac{1}{2}\left[\frac{(W/\bar{V}_*)_{i,j+1} - (W/\bar{V}_*)_{i,j}}{y_{j+1} - y_j} + \frac{(W/\bar{V}_*)_{i,j} - (W/\bar{V}_*)_{i,j-1}}{y_j - y_{j-1}}\right] \tag{4.17}$$

$$\frac{\partial(V/\bar{V}_*)}{\partial z} = \frac{1}{2}\left[\frac{(V/\bar{V}_*)_{i+1,j} - (V/\bar{V}_*)_{i,j}}{z_{i+1} - z_i} + \frac{(V/\bar{V}_*)_{i,j} - (V/\bar{V}_*)_{i-1,j}}{z_i - z_{i-1}}\right] \tag{4.18}$$

$$\Omega = \bar{V}_* \left[\frac{\partial(W/\bar{V}_*)}{\partial y} - \frac{\partial(V/\bar{V}_*)}{\partial z}\right] \tag{4.19}$$

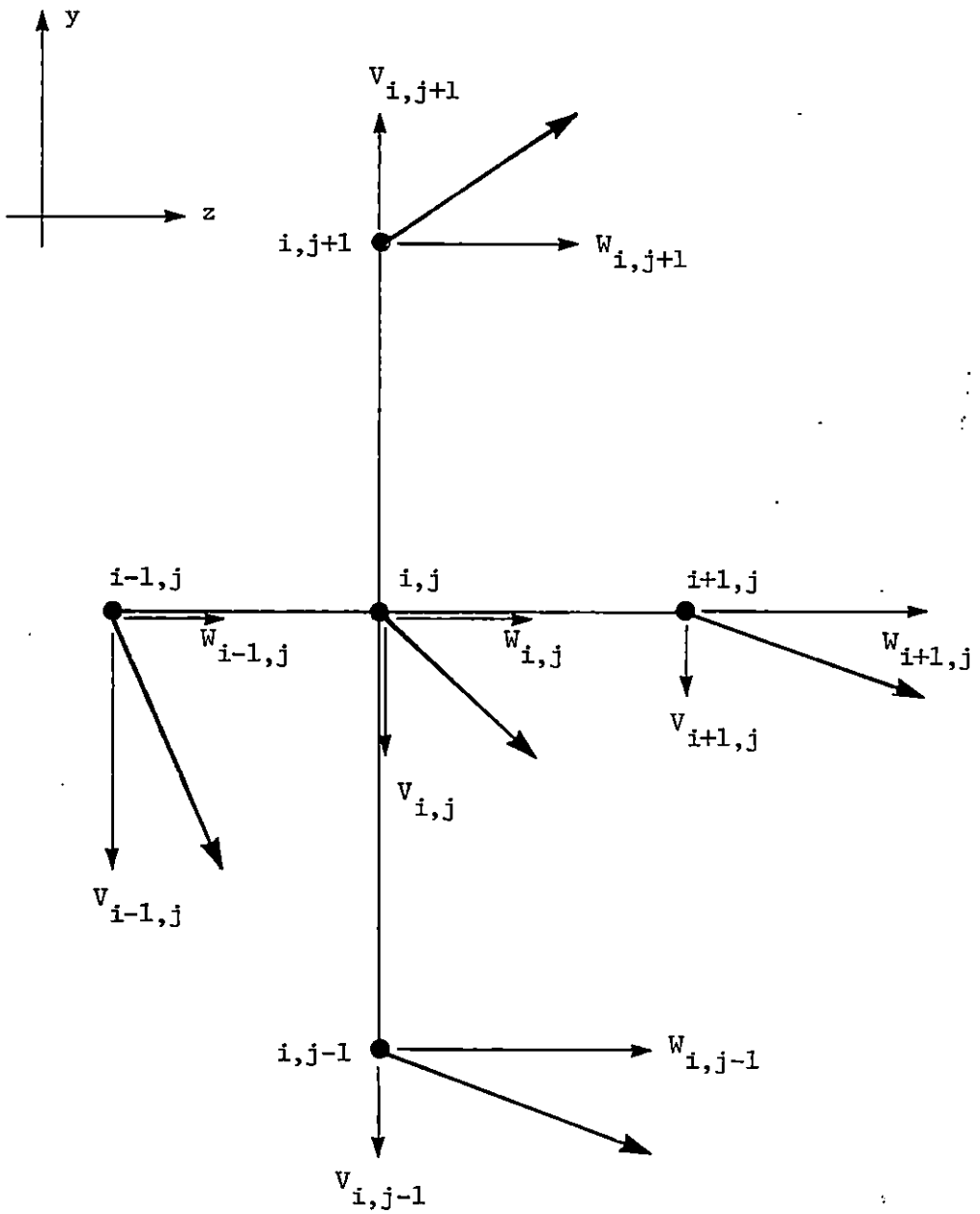

Fig. 4.28 Finite Difference Grid for the Computation of Streamwise Vorticity

Approximations at the corners and sides of the data grid consisted of forward or backward differences only, as appropriate. The calculations were performed using the dimensionless data and then scaled to the nominal laboratory conditions described in Table 2.1. The computed vorticity, in cycles per second (hertz) at nominal laboratory conditions, is shown in Fig. 4.29 and Fig. 4.30. At 43 percent chord, the mean streamwise vorticity at the center of the vortex is on the order of 120 Hz. At 100 percent chord, the vortex has decreased in strength and increased in cross sectional area with vorticity in the core on the order of 45 Hz.

The total pressure distributions and the static pressure distributions in the planes at 100 percent chord and 43 percent chord are shown in Fig. 4.31 through 4.34. These figures indicate that the vortex core consists of both low total pressure and low static pressure fluid. The total pressure distribution in Fig. 4.31 shows the total pressure defect resulting from the rapid boundary layer growth on the straight sides of the body. This defect appears near the centerline as a layer with a thickness in excess of 25 mm, in fair agreement with the idealized boundary layer analysis described in Section 4.2. The total pressure distribution shown in Fig. 4.32 agrees with the Kiel probe data shown in Fig. 4.21 to within the estimated uncertainties. The spanwise positions of the static pressure contours shown in Fig. 4.34 are consistent with the surface pressure distribution shown in Fig. 4.15.

The velocity distribution, the total pressure distribution, and the static pressure distribution on the plane of symmetry are shown in Fig.

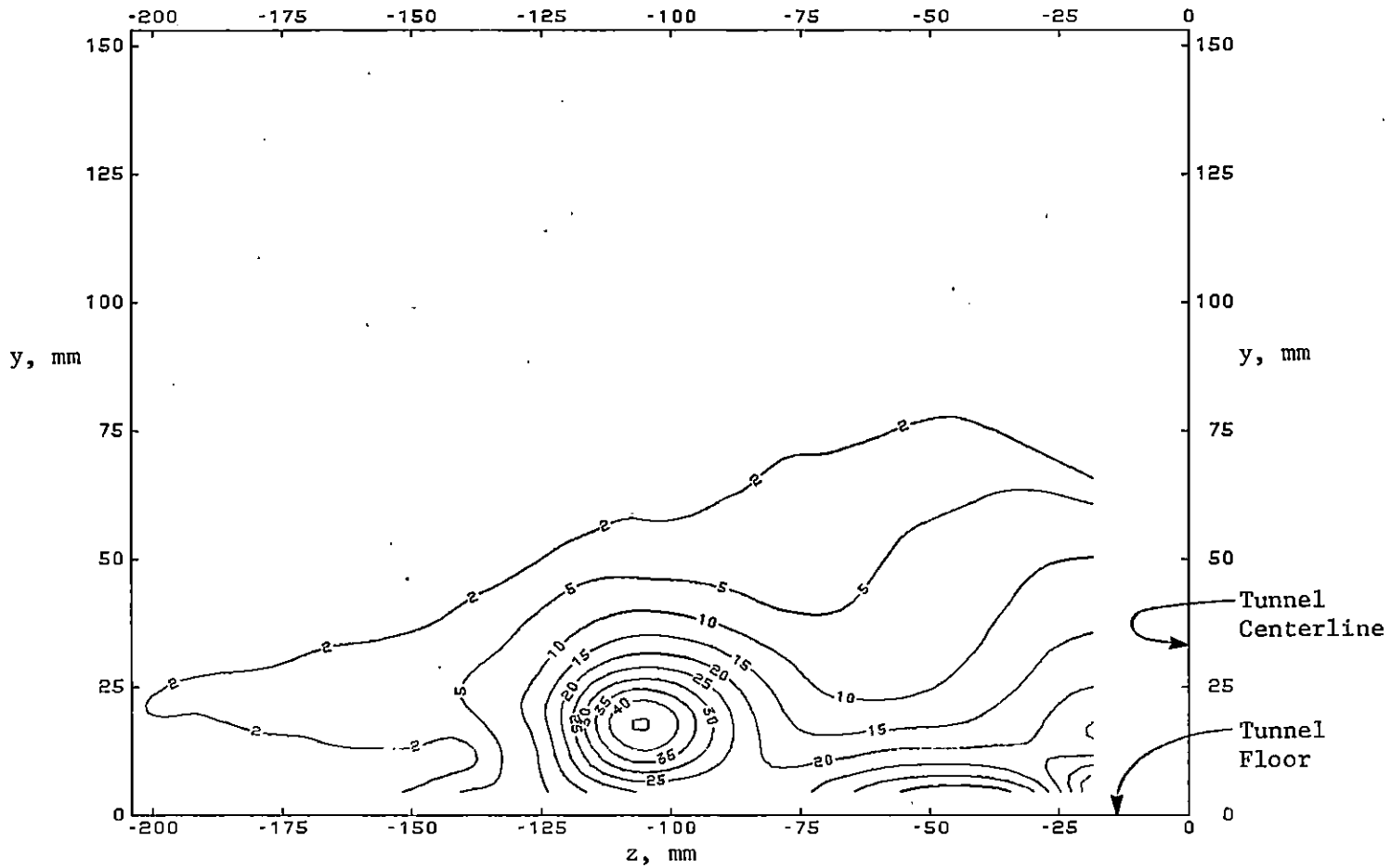

Fig. 4.29 Streamwise Vorticity Distribution at 100 Percent Chord

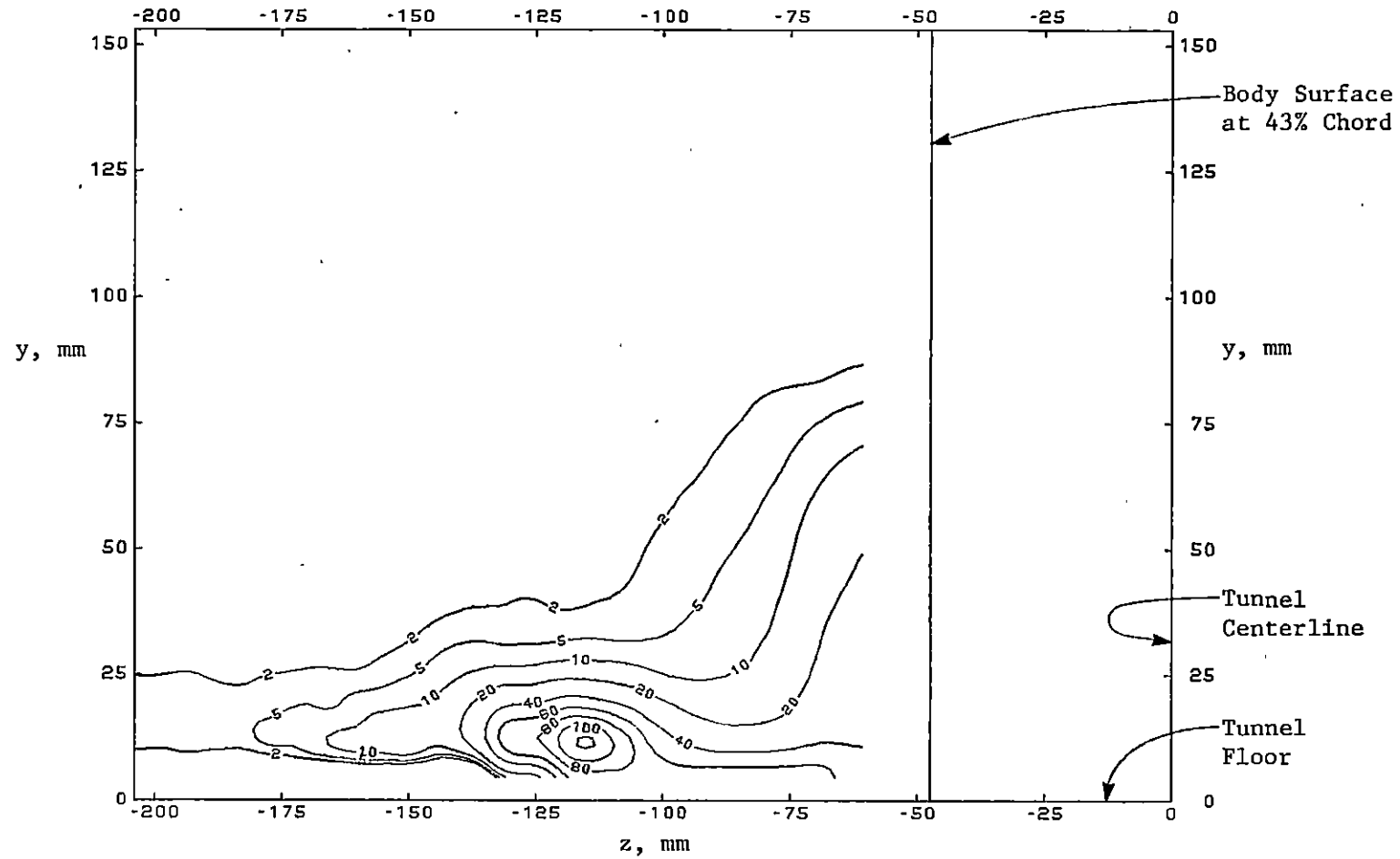

Fig. 4.30 Streamwise Vorticity Distribution at 43 Percent Chord

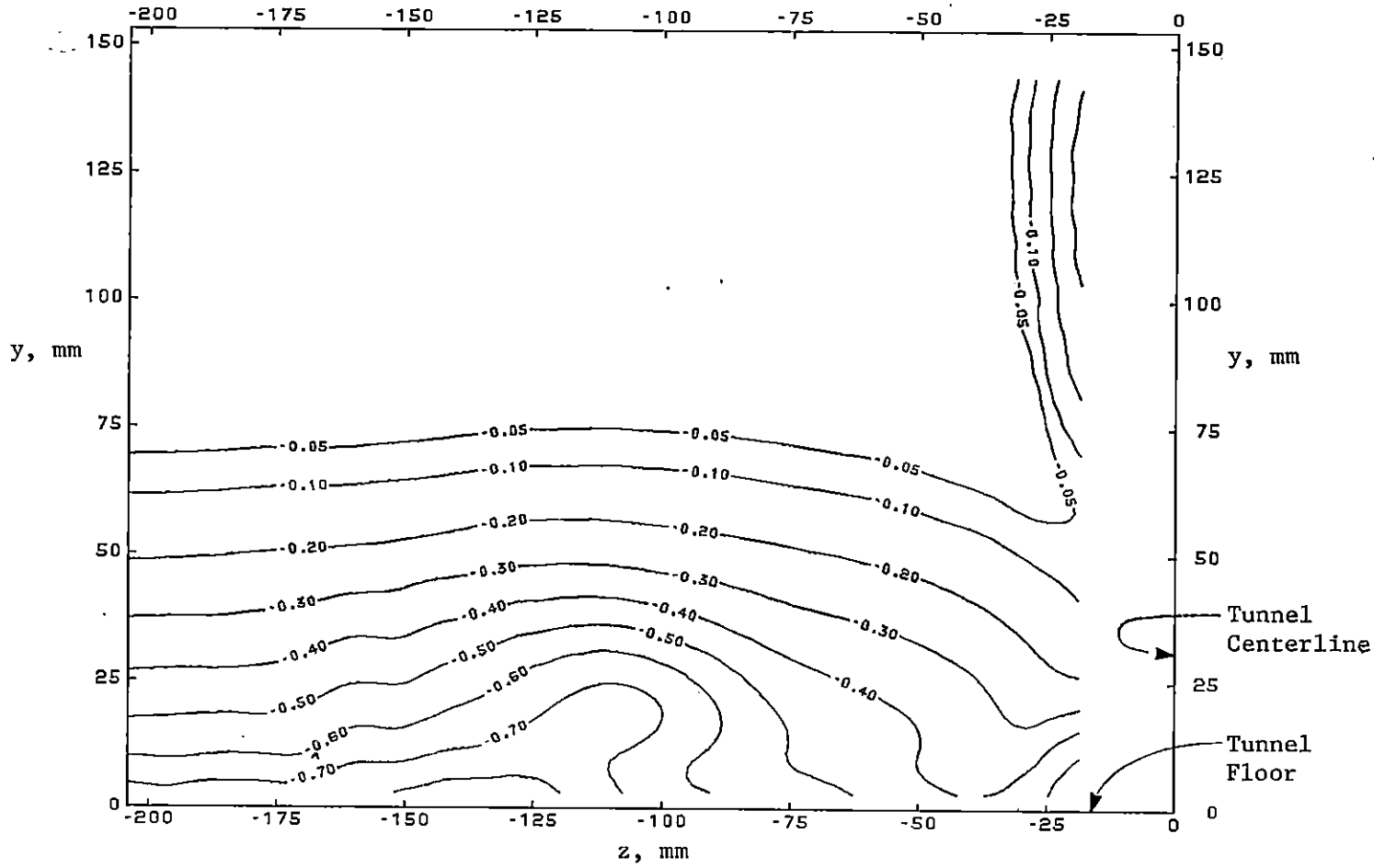

Fig. 4.31 Total Pressure Coefficient at 100 Percent Chord

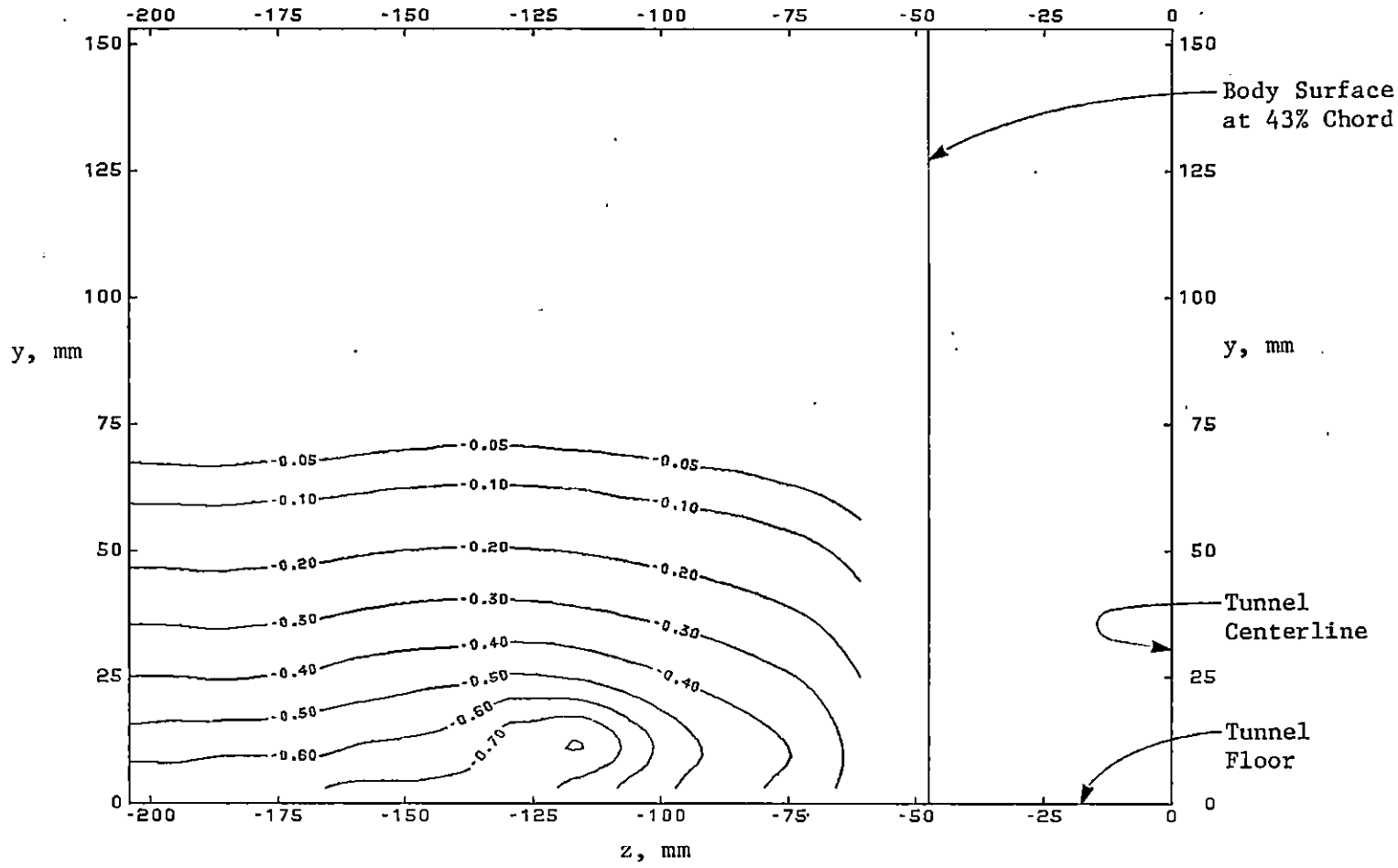

Fig. 4.32 Total Pressure Coefficient at 43 Percent Chord

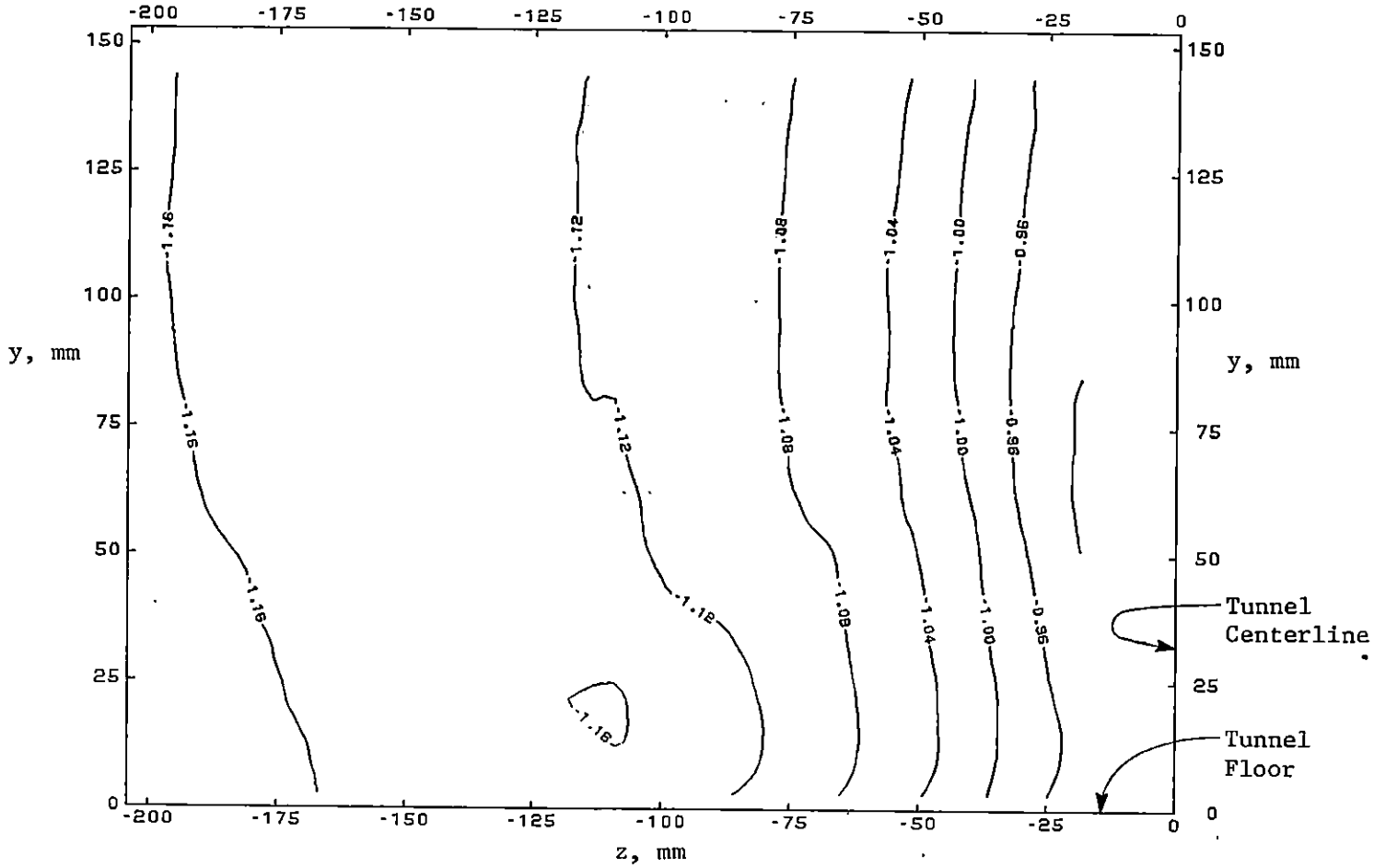

Fig. 4.33 Static Pressure Coefficient at 100 Percent Chord

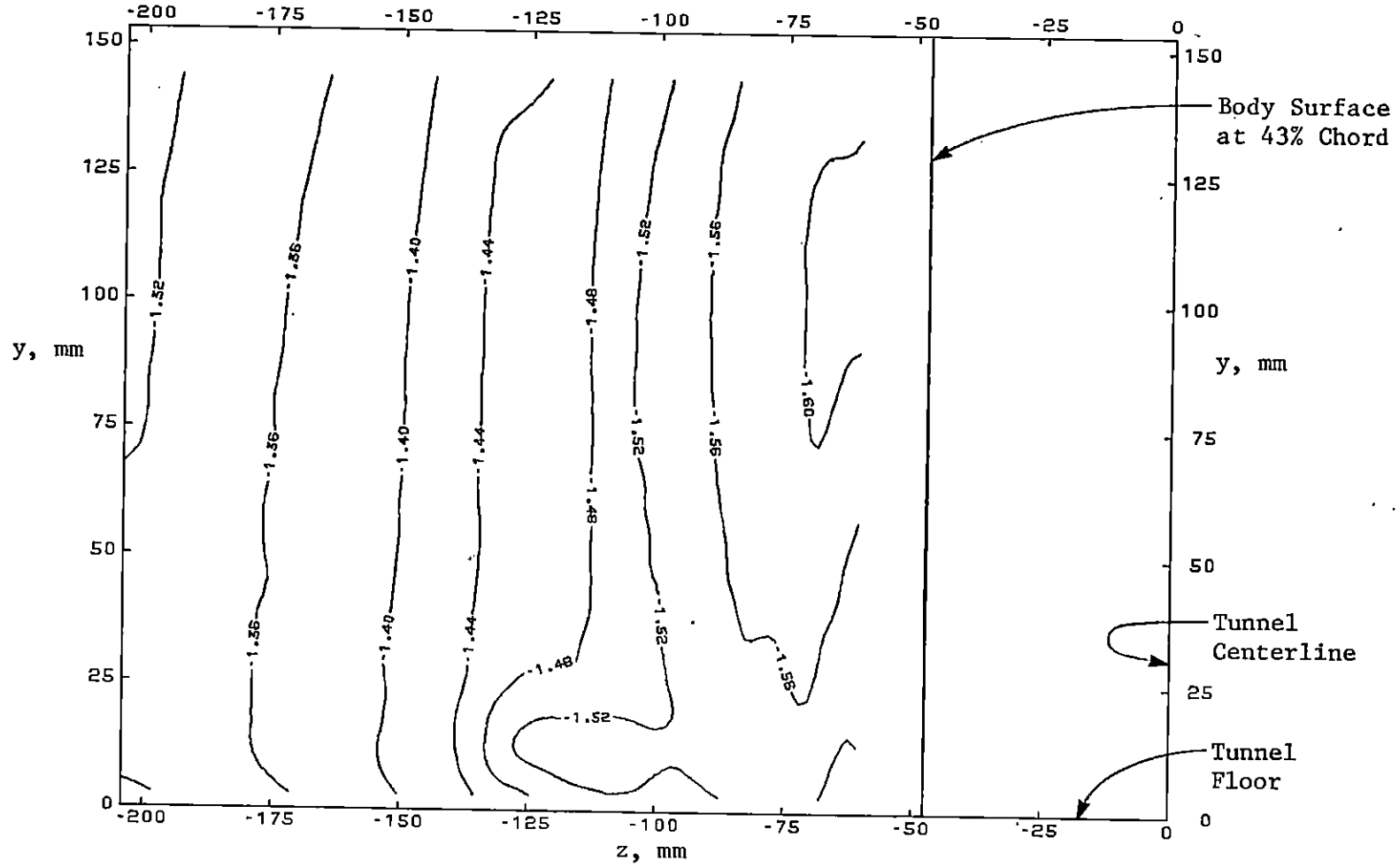

Fig. 4.34 Static Pressure Coefficient at 43 Percent Chord

4.35 through Fig. 4.37, respectively. Only one vortex is apparent in the velocity vector diagram. The extent of the reversed flow is consistent with the data obtained from the Kiel probe and shown in Fig. 4.23. It was not possible to resolve the flow field within 19 mm of the stagnation line or 3 mm of the floor because of the physical size of the probe.

Some of the data shown in these figures was obtained by extrapolating the calibration functions beyond their pitch angle limits of ±15°. The extent of this data is indicated by dashed lines. Extrapolating estimated functions beyond the range of the data used to evaluate the coefficients is an admittedly dangerous procedure. Nevertheless, the data within the dashed lines is included for its qualitative merit and should be weighted accordingly.

4.5.2 Some Comparisons with Previous Data

The flow field was surveyed at five x-z positions considered by Menna [1] to ensure repeatability and consistency between the two experimental studies. There are three overlapping positions on the plane of symmetry and two at 43 percent chord. These comparisons are shown in Fig. 4.38 through Fig. 4.42. The agreement between the two studies is good with differences in the measured streamwise component of velocity no larger than 5 percent. The differences in the spanwise component of velocity are within the estimated uncertainties in the results.

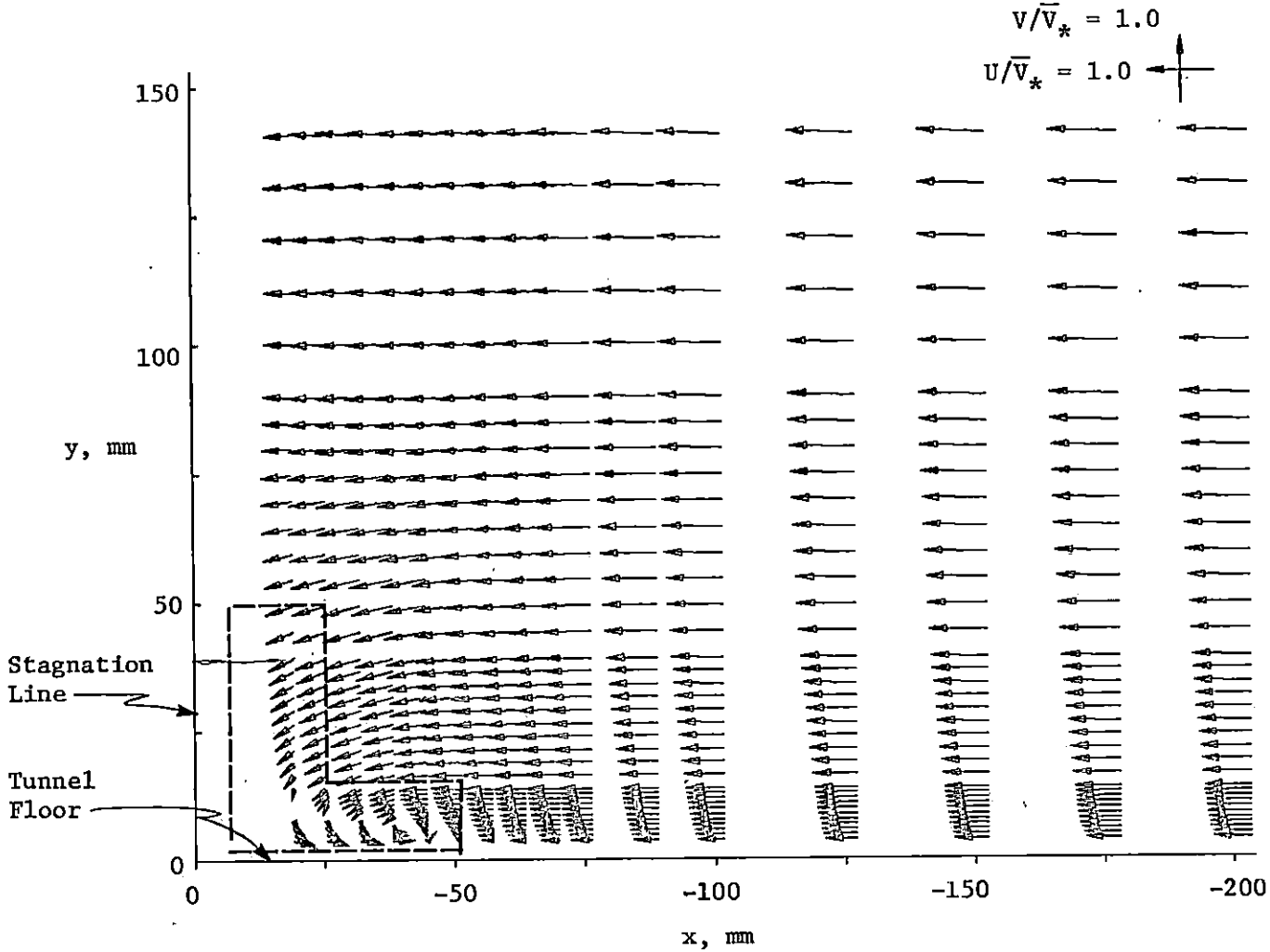

Fig. 4.35 Velocity Distribution on the Plane of Symmetry

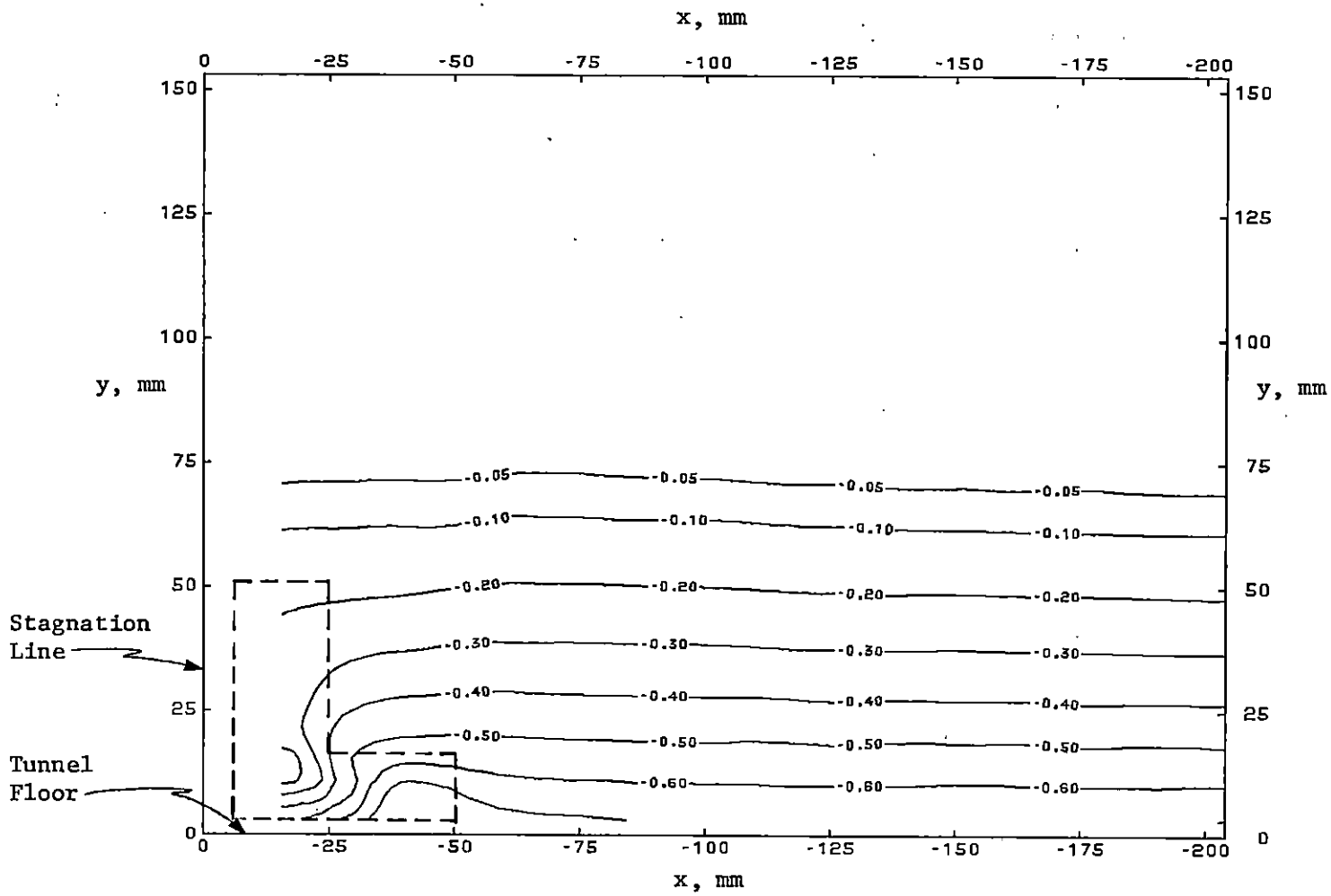

Fig. 4.36 Total Pressure Coefficient on the Plane of Symmetry

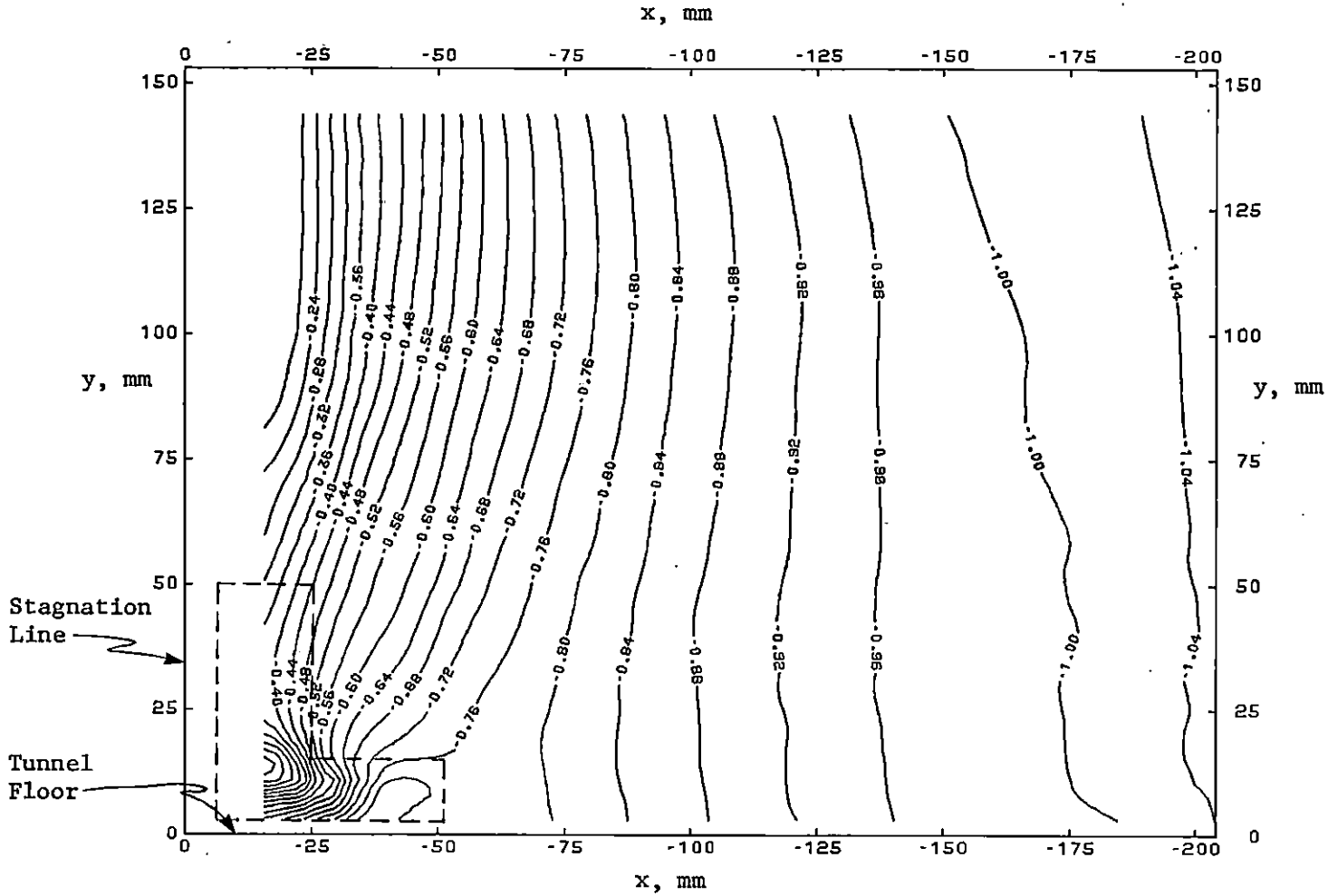

Fig. 4.37 Static Pressure Coefficient on the Plane of Symmetry

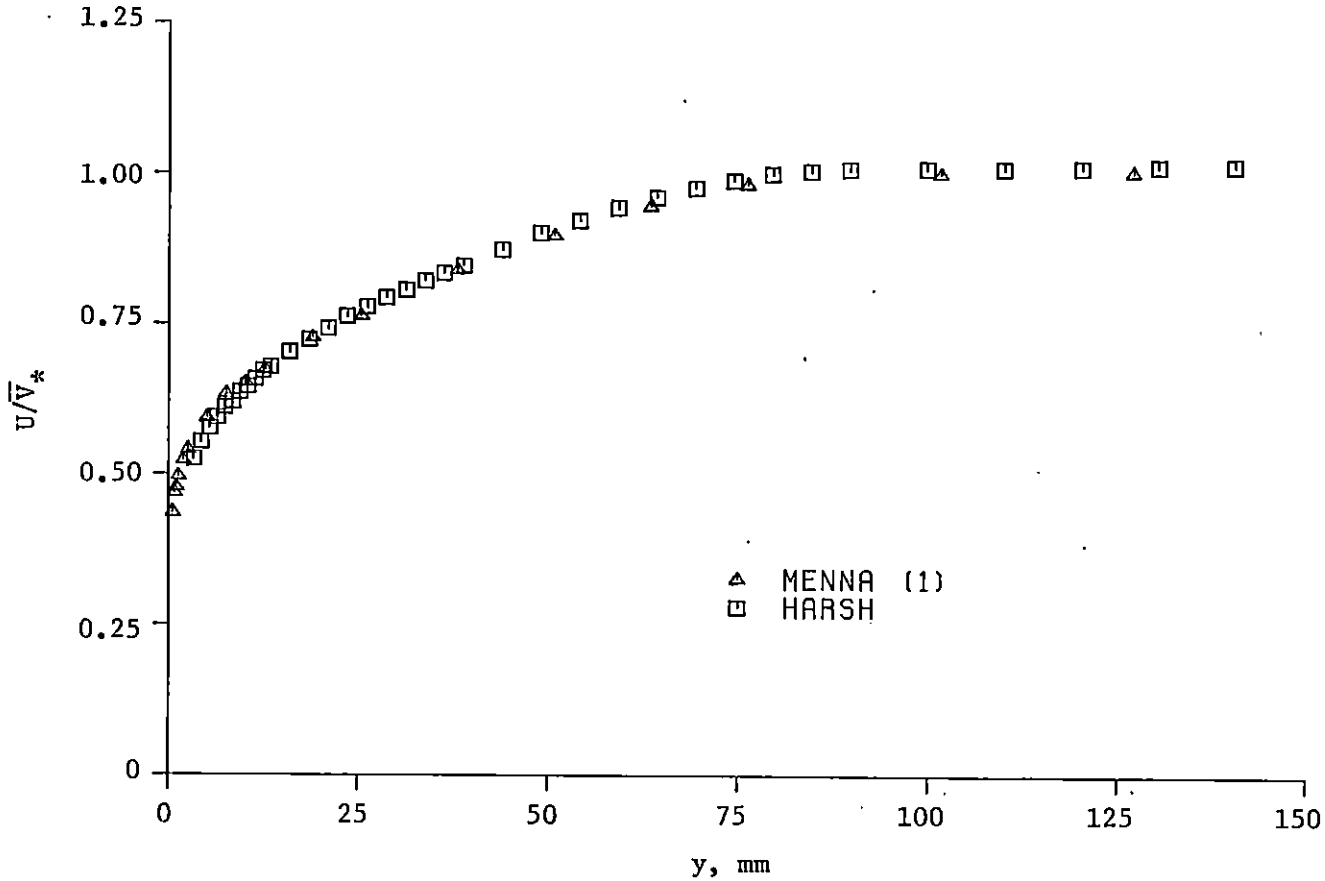

Fig. 4.38 Comparison with Menna's [1] Mean Velocity Data at (x,z) = (-178 mm, 0).

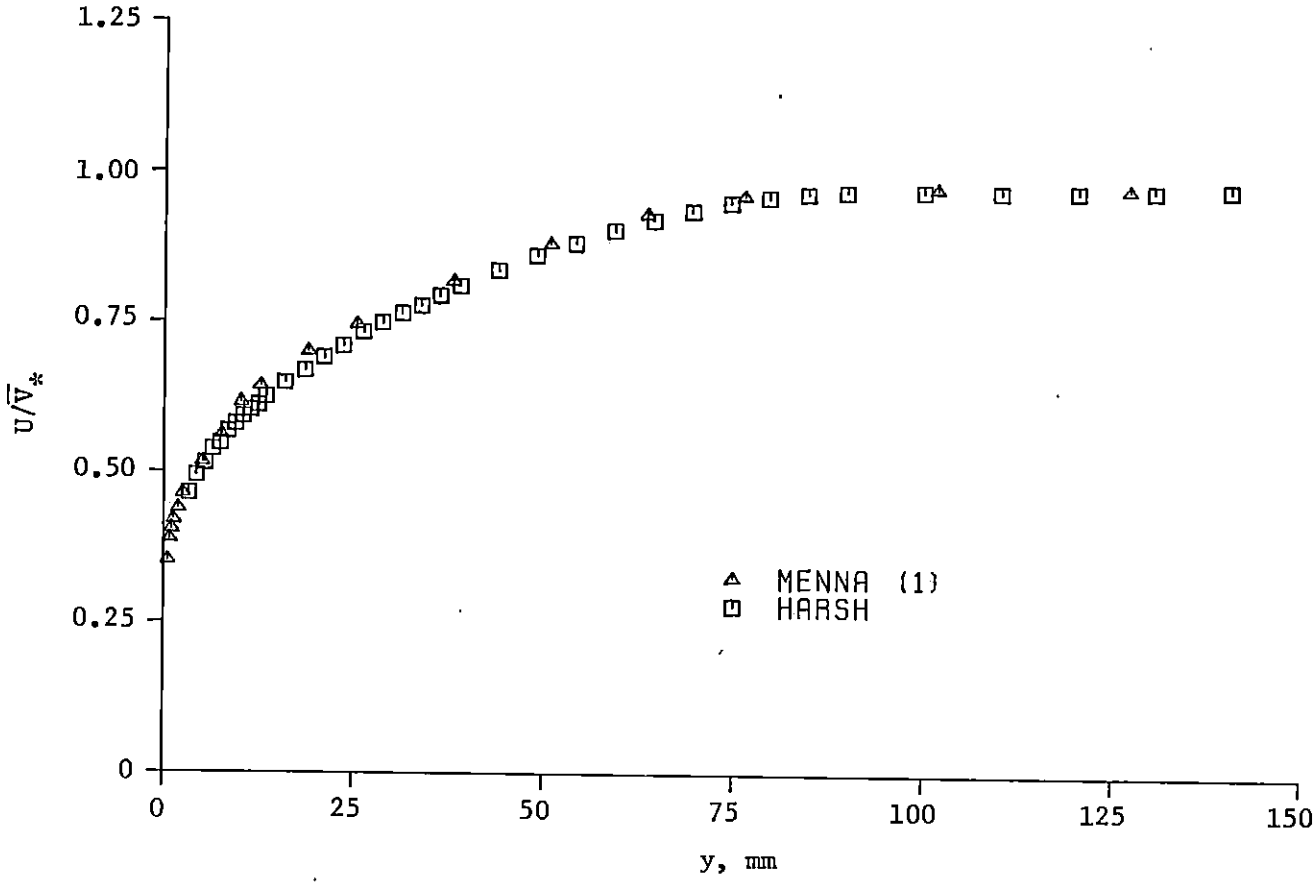

Fig. 4.39 Comparison with Menna's [1] Mean Velocity Data at (x,z) = (-127 mm, 0)

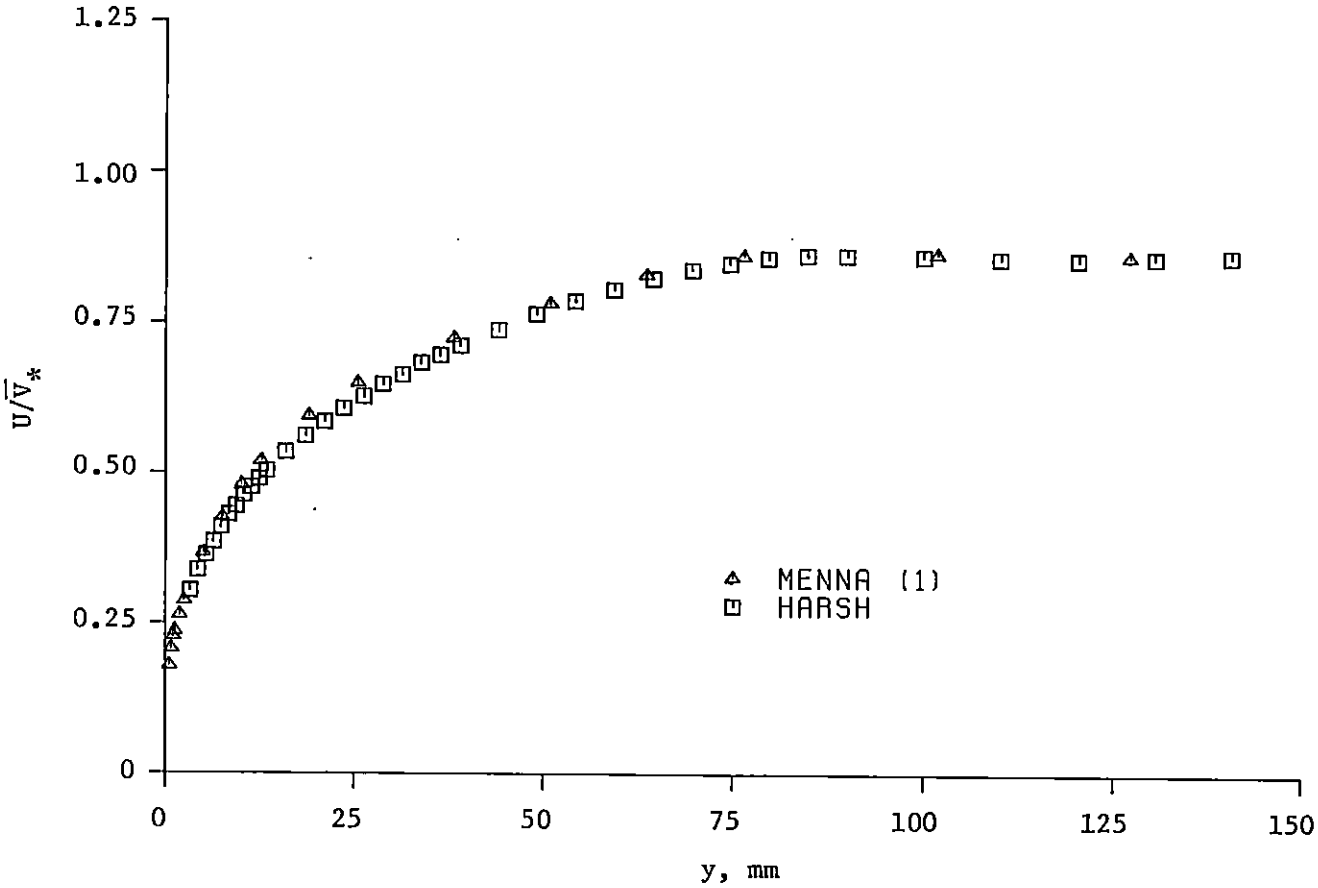

Fig. 4.40 Comparison with Menna's [1] Mean Velocity Data at (x,z) = (-76 mm, 0)

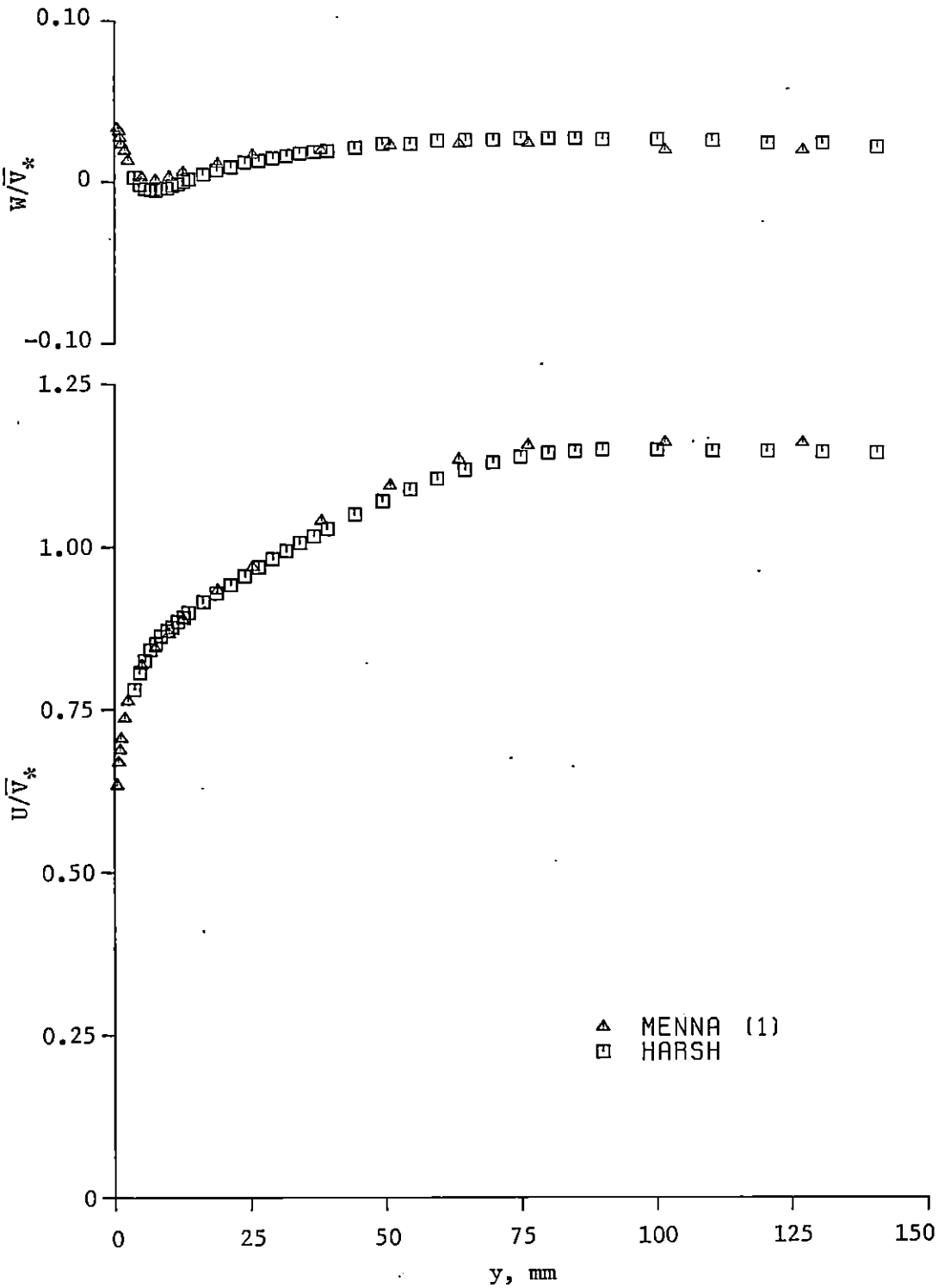

Fig. 4.41 Comparison with Menna's [1] Mean Velocity Data at (x,z) = (127 mm, -203 mm)

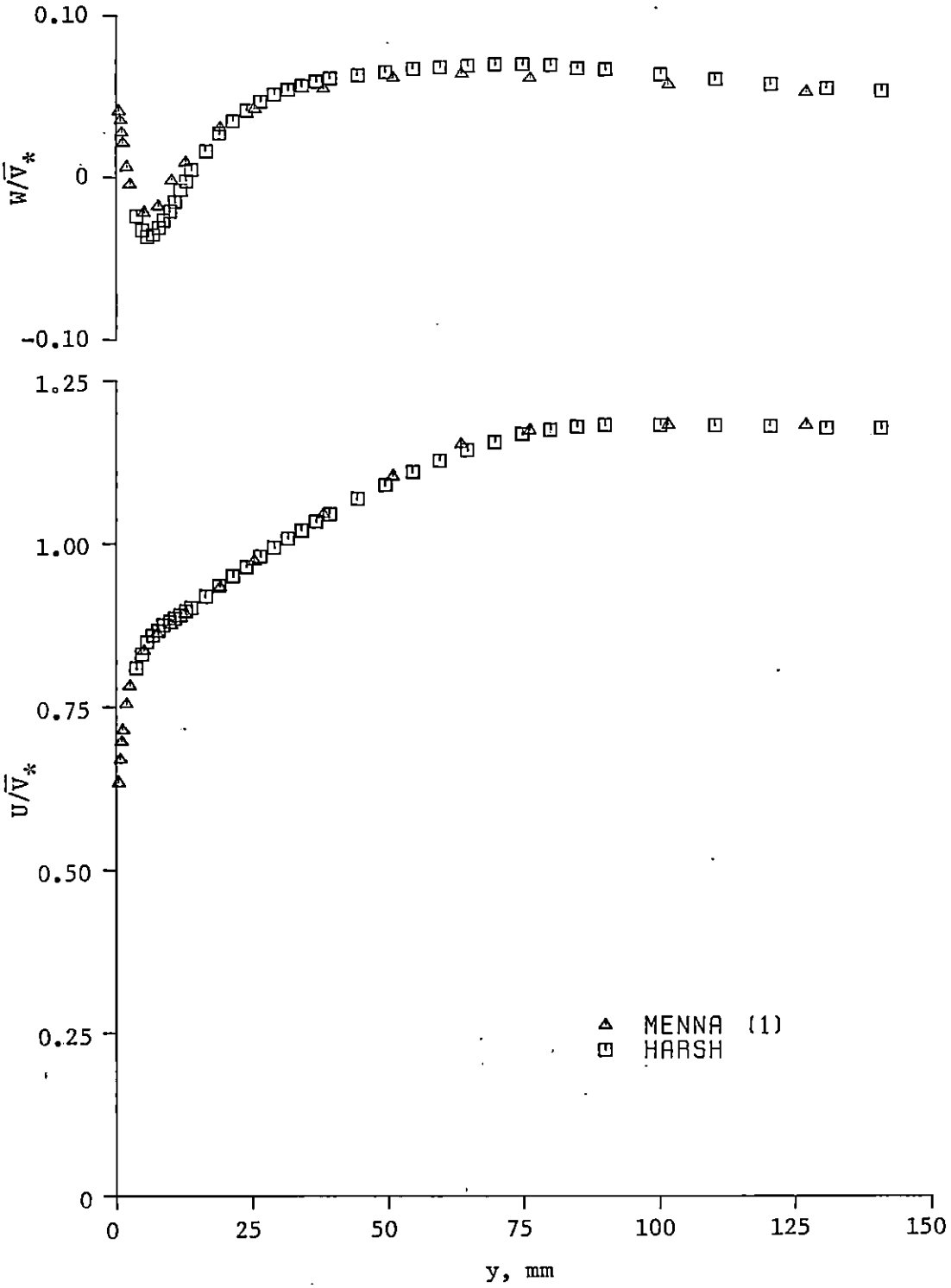

Fig. 4.42 Comparison with Menna's [1] Mean Velocity Data at (x,z) = (127 mm, -152 mm)

4.5.3 A Comparison Between Two Pressure Probes

The five-hole probe was used to measure the two-dimensional turbulent boundary layer in the center of the test section. This data was compared to the results obtained with the three-tube Conrad probe. The velocity distributions are shown in Fig. 4.43 and Fig. 4.44. The second figure shows the velocity profiles in law-of-the-wall coordinates where the friction velocity obtained from the Conrad probe was used to generate the five-hole probe coordinates. The agreement is good with no large noticeable effects attributed to the velocity gradient, the turbulence distribution, the probe geometries or wall proximity.

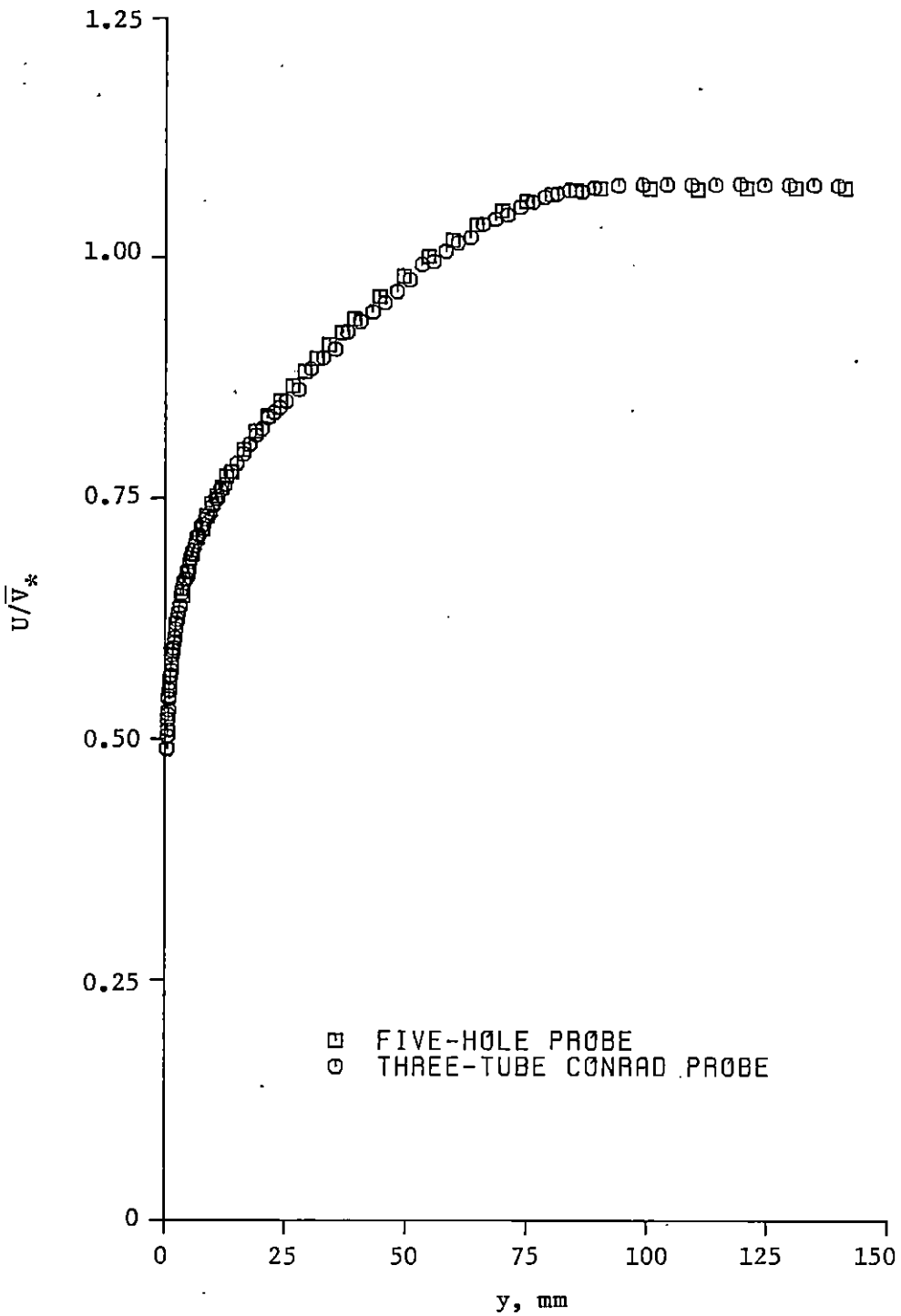

Fig. 4.43 Comparison Between the Three-Tube Conrad Probe and the Five-Hole Probe in the Two-Dimensional Turbulent Boundary Layer at (x,z) = (0,0)

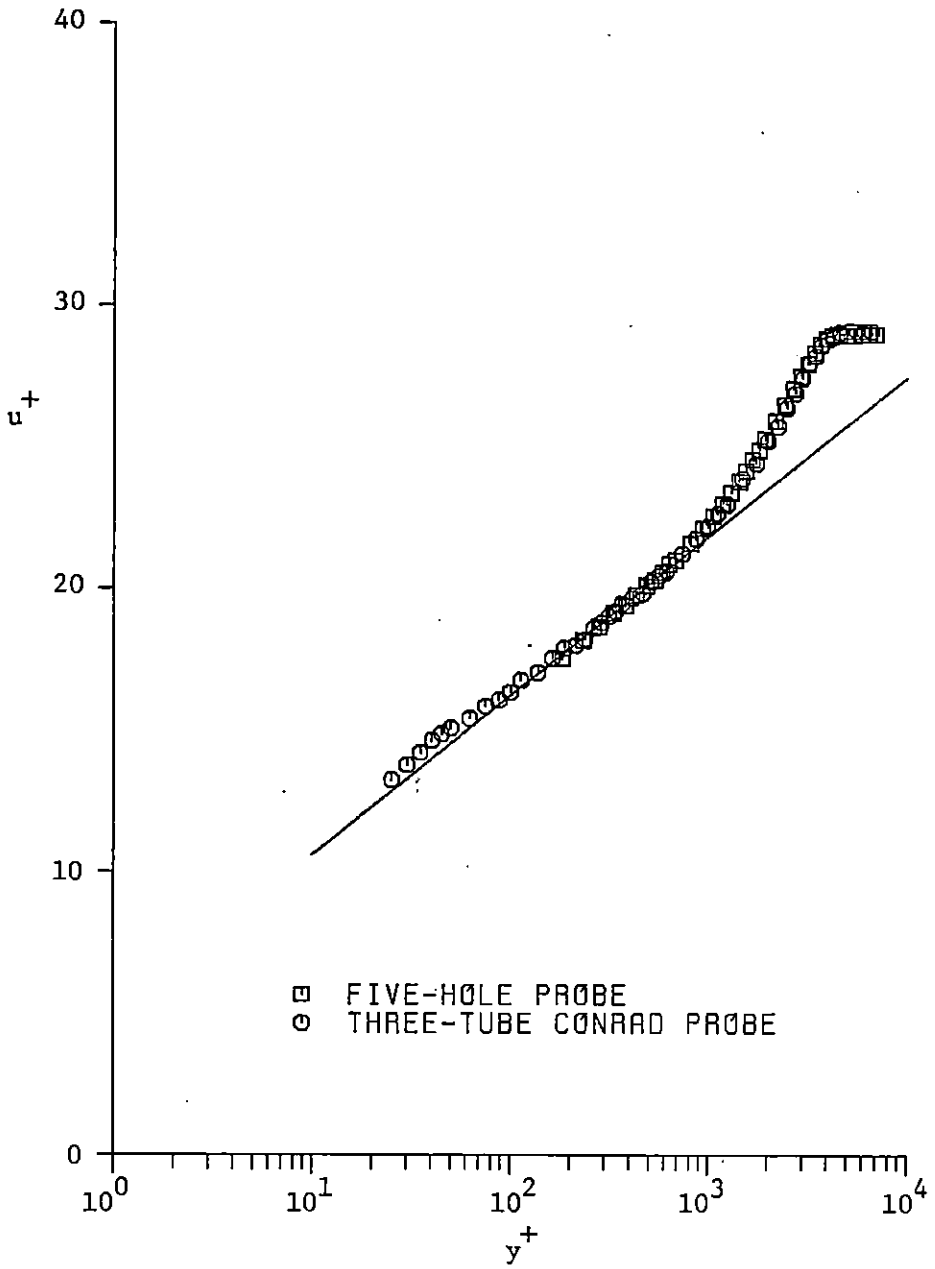

Fig. 4.44 Comparison Between the Three-Tube Conrad Probe and the Five-Hole Probe in the Two-Dimensional Turbulent Boundary Layer at (x,z) = (0,0), in Law-of-the-Wall Coordinates

5. SUMMARY

The incompressible, three-dimensional, turbulent flow separation around the base of a bluff obstacle on a flat surface was experimentally studied. The prominent feature of this type of flow is the horseshoe-shaped vortex (or system of vortices) formed in the corner between the obstacle and the surface.

The experimental program consisted of five parts:

(1) a study of the two-dimensional turbulent boundary layer on the flat surface,

(2) oil-film surface flow visualizations on the flat surface and on the vertical sides of the bluff obstacle,

(3) surface pressure measurements on the flat surface near the leading edge and on the sides of the obstacle,

(4) total pressure measurements using a miniature Kiel probe in two planes near the junction between the obstacle and the flat surface, and

(5) three-dimensional mean flow measurements using a five-hole pressure probe in three planes near the junction.

The objective of the two-dimensional turbulent boundary layer study was to confirm previously documented, small spanwise nonuniformities in the boundary layer on the flat surface. The displacement thickness, the momentum thickness, and the skin friction coefficient were used to assess the monuniformity of this boundary layer. Measured velocity distributions were integrated to obtain the displacement and momentum thicknesses. A systematic approach for estimating the wall shear stress

from velocity profile data, based on the method of least squares, was used to obtain the skin friction coefficient. The results confirm the existence of small spanwise nonuniformities. The largest deviations from the spanwise averages of these boundary layer-parameters occurred at the centerline position. The physical mechanism responsible for the spanwise variations was not identified.

The oil-film surface flow visualizations were conducted to define the extent of the three-dimensional separation and to give some indication of flow direction. The prominent features of the floor surface visualization include a singular separation point on the floor centerline 60 mm upstream of the leading edge and a line of ordinary separation emanating from this point. The floor flow visualization process also gave some indication of high wall shear stresses deep in the corner between the obstacle and the flat floor. The body surface visualizations showed an additional separation point on the stagnation line near the intersection between the leading edge and the floor centerline.

Extensive surface pressure measurements also showed the extent of the junction vortex. On the floor centerline, a relative maximum pressure was observed at the position corresponding to the singular separation point on the floor. This high pressure region was identified with the stagnating flow resulting from the streamwise flow meeting with the reversed flow at the singular separation point. Downstream of the singular separation point and 37 mm to 38 mm upstream of the leading edge, a relative minimum pressure was observed. This relative minimum was associated with the center of the vortex core.

The mean, three-dimensional flow field was surveyed with five-hole and Kiel pressure probes. The agreement between these probes was good. On the plane of symmetry, the mean flow results indicated that the three-dimensional separation and subsequent junction vortex were confined to a region very near the floor. The vortex in the plane of symmetry was, in fact, too close to the floor for any precise mean flow measurements in the region of reversed flow. One dominant vortex was observed in the other planes, downstream of the stagnation line.

REFERENCES

1. Menna, J. D., "A Three-Dimensional Turbulent Boundary Layer Upstream and Around a Junction Vortex Flow," Dissertation, Mechanical Engineering, Virginia Polytechnic Institute and State University, Blacksburg, Virginia, May, 1984.

2. Schwind, R. G., "The Three-Dimensional Boundary Layer Near a Strut," Gas Turbine Laboratory Report No. 57, Massachusetts Institute of Technology, Cambridge, Massachusetts, May, 1962.

3. Peake, D. J, and Galway, R. D., "The Three-Dimensional Separation of a Plane Incompressible Laminar Boundary Layer Produced by a Circular Cylinder Mounted Normal to a Flat Plate," Recent Developments in Boundary Layer Research, Part II, NATO Agardograph No. 97, North Atlantic Treaty Organization Advisory Group for Aerospace Research and Development, May, 1965, pp. 1049-1080.

4. Peake, D. J., Galway, R. D., and Rainbird, W. J., "The Three-Dimensional Separation of a Plane, Incompressible, Laminar Boundary Layer Produced by a Rankine Oval Mounted Normal to a Flat Plate," Report No. LR-446, National Aeronautical Establishment, Ottawa, Ontario, Canada, November, 1965.

5. Steinheuer, J., "Three-Dimensional Boundary Layers on Rotating Bodies and in Corners," Recent Developments in Boundary Layer Research, Part II, NATO Agardograph No. 97, North Atlantic Treaty Organization Advisory Group for Aerospace Research and Development, May, 1965, pp. 567-612.

6. Shen, P. S., and Jones, D. J., "Three-Dimensional Flow Separation of a Plane, Incompressible, Laminar Boundary Layer Caused by a Half-Delta Wing on a Flat Plate," Report No. LR-471, National Aeronautical Establishment, Ottawa, Ontario, Canada, February, 1967.

7. Shen, P. S., and Jones, D. J., "Three-Dimensional Laminar Boundary-Layer Separation on a Flat Plate Due to a Flow Confrontation with a Half-Cone at Incidence," Report No. LR-485, National Aeronautical Establishment, Ottawa, Ontario, Canada, June, 1967.

8. Roper, A. T., "A Cylinder in a Turbulent Shear Layer," Dissertation, Civil Engineering, Colorado State University, Fort Collins, Colorado, August, 1967.

9. Belik, L., "The Secondary Flow About Circular Cylinders Mounted Normal to a Flat Plate," Aeronautical Quarterly, Vol. 26, February, 1973, pp. 47-54.

10. Dechow, R., "Mittlere Geschwindigkeit und Reynoldsscher Spannungstensor in der dreidimensionalen turbulenten Wandgrezschicht vor einen stehenden Zylinder," Stromungsmechanik und Stromungsmaschinen, Heft 21, Marz, 1977, pp. 1-78.

11. Dechow, R., and Felsch, K. O., "Measurements of the Mean Velocity and of the Reynolds Stress Tensor in a Three-Dimensional Turbulent Boundary Layer Induced by a Cylinder Standing on a Flat Wall," Symposium on Turbulent Shear Flows, Vol. 1, American Society of Mechanical Engineers, University Park, Pennsylvania, April 18-20, 1977, pp. 9.11-9.20.

12. Barber, T. J., "An Investigation of Strut-Wall Intersection Losses," Journal of Aircraft, Vol. 15, No. 10, October, 1978, pp. 676-681.

13. Baker, C. J., "The Laminar Horseshoe Vortex," Journal of Fluid Mechanics, Vol. 95, Part 2, November, 1979, pp. 347-368.

14. Baker, C. J., "The Turbulent Horseshoe Vortex," Journal of Wind Engineering and Industrial Aerodynamics, Vol. 6, No. 1-2, July, 1980, pp. 9-23.

15. Shabaka, I. M. M. A., "Turbulent Flow in an Idealized Wing-Body Junction," Dissertation, Aeronautical Engineering, Imperial College of Science and Technology, London, England, April, 1979.

16. Shabaka, I. M. M. A., and Bradshaw, P., "Turbulent Flow Measurements in an Idealized Wing/Body Junction," AIAA Journal, Vol. 19, No. 2, February, 1981, pp. 131-132.

17. McMahon, H., Hubbartt, J., and Kubendran, L., "Mean Velocities and Reynolds Stresses in a Juncture Flow," NASA Contractor Report No. 3605, National Aeronautics and Space Administration, Langley Research Center, Hampton, Virginia, 1982.

18. McMahon, H., Hubbartt, J., and Kubendran, L., "Mean Velocities and Reynolds Stresses Upstream of a Simulated Wing Fuselage Juncture," NASA Contractor Report No. 3695, National Aeronautics and Space Administration, Langley Research Center, Hampton, Virginia, 1983.

19. Kubendran, L., McMahon, H., and Hubbartt, J., "Interference Drag in a Simulated Wing-Fuselage Juncture," NASA Contractor Report No. 3814, National Aeronautics and Space Administration, Langley Research Center, Hampton, Virginia, 1984.

20. Dickinson, S. C., "Flow Visualization and Velocity Measurements in the Separated Region of an Appendage-Flat Plate Junction," Proceedings of the Ninth Biennial Symposium on Turbulence, University of Missouri-Rolla, Rolla, Missouri, October 1-3, 1984.

21. Hsing, T. D., and Teng, H. Y., "Experimental Study of the Behavior of 3D-Turbulent Boundary Layer in a Simplified Wing/Body Junction," Paper No. AIAA-84-1529, presented at the American Institute of Aeronautics and Astronautics 17th Fluid Dynamics, Plasma Dynamics, and Lasers Conference, Snowmass, Colorado, June 25-27, 1984.

22. Moore, J., and Forlini, T. J., "A Horseshoe Vortex in a Duct," Paper No. 84-GT-202, presented at the American Society of Mechanical Engineers 29th International Gas Turbine Conference and Exhibit, Amsterdam, The Netherlands, June 4-7, 1984.

23. Rood, E. P., "Experimental Investigation of the Turbulent Large Scale Temporal Flow in the Wing-Body Junction," Dissertation, School of Engineering and Architecture, The Catholic University of America, Washington, District of Columbia, 1984.

24. Tree, I. K., "Laser-Doppler Measurements in a Turbulent Junction Vortex," Dissertation, Mechanical Engineering, Virginia Polytechnic Institute and State University, Blacksburg, Virginia, to be published in 1985.

25. Aggarwal, J. K., "Development of a Hot-Film Gauge Suitable for the Measurement of a Three-Dimensional Velocity Vector," Journal of Physics E: Scientific Instruments, Vol. 7, 1974, pp. 733-737.

26. Bank, N., and Gauvin, W. H., "Inclined Hot-Wire Response Equations for a Flow Field Having a Dominant Tangential Velocity Component," Canadian Journal of Chemical Engineering, Vol. 55, October, 1977, pp. 516-520.

27. Dau, K., McLeod, M., and Surry, D., "Two Probes for the Measurement of the Complete Velocity Vector in Subsonic Flow," Aeronautical Journal, Vol. 72, December, 1968, pp. 1066-1068.

28. De Grande, G., and Kool, P., "An Improved Experimental Method to Determine the Complete Reynolds Stress Tensor with a Single Rotating Slanting Hot Wire," Journal of Physics E: Scientific Instruments, Vol. 14, 1981, pp. 196-201.

29. Hirsch, C., and Kool, P., "Measurement of the Three-Dimensional Flow Field Behind an Axial Compressor Stage," Transactions of the American Society of Mechanical Engineers, Journal of Engineering for Power, Vol. 99, No. 2, April, 1977, pp. 168-180.

30. Hoffmeister, M., "Using a Single Hot-Wire Probe in Three-Dimensional Turbulent Flow Fields," DISA Information, No. 13, May, 1972, pp. 26-28.

31. Kirchhoff, R. H., and Struziak, R. M., "Direct Measurement of the Mean Flow Velocity Vector," Transactions of the American Society of Mechanical Engineers, Journal of Fluids Engineering, Vol. 98, No. 4, December, 1976, pp. 736-739.

32. Moussa, Z. M., and Eskinazi, S., "Directional Mean Flow Measurements Using a Single Inclined Hot Wire," Physics of Fluids, Vol. 18, No. 3, March, 1975, pp. 298-305.

33. Neuerburg, W., "Directional Hot-Wire Probe," DISA Information, No. 7, 1969, pp. 30-31.

34. Rosenberg, R. E., "A Three-Dimensional Hot-Wire Anemometry Technique Employing a Single Wire Probe," Report No. ARL-71-0039, Aerospace Research Laboratories, Air Force Systems Command, United States Air Force, Wright-Patterson Air Force Base, Ohio, March, 1971.

35. Sampath, S., Ganesan, V., and Gowda, B. H. L., "Improved Method for the Measurement of Turbulence Quantities," AIAA Journal, Vol. 20, No. 1, January, 1982, pp. 148-149.

36. Tabakoff, W., Vittal, B. V. R., and Wood, B., "Three-Dimensional Flow Measurements in a Turbine Scroll," Paper No. 83-GT-128, presented at the American Society of Mechanical Engineers 28th International Gas Turbine Conference and Exhibit, Phoenix, Arizona, March 27-31, 1983.

37. Arya, S. P. S., and Cermak, J. E., "Measurement of Turbulence in Three-Dimensional Mean Flow," Project THEMIS Technical Report No. 2, Fluid Dynamics and Diffusion Laboratory, Colorado State University, Fort Collins, Colorado, April, 1969.

38. Butler, T. L., and Wagner, J. W., "Application of a Three-Sensor Hot-Wire Probe for Incompressible Flow," AIAA Journal, Vol. 21, No. 5, May, 1983, pp. 726-732.

39. Cook, N. J., and Redfearn, D., "Calibration and Use of a Hot-Wire Probe for Highly Turbulent and Reversing Flows," Journal of Industrial Aerodynamics, Vol. 1, No. 3, February, 1976, pp. 221-231.

40. Davies, T. W., "Hot-Wire Anemometry in Highly Turbulent Flows," Symposium on External Flows, University of Bristol, England, 1972, pp. a.1-a.8.

41. Downing, P. M., "Reverse Flow Sensing Hot-Wire Anemometer," Journal of Physics E: Scientific Instruments, Vol. 5, No. 8, 1972, pp. 849-851.

42. Fabris, G., "Probe and Method for Simultaneous Measurement of Instantaneous Temperature and Three Velocity Components in Turbulent Flow," Review of Scientific Instruments, Vol. 49, No. 5, May, 1978, pp. 654-664.

43. Frota, M. N., and Moffat, R. J., "Effect of Combined Roll and Pitch Angles on Triple Hot-Wire Measurements of Mean and Turbulence Structure," DISA Information, No. 28, February, 1983, pp. 15-23.

44. Gaulier, C., "Measurement of Air Velocity by Means of a Triple Hot-Wire Probe," DISA Information, No. 21, April, 1977, pp. 16-20.

45. Gorton, C. A., and Lakshminarayana, B., "A Method for Measuring the Three-Dimensional Mean Flow and Turbulence Quantities Inside a Rotating Turbomachinery Passage," Transactions of the American Society of Mechanical Engineers, Journal of Engineering for Power, Vol. 98, No. 2, April, 1976, pp. 137-146.

46. Gunkel, A. A., Patel, R. P., and Weber, M. E., "A Shielded Hot-Wire Probe for Highly Turbulent and Rapidly Reversing Flows," Industrial and Engineering Chemistry, Fundamentals, Vol. 10, No. 4, November, 1971, pp. 627-631.

47. Jacobs, J., "Die Verwendung von Hitzdrahtsonden zur Ausmessung raumlicher Stromungen unter Berucksichtigung der Richtungsempfindlichkeit der Geber," Archiv fur technisches Messen, Lieferung 434, Marz, 1972, pp. R35-R39.

48. Lakshminarayana, B., "Three Sensor Hot Wire/Film Technique for Three Dimensional Mean and Turbulence Flow Field Measurement," TSI Quarterly, Vol. VIII, Issue 1, January-March, 1982.

49. "Data Reduction for Model 1294 - 3D Orthogonal Sensors," TSI Technical Bulletin No. 8, Thermo Systems Incorporated, St. Paul, Minnesota.

50. "Data Reduction Using 3-Sensor Probes (Model 1295, 1298) for Components and Correlations," TSI Technical Bulletin No. 24, Thermo Systems Incorporated, St. Paul, Minnesota.

51. Bradbury, L. J. S., "A Pulsed Wire Technique for Velocity Measurements in Highly Turbulent Flows," NPL AERO Report 1284, National Physical Laboratory, Teddington, England, January, 1969.

52. Bradbury, L. J. S., "Measurements with a Pulsed-Wire and a Hot-Wire Anemometer in the Highly Turbulent Wake of a Normal Flat Plate," Journal of Fluid Mechanics, Vol. 77, Part 3, October, 1976, pp. 473-497.

53. Bradbury, L. J. S., and Castro, I. P., "A Pulsed-Wire Technique for Velocity Measurements in Highly Turbulent Flows," Journal of Fluid Mechanics, Vol. 49, Part 4, October, 1971, pp. 657-691.

54. Bradbury, L. J. S., and Moss, W. D., "Pulsed Wire Anemometer Measurements in the Flow Past a Normal Flat Plate in a Uniform Flow and in a Sheared Flow," Wind Effects on Buildings and Structures, Proceedings of the Fourth International Conference on Wind Effects on Buildings and Structures, edited by K. J. Eaton, London, September 8-12, 1975, pp. 485-496.

55. Castro, I. P., and Cheun, B. S., "The Measurement of Reynolds Stresses with a Pulsed-Wire Anemometer," Journal of Fluid Mechanics, Vol. 118, May, 1982, pp. 41-58.

56. Gaster, M., and Bradbury, L. J. S., "The Measurement of the Spectra of Highly Turbulent Flows by a Randomly Triggered Pulsed-Wire Anemometer," Journal of Fluid Mechanics, Vol. 77, Part 3, 1976, pp. 499-509.

57. Tombach, I. H., "Velocity Measurements with a New Probe in Inhomogeneous Turbulent Jets," Dissertation, Aeronautical Engineering, California Institute of Technology, Pasadena, California, May, 1969.

58. Tombach, I. H., "An Evaluation of the Heat Pulse Anemometer for Velocity Measurement in Inhomogeneous Turbulent Flow," The Review of Scientific Instruments, Vol. 14, No. 2, February, 1973, pp. 141-148.

59. Bryer, D. W., and Pankhurst, R. C., Pressure-Probe Methods for Determining Wind Speed and Flow Direction, Her Majesty's Stationery Office, London, 1971.

60. Bryer, D. W., Walshe, D. E., and Garner, H. C., "Pressure Probes Selected for Three-Dimensional Flow Measurement," Reports and Memoranda No. 3037, National Physical Laboratory, Teddington, England, November, 1955.

61. Everett, K. N., Gerner, A. A., and Durston, D. A., "Seven Hole Cone Probes for High Angle Flow Measurement: Theory and Calibration," AIAA Journal, Vol. 21, No. 7, July, 1983, pp. 992-998.

62. Judd, A. M., "Calibration of a Five Tube Probe for Measuring Wind Speed and Direction," Journal of Physics E: Scientific Instruments, Vol. 8, February, 1975, pp. 115-116.

63. Lee, J. C., and Ash, J. E., "A Three-Dimensional Spherical Pitot Probe," Transactions of the American Society of Mechanical Engineers, Vol. 78, 1956, pp. 603-608.

64. Merrington, G. L., "A Pitch and Yaw Meter," Transactions of the American Society of Mechanical Engineers, Journal of Basic Engineering, Vol. 90, June, 1968, pp. 314-316.

65. Raghava, A. K., Kumar, K. L., Malhotra, R. C., and Agrawal, D. P., "A Probe for the Measurement of the Velocity Field," Transactions of the American Society of Mechanical Engineers, Journal of Fluids Engineering, Vol. 101, No. 1, March, 1979, pp. 143-146.

66. Shepherd, I. C., "A Four-Hole Pressure Probe for Fluid Flow Measurements in Three Dimensions," Transactions of the American Society of Mechanical Engineers, Journal of Fluids Engineering, Vol. 103, No. 4, December, 1981, pp. 590-594.

67. Treaster, A. L., and Yocum, A. M., "The Calibration and Application of Five-Hole Probes," Instrument Society of America, Transactions, Vol. 18, No. 3, 1979, pp. 23-34.

68. Winternitz, F. A. L., "Probe Measurements in Three-Dimensional Flow," Aircraft Engineering, Vol. 28, No. 330, August, 1956, pp. 273-278.

69. Wright, M. A., "The Evaluation of a Simplified Form of Presentation for Five-Hole Spherical and Hemispherical Pitometer Calibration Data," Journal of Physics E: Scientific Instruments, Vol. 3, No. 5, 1970, pp. 356-362.

70. Yajnik, K. S., and Gupta, R. P., "A New Probe for Measurement of Velocity and Flow Direction in Separated Flows," Journal of Physics E: Scientific Instruments, Vol. 6, 1973, pp. 82-86.

71. Simpson, R. L., "REVIEW - A Review of Some Phenomena in Turbulent Flow Separation," Transactions of the American Society of Mechanical Engineers, Journal of Fluids Engineering, Vol. 103, No. 4, December, 1981, pp. 520-533.

72. Lakshminarayana, B., "Techniques for Aerodynamic and Turbulence Measurements in Turbomachinery Rotors," Transactions of the American Society of Mechanical Engineers, Journal of Engineering for Power, Vol. 103, No. 2, April, 1981, pp. 374-392.

73. Coder, D. W., Besch, P. K., Rood, E. P., and Chappelear, J. E., "Complimentary Use of a Tri-Axial Hot-Film Probe and a Five-Hole Pitot Tube to Determine Vehicle Wake Characteristics," Three-Dimensional Turbulent Shear Flows, edited by S. Carmi, A. Hamed, J. Herring, and F. Peterson, selected papers from the American Institute of Aeronautics and Astronautics - American Society of Mechanical Engineers 3rd Joint Thermophysics, Fluids, Plasma, and Heat Transfer Conference, June 7-11, 1982, pp. 113-119.

74. Tennant, M. H., "Near-Wall Similarity in Three Dimensional Turbulent Bounary Layers," Dissertation, Mechanical Engineering, Virginia Polytechnic Institute and State University, Blacksburg, Virginia, November, 1977.

75. Herwig, N. L., "Design of a Data Acquisition System to Control and Monitor a Velocity Probe in a Fluid Flow Field," Thesis, Mechanical Engineering, Virginia Polytechnic Institute and State University, Blacksburg, Virginia, December, 1982.

76. Beck, J. V., and Arnold, K. J., Parameter Estimation in Engineering and Science, Wiley, New York, 1977.

77. Walpole, R. E., and Myers, R. E., Probability and Statistics for Engineers and Scientists, 2nd edition, Macmillan, New York, 1978.

78. Draper, N., and Smith, H., Applied Regression Analysis, 2nd edition, Wiley, New York, 1981.

79. Montgomery, D. C., and Peck, E. A., Introduction to Linear Regression Analysis, Wiley, New York, 1982.

80. Junkins, J. L., An Introduction to Optimal Estimation of Dynamical Systems, Sijthoff and Noordhoff, Alphen aan den Rijn, The Netherlands, 1978.

81. Winter, K. G., "An Outline of the Techniques Available for the Measurement of Skin Friction in Turbulent Boundary Layers," Compressible Turbulent Boundary Layers, Vol. 1, Lecture Series 86, von Karman Institute for Fluid Dynamics, March 1-5, 1976.

82. Winter, K. G., "An Outline of the Techniques Available for the Measurement of Skin Friction in Turbulent Boundary Layers," Progress in Aerospace Sciences, Vol. 18, 1977, pp. 1-57.

83. Rechenberg, I., "Messung der turbulenten Wandschubspannung," Zeitschrift fuer Flugwissenschaften, Heft 11, November, 1963, pp. 429-438.

84. Clauser, F. H., "The Turbulent Boundary Layer," Advances in Applied Mechanics, Vol. IV, 1956, pp. 1-51.

85. Bradshaw, P., "A Simple Method for Determining Turbulent Skin Friction from Velocity Profiles," Journal of the Aerospace Sciences, Vol. 26, No. 12, December, 1959, p. 841.

86. Schraub, F. A., and Kline, S. J., "A Study of the Structure of the Turbulent Boundary Layer with and without Longitudinal Pressure Gradients," Report No. MD-12, Thermosciences Division, Department of Mechanical Engineering, Stanford University, Stanford, California, March, 1965.

87. Rajaratnam, N., and Froelich, C. R., "Boundary Shear Stress in Turbulent Boundary Layers on Smooth Boundarys," Journal of the Royal Aeronautical Society, Vol. 71, No. 673, January, 1967, pp. 52-53.

88. Coles, D., "The Young Person's Guide to the Data," Computation of Turbulent Boundary Layers - 1968 AFOSR-IFP-Stanford Conference, Vol. II, Thermosciences Division, Department of Mechanical Engineering, Stanford University, Stanford, California, 1968, pp. 1-54.

89. Pierce, F. J., and Zimmerman, B. B., "Wall Shear Stress Inference from Two- and Three-Dimensional Turbulent Boundary Layer Velocity Profiles," Transactions of the American Society of Mechanical Engineers, Journal of Fluids Engineering, Vol. 95, No. 1, March, 1973, pp. 61-67.

90. Ludwieg, H., and Tillmann, W., "Investigations of the Wall-Shearing Stress in Turbulent Boundary Layers," NACA Technical Memorandum No. 1285, National Advisory Committee for Aeronautics, Washington, District of Columbia, May, 1950.

91. Squire, L. C., Maltby, R. L., Keating, R. F. A., and Stanbrook, A., "The Surface Oil Flow Technique," Flow Visualization in Wind Tunnels Using Indicators, NATO Agardograph No. 70, North Atlantic Treaty Organization Advisory Group for Aerospace Research and Development, April, 1962, pp. 1-74.

92. Kline, S. J., and McClintock, F. A., "Describing Uncertainties in Single-Sample Experiments," Mechanical Engineering, January, 1953, pp. 3-8.

93. Moffat, R. J., "Contributions to the Theory of Single-Sample Uncertainty Analysis," Transactions of the American Society of Mechanical Engineers, Journal of Fluids Engineering, Vol. 104, No. 2, June, 1982, pp. 250-260.

94. Schenck, H., Theories of Engineering Experimentation, 3rd edition, McGraw-Hill, New York, 1979, pp. 53-79.

95. Holman, J. P., Experimental Methods for Engineers, 3rd edition, McGraw-Hill, New York, 1978, pp. 44-51.

96. Sampson, R. J., Surface II Graphics System, Kansas Geological Survey, Lawrence, Kansas, 1978.

97. Fitts, D. O., "A Study of Two- and Three-Dimensional Turbulent Boundary Layer Data Sets Using Momentum Integral Techniques," Thesis, Mechanical Engineering, Virginia Polytechnic Institute and State University, Blacksburg, Virginia, March, 1982.

98. Townsend, A. A., The Structure of Turbulent Shear Flow, 2nd edition, Cambridge University Press, Cambridge, England, 1976, pp. 328-333.

99. McAllister, J. E., "Near-Wall Similarity in Two- and Three-Dimensional Turbulent Boundary Layers," Dissertation, Mechanical Engineering, Virginia Polytechnic Institute and State University, Blacksburg, Virginia, December, 1979.

100. Schlicting, H., Boundary-Layer Theory, 7th edition, McGraw-Hill, New York, 1979, pp. 206-214.

101. Moses, H. L., "A Strip-Integral Method for Predicting the Behavior of Turbulent Boundary Layers," Computation of Turbulent Boundary Layers - 1968 AFOSR-IFP-Stanford Conference, Vol. I, Thermosciences Division, Department of Mechanical Engineering, Stanford University, Stanford, California, 1968, pp. 76-82.

APPENDIX A

Two-Dimensional Turbulent Boundary Layer Data

In this appendix:

BETA $\equiv \beta$,

SPEED $\equiv U/U_e$.

The estimated uncertainties are at the 5 percent significance level (95 percent confidence intervals or 19 to 1 odds).

Table A.1 Two-Dimensional Turbulent Boundary Layer Data at (x,z)=(0,-203 mm)

y, mm	BETA, deg	SPEED	y, mm	BETA, deg	SPEED	y, mm	BETA, deg	SPEED
0.51	0.0±0.8	0.474±0.009	5.33	-0.2±0.4	0.672±0.006	35.31	-0.2±0.2	0.876±0.005
0.56	-0.1±0.8	0.484±0.008	5.59	-0.2±0.4	0.676±0.006	37.85	-0.3±0.2	0.887±0.005
0.61	0.0±0.7	0.497±0.008	5.84	-0.1±0.4	0.678±0.006	40.39	-0.2±0.2	0.900±0.005
0.66	-0.1±0.7	0.506±0.008	6.10	-0.2±0.4	0.683±0.006	42.93	-0.2±0.2	0.911±0.005
0.71	-0.1±0.7	0.513±0.008	6.35	-0.2±0.4	0.682±0.006	45.47	-0.3±0.2	0.919±0.005
0.76	-0.1±0.7	0.517±0.008	6.60	-0.2±0.4	0.688±0.006	48.01	-0.3±0.2	0.930±0.005
0.81	-0.0±0.6	0.525±0.008	6.86	-0.2±0.4	0.694±0.006	50.55	-0.3±0.2	0.941±0.005
0.86	-0.1±0.6	0.527±0.008	7.11	-0.2±0.4	0.693±0.006	53.09	-0.3±0.2	0.949±0.005
0.91	-0.1±0.6	0.536±0.008	7.37	-0.2±0.4	0.698±0.006	55.63	-0.3±0.2	0.958±0.005
0.97	-0.1±0.6	0.537±0.008	7.87	-0.2±0.4	0.706±0.006	58.17	-0.2±0.2	0.963±0.005
1.02	-0.1±0.6	0.543±0.008	8.38	-0.2±0.3	0.710±0.006	60.71	-0.2±0.2	0.971±0.005
1.14	-0.1±0.6	0.550±0.007	8.89	-0.2±0.3	0.715±0.006	63.25	-0.3±0.2	0.977±0.005
1.27	-0.1±0.6	0.555±0.007	9.40	-0.2±0.3	0.720±0.006	65.79	-0.2±0.2	0.982±0.005
1.40	-0.1±0.6	0.563±0.007	9.91	-0.2±0.3	0.729±0.006	68.33	-0.2±0.2	0.987±0.005
1.52	-0.1±0.5	0.570±0.007	10.41	-0.2±0.3	0.731±0.006	70.87	-0.2±0.2	0.989±0.005
1.65	-0.1±0.5	0.579±0.007	10.92	-0.2±0.3	0.733±0.006	73.41	-0.2±0.2	0.994±0.005
1.78	-0.2±0.5	0.583±0.007	11.43	-0.2±0.3	0.739±0.006	75.95	-0.2±0.2	0.996±0.005
1.90	-0.1±0.5	0.591±0.007	11.94	-0.2±0.3	0.744±0.006	78.49	-0.1±0.2	0.999±0.005
2.03	-0.1±0.5	0.596±0.007	12.45	-0.2±0.3	0.745±0.006	81.03	-0.1±0.2	0.999±0.005
2.16	-0.2±0.5	0.597±0.007	13.72	-0.2±0.3	0.756±0.006	83.57	-0.1±0.2	0.999±0.005
2.29	-0.2±0.5	0.603±0.007	14.99	-0.2±0.3	0.763±0.006	86.11	-0.1±0.2	1.000±0.005
2.54	-0.1±0.5	0.613±0.007	16.26	-0.2±0.3	0.777±0.006	88.65	-0.1±0.2	1.001±0.005
2.79	-0.1±0.5	0.618±0.007	17.53	-0.2±0.3	0.782±0.006	93.73	-0.1±0.2	1.000±0.005
3.05	-0.2±0.4	0.627±0.007	18.80	-0.2±0.3	0.789±0.006	98.81	-0.0±0.2	1.000±0.005
3.30	-0.1±0.4	0.630±0.007	20.07	-0.2±0.3	0.797±0.006	103.89	-0.0±0.2	1.001±0.005
3.56	-0.1±0.4	0.639±0.007	21.34	-0.2±0.3	0.806±0.006	108.97	0.0±0.2	1.000±0.005
3.81	-0.1±0.4	0.646±0.007	22.61	-0.2±0.3	0.812±0.006	114.05	0.0±0.2	1.000±0.005
4.06	-0.2±0.4	0.648±0.007	23.88	-0.2±0.3	0.819±0.005	119.13	-0.0±0.2	1.000±0.005
4.32	-0.1±0.4	0.657±0.006	25.15	-0.2±0.3	0.828±0.005	124.21	-0.0±0.2	1.000±0.005
4.57	-0.2±0.4	0.658±0.006	27.69	-0.2±0.2	0.840±0.005	129.29	-0.0±0.2	1.000±0.005
4.83	-0.2±0.4	0.666±0.006	30.23	-0.2±0.2	0.855±0.005	134.37	0.0±0.2	0.999±0.005
5.08	-0.2±0.4	0.666±0.006	32.77	-0.3±0.2	0.866±0.005	139.45	0.0±0.2	1.000±0.005

Table A.2 Two-Dimensional Turbulent Boundary Layer Data at (x,z)=(0,-152 mm)

y, mm	BETA, deg	SPEED	y, mm	BETA, deg	SPEED	y, mm	BETA, deg	SPEED
0.51	0.3±0.7	0.489±0.008	5.33	0.1±0.4	0.688±0.006	35.31	-0.2±0.2	0.887±0.005
0.56	0.2±0.7	0.503±0.008	5.59	0.1±0.4	0.691±0.006	37.85	-0.2±0.2	0.900±0.005
0.61	0.2±0.7	0.511±0.008	5.84	0.1±0.4	0.692±0.006	40.39	-0.3±0.2	0.908±0.005
0.66	0.3±0.7	0.517±0.008	6.10	0.1±0.4	0.699±0.006	42.93	-0.2±0.2	0.918±0.005
0.71	0.2±0.6	0.524±0.008	6.35	0.1±0.4	0.703±0.006	45.47	-0.2±0.2	0.927±0.005
0.76	0.2±0.6	0.531±0.008	6.60	0.1±0.4	0.707±0.006	48.01	-0.3±0.2	0.937±0.005
0.81	0.3±0.6	0.536±0.008	6.86	0.0±0.4	0.708±0.006	50.55	-0.3±0.2	0.945±0.005
0.86	0.2±0.6	0.542±0.008	7.11	0.0±0.3	0.711±0.006	53.09	-0.3±0.2	0.954±0.005
0.91	0.2±0.6	0.545±0.008	7.37	0.0±0.3	0.714±0.006	55.63	-0.2±0.2	0.963±0.005
0.97	0.3±0.6	0.549±0.008	7.87	0.0±0.3	0.720±0.006	58.17	-0.3±0.2	0.967±0.005
1.02	0.2±0.6	0.552±0.007	8.38	0.0±0.3	0.727±0.006	60.71	-0.3±0.2	0.973±0.005
1.14	0.2±0.6	0.560±0.007	8.89	-0.0±0.3	0.730±0.006	63.25	-0.3±0.2	0.979±0.005
1.27	0.2±0.5	0.570±0.007	9.40	0.0±0.3	0.735±0.006	65.79	-0.2±0.2	0.986±0.005
1.40	0.2±0.5	0.578±0.007	9.91	0.0±0.3	0.742±0.006	68.33	-0.2±0.2	0.989±0.005
1.52	0.2±0.5	0.587±0.007	10.41	-0.0±0.3	0.744±0.006	70.87	-0.2±0.2	0.993±0.005
1.65	0.2±0.5	0.591±0.007	10.92	-0.0±0.3	0.748±0.006	73.41	-0.2±0.2	0.995±0.005
1.78	0.2±0.5	0.598±0.007	11.43	-0.0±0.3	0.755±0.006	75.95	-0.2±0.2	0.998±0.005
1.90	0.2±0.5	0.601±0.007	11.94	-0.0±0.3	0.760±0.006	78.49	-0.2±0.2	0.999±0.005
2.03	0.2±0.5	0.608±0.007	12.45	-0.1±0.3	0.763±0.006	81.03	-0.2±0.2	1.000±0.005
2.16	0.2±0.5	0.612±0.007	13.72	-0.1±0.3	0.773±0.006	83.57	-0.2±0.2	1.000±0.005
2.29	0.2±0.5	0.616±0.007	14.99	-0.1±0.3	0.782±0.006	86.11	-0.2±0.2	1.000±0.005
2.54	0.2±0.5	0.623±0.007	16.26	-0.1±0.3	0.786±0.006	88.65	-0.2±0.2	1.000±0.005
2.79	0.2±0.4	0.632±0.007	17.53	-0.1±0.3	0.797±0.006	93.73	-0.1±0.2	1.000±0.005
3.05	0.2±0.4	0.641±0.007	18.80	-0.1±0.3	0.807±0.006	98.81	-0.1±0.2	1.000±0.005
3.30	0.1±0.4	0.645±0.007	20.07	-0.1±0.3	0.814±0.006	103.89	-0.1±0.2	1.000±0.005
3.56	0.1±0.4	0.654±0.006	21.34	-0.2±0.3	0.821±0.005	108.97	-0.1±0.2	1.000±0.005
3.81	0.1±0.4	0.658±0.006	22.61	-0.2±0.3	0.828±0.005	114.05	-0.0±0.2	1.000±0.005
4.06	0.2±0.4	0.665±0.006	23.88	-0.2±0.3	0.833±0.005	119.13	-0.0±0.2	1.000±0.005
4.32	0.1±0.4	0.668±0.006	25.15	-0.2±0.2	0.840±0.005	124.21	0.0±0.2	0.999±0.005
4.57	0.2±0.4	0.674±0.006	27.69	-0.2±0.2	0.854±0.005	129.29	0.1±0.2	1.000±0.005
4.83	0.1±0.4	0.676±0.006	30.23	-0.2±0.2	0.865±0.005	134.37	0.1±0.2	1.000±0.005
5.08	0.1±0.4	0.681±0.006	32.77	-0.3±0.2	0.877±0.005	139.45	0.1±0.2	1.000±0.005

Table A.3 Two-Dimensional Turbulent Boundary Layer Data at (x,z)=(0,-102 mm)

y, mm	BETA, deg	SPEED	y, mm	BETA, deg	SPEED	y, mm	BETA, deg	SPEED
0.51	0.4±0.8	0.474±0.009	5.33	0.2±0.4	0.666±0.006	35.31	-0.1±0.2	0.871±0.005
0.56	0.5±0.8	0.483±0.009	5.59	0.1±0.4	0.669±0.006	37.85	-0.1±0.2	0.881±0.005
0.61	0.5±0.7	0.493±0.008	5.84	0.2±0.4	0.672±0.006	40.39	-0.1±0.2	0.892±0.005
0.66	0.4±0.7	0.500±0.008	6.10	0.2±0.4	0.675±0.006	42.93	-0.1±0.2	0.903±0.005
0.71	0.3±0.7	0.511±0.008	6.35	0.2±0.4	0.681±0.006	45.47	-0.1±0.2	0.913±0.005
0.76	0.4±0.7	0.514±0.008	6.60	0.2±0.4	0.684±0.006	48.01	-0.1±0.2	0.923±0.005
0.81	0.4±0.7	0.518±0.008	6.86	0.2±0.4	0.683±0.006	50.55	-0.1±0.2	0.931±0.005
0.86	0.4±0.6	0.523±0.008	7.11	0.2±0.4	0.687±0.006	53.09	-0.1±0.2	0.939±0.005
0.91	0.4±0.6	0.528±0.008	7.37	0.2±0.4	0.691±0.006	55.63	-0.1±0.2	0.949±0.005
0.97	0.4±0.6	0.533±0.008	7.87	0.2±0.4	0.698±0.006	58.17	-0.1±0.2	0.956±0.005
1.02	0.4±0.6	0.537±0.008	8.38	0.1±0.4	0.704±0.006	60.71	-0.2±0.2	0.965±0.005
1.14	0.4±0.6	0.547±0.008	8.89	0.2±0.4	0.707±0.006	63.25	-0.2±0.2	0.970±0.005
1.27	0.3±0.6	0.552±0.008	9.40	0.1±0.3	0.713±0.006	65.79	-0.2±0.2	0.975±0.005
1.40	0.3±0.6	0.561±0.007	9.91	0.1±0.3	0.717±0.006	68.33	-0.1±0.2	0.981±0.005
1.52	0.4±0.6	0.565±0.007	10.41	0.1±0.3	0.723±0.006	70.87	-0.2±0.2	0.987±0.005
1.65	0.4±0.5	0.573±0.007	10.92	0.1±0.3	0.729±0.006	73.41	-0.1±0.2	0.989±0.005
1.78	0.3±0.5	0.579±0.007	11.43	0.1±0.3	0.732±0.006	75.95	-0.1±0.2	0.992±0.005
1.90	0.3±0.5	0.586±0.007	11.94	0.1±0.3	0.734±0.006	78.49	-0.1±0.2	0.994±0.005
2.03	0.3±0.5	0.589±0.007	12.45	0.1±0.3	0.739±0.006	81.03	-0.1±0.2	0.996±0.005
2.16	0.3±0.5	0.593±0.007	13.72	0.0±0.3	0.747±0.006	83.57	-0.1±0.2	0.998±0.005
2.29	0.3±0.5	0.598±0.007	14.99	-0.0±0.3	0.756±0.006	86.11	-0.0±0.2	0.998±0.005
2.54	0.3±0.5	0.608±0.007	16.26	0.0±0.3	0.769±0.006	88.65	-0.0±0.2	1.000±0.005
2.79	0.4±0.5	0.613±0.007	17.53	0.0±0.3	0.772±0.006	93.73	-0.0±0.2	1.001±0.005
3.05	0.3±0.5	0.620±0.007	18.80	-0.0±0.3	0.784±0.006	98.81	-0.0±0.2	1.000±0.005
3.30	0.3±0.5	0.623±0.007	20.07	-0.0±0.3	0.788±0.006	103.89	0.0±0.2	1.001±0.005
3.56	0.3±0.4	0.632±0.007	21.34	-0.0±0.3	0.797±0.006	108.97	0.0±0.2	1.001±0.005
3.81	0.3±0.4	0.638±0.007	22.61	-0.0±0.3	0.807±0.006	114.05	0.0±0.2	1.000±0.005
4.06	0.2±0.4	0.646±0.007	23.88	-0.1±0.3	0.813±0.006	119.13	0.0±0.2	1.000±0.005
4.32	0.2±0.4	0.649±0.007	25.15	-0.1±0.3	0.820±0.006	124.21	0.0±0.2	0.999±0.005
4.57	0.3±0.4	0.653±0.007	27.69	-0.1±0.3	0.833±0.005	129.29	0.0±0.2	1.000±0.005
4.83	0.2±0.4	0.657±0.006	30.23	-0.1±0.2	0.845±0.005	134.37	-0.0±0.2	1.000±0.005
5.08	0.2±0.4	0.662±0.006	32.77	-0.1±0.2	0.859±0.005	139.45	-0.0±0.2	0.999±0.005

Table A.4 Two-Dimensional Turbulent Boundary Layer Data at (x,z)=(0,-51 mm)

y, mm	BETA, deg	SPEED	y, mm	BETA, deg	SPEED	y, mm	BETA, deg	SPEED
0.51	0.5±0.8	0.475±0.009	5.33	0.4±0.4	0.668±0.006	35.31	-0.0±0.2	0.872±0.005
0.56	0.5±0.8	0.485±0.008	5.59	0.4±0.4	0.672±0.006	37.85	-0.0±0.2	0.880±0.005
0.61	0.5±0.7	0.494±0.008	5.84	0.4±0.4	0.674±0.006	40.39	-0.0±0.2	0.891±0.005
0.66	0.6±0.7	0.504±0.008	6.10	0.4±0.4	0.678±0.006	42.93	-0.0±0.2	0.902±0.005
0.71	0.5±0.7	0.510±0.008	6.35	0.4±0.4	0.678±0.006	45.47	-0.0±0.2	0.910±0.005
0.76	0.5±0.7	0.516±0.008	6.60	0.4±0.4	0.682±0.006	48.01	-0.0±0.2	0.920±0.005
0.81	0.5±0.7	0.521±0.008	6.86	0.3±0.4	0.686±0.006	50.55	-0.0±0.2	0.927±0.005
0.86	0.5±0.6	0.524±0.008	7.11	0.3±0.4	0.690±0.006	53.09	-0.0±0.2	0.935±0.005
0.91	0.5±0.6	0.530±0.008	7.37	0.3±0.4	0.694±0.006	55.63	-0.0±0.2	0.946±0.005
0.97	0.5±0.6	0.534±0.008	7.87	0.3±0.4	0.698±0.006	58.17	-0.0±0.2	0.953±0.005
1.02	0.5±0.6	0.539±0.008	8.38	0.3±0.4	0.706±0.006	60.71	0.0±0.2	0.960±0.005
1.14	0.5±0.6	0.545±0.008	8.89	0.3±0.4	0.708±0.006	63.25	0.0±0.2	0.966±0.005
1.27	0.5±0.6	0.553±0.007	9.40	0.3±0.3	0.714±0.006	65.79	0.0±0.2	0.971±0.005
1.40	0.5±0.6	0.562±0.007	9.91	0.3±0.3	0.720±0.006	68.33	0.0±0.2	0.980±0.005
1.52	0.5±0.6	0.564±0.007	10.41	0.3±0.3	0.724±0.006	70.87	0.1±0.2	0.983±0.005
1.65	0.5±0.5	0.574±0.007	10.92	0.2±0.3	0.730±0.006	73.41	0.1±0.2	0.987±0.005
1.78	0.5±0.5	0.579±0.007	11.43	0.2±0.3	0.733±0.006	75.95	0.1±0.2	0.991±0.005
1.90	0.5±0.5	0.585±0.007	11.94	0.2±0.3	0.736±0.006	78.49	0.1±0.2	0.994±0.005
2.03	0.5±0.5	0.589±0.007	12.45	0.2±0.3	0.739±0.006	81.03	0.1±0.2	0.996±0.005
2.16	0.5±0.5	0.591±0.007	13.72	0.2±0.3	0.751±0.006	83.57	0.1±0.2	0.998±0.005
2.29	0.5±0.5	0.597±0.007	14.99	0.2±0.3	0.760±0.006	86.11	0.1±0.2	1.000±0.005
2.54	0.5±0.5	0.607±0.007	16.26	0.2±0.3	0.769±0.006	88.65	0.1±0.2	1.000±0.005
2.79	0.5±0.5	0.615±0.007	17.53	0.1±0.3	0.778±0.006	93.73	0.1±0.2	1.000±0.005
3.05	0.5±0.5	0.621±0.007	18.80	0.1±0.3	0.784±0.006	98.81	0.1±0.2	1.000±0.005
3.30	0.5±0.5	0.626±0.007	20.07	0.1±0.3	0.790±0.006	103.89	0.1±0.2	1.000±0.005
3.56	0.5±0.4	0.632±0.007	21.34	0.1±0.3	0.798±0.006	108.97	0.1±0.2	1.000±0.005
3.81	0.5±0.4	0.638±0.007	22.61	0.1±0.3	0.806±0.006	114.05	0.1±0.2	1.000±0.005
4.06	0.5±0.4	0.644±0.007	23.88	0.0±0.3	0.814±0.006	119.13	0.1±0.2	1.000±0.005
4.32	0.4±0.4	0.648±0.007	25.15	0.0±0.3	0.819±0.005	124.21	0.1±0.2	1.000±0.005
4.57	0.5±0.4	0.653±0.006	27.69	0.0±0.3	0.834±0.005	129.29	0.0±0.2	1.000±0.005
4.83	0.4±0.4	0.657±0.006	30.23	0.0±0.2	0.846±0.005	134.37	0.0±0.2	1.000±0.005
5.08	0.4±0.4	0.663±0.006	32.77	0.0±0.2	0.860±0.005	139.45	0.0±0.2	1.000±0.005

Table A.5 Two-Dimensional Turbulent Boundary Layer Data at (x,z)=(0,0)

y, mm	BETA, deg	SPEED	y, mm	BETA, deg	SPEED	y, mm	BETA, deg	SPEED
0.51	0.4±0.9	0.455±0.009	5.33	0.3±0.4	0.639±0.007	35.31	0.3±0.3	0.840±0.005
0.56	0.4±0.8	0.467±0.009	5.59	0.2±0.4	0.643±0.007	37.85	0.2±0.2	0.857±0.005
0.61	0.4±0.8	0.473±0.009	5.84	0.4±0.4	0.646±0.007	40.39	0.2±0.2	0.867±0.005
0.66	0.5±0.8	0.483±0.009	6.10	0.4±0.4	0.650±0.007	42.93	0.2±0.2	0.876±0.005
0.71	0.4±0.7	0.488±0.008	6.35	0.4±0.4	0.654±0.006	45.47	0.2±0.2	0.885±0.005
0.76	0.5±0.7	0.492±0.008	6.60	0.2±0.4	0.659±0.006	48.01	0.2±0.2	0.896±0.005
0.81	0.4±0.7	0.503±0.008	6.86	0.4±0.4	0.660±0.006	50.55	0.2±0.2	0.907±0.005
0.86	0.2±0.7	0.505±0.008	7.11	0.3±0.4	0.661±0.006	53.09	0.2±0.2	0.922±0.005
0.91	0.6±0.7	0.511±0.008	7.37	0.3±0.4	0.669±0.006	55.63	0.2±0.2	0.925±0.005
0.97	0.4±0.7	0.511±0.008	7.87	0.3±0.4	0.671±0.006	58.17	0.2±0.2	0.935±0.005
1.02	0.4±0.7	0.518±0.008	8.38	0.5±0.4	0.676±0.006	60.71	0.2±0.2	0.943±0.005
1.14	0.3±0.6	0.525±0.008	8.89	0.3±0.4	0.679±0.006	63.25	0.2±0.2	0.948±0.005
1.27	0.3±0.6	0.530±0.008	9.40	0.2±0.4	0.682±0.006	65.79	0.1±0.2	0.961±0.005
1.40	0.4±0.6	0.536±0.008	9.91	0.3±0.4	0.689±0.006	68.33	0.1±0.2	0.966±0.005
1.52	0.5±0.6	0.545±0.008	10.41	0.4±0.4	0.696±0.006	70.87	0.1±0.2	0.970±0.005
1.65	0.4±0.6	0.549±0.008	10.92	0.3±0.4	0.696±0.006	73.41	0.1±0.2	0.978±0.005
1.78	0.4±0.6	0.552±0.008	11.43	0.3±0.4	0.704±0.006	75.95	0.1±0.2	0.983±0.005
1.90	0.5±0.6	0.557±0.007	11.94	0.3±0.4	0.707±0.006	78.49	0.1±0.2	0.988±0.005
2.03	0.4±0.6	0.562±0.007	12.45	0.3±0.4	0.709±0.006	81.03	0.1±0.2	0.991±0.005
2.16	0.4±0.5	0.570±0.007	13.72	0.3±0.3	0.722±0.006	83.57	0.0±0.2	0.994±0.005
2.29	0.3±0.5	0.576±0.007	14.99	0.4±0.3	0.730±0.006	86.11	0.0±0.2	0.993±0.005
2.54	0.3±0.5	0.579±0.007	16.26	0.3±0.3	0.739±0.006	88.65	0.0±0.2	0.997±0.005
2.79	0.6±0.5	0.586±0.007	17.53	0.3±0.3	0.748±0.006	93.73	0.1±0.2	0.999±0.005
3.05	0.4±0.5	0.592±0.007	18.80	0.3±0.3	0.757±0.006	98.81	0.1±0.2	1.000±0.005
3.30	0.4±0.5	0.603±0.007	20.07	0.3±0.3	0.763±0.006	103.89	0.2±0.2	1.000±0.005
3.56	0.4±0.5	0.609±0.007	21.34	0.3±0.3	0.774±0.006	108.97	0.2±0.2	1.000±0.005
3.81	0.4±0.5	0.615±0.007	22.61	0.3±0.3	0.779±0.006	114.05	0.2±0.2	1.000±0.005
4.06	0.5±0.5	0.617±0.007	23.88	0.3±0.3	0.784±0.006	119.13	0.1±0.2	1.001±0.005
4.32	0.3±0.5	0.619±0.007	25.15	0.3±0.3	0.790±0.006	124.21	0.0±0.2	1.000±0.005
4.57	0.5±0.5	0.626±0.007	27.69	0.3±0.3	0.801±0.006	129.29	-0.0±0.2	1.000±0.005
4.83	0.2±0.5	0.626±0.007	30.23	0.3±0.3	0.821±0.005	134.37	-0.1±0.2	1.000±0.005
5.08	0.3±0.4	0.635±0.007	32.77	0.3±0.3	0.832±0.005	139.45	-0.1±0.2	0.999±0.005

Table A.6 Two-Dimensional Turbulent Boundary Layer Data at (x,z)=(0,51 mm)

y, mm	BETA, deg	SPEED	y, mm	BETA, deg	SPEED	y, mm	BETA, deg	SPEED
0.51	1.1±0.8	0.479±0.009	5.33	0.9±0.4	0.672±0.006	35.31	0.3±0.2	0.883±0.005
0.56	1.1±0.7	0.493±0.008	5.59	0.8±0.4	0.674±0.006	37.85	0.3±0.2	0.894±0.005
0.61	1.1±0.7	0.490±0.008	5.84	0.8±0.4	0.677±0.006	40.39	0.3±0.2	0.900±0.005
0.66	1.0±0.7	0.509±0.008	6.10	0.9±0.4	0.686±0.006	42.93	0.2±0.2	0.905±0.005
0.71	1.1±0.7	0.516±0.008	6.35	0.9±0.4	0.695±0.006	45.47	0.2±0.2	0.921±0.005
0.76	1.0±0.6	0.523±0.008	6.60	0.8±0.4	0.687±0.006	48.01	0.1±0.2	0.934±0.005
0.81	1.0±0.6	0.528±0.008	6.86	0.9±0.4	0.708±0.006	50.55	0.1±0.2	0.933±0.005
0.86	1.0±0.6	0.533±0.008	7.11	0.8±0.4	0.695±0.006	53.09	0.1±0.2	0.955±0.005
0.91	1.0±0.6	0.535±0.008	7.37	0.8±0.4	0.704±0.006	55.63	0.2±0.2	0.956±0.005
0.97	1.0±0.6	0.541±0.008	7.87	0.9±0.3	0.714±0.006	58.17	0.1±0.2	0.959±0.005
1.02	1.1±0.6	0.545±0.008	8.38	0.7±0.4	0.710±0.006	60.71	0.1±0.2	0.970±0.005
1.14	1.0±0.6	0.549±0.008	8.89	0.8±0.3	0.715±0.006	63.25	0.1±0.2	0.971±0.005
1.27	0.9±0.6	0.556±0.007	9.40	0.8±0.3	0.730±0.006	65.79	0.2±0.2	0.980±0.005
1.40	1.0±0.5	0.573±0.007	9.91	0.7±0.3	0.730±0.006	68.33	0.1±0.2	0.988±0.005
1.52	1.0±0.5	0.570±0.007	10.41	0.7±0.3	0.734±0.006	70.87	0.1±0.2	0.985±0.005
1.65	1.0±0.5	0.578±0.007	10.92	0.8±0.3	0.737±0.006	73.41	0.1±0.2	0.991±0.005
1.78	1.0±0.5	0.580±0.007	11.43	0.7±0.3	0.741±0.006	75.95	0.1±0.2	0.994±0.005
1.90	1.0±0.5	0.588±0.007	11.94	0.7±0.3	0.746±0.006	78.49	0.1±0.2	0.995±0.005
2.03	1.0±0.5	0.596±0.007	12.45	0.6±0.3	0.745±0.006	81.03	0.1±0.2	0.998±0.005
2.16	0.9±0.5	0.606±0.007	13.72	0.7±0.3	0.758±0.006	83.57	0.0±0.2	0.997±0.005
2.29	1.0±0.5	0.603±0.007	14.99	0.7±0.3	0.763±0.006	86.11	0.1±0.2	0.999±0.005
2.54	0.9±0.5	0.610±0.007	16.26	0.6±0.3	0.772±0.006	88.65	0.1±0.2	0.999±0.005
2.79	0.9±0.5	0.626±0.007	17.53	0.5±0.3	0.789±0.006	93.73	0.1±0.2	1.000±0.005
3.05	0.9±0.5	0.622±0.007	18.80	0.5±0.3	0.793±0.006	98.81	0.1±0.2	1.000±0.005
3.30	1.0±0.5	0.625±0.007	20.07	0.5±0.3	0.792±0.006	103.89	0.1±0.2	1.000±0.005
3.56	0.9±0.4	0.637±0.007	21.34	0.5±0.3	0.805±0.006	108.97	0.1±0.2	1.000±0.005
3.81	0.9±0.4	0.649±0.007	22.61	0.5±0.3	0.816±0.006	114.05	0.1±0.2	1.001±0.005
4.06	0.9±0.4	0.648±0.007	23.88	0.5±0.3	0.822±0.005	119.13	0.0±0.2	1.000±0.005
4.32	0.9±0.4	0.659±0.006	25.15	0.4±0.3	0.818±0.006	124.21	0.0±0.2	1.000±0.005
4.57	0.9±0.4	0.658±0.006	27.69	0.3±0.3	0.839±0.005	129.29	-0.0±0.2	1.000±0.005
4.83	0.8±0.4	0.665±0.006	30.23	0.4±0.2	0.854±0.005	134.37	-0.1±0.2	0.999±0.005
5.08	0.9±0.4	0.669±0.006	32.77	0.3±0.2	0.867±0.005	139.45	-0.1±0.2	1.000±0.005

Table A.7 Two-Dimensional Turbulent Boundary Layer Data at (x,z)=(0,102 mm)

y, mm	BETA, deg	SPEED	y, mm	BETA, deg	SPEED	y, mm	BETA, deg	SPEED
0.51	0.4±0.8	0.476±0.009	5.33	0.2±0.4	0.675±0.006	35.31	0.3±0.2	0.885±0.005
0.56	0.4±0.8	0.488±0.009	5.59	0.3±0.4	0.677±0.006	37.85	0.3±0.2	0.894±0.005
0.61	0.4±0.7	0.497±0.008	5.84	0.2±0.4	0.680±0.006	40.39	0.4±0.2	0.905±0.005
0.66	0.4±0.7	0.506±0.008	6.10	0.3±0.4	0.685±0.006	42.93	0.3±0.2	0.915±0.005
0.71	0.5±0.7	0.513±0.008	6.35	0.3±0.4	0.688±0.006	45.47	0.3±0.2	0.925±0.005
0.76	0.3±0.7	0.521±0.008	6.60	0.3±0.4	0.690±0.006	48.01	0.3±0.2	0.935±0.005
0.81	0.4±0.7	0.522±0.008	6.86	0.3±0.4	0.694±0.006	50.55	0.2±0.2	0.946±0.005
0.86	0.5±0.6	0.528±0.008	7.11	0.3±0.4	0.695±0.006	53.09	0.2±0.2	0.955±0.005
0.91	0.4±0.6	0.534±0.008	7.37	0.2±0.4	0.699±0.006	55.63	0.2±0.2	0.961±0.005
0.97	0.4±0.6	0.543±0.008	7.87	0.3±0.4	0.708±0.006	58.17	0.2±0.2	0.970±0.005
1.02	0.3±0.6	0.545±0.008	8.38	0.3±0.4	0.713±0.006	60.71	0.1±0.2	0.974±0.005
1.14	0.3±0.6	0.549±0.008	8.89	0.3±0.4	0.715±0.006	63.25	0.1±0.2	0.981±0.005
1.27	0.4±0.6	0.557±0.008	9.40	0.3±0.3	0.720±0.006	65.79	0.1±0.2	0.984±0.005
1.40	0.3±0.6	0.563±0.007	9.91	0.3±0.3	0.729±0.006	68.33	0.0±0.2	0.992±0.005
1.52	0.3±0.5	0.573±0.007	10.41	0.3±0.3	0.731±0.006	70.87	0.0±0.2	0.994±0.005
1.65	0.3±0.5	0.579±0.007	10.92	0.3±0.3	0.736±0.006	73.41	0.1±0.2	0.996±0.005
1.78	0.3±0.5	0.584±0.007	11.43	0.3±0.3	0.740±0.006	75.95	0.1±0.2	0.997±0.005
1.90	0.2±0.5	0.590±0.007	11.94	0.3±0.3	0.743±0.006	78.49	0.1±0.2	0.999±0.005
2.03	0.2±0.5	0.593±0.007	12.45	0.3±0.3	0.746±0.006	81.03	0.1±0.2	0.999±0.005
2.16	0.3±0.5	0.595±0.007	13.72	0.3±0.3	0.760±0.006	83.57	0.1±0.2	0.999±0.005
2.29	0.3±0.5	0.605±0.007	14.99	0.3±0.3	0.768±0.006	86.11	0.1±0.2	1.001±0.005
2.54	0.3±0.5	0.614±0.007	16.26	0.4±0.3	0.776±0.006	88.65	0.1±0.2	1.000±0.005
2.79	0.2±0.5	0.620±0.007	17.53	0.4±0.3	0.786±0.006	93.73	0.0±0.2	1.001±0.005
3.05	0.3±0.5	0.623±0.007	18.80	0.4±0.3	0.795±0.006	98.81	0.0±0.2	0.999±0.005
3.30	0.3±0.5	0.627±0.007	20.07	0.4±0.3	0.801±0.006	103.89	0.0±0.2	1.001±0.005
3.56	0.2±0.4	0.637±0.007	21.34	0.3±0.3	0.808±0.006	108.97	0.0±0.2	1.000±0.005
3.81	0.3±0.4	0.648±0.007	22.61	0.4±0.3	0.817±0.006	114.05	0.0±0.2	1.001±0.005
4.06	0.3±0.4	0.651±0.007	23.88	0.4±0.3	0.827±0.006	119.13	-0.0±0.2	1.000±0.005
4.32	0.3±0.4	0.657±0.007	25.15	0.4±0.3	0.829±0.006	124.21	-0.0±0.2	1.000±0.005
4.57	0.3±0.4	0.659±0.007	27.69	0.4±0.3	0.841±0.005	129.29	-0.0±0.2	1.000±0.005
4.83	0.3±0.4	0.665±0.006	30.23	0.4±0.2	0.862±0.005	134.37	-0.0±0.2	0.999±0.005
5.08	0.2±0.4	0.674±0.006	32.77	0.3±0.2	0.870±0.005	139.45	-0.0±0.2	0.999±0.005

Table A.8 Two-Dimensional Turbulent Boundary Layer Data at (x,z)=(0,152 mm)

y, mm	BETA, deg	SPEED	y, mm	BETA, deg	SPEED	y, mm	BETA, deg	SPEED
0.51	0.8±0.8	0.476±0.009	5.33	0.8±0.4	0.663±0.007	35.31	0.4±0.2	0.875±0.005
0.56	0.9±0.8	0.484±0.009	5.59	0.6±0.4	0.669±0.006	37.85	0.4±0.2	0.884±0.005
0.61	0.9±0.8	0.489±0.009	5.84	0.7±0.4	0.673±0.006	40.39	0.4±0.2	0.895±0.005
0.66	0.9±0.7	0.496±0.008	6.10	0.6±0.4	0.676±0.006	42.93	0.4±0.2	0.907±0.005
0.71	0.9±0.7	0.507±0.008	6.35	0.6±0.4	0.679±0.006	45.47	0.3±0.2	0.918±0.005
0.76	0.9±0.7	0.514±0.008	6.60	0.7±0.4	0.680±0.006	48.01	0.3±0.2	0.929±0.005
0.81	0.9±0.7	0.515±0.008	6.86	0.7±0.4	0.683±0.006	50.55	0.3±0.2	0.933±0.005
0.86	0.8±0.7	0.523±0.008	7.11	0.7±0.4	0.686±0.006	53.09	0.3±0.2	0.944±0.005
0.91	0.8±0.6	0.528±0.008	7.37	0.7±0.4	0.687±0.006	55.63	0.3±0.2	0.954±0.005
0.97	0.8±0.6	0.530±0.008	7.87	0.7±0.4	0.695±0.006	58.17	0.3±0.2	0.960±0.005
1.02	0.8±0.6	0.534±0.008	8.38	0.6±0.4	0.703±0.006	60.71	0.2±0.2	0.971±0.005
1.14	0.8±0.6	0.545±0.008	8.89	0.6±0.4	0.708±0.006	63.25	0.2±0.2	0.976±0.005
1.27	0.8±0.6	0.551±0.008	9.40	0.7±0.4	0.712±0.006	65.79	0.1±0.2	0.981±0.005
1.40	0.8±0.6	0.555±0.008	9.91	0.7±0.3	0.718±0.006	68.33	0.1±0.2	0.986±0.005
1.52	0.9±0.6	0.562±0.008	10.41	0.6±0.3	0.719±0.006	70.87	0.1±0.2	0.991±0.005
1.65	0.9±0.6	0.567±0.007	10.92	0.6±0.3	0.730±0.006	73.41	0.1±0.2	0.995±0.005
1.78	0.9±0.5	0.573±0.007	11.43	0.7±0.3	0.730±0.006	75.95	0.0±0.2	0.997±0.005
1.90	0.9±0.5	0.581±0.007	11.94	0.7±0.3	0.736±0.006	78.49	0.0±0.2	0.998±0.005
2.03	0.7±0.5	0.588±0.007	12.45	0.6±0.3	0.742±0.006	81.03	-0.0±0.2	0.999±0.005
2.16	0.8±0.5	0.593±0.007	13.72	0.6±0.3	0.748±0.006	83.57	-0.0±0.2	0.999±0.005
2.29	0.8±0.5	0.596±0.007	14.99	0.6±0.3	0.759±0.006	86.11	-0.0±0.2	0.999±0.005
2.54	0.8±0.5	0.604±0.007	16.26	0.5±0.3	0.771±0.006	88.65	-0.0±0.2	1.000±0.005
2.79	0.7±0.5	0.611±0.007	17.53	0.6±0.3	0.777±0.006	93.73	-0.1±0.2	1.000±0.005
3.05	0.8±0.5	0.619±0.007	18.80	0.5±0.3	0.785±0.006	98.81	-0.1±0.2	1.000±0.005
3.30	0.7±0.5	0.629±0.007	20.07	0.5±0.3	0.790±0.006	103.89	-0.1±0.2	1.000±0.005
3.56	0.7±0.5	0.631±0.007	21.34	0.5±0.3	0.799±0.006	108.97	-0.1±0.2	1.000±0.005
3.81	0.8±0.4	0.635±0.007	22.61	0.5±0.3	0.807±0.006	114.05	-0.1±0.2	1.000±0.005
4.06	0.7±0.4	0.640±0.007	23.88	0.5±0.3	0.818±0.006	119.13	-0.1±0.2	1.000±0.005
4.32	0.8±0.4	0.646±0.007	25.15	0.5±0.3	0.821±0.006	124.21	-0.1±0.2	1.000±0.005
4.57	0.7±0.4	0.653±0.007	27.69	0.5±0.3	0.839±0.005	129.29	-0.2±0.2	0.999±0.005
4.83	0.7±0.4	0.656±0.007	30.23	0.4±0.2	0.854±0.005	134.37	-0.1±0.2	1.000±0.005
5.08	0.7±0.4	0.658±0.007	32.77	0.4±0.2	0.866±0.005	139.45	-0.1±0.2	0.999±0.005

Table A.9 Two-Dimensional Turbulent Boundary Layer Data at (x,z)=(0,203 mm)

y, mm	BETA, deg	SPEED	y, mm	BETA, deg	SPEED	y, mm	BETA, deg	SPEED
0.51	0.9±0.8	0.482±0.009	5.33	0.8±0.4	0.677±0.006	35.31	0.5±0.2	0.885±0.005
0.56	1.0±0.8	0.491±0.009	5.59	0.8±0.4	0.680±0.006	37.85	0.5±0.2	0.893±0.005
0.61	0.9±0.7	0.498±0.008	5.84	0.8±0.4	0.677±0.006	40.39	0.5±0.2	0.908±0.005
0.66	0.9±0.7	0.503±0.008	6.10	0.8±0.4	0.685±0.006	42.93	0.5±0.2	0.916±0.005
0.71	1.0±0.7	0.515±0.008	6.35	0.8±0.4	0.685±0.006	45.47	0.4±0.2	0.926±0.005
0.76	1.0±0.7	0.521±0.008	6.60	0.8±0.4	0.691±0.006	48.01	0.4±0.2	0.934±0.005
0.81	0.9±0.6	0.528±0.008	6.86	0.8±0.4	0.690±0.006	50.55	0.4±0.2	0.945±0.005
0.86	1.0±0.6	0.528±0.008	7.11	0.8±0.4	0.697±0.006	53.09	0.4±0.2	0.951±0.005
0.91	0.9±0.6	0.533±0.008	7.37	0.8±0.4	0.702±0.006	55.63	0.3±0.2	0.960±0.005
0.97	0.9±0.6	0.538±0.008	7.87	0.8±0.4	0.707±0.006	58.17	0.3±0.2	0.967±0.005
1.02	0.9±0.6	0.543±0.008	8.38	0.8±0.4	0.716±0.006	60.71	0.3±0.2	0.974±0.005
1.14	0.9±0.6	0.551±0.008	8.89	0.9±0.3	0.720±0.006	63.25	0.2±0.2	0.979±0.005
1.27	0.9±0.6	0.557±0.008	9.40	0.8±0.3	0.720±0.006	65.79	0.2±0.2	0.985±0.005
1.40	0.9±0.6	0.564±0.008	9.91	0.8±0.3	0.729±0.006	68.33	0.2±0.2	0.991±0.005
1.52	0.9±0.6	0.569±0.007	10.41	0.8±0.3	0.734±0.006	70.87	0.2±0.2	0.993±0.005
1.65	0.9±0.5	0.576±0.007	10.92	0.8±0.3	0.736±0.006	73.41	0.1±0.2	0.996±0.005
1.78	1.0±0.5	0.583±0.007	11.43	0.8±0.3	0.741±0.006	75.95	0.1±0.2	0.998±0.005
1.90	0.9±0.5	0.589±0.007	11.94	0.8±0.3	0.742±0.006	78.49	0.1±0.2	0.999±0.005
2.03	0.8±0.5	0.595±0.007	12.45	0.7±0.3	0.746±0.006	81.03	0.1±0.2	0.999±0.005
2.16	0.8±0.5	0.599±0.007	13.72	0.8±0.3	0.758±0.006	83.57	0.1±0.2	1.000±0.005
2.29	0.8±0.5	0.607±0.007	14.99	0.7±0.3	0.767±0.006	86.11	0.1±0.2	1.000±0.005
2.54	0.8±0.5	0.615±0.007	16.26	0.8±0.3	0.775±0.006	88.65	0.0±0.2	1.000±0.005
2.79	0.8±0.5	0.624±0.007	17.53	0.7±0.3	0.787±0.006	93.73	0.0±0.2	1.001±0.005
3.05	0.9±0.5	0.625±0.007	18.80	0.8±0.3	0.793±0.006	98.81	0.0±0.2	1.000±0.005
3.30	0.8±0.5	0.630±0.007	20.07	0.7±0.3	0.799±0.006	103.89	-0.0±0.2	1.001±0.005
3.56	0.9±0.4	0.645±0.007	21.34	0.7±0.3	0.806±0.006	108.97	-0.0±0.2	1.000±0.005
3.81	0.8±0.4	0.645±0.007	22.61	0.6±0.3	0.817±0.006	114.05	-0.0±0.2	1.000±0.005
4.06	0.8±0.4	0.652±0.007	23.88	0.6±0.3	0.824±0.006	119.13	-0.1±0.2	1.000±0.005
4.32	0.9±0.4	0.656±0.007	25.15	0.6±0.3	0.828±0.006	124.21	-0.1±0.2	1.000±0.005
4.57	0.9±0.4	0.657±0.007	27.69	0.6±0.3	0.841±0.005	129.29	-0.1±0.2	1.000±0.005
4.83	0.8±0.4	0.666±0.007	30.23	0.6±0.2	0.854±0.005	134.37	-0.2±0.2	1.000±0.005
5.08	0.8±0.4	0.670±0.006	32.77	0.5±0.2	0.878±0.005	139.45	-0.2±0.2	1.000±0.005

APPENDIX B

Surface Pressure Data

In this appendix:

$$CP \equiv C_p \quad .$$

The estimated uncertainties are at the 5 percent significance level (95 percent confidence intervals or 19 to 1 odds).

Table B.1 Pressure Coefficient Data on the Side of the Bluff Body

x, mm	y, mm	CP	x, mm	y, mm	CP
0	176	-0.03±0.005	0	47	-0.22±0.005
13	176	-1.39±0.009	13	47	-1.45±0.009
25	176	-2.35±0.013	25	47	-2.36±0.013
38	176	-2.97±0.016	38	47	-2.94±0.016
51	176	-3.19±0.017	51	47	-3.18±0.017
64	176	-3.63±0.020	64	47	-3.68±0.020
76	176	-2.53±0.014	76	47	-2.64±0.015
90	176	-2.04±0.012	90	47	-2.09±0.012
119	176	-1.57±0.009	119	47	-1.63±0.010
149	176	-1.40±0.009	149	47	-1.43±0.009
179	176	-1.30±0.008	179	47	-1.31±0.008
209	176	-1.23±0.008	209	47	-1.20±0.008
239	176	-1.14±0.007	239	47	-1.11±0.007
0	118	-0.01±0.005	0	24	-0.40±0.005
13	118	-1.45±0.009	13	24	-1.48±0.009
25	118	-2.51±0.014	25	24	-2.28±0.013
38	118	-3.15±0.017	38	24	-2.81±0.015
51	118	-3.39±0.018	51	24	-2.99±0.016
64	118	-3.88±0.021	64	24	-2.97±0.016
76	118	-2.69±0.015	76	24	-2.48±0.014
90	118	-2.15±0.012	90	24	-1.99±0.011
119	118	-1.64±0.010	119	24	-1.60±0.010
149	118	-1.43±0.009	149	24	-1.41±0.009
179	118	-1.30±0.008	179	24	-1.30±0.008
209	118	-1.19±0.008	209	24	-1.19±0.008
239	118	-1.10±0.007	239	24	-1.11±0.007
0	59	-0.14±0.005	0	12	-0.41±0.005
13	59	-1.45±0.009	13	12	-1.42±0.009
25	59	-2.41±0.013	25	12	-2.18±0.012
38	59	-2.99±0.016	38	12	-2.67±0.015
51	59	-3.26±0.018	51	12	-2.86±0.016
64	59	-3.81±0.021	64	12	-2.74±0.015
76	59	-2.66±0.015	76	12	-2.39±0.013
90	59	-2.11±0.012	90	12	-1.95±0.011
119	59	-1.64±0.010	119	12	-1.60±0.009
149	59	-1.43±0.009	149	12	-1.41±0.009
179	59	-1.31±0.008	179	12	-1.30±0.008
209	59	-1.20±0.008	209	12	-1.20±0.008
239	59	-1.11±0.007	239	12	-1.11±0.007

Table B.2 Pressure Coefficient Data on the Flat Floor

x, mm	z, mm	CP	x, mm	z, mm	CP
-102	0	-0.89±0.006	-6	-13	-0.45±0.005
-95	0	-0.88±0.006	-51	-19	-0.81±0.006
-89	0	-0.86±0.006	-44	-19	-0.83±0.006
-83	0	-0.85±0.006	-38	-19	-0.86±0.006
-76	0	-0.83±0.006	-32	-19	-0.87±0.006
-70	0	-0.82±0.006	-25	-19	-0.79±0.006
-64	0	-0.80±0.006	-102	-25	-0.90±0.007
-57	0	-0.79±0.006	-95	-25	-0.89±0.006
-51	0	-0.79±0.006	-89	-25	-0.88±0.006
-44	0	-0.81±0.006	-83	-25	-0.87±0.006
-38	0	-0.83±0.006	-76	-25	-0.86±0.006
-32	0	-0.80±0.006	-70	-25	-0.84±0.006
-25	0	-0.70±0.006	-64	-25	-0.83±0.006
-19	0	-0.58±0.005	-57	-25	-0.83±0.006
-13	0	-0.48±0.005	-51	-25	-0.82±0.006
-6	0	-0.33±0.005	-44	-25	-0.84±0.006
-51	-6	-0.79±0.006	-38	-25	-0.88±0.006
-44	-6	-0.80±0.006	-32	-25	-0.90±0.007
-38	-6	-0.82±0.006	-25	-25	-0.85±0.006
-32	-6	-0.81±0.006	-19	-25	-0.77±0.006
-25	-6	-0.71±0.006	-13	-25	-0.72±0.006
-95	-13	-0.88±0.006	-6	-25	-0.69±0.006
-89	-13	-0.87±0.006	0	-25	-0.60±0.005
-83	-13	-0.86±0.006	-44	-32	-0.86±0.006
-76	-13	-0.84±0.006	-38	-32	-0.90±0.007
-70	-13	-0.82±0.006	-32	-32	-0.94±0.007
-64	-13	-0.81±0.006	-25	-32	-0.93±0.007
-57	-13	-0.80±0.006	-19	-32	-0.87±0.006
-51	-13	-0.80±0.006	-102	-38	-0.92±0.007
-44	-13	-0.82±0.006	-95	-38	-0.91±0.007
-38	-13	-0.85±0.006	-89	-38	-0.90±0.007
-32	-13	-0.83±0.006	-83	-38	-0.89±0.006
-25	-13	-0.74±0.006	-76	-38	-0.88±0.006
-19	-13	-0.63±0.006	-70	-38	-0.87±0.006
-13	-13	-0.56±0.005	-64	-38	-0.87±0.006

Table B.2 Continued

x, mm	z, mm	CP	x, mm	z, mm	CP
-57	-38	-0.86±0.006	-32	-57	-1.04±0.007
-51	-38	-0.87±0.006	-25	-57	-1.11±0.007
-44	-38	-0.88±0.006	-19	-57	-1.18±0.008
-38	-38	-0.93±0.007	-13	-57	-1.22±0.008
-32	-38	-0.97±0.007	-6	-57	-1.24±0.008
-25	-38	-0.99±0.007	-102	-64	-0.96±0.007
-19	-38	-0.96±0.007	-89	-64	-0.96±0.007
-13	-38	-0.93±0.007	-76	-64	-0.95±0.007
-6	-38	-0.94±0.007	-70	-64	-0.95±0.007
0	-38	-0.98±0.007	-64	-64	-0.95±0.007
6	-38	-1.00±0.007	-57	-64	-0.96±0.007
-38	-44	-0.94±0.007	-51	-64	-0.97±0.007
-32	-44	-1.00±0.007	-44	-64	-0.99±0.007
-25	-44	-1.05±0.007	-38	-64	-1.01±0.007
-19	-44	-1.05±0.007	-32	-64	-1.06±0.007
-13	-44	-1.03±0.007	-25	-64	-1.12±0.007
-89	-51	-0.93±0.007	-19	-64	-1.22±0.008
-83	-51	-0.92±0.007	-13	-64	-1.27±0.008
-76	-51	-0.92±0.007	-6	-64	-1.32±0.008
-70	-51	-0.91±0.007	0	-64	-1.37±0.008
-64	-51	-0.91±0.007	6	-64	-1.45±0.009
-57	-51	-0.91±0.007	13	-64	-1.57±0.009
-51	-51	-0.92±0.007	19	-64	-1.73±0.010
-44	-51	-0.93±0.007	25	-64	-1.91±0.011
-38	-51	-0.96±0.007	32	-64	-2.10±0.012
-32	-51	-1.02±0.007	38	-64	-2.29±0.013
-25	-51	-1.09±0.007	-19	-70	-1.21±0.008
-19	-51	-1.13±0.007	-13	-70	-1.30±0.008
-13	-51	-1.13±0.007	-6	-70	-1.38±0.008
-6	-51	-1.14±0.007	0	-70	-1.44±0.009
0	-51	-1.21±0.008	6	-70	-1.50±0.009
6	-51	-1.32±0.008	-102	-76	-0.99±0.007
13	-51	-1.46±0.009	-89	-76	-0.99±0.007
19	-51	-1.63±0.010	-76	-76	-0.99±0.007
25	-51	-2.01±0.011	-64	-76	-1.00±0.007

Table B.2 Continued

x, mm	z, mm	CP	x, mm	z, mm	CP
-57	-76	-1.01±0.007	-76	-89	-1.03±0.007
-51	-76	-1.02±0.007	-64	-89	-1.04±0.007
-44	-76	-1.04±0.007	-51	-89	-1.06±0.007
-38	-76	-1.06±0.007	-44	-89	-1.08±0.007
-32	-76	-1.10±0.007	-38	-89	-1.10±0.007
-25	-76	-1.14±0.007	-32	-89	-1.14±0.007
-19	-76	-1.21±0.008	-25	-89	-1.17±0.008
-13	-76	-1.30±0.008	-19	-89	-1.22±0.008
-6	-76	-1.40±0.009	-13	-89	-1.28±0.008
0	-76	-1.47±0.009	-6	-89	-1.35±0.008
6	-76	-1.54±0.009	0	-89	-1.44±0.009
13	-76	-1.61±0.010	6	-89	-1.53±0.009
19	-76	-1.69±0.010	13	-89	-1.62±0.010
25	-76	-1.80±0.010	19	-89	-1.69±0.010
32	-76	-1.91±0.011	25	-89	-1.74±0.010
38	-76	-2.03±0.012	32	-89	-1.80±0.010
44	-76	-2.14±0.012	38	-89	-1.85±0.011
51	-76	-2.22±0.012	44	-89	-1.90±0.011
57	-76	-2.25±0.013	51	-89	-1.93±0.011
64	-76	-2.23±0.013	57	-89	-1.95±0.011
70	-76	-2.16±0.012	64	-89	-1.94±0.011
76	-76	-2.06±0.012	70	-89	-1.92±0.011
83	-76	-1.96±0.011	76	-89	-1.88±0.011
89	-76	-1.87±0.011	83	-89	-1.83±0.011
95	-76	-1.79±0.010	89	-89	-1.78±0.010
102	-76	-1.72±0.010	95	-89	-1.73±0.010
0	-83	-1.47±0.009	102	-89	-1.68±0.010
6	-83	-1.56±0.009	6	-95	-1.49±0.009
13	-83	-1.63±0.010	13	-95	-1.57±0.009
19	-83	-1.69±0.010	19	-95	-1.65±0.010
25	-83	-1.76±0.010	25	-95	-1.71±0.010
32	-83	-1.85±0.011	32	-95	-1.77±0.010
38	-83	-1.93±0.011	38	-95	-1.81±0.010
-102	-89	-1.02±0.007	44	-95	-1.83±0.011
-89	-89	-1.02±0.007	51	-95	-1.85±0.011

Table B.2 Continued

x, mm	z, mm	CP	x, mm	z, mm	CP
57	-95	-1.86±0.011	38	-108	-1.69±0.010
64	-95	-1.86±0.011	44	-108	-1.72±0.010
70	-95	-1.84±0.011	51	-108	-1.74±0.010
76	-95	-1.81±0.011	57	-108	-1.75±0.010
83	-95	-1.77±0.010	64	-108	-1.75±0.010
89	-95	-1.73±0.010	70	-108	-1.74±0.010
95	-95	-1.69±0.010	76	-108	-1.72±0.010
102	-95	-1.65±0.010	83	-108	-1.70±0.010
-89	-102	-1.05±0.007	89	-108	-1.67±0.010
-76	-102	-1.06±0.007	95	-108	-1.64±0.010
-64	-102	-1.07±0.007	102	-108	-1.61±0.010
-51	-102	-1.10±0.007	-89	-114	-1.07±0.007
-38	-102	-1.14±0.007	-76	-114	-1.08±0.007
-32	-102	-1.16±0.008	-64	-114	-1.10±0.007
-25	-102	-1.19±0.008	-51	-114	-1.13±0.007
-19	-102	-1.23±0.008	-38	-114	-1.16±0.008
-13	-102	-1.27±0.008	-25	-114	-1.21±0.008
-6	-102	-1.33±0.008	-13	-114	-1.27±0.008
0	-102	-1.38±0.009	-6	-114	-1.31±0.008
6	-102	-1.44±0.009	0	-114	-1.35±0.008
13	-102	-1.52±0.009	6	-114	-1.40±0.009
19	-102	-1.59±0.009	13	-114	-1.44±0.009
25	-102	-1.65±0.010	19	-114	-1.49±0.009
32	-102	-1.71±0.010	25	-114	-1.53±0.009
38	-102	-1.75±0.010	32	-114	-1.58±0.009
44	-102	-1.78±0.010	38	-114	-1.61±0.010
51	-102	-1.80±0.010	44	-114	-1.65±0.010
57	-102	-1.80±0.010	51	-114	-1.67±0.010
64	-102	-1.80±0.010	57	-114	-1.68±0.010
70	-102	-1.78±0.010	64	-114	-1.69±0.010
76	-102	-1.76±0.010	70	-114	-1.69±0.010
83	-102	-1.73±0.010	76	-114	-1.67±0.010
89	-102	-1.70±0.010	83	-114	-1.66±0.010
95	-102	-1.66±0.010	89	-114	-1.64±0.010
102	-102	-1.63±0.010	95	-114	-1.61±0.010

Table B.2 Continued

x, mm	z, mm	CP	x, mm	z, mm	CP
102	-114	-1.59±0.009	38	-140	-1.46±0.009
-89	-127	-1.10±0.007	51	-140	-1.48±0.009
-76	-127	-1.11±0.007	64	-140	-1.50±0.009
-64	-127	-1.13±0.007	76	-140	-1.50±0.009
-51	-127	-1.15±0.008	89	-140	-1.50±0.009
-38	-127	-1.19±0.008	102	-140	-1.48±0.009
-25	-127	-1.23±0.008	-89	-152	-1.13±0.007
-13	-127	-1.28±0.008	-76	-152	-1.14±0.007
0	-127	-1.34±0.008	-64	-152	-1.16±0.008
6	-127	-1.37±0.008	-51	-152	-1.18±0.008
13	-127	-1.40±0.009	-38	-152	-1.21±0.008
19	-127	-1.43±0.009	-25	-152	-1.24±0.008
25	-127	-1.47±0.009	-13	-152	-1.27±0.008
32	-127	-1.49±0.009	13	-152	-1.34±0.008
38	-127	-1.52±0.009	25	-152	-1.38±0.008
44	-127	-1.55±0.009	38	-152	-1.41±0.009
51	-127	-1.56±0.009	51	-152	-1.43±0.009
57	-127	-1.57±0.009	64	-152	-1.44±0.009
64	-127	-1.58±0.009	76	-152	-1.45±0.009
70	-127	-1.58±0.009	89	-152	-1.44±0.009
76	-127	-1.58±0.009	102	-152	-1.43±0.009
83	-127	-1.57±0.009	-13	-165	-1.27±0.008
89	-127	-1.56±0.009	0	-165	-1.30±0.008
95	-127	-1.55±0.009	13	-165	-1.33±0.008
102	-127	-1.53±0.009	25	-165	-1.35±0.008
-89	-140	-1.11±0.007	38	-165	-1.38±0.008
-76	-140	-1.13±0.007	51	-165	-1.40±0.009
-64	-140	-1.15±0.007	64	-165	-1.40±0.009
-51	-140	-1.17±0.008	76	-165	-1.41±0.009
-38	-140	-1.20±0.008	89	-165	-1.40±0.009
-25	-140	-1.23±0.008	102	-165	-1.40±0.009
-13	-140	-1.27±0.008	-89	-178	-1.15±0.007
0	-140	-1.32±0.008	-64	-178	-1.18±0.008
13	-140	-1.37±0.008	-38	-178	-1.22±0.008
25	-140	-1.41±0.009	-13	-178	-1.26±0.008

Table B.2 Continued

x, mm	z, mm	CP
13	-178	-1.31±0.008
38	-178	-1.35±0.008
64	-178	-1.37±0.008
89	-178	-1.38±0.008
-89	-203	-1.16±0.008
-64	-203	-1.19±0.008
-38	-203	-1.22±0.008
-25	-203	-1.23±0.008
-13	-203	-1.25±0.008
13	-203	-1.29±0.008
38	-203	-1.31±0.008
64	-203	-1.32±0.008
89	-203	-1.33±0.008

APPENDIX C

Kiel Probe Total Pressure Data

In this appendix:

$$CPT \equiv C_{P,T} \quad .$$

The estimated uncertainties are at the 5 percent significance level (95 percent confidence intervals or 19 to 1 odds).

Table C.1 Kiel Probe Total Pressure Data at (x,z)=(127 mm,-203 mm)

y, mm	CPT	y, mm	CPT	y, mm	CPT
0.8	-0.860±0.006	12.0	-0.533±0.005	49.0	-0.177±0.005
1.0	-0.842±0.006	12.5	-0.525±0.005	51.6	-0.157±0.005
1.3	-0.821±0.006	13.0	-0.520±0.005	54.1	-0.138±0.005
1.5	-0.799±0.006	13.5	-0.514±0.005	56.7	-0.118±0.005
1.8	-0.781±0.006	14.8	-0.503±0.005	59.2	-0.101±0.005
2.1	-0.766±0.006	16.0	-0.487±0.005	61.7	-0.084±0.005
2.3	-0.748±0.006	17.3	-0.472±0.005	64.3	-0.067±0.005
2.6	-0.734±0.006	18.6	-0.459±0.005	66.8	-0.053±0.005
2.8	-0.723±0.006	19.8	-0.446±0.005	69.4	-0.041±0.005
3.1	-0.710±0.006	21.1	-0.433±0.005	71.9	-0.030±0.005
3.3	-0.699±0.006	22.4	-0.421±0.005	74.4	-0.021±0.005
3.8	-0.680±0.006	23.6	-0.407±0.005	77.0	-0.014±0.005
4.3	-0.663±0.006	24.9	-0.396±0.005	79.5	-0.009±0.005
4.9	-0.648±0.006	26.2	-0.383±0.005	82.1	-0.005±0.005
5.4	-0.634±0.006	27.5	-0.371±0.005	84.6	-0.002±0.005
5.9	-0.625±0.006	28.7	-0.358±0.005	87.1	-0.000±0.005
6.4	-0.613±0.005	30.0	-0.346±0.005	89.7	0.001±0.005
6.9	-0.603±0.005	31.3	-0.333±0.005	94.8	0.002±0.005
7.4	-0.596±0.005	32.5	-0.321±0.005	99.8	0.003±0.005
7.9	-0.586±0.005	33.8	-0.311±0.005	104.9	0.003±0.005
8.4	-0.577±0.005	35.1	-0.298±0.005	110.0	0.003±0.005
8.9	-0.571±0.005	36.3	-0.288±0.005	115.1	0.002±0.005
9.4	-0.566±0.005	37.6	-0.276±0.005	120.2	0.002±0.005
9.9	-0.559±0.005	38.9	-0.263±0.005	125.2	0.002±0.005
10.4	-0.551±0.005	41.4	-0.242±0.005	130.3	0.002±0.005
10.9	-0.545±0.005	44.0	-0.221±0.005	135.4	0.002±0.005
11.5	-0.538±0.005	46.5	-0.197±0.005	140.5	0.002±0.005

Table C.2 Kiel Probe Total Pressure Data at (x,z)=(127 mm,-178 mm)

y, mm	CPT	y, mm	CPT	y, mm	CPT
0.8	-0.888±0.006	12.0	-0.540±0.005	49.0	-0.178±0.005
1.0	-0.867±0.006	12.5	-0.538±0.005	51.6	-0.160±0.005
1.3	-0.840±0.006	13.0	-0.527±0.005	54.1	-0.139±0.005
1.5	-0.819±0.006	13.5	-0.525±0.005	56.7	-0.120±0.005
1.8	-0.796±0.006	14.8	-0.509±0.005	59.2	-0.102±0.005
2.1	-0.780±0.006	16.0	-0.491±0.005	61.7	-0.086±0.005
2.3	-0.763±0.006	17.3	-0.476±0.005	64.3	-0.070±0.005
2.6	-0.748±0.006	18.6	-0.461±0.005	66.8	-0.053±0.005
2.8	-0.737±0.006	19.8	-0.447±0.005	69.4	-0.042±0.005
3.1	-0.725±0.006	21.1	-0.432±0.005	71.9	-0.031±0.005
3.3	-0.712±0.006	22.4	-0.418±0.005	74.4	-0.022±0.005
3.8	-0.693±0.006	23.6	-0.407±0.005	77.0	-0.015±0.005
4.3	-0.675±0.006	24.9	-0.393±0.005	79.5	-0.009±0.005
4.9	-0.661±0.006	26.2	-0.381±0.005	82.1	-0.005±0.005
5.4	-0.648±0.006	27.5	-0.368±0.005	84.6	-0.002±0.005
5.9	-0.635±0.006	28.7	-0.355±0.005	87.1	-0.000±0.005
6.4	-0.622±0.006	30.0	-0.342±0.005	89.7	0.001±0.005
6.9	-0.616±0.005	31.3	-0.331±0.005	94.8	0.002±0.005
7.4	-0.607±0.005	32.5	-0.317±0.005	99.8	0.002±0.005
7.9	-0.598±0.005	33.8	-0.307±0.005	104.9	0.002±0.005
8.4	-0.592±0.005	35.1	-0.294±0.005	110.0	0.002±0.005
8.9	-0.585±0.005	36.3	-0.283±0.005	115.1	0.002±0.005
9.4	-0.576±0.005	37.6	-0.273±0.005	120.2	0.002±0.005
9.9	-0.571±0.005	38.9	-0.262±0.005	125.2	0.002±0.005
10.4	-0.561±0.005	41.4	-0.241±0.005	130.3	0.002±0.005
10.9	-0.555±0.005	44.0	-0.216±0.005	135.4	0.002±0.005
11.5	-0.550±0.005	46.5	-0.197±0.005	140.5	0.002±0.005

Table C.3 Kiel Probe Total Pressure Data at (x,z)=(127 mm,-165 mm)

y, mm	CPT	y, mm	CPT	y, mm	CPT
0.8	-0.917±0.006	12.0	-0.574±0.005	49.0	-0.182±0.005
1.0	-0.885±0.006	12.5	-0.568±0.005	51.6	-0.162±0.005
1.3	-0.858±0.006	13.0	-0.560±0.005	54.1	-0.141±0.005
1.5	-0.837±0.006	13.5	-0.554±0.005	56.7	-0.123±0.005
1.8	-0.818±0.006	14.8	-0.539±0.005	59.2	-0.104±0.005
2.1	-0.803±0.006	16.0	-0.521±0.005	61.7	-0.087±0.005
2.3	-0.783±0.006	17.3	-0.505±0.005	64.3	-0.071±0.005
2.6	-0.769±0.006	18.6	-0.491±0.005	66.8	-0.057±0.005
2.8	-0.756±0.006	19.8	-0.475±0.005	69.4	-0.043±0.005
3.1	-0.745±0.006	21.1	-0.460±0.005	71.9	-0.031±0.005
3.3	-0.732±0.006	22.4	-0.445±0.005	74.4	-0.022±0.005
3.8	-0.713±0.006	23.6	-0.432±0.005	77.0	-0.015±0.005
4.3	-0.695±0.006	24.9	-0.416±0.005	79.5	-0.009±0.005
4.9	-0.681±0.006	26.2	-0.402±0.005	82.1	-0.005±0.005
5.4	-0.669±0.006	27.5	-0.385±0.005	84.6	-0.002±0.005
5.9	-0.659±0.006	28.7	-0.376±0.005	87.1	0.000±0.005
6.4	-0.649±0.006	30.0	-0.360±0.005	89.7	0.001±0.005
6.9	-0.642±0.006	31.3	-0.346±0.005	94.8	0.002±0.005
7.4	-0.633±0.006	32.5	-0.337±0.005	99.8	0.003±0.005
7.9	-0.626±0.005	33.8	-0.321±0.005	104.9	0.003±0.005
8.4	-0.619±0.005	35.1	-0.309±0.005	110.0	0.002±0.005
8.9	-0.611±0.005	36.3	-0.298±0.005	115.1	0.003±0.005
9.4	-0.606±0.005	37.6	-0.283±0.005	120.2	0.002±0.005
9.9	-0.598±0.005	38.9	-0.273±0.005	125.2	0.002±0.005
10.4	-0.593±0.005	41.4	-0.250±0.005	130.3	0.002±0.005
10.9	-0.586±0.005	44.0	-0.225±0.005	135.4	0.002±0.005
11.5	-0.579±0.005	46.5	-0.202±0.005	140.5	0.002±0.005

Table C.4 Kiel Probe Total Pressure Data at (x,z)=(127 mm,-152 mm)

y, mm	CPT	y, mm	CPT	y, mm	CPT
0.8	-0.933±0.007	12.0	-0.601±0.005	49.0	-0.199±0.005
1.0	-0.901±0.006	12.5	-0.596±0.005	51.6	-0.178±0.005
1.3	-0.875±0.006	13.0	-0.589±0.005	54.1	-0.158±0.005
1.5	-0.852±0.006	13.5	-0.585±0.005	56.7	-0.138±0.005
1.8	-0.831±0.006	14.8	-0.569±0.005	59.2	-0.118±0.005
2.1	-0.811±0.006	16.0	-0.555±0.005	61.7	-0.102±0.005
2.3	-0.795±0.006	17.3	-0.540±0.005	64.3	-0.083±0.005
2.6	-0.779±0.006	18.6	-0.523±0.005	66.8	-0.065±0.005
2.8	-0.766±0.006	19.8	-0.506±0.005	69.4	-0.051±0.005
3.1	-0.753±0.006	21.1	-0.494±0.005	71.9	-0.039±0.005
3.3	-0.742±0.006	22.4	-0.476±0.005	74.4	-0.028±0.005
3.8	-0.721±0.006	23.6	-0.462±0.005	77.0	-0.020±0.005
4.3	-0.706±0.006	24.9	-0.449±0.005	79.5	-0.013±0.005
4.9	-0.691±0.006	26.2	-0.434±0.005	82.1	-0.008±0.005
5.4	-0.680±0.006	27.5	-0.419±0.005	84.6	-0.004±0.005
5.9	-0.671±0.006	28.7	-0.405±0.005	87.1	-0.001±0.005
6.4	-0.662±0.006	30.0	-0.392±0.005	89.7	0.000±0.005
6.9	-0.653±0.006	31.3	-0.376±0.005	94.8	0.002±0.005
7.4	-0.647±0.006	32.5	-0.361±0.005	99.8	0.003±0.005
7.9	-0.644±0.006	33.8	-0.349±0.005	104.9	0.003±0.005
8.4	-0.637±0.006	35.1	-0.336±0.005	110.0	0.003±0.005
8.9	-0.632±0.006	36.3	-0.321±0.005	115.1	0.002±0.005
9.4	-0.626±0.006	37.6	-0.310±0.005	120.2	0.002±0.005
9.9	-0.621±0.005	38.9	-0.299±0.005	125.2	0.002±0.005
10.4	-0.616±0.005	41.4	-0.272±0.005	130.3	0.002±0.005
10.9	-0.611±0.005	44.0	-0.249±0.005	135.4	0.002±0.005
11.5	-0.603±0.005	46.5	-0.222±0.005	140.5	0.002±0.005

Table C.5 Kiel Probe Total Pressure Data at (x,z)=(127 mm,-146 mm)

y, mm	CPT	y, mm	CPT	y, mm	CPT
0.8	-0.932±0.007	12.0	-0.612±0.005	49.0	-0.213±0.005
1.0	-0.897±0.006	12.5	-0.607±0.005	51.6	-0.188±0.005
1.3	-0.870±0.006	13.0	-0.602±0.005	54.1	-0.164±0.005
1.5	-0.845±0.006	13.5	-0.596±0.005	56.7	-0.145±0.005
1.8	-0.824±0.006	14.8	-0.584±0.005	59.2	-0.126±0.005
2.1	-0.805±0.006	16.0	-0.571±0.005	61.7	-0.108±0.005
2.3	-0.791±0.006	17.3	-0.557±0.005	64.3	-0.090±0.005
2.6	-0.775±0.006	18.6	-0.539±0.005	66.8	-0.072±0.005
2.8	-0.761±0.006	19.8	-0.522±0.005	69.4	-0.057±0.005
3.1	-0.748±0.006	21.1	-0.505±0.005	71.9	-0.043±0.005
3.3	-0.737±0.006	22.4	-0.494±0.005	74.4	-0.033±0.005
3.8	-0.718±0.006	23.6	-0.479±0.005	77.0	-0.023±0.005
4.3	-0.704±0.006	24.9	-0.463±0.005	79.5	-0.016±0.005
4.9	-0.692±0.006	26.2	-0.452±0.005	82.1	-0.010±0.005
5.4	-0.683±0.006	27.5	-0.435±0.005	84.6	-0.005±0.005
5.9	-0.672±0.006	28.7	-0.422±0.005	87.1	-0.002±0.005
6.4	-0.666±0.006	30.0	-0.406±0.005	89.7	-0.000±0.005
6.9	-0.659±0.006	31.3	-0.392±0.005	94.8	0.002±0.005
7.4	-0.654±0.006	32.5	-0.377±0.005	99.8	0.002±0.005
7.9	-0.649±0.006	33.8	-0.361±0.005	104.9	0.002±0.005
8.4	-0.643±0.006	35.1	-0.350±0.005	110.0	0.002±0.005
8.9	-0.639±0.006	36.3	-0.337±0.005	115.1	0.002±0.005
9.4	-0.636±0.006	37.6	-0.325±0.005	120.2	0.002±0.005
9.9	-0.632±0.006	38.9	-0.312±0.005	125.2	0.002±0.005
10.4	-0.625±0.006	41.4	-0.282±0.005	130.3	0.002±0.005
10.9	-0.623±0.005	44.0	-0.259±0.005	135.4	0.002±0.005
11.5	-0.617±0.005	46.5	-0.232±0.005	140.5	0.002±0.005

Table C.6 Kiel Probe Total Pressure Data at (x,z)=(127 mm,-140 mm)

y, mm	CPT	y, mm	CPT	y, mm	CPT
0.8	-0.927±0.007	12.0	-0.632±0.006	49.0	-0.221±0.005
1.0	-0.894±0.006	12.5	-0.625±0.006	51.6	-0.197±0.005
1.3	-0.866±0.006	13.0	-0.624±0.006	54.1	-0.176±0.005
1.5	-0.839±0.006	13.5	-0.619±0.005	56.7	-0.152±0.005
1.8	-0.818±0.006	14.8	-0.607±0.005	59.2	-0.134±0.005
2.1	-0.801±0.006	16.0	-0.592±0.005	61.7	-0.116±0.005
2.3	-0.785±0.006	17.3	-0.575±0.005	64.3	-0.096±0.005
2.6	-0.770±0.006	18.6	-0.562±0.005	66.8	-0.079±0.005
2.8	-0.757±0.006	19.8	-0.542±0.005	69.4	-0.064±0.005
3.1	-0.746±0.006	21.1	-0.526±0.005	71.9	-0.049±0.005
3.3	-0.736±0.006	22.4	-0.512±0.005	74.4	-0.038±0.005
3.8	-0.720±0.006	23.6	-0.495±0.005	77.0	-0.027±0.005
4.3	-0.708±0.006	24.9	-0.478±0.005	79.5	-0.020±0.005
4.9	-0.698±0.006	26.2	-0.460±0.005	82.1	-0.012±0.005
5.4	-0.691±0.006	27.5	-0.446±0.005	84.6	-0.007±0.005
5.9	-0.685±0.006	28.7	-0.432±0.005	87.1	-0.004±0.005
6.4	-0.679±0.006	30.0	-0.420±0.005	89.7	-0.001±0.005
6.9	-0.674±0.006	31.3	-0.403±0.005	94.8	0.001±0.005
7.4	-0.670±0.006	32.5	-0.389±0.005	99.8	0.002±0.005
7.9	-0.664±0.006	33.8	-0.375±0.005	104.9	0.003±0.005
8.4	-0.661±0.006	35.1	-0.359±0.005	110.0	0.003±0.005
8.9	-0.656±0.006	36.3	-0.349±0.005	115.1	0.003±0.005
9.4	-0.652±0.006	37.6	-0.330±0.005	120.2	0.002±0.005
9.9	-0.650±0.006	38.9	-0.321±0.005	125.2	0.002±0.005
10.4	-0.646±0.006	41.4	-0.296±0.005	130.3	0.002±0.005
10.9	-0.645±0.006	44.0	-0.272±0.005	135.4	0.002±0.005
11.5	-0.638±0.006	46.5	-0.246±0.005	140.5	0.002±0.005

Table C.7 Kiel Probe Total Pressure Data at (x,z)=(127 mm,-133 mm)

y, mm	CPT	y, mm	CPT	y, mm	CPT
0.8	-0.910±0.006	12.0	-0.662±0.006	49.0	-0.218±0.005
1.0	-0.874±0.006	12.5	-0.658±0.006	51.6	-0.194±0.005
1.3	-0.847±0.006	13.0	-0.652±0.006	54.1	-0.173±0.005
1.5	-0.826±0.006	13.5	-0.649±0.006	56.7	-0.151±0.005
1.8	-0.808±0.006	14.8	-0.632±0.006	59.2	-0.132±0.005
2.1	-0.791±0.006	16.0	-0.620±0.005	61.7	-0.112±0.005
2.3	-0.777±0.006	17.3	-0.601±0.005	64.3	-0.093±0.005
2.6	-0.765±0.006	18.6	-0.583±0.005	66.8	-0.079±0.005
2.8	-0.753±0.006	19.8	-0.565±0.005	69.4	-0.062±0.005
3.1	-0.744±0.006	21.1	-0.542±0.005	71.9	-0.048±0.005
3.3	-0.736±0.006	22.4	-0.523±0.005	74.4	-0.036±0.005
3.8	-0.724±0.006	23.6	-0.501±0.005	77.0	-0.026±0.005
4.3	-0.715±0.006	24.9	-0.485±0.005	79.5	-0.018±0.005
4.9	-0.709±0.006	26.2	-0.467±0.005	82.1	-0.011±0.005
5.4	-0.703±0.006	27.5	-0.451±0.005	84.6	-0.006±0.005
5.9	-0.699±0.006	28.7	-0.433±0.005	87.1	-0.003±0.005
6.4	-0.696±0.006	30.0	-0.416±0.005	89.7	-0.000±0.005
6.9	-0.694±0.006	31.3	-0.401±0.005	94.8	0.002±0.005
7.4	-0.691±0.006	32.5	-0.388±0.005	99.8	0.003±0.005
7.9	-0.687±0.006	33.8	-0.371±0.005	104.9	0.004±0.005
8.4	-0.685±0.006	35.1	-0.358±0.005	110.0	0.004±0.005
8.9	-0.682±0.006	36.3	-0.345±0.005	115.1	0.004±0.005
9.4	-0.677±0.006	37.6	-0.330±0.005	120.2	0.004±0.005
9.9	-0.677±0.006	38.9	-0.317±0.005	125.2	0.004±0.005
10.4	-0.673±0.006	41.4	-0.289±0.005	130.3	0.004±0.005
10.9	-0.669±0.006	44.0	-0.267±0.005	135.4	0.004±0.005
11.5	-0.667±0.006	46.5	-0.240±0.005	140.5	0.004±0.005

Table C.8 Kiel Probe Total Pressure Data at (x,z)=(127 mm,-127 mm)

y, mm	CPT	y, mm	CPT	y, mm	CPT
0.8	-0.908±0.006	12.0	-0.720±0.006	49.0	-0.217±0.005
1.0	-0.864±0.006	12.5	-0.715±0.006	51.6	-0.194±0.005
1.3	-0.835±0.006	13.0	-0.714±0.006	54.1	-0.173±0.005
1.5	-0.805±0.006	13.5	-0.709±0.006	56.7	-0.151±0.005
1.8	-0.787±0.006	14.8	-0.695±0.006	59.2	-0.132±0.005
2.1	-0.770±0.006	16.0	-0.671±0.006	61.7	-0.112±0.005
2.3	-0.755±0.006	17.3	-0.647±0.006	64.3	-0.096±0.005
2.6	-0.747±0.006	18.6	-0.624±0.006	66.8	-0.079±0.005
2.8	-0.739±0.006	19.8	-0.597±0.005	69.4	-0.064±0.005
3.1	-0.731±0.006	21.1	-0.572±0.005	71.9	-0.050±0.005
3.3	-0.727±0.006	22.4	-0.544±0.005	74.4	-0.038±0.005
3.8	-0.719±0.006	23.6	-0.519±0.005	77.0	-0.026±0.005
4.3	-0.716±0.006	24.9	-0.496±0.005	79.5	-0.018±0.005
4.9	-0.714±0.006	26.2	-0.475±0.005	82.1	-0.012±0.005
5.4	-0.715±0.006	27.5	-0.455±0.005	84.6	-0.007±0.005
5.9	-0.716±0.006	28.7	-0.437±0.005	87.1	-0.003±0.005
6.4	-0.717±0.006	30.0	-0.421±0.005	89.7	-0.001±0.005
6.9	-0.721±0.006	31.3	-0.404±0.005	94.8	0.002±0.005
7.4	-0.724±0.006	32.5	-0.390±0.005	99.8	0.003±0.005
7.9	-0.724±0.006	33.8	-0.372±0.005	104.9	0.004±0.005
8.4	-0.728±0.006	35.1	-0.357±0.005	110.0	0.004±0.005
8.9	-0.730±0.006	36.3	-0.343±0.005	115.1	0.004±0.005
9.4	-0.727±0.006	37.6	-0.330±0.005	120.2	0.004±0.005
9.9	-0.728±0.006	38.9	-0.314±0.005	125.2	0.004±0.005
10.4	-0.730±0.006	41.4	-0.291±0.005	130.3	0.003±0.005
10.9	-0.730±0.006	44.0	-0.266±0.005	135.4	0.003±0.005
11.5	-0.728±0.006	46.5	-0.241±0.005	140.5	0.003±0.005

Table C.9 Kiel Probe Total Pressure Data at (x,z)=(127 mm,-121 mm)

y, mm	CPT	y, mm	CPT	y, mm	CPT
0.8	-0.829±0.006	12.0	-0.790±0.006	49.0	-0.210±0.005
1.0	-0.784±0.006	12.5	-0.784±0.006	51.6	-0.189±0.005
1.3	-0.754±0.006	13.0	-0.779±0.006	54.1	-0.166±0.005
1.5	-0.728±0.006	13.5	-0.771±0.006	56.7	-0.147±0.005
1.8	-0.709±0.006	14.8	-0.746±0.006	59.2	-0.127±0.005
2.1	-0.699±0.006	16.0	-0.711±0.006	61.7	-0.107±0.005
2.3	-0.692±0.006	17.3	-0.679±0.006	64.3	-0.093±0.005
2.6	-0.686±0.006	18.6	-0.643±0.006	66.8	-0.078±0.005
2.8	-0.682±0.006	19.8	-0.612±0.005	69.4	-0.060±0.005
3.1	-0.681±0.006	21.1	-0.581±0.005	71.9	-0.047±0.005
3.3	-0.682±0.006	22.4	-0.552±0.005	74.4	-0.036±0.005
3.8	-0.688±0.006	23.6	-0.524±0.005	77.0	-0.026±0.005
4.3	-0.695±0.006	24.9	-0.492±0.005	79.5	-0.019±0.005
4.9	-0.703±0.006	26.2	-0.473±0.005	82.1	-0.011±0.005
5.4	-0.715±0.006	27.5	-0.449±0.005	84.6	-0.007±0.005
5.9	-0.724±0.006	28.7	-0.430±0.005	87.1	-0.004±0.005
6.4	-0.736±0.006	30.0	-0.413±0.005	89.7	-0.001±0.005
6.9	-0.747±0.006	31.3	-0.395±0.005	94.8	0.001±0.005
7.4	-0.756±0.006	32.5	-0.380±0.005	99.8	0.002±0.005
7.9	-0.765±0.006	33.8	-0.365±0.005	104.9	0.002±0.005
8.4	-0.773±0.006	35.1	-0.350±0.005	110.0	0.002±0.005
8.9	-0.781±0.006	36.3	-0.336±0.005	115.1	0.002±0.005
9.4	-0.785±0.006	37.6	-0.322±0.005	120.2	0.002±0.005
9.9	-0.793±0.006	38.9	-0.312±0.005	125.2	0.002±0.005
10.4	-0.795±0.006	41.4	-0.281±0.005	130.3	0.002±0.005
10.9	-0.793±0.006	44.0	-0.257±0.005	135.4	0.002±0.005
11.5	-0.796±0.006	46.5	-0.234±0.005	140.5	0.002±0.005

Table C.10 Kiel Probe Total Pressure Data at (x,z)=(127 mm,-114 mm)

y, mm	CPT	y, mm	CPT	y, mm	CPT
0.8	-0.738±0.006	12.0	-0.804±0.006	49.0	-0.205±0.005
1.0	-0.691±0.006	12.5	-0.797±0.006	51.6	-0.180±0.005
1.3	-0.654±0.006	13.0	-0.787±0.006	54.1	-0.162±0.005
1.5	-0.632±0.006	13.5	-0.777±0.006	56.7	-0.141±0.005
1.8	-0.617±0.005	14.8	-0.741±0.006	59.2	-0.122±0.005
2.1	-0.610±0.005	16.0	-0.703±0.006	61.7	-0.104±0.005
2.3	-0.606±0.005	17.3	-0.665±0.006	64.3	-0.087±0.005
2.6	-0.606±0.005	18.6	-0.629±0.006	66.8	-0.073±0.005
2.8	-0.608±0.005	19.8	-0.593±0.005	69.4	-0.058±0.005
3.1	-0.618±0.006	21.1	-0.558±0.005	71.9	-0.045±0.005
3.3	-0.622±0.006	22.4	-0.530±0.005	74.4	-0.035±0.005
3.8	-0.639±0.006	23.6	-0.501±0.005	77.0	-0.025±0.005
4.3	-0.655±0.006	24.9	-0.478±0.005	79.5	-0.017±0.005
4.9	-0.673±0.006	26.2	-0.455±0.005	82.1	-0.011±0.005
5.4	-0.691±0.006	27.5	-0.435±0.005	84.6	-0.007±0.005
5.9	-0.709±0.006	28.7	-0.419±0.005	87.1	-0.003±0.005
6.4	-0.725±0.006	30.0	-0.402±0.005	89.7	-0.001±0.005
6.9	-0.742±0.006	31.3	-0.385±0.005	94.8	0.001±0.005
7.4	-0.754±0.006	32.5	-0.369±0.005	99.8	0.002±0.005
7.9	-0.767±0.006	33.8	-0.355±0.005	104.9	0.003±0.005
8.4	-0.778±0.006	35.1	-0.340±0.005	110.0	0.003±0.005
8.9	-0.790±0.006	36.3	-0.328±0.005	115.1	0.002±0.005
9.4	-0.799±0.006	37.6	-0.313±0.005	120.2	0.002±0.005
9.9	-0.806±0.006	38.9	-0.299±0.005	125.2	0.002±0.005
10.4	-0.807±0.006	41.4	-0.273±0.005	130.3	0.002±0.005
10.9	-0.809±0.006	44.0	-0.249±0.005	135.4	0.002±0.005
11.5	-0.808±0.006	46.5	-0.228±0.005	140.5	0.002±0.005

Table C.11 Kiel Probe Total Pressure Data at (x,z)=(127 mm,-108 mm)

y, mm	CPT	y, mm	CPT	y, mm	CPT
0.8	-0.672±0.006	12.0	-0.735±0.006	49.0	-0.197±0.005
1.0	-0.613±0.005	12.5	-0.727±0.006	51.6	-0.176±0.005
1.3	-0.580±0.005	13.0	-0.717±0.006	54.1	-0.154±0.005
1.5	-0.557±0.005	13.5	-0.708±0.006	56.7	-0.135±0.005
1.8	-0.544±0.005	14.8	-0.674±0.006	59.2	-0.116±0.005
2.1	-0.538±0.005	16.0	-0.640±0.006	61.7	-0.099±0.005
2.3	-0.540±0.005	17.3	-0.610±0.005	64.3	-0.084±0.005
2.6	-0.542±0.005	18.6	-0.576±0.005	66.8	-0.067±0.005
2.8	-0.548±0.005	19.8	-0.546±0.005	69.4	-0.053±0.005
3.1	-0.555±0.005	21.1	-0.515±0.005	71.9	-0.042±0.005
3.3	-0.564±0.005	22.4	-0.494±0.005	74.4	-0.031±0.005
3.8	-0.582±0.005	23.6	-0.468±0.005	77.0	-0.022±0.005
4.3	-0.602±0.005	24.9	-0.449±0.005	79.5	-0.015±0.005
4.9	-0.622±0.005	26.2	-0.430±0.005	82.1	-0.010±0.005
5.4	-0.640±0.006	27.5	-0.413±0.005	84.6	-0.005±0.005
5.9	-0.657±0.006	28.7	-0.397±0.005	87.1	-0.003±0.005
6.4	-0.673±0.006	30.0	-0.380±0.005	89.7	-0.001±0.005
6.9	-0.683±0.006	31.3	-0.368±0.005	94.8	0.001±0.005
7.4	-0.698±0.006	32.5	-0.353±0.005	99.8	0.002±0.005
7.9	-0.706±0.006	33.8	-0.338±0.005	104.9	0.002±0.005
8.4	-0.714±0.006	35.1	-0.326±0.005	110.0	0.002±0.005
8.9	-0.723±0.006	36.3	-0.316±0.005	115.1	0.002±0.005
9.4	-0.730±0.006	37.6	-0.298±0.005	120.2	0.002±0.005
9.9	-0.732±0.006	38.9	-0.287±0.005	125.2	0.002±0.005
10.4	-0.734±0.006	41.4	-0.260±0.005	130.3	0.002±0.005
10.9	-0.733±0.006	44.0	-0.238±0.005	135.4	0.002±0.005
11.5	-0.739±0.006	46.5	-0.215±0.005	140.5	0.002±0.005

Table C.12 Kiel Probe Total Pressure Data at (x,z)=(127 mm,-102 mm)

y, mm	CPT	y, mm	CPT	y, mm	CPT
0.8	-0.634±0.006	12.0	-0.615±0.005	49.0	-0.183±0.005
1.0	-0.575±0.005	12.5	-0.610±0.005	51.6	-0.163±0.005
1.3	-0.539±0.005	13.0	-0.604±0.005	54.1	-0.144±0.005
1.5	-0.513±0.005	13.5	-0.596±0.005	56.7	-0.123±0.005
1.8	-0.499±0.005	14.8	-0.576±0.005	59.2	-0.107±0.005
2.1	-0.492±0.005	16.0	-0.555±0.005	61.7	-0.090±0.005
2.3	-0.489±0.005	17.3	-0.530±0.005	64.3	-0.077±0.005
2.6	-0.491±0.005	18.6	-0.508±0.005	66.8	-0.060±0.005
2.8	-0.495±0.005	19.8	-0.486±0.005	69.4	-0.048±0.005
3.1	-0.501±0.005	21.1	-0.467±0.005	71.9	-0.037±0.005
3.3	-0.509±0.005	22.4	-0.447±0.005	74.4	-0.027±0.005
3.8	-0.525±0.005	23.6	-0.432±0.005	77.0	-0.019±0.005
4.3	-0.543±0.005	24.9	-0.414±0.005	79.5	-0.013±0.005
4.9	-0.559±0.005	26.2	-0.401±0.005	82.1	-0.008±0.005
5.4	-0.574±0.005	27.5	-0.386±0.005	84.6	-0.004±0.005
5.9	-0.584±0.005	28.7	-0.373±0.005	87.1	-0.002±0.005
6.4	-0.596±0.005	30.0	-0.358±0.005	89.7	-0.000±0.005
6.9	-0.605±0.005	31.3	-0.345±0.005	94.8	0.002±0.005
7.4	-0.612±0.005	32.5	-0.333±0.005	99.8	0.002±0.005
7.9	-0.616±0.005	33.8	-0.320±0.005	104.9	0.002±0.005
8.4	-0.623±0.005	35.1	-0.310±0.005	110.0	0.002±0.005
8.9	-0.627±0.006	36.3	-0.295±0.005	115.1	0.002±0.005
9.4	-0.626±0.005	37.6	-0.284±0.005	120.2	0.002±0.005
9.9	-0.629±0.006	38.9	-0.272±0.005	125.2	0.002±0.005
10.4	-0.625±0.005	41.4	-0.249±0.005	130.3	0.002±0.005
10.9	-0.627±0.006	44.0	-0.226±0.005	135.4	0.002±0.005
11.5	-0.620±0.005	46.5	-0.204±0.005	140.5	0.002±0.005

Table C.13 Kiel Probe Total Pressure Data at (x,z)=(127 mm,-95 mm) .

y, mm	CPT	y, mm	CPT	y, mm	CPT
0.8	-0.614±0.005	12.0	-0.532±0.005	49.0	-0.172±0.005
1.0	-0.550±0.005	12.5	-0.524±0.005	51.6	-0.152±0.005
1.3	-0.512±0.005	13.0	-0.521±0.005	54.1	-0.134±0.005
1.5	-0.484±0.005	13.5	-0.515±0.005	56.7	-0.115±0.005
1.8	-0.467±0.005	14.8	-0.501±0.005	59.2	-0.099±0.005
2.1	-0.458±0.005	16.0	-0.490±0.005	61.7	-0.084±0.005
2.3	-0.452±0.005	17.3	-0.474±0.005	64.3	-0.069±0.005
2.6	-0.449±0.005	18.6	-0.459±0.005	66.8	-0.055±0.005
2.8	-0.453±0.005	19.8	-0.445±0.005	69.4	-0.043±0.005
3.1	-0.458±0.005	21.1	-0.431±0.005	71.9	-0.032±0.005
3.3	-0.461±0.005	22.4	-0.412±0.005	74.4	-0.024±0.005
3.8	-0.475±0.005	23.6	-0.401±0.005	77.0	-0.016±0.005
4.3	-0.488±0.005	24.9	-0.387±0.005	79.5	-0.011±0.005
4.9	-0.500±0.005	26.2	-0.375±0.005	82.1	-0.007±0.005
5.4	-0.511±0.005	27.5	-0.364±0.005	84.6	-0.004±0.005
5.9	-0.521±0.005	28.7	-0.351±0.005	87.1	-0.002±0.005
6.4	-0.528±0.005	30.0	-0.341±0.005	89.7	-0.000±0.005
6.9	-0.534±0.005	31.3	-0.331±0.005	94.8	0.001±0.005
7.4	-0.539±0.005	32.5	-0.319±0.005	99.8	0.002±0.005
7.9	-0.541±0.005	33.8	-0.306±0.005	104.9	0.002±0.005
8.4	-0.544±0.005	35.1	-0.290±0.005	110.0	0.002±0.005
8.9	-0.545±0.005	36.3	-0.278±0.005	115.1	0.002±0.005
9.4	-0.546±0.005	37.6	-0.269±0.005	120.2	0.002±0.005
9.9	-0.543±0.005	38.9	-0.256±0.005	125.2	0.002±0.005
10.4	-0.543±0.005	41.4	-0.234±0.005	130.3	0.002±0.005
10.9	-0.540±0.005	44.0	-0.211±0.005	135.4	0.002±0.005
11.5	-0.535±0.005	46.5	-0.191±0.005	140.5	0.002±0.005

Table C.14 Kiel Probe Total Pressure Data at (x,z)=(127 mm,-89 mm)

y, mm	CPT	y, mm	CPT	y, mm	CPT
0.8	-0.612±0.005	12.0	-0.478±0.005	49.0	-0.159±0.005
1.0	-0.546±0.005	12.5	-0.472±0.005	51.6	-0.141±0.005
1.3	-0.502±0.005	13.0	-0.468±0.005	54.1	-0.124±0.005
1.5	-0.469±0.005	13.5	-0.464±0.005	56.7	-0.106±0.005
1.8	-0.449±0.005	14.8	-0.454±0.005	59.2	-0.092±0.005
2.1	-0.435±0.005	16.0	-0.441±0.005	61.7	-0.076±0.005
2.3	-0.427±0.005	17.3	-0.430±0.005	64.3	-0.062±0.005
2.6	-0.425±0.005	18.6	-0.419±0.005	66.8	-0.049±0.005
2.8	-0.427±0.005	19.8	-0.407±0.005	69.4	-0.039±0.005
3.1	-0.428±0.005	21.1	-0.397±0.005	71.9	-0.029±0.005
3.3	-0.432±0.005	22.4	-0.383±0.005	74.4	-0.021±0.005
3.8	-0.442±0.005	23.6	-0.373±0.005	77.0	-0.015±0.005
4.3	-0.451±0.005	24.9	-0.361±0.005	79.5	-0.010±0.005
4.9	-0.460±0.005	26.2	-0.349±0.005	82.1	-0.006±0.005
5.4	-0.470±0.005	27.5	-0.339±0.005	84.6	-0.003±0.005
5.9	-0.478±0.005	28.7	-0.328±0.005	87.1	-0.001±0.005
6.4	-0.483±0.005	30.0	-0.316±0.005	89.7	0.000±0.005
6.9	-0.487±0.005	31.3	-0.305±0.005	94.8	0.001±0.005
7.4	-0.489±0.005	32.5	-0.294±0.005	99.8	0.002±0.005
7.9	-0.491±0.005	33.8	-0.285±0.005	104.9	0.002±0.005
8.4	-0.491±0.005	35.1	-0.272±0.005	110.0	0.002±0.005
8.9	-0.490±0.005	36.3	-0.262±0.005	115.1	0.002±0.005
9.4	-0.489±0.005	37.6	-0.251±0.005	120.2	0.002±0.005
9.9	-0.488±0.005	38.9	-0.239±0.005	125.2	0.002±0.005
10.4	-0.485±0.005	41.4	-0.219±0.005	130.3	0.002±0.005
10.9	-0.482±0.005	44.0	-0.199±0.005	135.4	0.002±0.005
11.5	-0.479±0.005	46.5	-0.179±0.005	140.5	0.002±0.005

Table C.15 Kiel Probe Total Pressure Data at (x,z)=(127 mm,-83 mm)

y, mm	CPT	y, mm	CPT	y, mm	CPT
0.8	-0.583±0.005	12.0	-0.439±0.005	49.0	-0.147±0.005
1.0	-0.518±0.005	12.5	-0.436±0.005	51.6	-0.130±0.005
1.3	-0.474±0.005	13.0	-0.435±0.005	54.1	-0.114±0.005
1.5	-0.443±0.005	13.5	-0.429±0.005	56.7	-0.099±0.005
1.8	-0.422±0.005	14.8	-0.420±0.005	59.2	-0.084±0.005
2.1	-0.411±0.005	16.0	-0.410±0.005	61.7	-0.069±0.005
2.3	-0.404±0.005	17.3	-0.400±0.005	64.3	-0.055±0.005
2.6	-0.403±0.005	18.6	-0.391±0.005	66.8	-0.044±0.005
2.8	-0.401±0.005	19.8	-0.379±0.005	69.4	-0.035±0.005
3.1	-0.404±0.005	21.1	-0.368±0.005	71.9	-0.026±0.005
3.3	-0.407±0.005	22.4	-0.358±0.005	74.4	-0.019±0.005
3.8	-0.415±0.005	23.6	-0.347±0.005	77.0	-0.012±0.005
4.3	-0.424±0.005	24.9	-0.337±0.005	79.5	-0.008±0.005
4.9	-0.434±0.005	26.2	-0.327±0.005	82.1	-0.005±0.005
5.4	-0.439±0.005	27.5	-0.318±0.005	84.6	-0.002±0.005
5.9	-0.443±0.005	28.7	-0.306±0.005	87.1	-0.001±0.005
6.4	-0.449±0.005	30.0	-0.296±0.005	89.7	0.001±0.005
6.9	-0.451±0.005	31.3	-0.284±0.005	94.8	0.002±0.005
7.4	-0.453±0.005	32.5	-0.274±0.005	99.8	0.002±0.005
7.9	-0.456±0.005	33.8	-0.262±0.005	104.9	0.002±0.005
8.4	-0.455±0.005	35.1	-0.253±0.005	110.0	0.002±0.005
8.9	-0.454±0.005	36.3	-0.244±0.005	115.1	0.002±0.005
9.4	-0.452±0.005	37.6	-0.234±0.005	120.2	0.002±0.005
9.9	-0.452±0.005	38.9	-0.222±0.005	125.2	0.002±0.005
10.4	-0.447±0.005	41.4	-0.204±0.005	130.3	0.002±0.005
10.9	-0.449±0.005	44.0	-0.186±0.005	135.4	0.002±0.005
11.5	-0.442±0.005	46.5	-0.166±0.005	140.5	0.002±0.005

Table C.16 Kiel Probe Total Pressure Data at (x,z)=(127 mm,-76 mm)

y, mm	CPT	y, mm	CPT	y, mm	CPT
0.8	-0.501±0.005	12.0	-0.404±0.005	49.0	-0.130±0.005
1.0	-0.438±0.005	12.5	-0.403±0.005	51.6	-0.114±0.005
1.3	-0.408±0.005	13.0	-0.399±0.005	54.1	-0.105±0.005
1.5	-0.385±0.005	13.5	-0.395±0.005	56.7	-0.084±0.005
1.8	-0.376±0.005	14.8	-0.388±0.005	59.2	-0.068±0.005
2.1	-0.369±0.005	16.0	-0.378±0.005	61.7	-0.059±0.005
2.3	-0.365±0.005	17.3	-0.368±0.005	64.3	-0.046±0.005
2.6	-0.365±0.005	18.6	-0.356±0.005	66.8	-0.037±0.005
2.8	-0.370±0.005	19.8	-0.346±0.005	69.4	-0.028±0.005
3.1	-0.375±0.005	21.1	-0.339±0.005	71.9	-0.020±0.005
3.3	-0.378±0.005	22.4	-0.330±0.005	74.4	-0.017±0.005
3.8	-0.386±0.005	23.6	-0.317±0.005	77.0	-0.016±0.005
4.3	-0.392±0.005	24.9	-0.309±0.005	79.5	-0.006±0.005
4.9	-0.399±0.005	26.2	-0.297±0.005	82.1	-0.010±0.005
5.4	-0.405±0.005	27.5	-0.288±0.005	84.6	-0.005±0.005
5.9	-0.411±0.005	28.7	-0.279±0.005	87.1	-0.002±0.005
6.4	-0.414±0.005	30.0	-0.267±0.005	89.7	0.006±0.005
6.9	-0.414±0.005	31.3	-0.258±0.005	94.8	0.006±0.005
7.4	-0.417±0.005	32.5	-0.246±0.005	99.8	0.004±0.005
7.9	-0.417±0.005	33.8	-0.239±0.005	104.9	0.011±0.005
8.4	-0.418±0.005	35.1	-0.227±0.005	110.0	0.005±0.005
8.9	-0.417±0.005	36.3	-0.219±0.005	115.1	0.003±0.005
9.4	-0.415±0.005	37.6	-0.211±0.005	120.2	0.003±0.005
9.9	-0.413±0.005	38.9	-0.200±0.005	125.2	0.002±0.005
10.4	-0.410±0.005	41.4	-0.183±0.005	130.3	0.002±0.005
10.9	-0.408±0.005	44.0	-0.161±0.005	135.4	0.004±0.005
11.5	-0.406±0.005	46.5	-0.148±0.005	140.5	0.004±0.005

Table C.17 Kiel Probe Total Pressure Data at (x,z)=(127 mm,-70 mm)

y, mm	CPT	y, mm	CPT	y, mm	CPT
0.8	-0.412±0.005	12.0	-0.362±0.005	49:0	-0.116±0.005
1.0	-0.363±0.005	12.5	-0.357±0.005	51.6	-0.100±0.005
1.3	-0.338±0.005	13.0	-0.355±0.005	54.1	-0.086±0.005
1.5	-0.327±0.005	13.5	-0.354±0.005	56.7	-0.073±0.005
1.8	-0.322±0.005	14.8	-0.346±0.005	59.2	-0.062±0.005
2.1	-0.320±0.005	16.0	-0.338±0.005	61.7	-0.051±0.005
2.3	-0.322±0.005	17.3	-0.329±0.005	64.3	-0.040±0.005
2.6	-0.325±0.005	18.6	-0.322±0.005	66.8	-0.031±0.005
2.8	-0.329±0.005	19.8	-0.311±0.005	69.4	-0.024±0.005
3.1	-0.335±0.005	21.1	-0.303±0.005	71.9	-0.017±0.005
3.3	-0.338±0.005	22.4	-0.294±0.005	74.4	-0.012±0.005
3.8	-0.347±0.005	23.6	-0.284±0.005	77.0	-0.008±0.005
4.3	-0.356±0.005	24.9	-0.276±0.005	79.5	-0.005±0.005
4.9	-0.361±0.005	26.2	-0.267±0.005	82.1	-0.003±0.005
5.4	-0.366±0.005	27.5	-0.259±0.005	84.6	-0.001±0.005
5.9	-0.369±0.005	28.7	-0.247±0.005	87.1	0.000±0.005
6.4	-0.370±0.005	30.0	-0.238±0.005	89.7	0.001±0.005
6.9	-0.373±0.005	31.3	-0.230±0.005	94.8	0.002±0.005
7.4	-0.374±0.005	32.5	-0.220±0.005	99.8	0.002±0.005
7.9	-0.374±0.005	33.8	-0.212±0.005	104.9	0.002±0.005
8.4	-0.372±0.005	35.1	-0.202±0.005	110.0	0.002±0.005
8.9	-0.371±0.005	36.3	-0.195±0.005	115.1	0.002±0.005
9.4	-0.371±0.005	37.6	-0.186±0.005	120.2	0.002±0.005
9.9	-0.369±0.005	38.9	-0.177±0.005	125.2	0.002±0.005
10.4	-0.366±0.005	41.4	-0.161±0.005	130.3	0.002±0.005
10.9	-0.364±0.005	44.0	-0.145±0.005	135.4	0.002±0.005
11.5	-0.361±0.005	46.5	-0.128±0.005	140.5	0.002±0.005

Table C.18 Kiel Probe Total Pressure Data at (x,z)=(127 mm,-64 mm)

y, mm	CPT	y, mm	CPT	y, mm	CPT
0.8	-0.296±0.005	12.0	-0.290±0.005	49.0	-0.092±0.005
1.0	-0.271±0.005	12.5	-0.289±0.005	51.6	-0.081±0.005
1.3	-0.266±0.005	13.0	-0.287±0.005	54.1	-0.067±0.005
1.5	-0.262±0.005	13.5	-0.287±0.005	56.7	-0.057±0.005
1.8	-0.266±0.005	14.8	-0.279±0.005	59.2	-0.049±0.005
2.1	-0.268±0.005	16.0	-0.274±0.005	61.7	-0.039±0.005
2.3	-0.271±0.005	17.3	-0.267±0.005	64.3	-0.030±0.005
2.6	-0.273±0.005	18.6	-0.261±0.005	66.8	-0.024±0.005
2.8	-0.275±0.005	19.8	-0.253±0.005	69.4	-0.017±0.005
3.1	-0.279±0.005	21.1	-0.247±0.005	71.9	-0.014±0.005
3.3	-0.280±0.005	22.4	-0.241±0.005	74.4	-0.009±0.005
3.8	-0.285±0.005	23.6	-0.231±0.005	77.0	-0.006±0.005
4.3	-0.289±0.005	24.9	-0.226±0.005	79.5	-0.004±0.005
4.9	-0.290±0.005	26.2	-0.217±0.005	82.1	-0.002±0.005
5.4	-0.294±0.005	27.5	-0.209±0.005	84.6	-0.001±0.005
5.9	-0.296±0.005	28.7	-0.203±0.005	87.1	0.001±0.005
6.4	-0.295±0.005	30.0	-0.195±0.005	89.7	0.001±0.005
6.9	-0.298±0.005	31.3	-0.187±0.005	94.8	0.002±0.005
7.4	-0.299±0.005	32.5	-0.180±0.005	99.8	0.002±0.005
7.9	-0.299±0.005	33.8	-0.174±0.005	104.9	0.002±0.005
8.4	-0.300±0.005	35.1	-0.167±0.005	110.0	0.002±0.005
8.9	-0.298±0.005	36.3	-0.161±0.005	115.1	0.002±0.005
9.4	-0.299±0.005	37.6	-0.151±0.005	120.2	0.002±0.005
9.9	-0.297±0.005	38.9	-0.145±0.005	125.2	0.002±0.005
10.4	-0.293±0.005	41.4	-0.133±0.005	130.3	0.002±0.005
10.9	-0.294±0.005	44.0	-0.120±0.005	135.4	0.002±0.005
11.5	-0.292±0.005	46.5	-0.104±0.005	140.5	0.002±0.005

Table C.19 Kiel Probe Total Pressure Data at (x,z)=(-203 mm,0)

y, mm	CPT	y, mm	CPT	y, mm	CPT
0.8	-0.804±0.006	12.0	-0.557±0.005	49.0	-0.184±0.005
1.0	-0.789±0.006	12.5	-0.547±0.005	51.6	-0.165±0.005
1.3	-0.776±0.006	13.0	-0.543±0.005	54.1	-0.146±0.005
1.5	-0.767±0.006	13.5	-0.535±0.005	56.7	-0.126±0.005
1.8	-0.754±0.006	14.8	-0.520±0.005	59.2	-0.110±0.005
2.1	-0.743±0.006	16.0	-0.505±0.005	61.7	-0.090±0.005
2.3	-0.736±0.006	17.3	-0.489±0.005	64.3	-0.077±0.005
2.6	-0.729±0.006	18.6	-0.475±0.005	66.8	-0.061±0.005
2.8	-0.722±0.006	19.8	-0.460±0.005	69.4	-0.046±0.005
3.1	-0.714±0.006	21.1	-0.448±0.005	71.9	-0.037±0.005
3.3	-0.709±0.006	22.4	-0.434±0.005	74.4	-0.025±0.005
3.8	-0.694±0.006	23.6	-0.420±0.005	77.0	-0.019±0.005
4.3	-0.680±0.006	24.9	-0.408±0.005	79.5	-0.011±0.005
4.9	-0.669±0.006	26.2	-0.394±0.005	82.1	-0.007±0.005
5.4	-0.660±0.006	27.5	-0.381±0.005	84.6	-0.003±0.005
5.9	-0.652±0.006	28.7	-0.369±0.005	87.1	-0.001±0.005
6.4	-0.639±0.006	30.0	-0.357±0.005	89.7	0.001±0.005
6.9	-0.629±0.006	31.3	-0.346±0.005	94.8	0.002±0.005
7.4	-0.620±0.006	32.5	-0.331±0.005	99.8	0.003±0.005
7.9	-0.613±0.005	33.8	-0.319±0.005	104.9	0.003±0.005
8.4	-0.605±0.005	35.1	-0.309±0.005	110.0	0.003±0.005
8.9	-0.595±0.005	36.3	-0.294±0.005	115.1	0.003±0.005
9.4	-0.587±0.005	37.6	-0.284±0.005	120.2	0.003±0.005
9.9	-0.579±0.005	38.9	-0.271±0.005	125.2	0.003±0.005
10.4	-0.575±0.005	41.4	-0.249±0.005	130.3	0.002±0.005
10.9	-0.568±0.005	44.0	-0.225±0.005	135.4	0.002±0.005
11.5	-0.561±0.005	46.5	-0.205±0.005	140.5	0.002±0.005

Table C.20 Kiel Probe Total Pressure Data at (x,z)=(-178 mm,0)

y, mm	CPT	y, mm	CPT	y, mm	CPT
0.8	-0.803±0.006	12.0	-0.560±0.005	49.0	-0.191±0.005
1.0	-0.791±0.006	12.5	-0.553±0.005	51.6	-0.168±0.005
1.3	-0.778±0.006	13.0	-0.545±0.005	54.1	-0.147±0.005
1.5	-0.768±0.006	13.5	-0.541±0.005	56.7	-0.129±0.005
1.8	-0.760±0.006	14.8	-0.524±0.005	59.2	-0.111±0.005
2.1	-0.749±0.006	16.0	-0.509±0.005	61.7	-0.096±0.005
2.3	-0.742±0.006	17.3	-0.495±0.005	64.3	-0.081±0.005
2.6	-0.734±0.006	18.6	-0.480±0.005	66.8	-0.064±0.005
2.8	-0.726±0.006	19.8	-0.464±0.005	69.4	-0.051±0.005
3.1	-0.718±0.006	21.1	-0.451±0.005	71.9	-0.039±0.005
3.3	-0.713±0.006	22.4	-0.439±0.005	74.4	-0.029±0.005
3.8	-0.700±0.006	23.6	-0.425±0.005	77.0	-0.019±0.005
4.3	-0.689±0.006	24.9	-0.411±0.005	79.5	-0.012±0.005
4.9	-0.675±0.006	26.2	-0.399±0.005	82.1	-0.008±0.005
5.4	-0.664±0.006	27.5	-0.387±0.005	84.6	-0.004±0.005
5.9	-0.656±0.006	28.7	-0.373±0.005	87.1	-0.001±0.005
6.4	-0.646±0.006	30.0	-0.361±0.005	89.7	0.001±0.005
6.9	-0.635±0.006	31.3	-0.348±0.005	94.8	0.002±0.005
7.4	-0.626±0.006	32.5	-0.337±0.005	99.8	0.003±0.005
7.9	-0.621±0.006	33.8	-0.323±0.005	104.9	0.003±0.005
8.4	-0.612±0.005	35.1	-0.310±0.005	110.0	0.003±0.005
8.9	-0.603±0.005	36.3	-0.300±0.005	115.1	0.003±0.005
9.4	-0.594±0.005	37.6	-0.287±0.005	120.2	0.002±0.005
9.9	-0.587±0.005	38.9	-0.276±0.005	125.2	0.003±0.005
10.4	-0.578±0.005	41.4	-0.255±0.005	130.3	0.003±0.005
10.9	-0.571±0.005	44.0	-0.231±0.005	135.4	0.002±0.005
11.5	-0.566±0.005	46.5	-0.209±0.005	140.5	0.003±0.005

Table C.21 Kiel Probe Total Pressure Data at (x,z)=(-165 mm,0)

y, mm	CPT	y, mm	CPT	y, mm	CPT
0.8	-0.798±0.006	12.0	-0.558±0.005	49.0	-0.190±0.005
1.0	-0.787±0.006	12.5	-0.552±0.005	51.6	-0.171±0.005
1.3	-0.776±0.006	13.0	-0.546±0.005	54.1	-0.151±0.005
1.5	-0.765±0.006	13.5	-0.538±0.005	56.7	-0.131±0.005
1.8	-0.754±0.006	14.8	-0.523±0.005	59.2	-0.115±0.005
2.1	-0.747±0.006	16.0	-0.508±0.005	61.7	-0.096±0.005
2.3	-0.736±0.006	17.3	-0.495±0.005	64.3	-0.080±0.005
2.6	-0.729±0.006	18.6	-0.479±0.005	66.8	-0.066±0.005
2.8	-0.722±0.006	19.8	-0.465±0.005	69.4	-0.052±0.005
3.1	-0.714±0.006	21.1	-0.452±0.005	71.9	-0.039±0.005
3.3	-0.708±0.006	22.4	-0.438±0.005	74.4	-0.029±0.005
3.8	-0.696±0.006	23.6	-0.425±0.005	77.0	-0.021±0.005
4.3	-0.683±0.006	24.9	-0.412±0.005	79.5	-0.013±0.005
4.9	-0.672±0.006	26.2	-0.398±0.005	82.1	-0.008±0.005
5.4	-0.662±0.006	27.5	-0.388±0.005	84.6	-0.004±0.005
5.9	-0.654±0.006	28.7	-0.373±0.005	87.1	-0.001±0.005
6.4	-0.643±0.006	30.0	-0.361±0.005	89.7	0.001±0.005
6.9	-0.633±0.006	31.3	-0.350±0.005	94.8	0.002±0.005
7.4	-0.626±0.006	32.5	-0.333±0.005	99.8	0.003±0.005
7.9	-0.616±0.005	33.8	-0.324±0.005	104.9	0.003±0.005
8.4	-0.611±0.005	35.1	-0.312±0.005	110.0	0.003±0.005
8.9	-0.601±0.005	36.3	-0.300±0.005	115.1	0.003±0.005
9.4	-0.593±0.005	37.6	-0.291±0.005	120.2	0.003±0.005
9.9	-0.587±0.005	38.9	-0.275±0.005	125.2	0.003±0.005
10.4	-0.581±0.005	41.4	-0.253±0.005	130.3	0.003±0.005
10.9	-0.570±0.005	44.0	-0.234±0.005	135.4	0.003±0.005
11.5	-0.565±0.005	46.5	-0.211±0.005	140.5	0.002±0.005

Table C.22 Kiel Probe Total Pressure Data at (x,z)=(-152 mm,0)

y, mm	CPT	y, mm	CPT	y, mm	CPT
0.8	-0.794±0.006	12.0	-0.562±0.005	49.0	-0.190±0.005
1.0	-0.783±0.006	12.5	-0.555±0.005	51.6	-0.171±0.005
1.3	-0.771±0.006	13.0	-0.548±0.005	54.1	-0.152±0.005
1.5	-0.762±0.006	13.5	-0.541±0.005	56.7	-0.135±0.005
1.8	-0.754±0.006	14.8	-0.527±0.005	59.2	-0.116±0.005
2.1	-0.746±0.006	16.0	-0.512±0.005	61.7	-0.097±0.005
2.3	-0.738±0.006	17.3	-0.497±0.005	64.3	-0.082±0.005
2.6	-0.730±0.006	18.6	-0.482±0.005	66.8	-0.066±0.005
2.8	-0.722±0.006	19.8	-0.468±0.005	69.4	-0.052±0.005
3.1	-0.715±0.006	21.1	-0.454±0.005	71.9	-0.039±0.005
3.3	-0.707±0.006	22.4	-0.442±0.005	74.4	-0.030±0.005
3.8	-0.696±0.006	23.6	-0.429±0.005	77.0	-0.020±0.005
4.3	-0.686±0.006	24.9	-0.416±0.005	79.5	-0.014±0.005
4.9	-0.675±0.006	26.2	-0.402±0.005	82.1	-0.008±0.005
5.4	-0.664±0.006	27.5	-0.390±0.005	84.6	-0.004±0.005
5.9	-0.655±0.006	28.7	-0.377±0.005	87.1	-0.001±0.005
6.4	-0.645±0.006	30.0	-0.362±0.005	89.7	0.000±0.005
6.9	-0.636±0.006	31.3	-0.351±0.005	94.8	0.002±0.005
7.4	-0.629±0.006	32.5	-0.340±0.005	99.8	0.003±0.005
7.9	-0.619±0.005	33.8	-0.327±0.005	104.9	0.003±0.005
8.4	-0.611±0.005	35.1	-0.313±0.005	110.0	0.003±0.005
8.9	-0.603±0.005	36.3	-0.304±0.005	115.1	0.003±0.005
9.4	-0.596±0.005	37.6	-0.290±0.005	120.2	0.003±0.005
9.9	-0.588±0.005	38.9	-0.280±0.005	125.2	0.003±0.005
10.4	-0.583±0.005	41.4	-0.257±0.005	130.3	0.003±0.005
10.9	-0.576±0.005	44.0	-0.233±0.005	135.4	0.003±0.005
11.5	-0.569±0.005	46.5	-0.214±0.005	140.5	0.002±0.005

Table C.23 Kiel Probe Total Pressure Data at (x,z)=(-140 mm,0)

y, mm	CPT	y, mm	CPT	y, mm	CPT
0.8	-0.793±0.006	12.0	-0.563±0.005	49.0	-0.194±0.005
1.0	-0.784±0.006	12.5	-0.556±0.005	51.6	-0.172±0.005
1.3	-0.773±0.006	13.0	-0.551±0.005	54.1	-0.155±0.005
1.5	-0.762±0.006	13.5	-0.543±0.005	56.7	-0.134±0.005
1.8	-0.753±0.006	14.8	-0.528±0.005	59.2	-0.118±0.005
2.1	-0.744±0.006	16.0	-0.512±0.005	61.7	-0.102±0.005
2.3	-0.736±0.006	17.3	-0.499±0.005	64.3	-0.081±0.005
2.6	-0.728±0.006	18.6	-0.485±0.005	66.8	-0.069±0.005
2.8	-0.721±0.006	19.8	-0.468±0.005	69.4	-0.056±0.005
3.1	-0.715±0.006	21.1	-0.456±0.005	71.9	-0.043±0.005
3.3	-0.708±0.006	22.4	-0.442±0.005	74.4	-0.032±0.005
3.8	-0.696±0.006	23.6	-0.430±0.005	77.0	-0.023±0.005
4.3	-0.684±0.006	24.9	-0.418±0.005	79.5	-0.015±0.005
4.9	-0.672±0.006	26.2	-0.404±0.005	82.1	-0.009±0.005
5.4	-0.665±0.006	27.5	-0.392±0.005	84.6	-0.005±0.005
5.9	-0.652±0.006	28.7	-0.379±0.005	87.1	-0.002±0.005
6.4	-0.645±0.006	30.0	-0.363±0.005	89.7	0.000±0.005
6.9	-0.636±0.006	31.3	-0.351±0.005	94.8	0.002±0.005
7.4	-0.627±0.006	32.5	-0.340±0.005	99.8	0.003±0.005
7.9	-0.617±0.006	33.8	-0.326±0.005	104.9	0.003±0.005
8.4	-0.612±0.006	35.1	-0.316±0.005	110.0	0.003±0.005
8.9	-0.604±0.006	36.3	-0.304±0.005	115.1	0.003±0.005
9.4	-0.595±0.005	37.6	-0.293±0.005	120.2	0.003±0.005
9.9	-0.589±0.005	38.9	-0.280±0.005	125.2	0.003±0.005
10.4	-0.582±0.005	41.4	-0.258±0.005	130.3	0.003±0.005
10.9	-0.575±0.005	44.0	-0.234±0.005	135.4	0.002±0.005
11.5	-0.569±0.005	46.5	-0.216±0.005	140.5	0.002±0.005

Table C.24 Kiel Probe Total Pressure Data at (x,z)=(-127 mm,0)

y, mm	CPT	y, mm	CPT	y, mm	CPT
0.8	-0.783±0.006	12.0	-0.567±0.005	49.0	-0.196±0.005
1.0	-0.774±0.006	12.5	-0.557±0.005	51.6	-0.176±0.005
1.3	-0.764±0.006	13.0	-0.553±0.005	54.1	-0.153±0.005
1.5	-0.757±0.006	13.5	-0.547±0.005	56.7	-0.138±0.005
1.8	-0.747±0.006	14.8	-0.530±0.005	59.2	-0.120±0.005
2.1	-0.740±0.006	16.0	-0.516±0.005	61.7	-0.106±0.005
2.3	-0.735±0.006	17.3	-0.501±0.005	64.3	-0.086±0.005
2.6	-0.728±0.006	18.6	-0.487±0.005	66.8	-0.069±0.005
2.8	-0.719±0.006	19.8	-0.474±0.005	69.4	-0.056±0.005
3.1	-0.713±0.006	21.1	-0.459±0.005	71.9	-0.042±0.005
3.3	-0.708±0.006	22.4	-0.442±0.005	74.4	-0.034±0.005
3.8	-0.696±0.006	23.6	-0.433±0.005	77.0	-0.026±0.005
4.3	-0.686±0.006	24.9	-0.420±0.005	79.5	-0.017±0.005
4.9	-0.675±0.006	26.2	-0.407±0.005	82.1	-0.010±0.005
5.4	-0.665±0.006	27.5	-0.394±0.005	84.6	-0.006±0.005
5.9	-0.653±0.006	28.7	-0.380±0.005	87.1	-0.003±0.005
6.4	-0.646±0.006	30.0	-0.367±0.005	89.7	-0.000±0.005
6.9	-0.639±0.006	31.3	-0.359±0.005	94.8	0.002±0.005
7.4	-0.631±0.006	32.5	-0.345±0.005	99.8	0.003±0.005
7.9	-0.621±0.006	33.8	-0.330±0.005	104.9	0.003±0.005
8.4	-0.614±0.006	35.1	-0.320±0.005	110.0	0.003±0.005
8.9	-0.608±0.006	36.3	-0.308±0.005	115.1	0.003±0.005
9.4	-0.602±0.005	37.6	-0.296±0.005	120.2	0.003±0.005
9.9	-0.592±0.005	38.9	-0.285±0.005	125.2	0.003±0.005
10.4	-0.586±0.005	41.4	-0.260±0.005	130.3	0.003±0.005
10.9	-0.579±0.005	44.0	-0.240±0.005	135.4	0.002±0.005
11.5	-0.573±0.005	46.5	-0.219±0.005	140.5	0.002±0.005

Table C.25 Kiel Probe Total Pressure Data at (x,z)=(-121 mm,0)

y, mm	CPT	y, mm	CPT	y, mm	CPT
0.8	-0.787±0.006	12.0	-0.567±0.005	49.0	-0.196±0.005
1.0	-0.779±0.006	12.5	-0.561±0.005	51.6	-0.180±0.005
1.3	-0.769±0.006	13.0	-0.555±0.005	54.1	-0.159±0.005
1.5	-0.761±0.006	13.5	-0.548±0.005	56.7	-0.140±0.005
1.8	-0.752±0.006	14.8	-0.532±0.005	59.2	-0.121±0.005
2.1	-0.744±0.006	16.0	-0.517±0.005	61.7	-0.104±0.005
2.3	-0.737±0.006	17.3	-0.503±0.005	64.3	-0.087±0.005
2.6	-0.730±0.006	18.6	-0.493±0.005	66.8	-0.073±0.005
2.8	-0.725±0.006	19.8	-0.478±0.005	69.4	-0.059±0.005
3.1	-0.717±0.006	21.1	-0.461±0.005	71.9	-0.044±0.005
3.3	-0.712±0.006	22.4	-0.449±0.005	74.4	-0.035±0.005
3.8	-0.700±0.006	23.6	-0.434±0.005	77.0	-0.023±0.005
4.3	-0.688±0.006	24.9	-0.421±0.005	79.5	-0.016±0.005
4.9	-0.679±0.006	26.2	-0.411±0.005	82.1	-0.011±0.005
5.4	-0.670±0.006	27.5	-0.397±0.005	84.6	-0.005±0.005
5.9	-0.660±0.006	28.7	-0.384±0.005	87.1	-0.002±0.005
6.4	-0.651±0.006	30.0	-0.373±0.005	89.7	-0.001±0.005
6.9	-0.642±0.006	31.3	-0.359±0.005	94.8	0.002±0.005
7.4	-0.632±0.006	32.5	-0.347±0.005	99.8	0.003±0.005
7.9	-0.625±0.006	33.8	-0.335±0.005	104.9	0.003±0.005
8.4	-0.618±0.006	35.1	-0.323±0.005	110.0	0.003±0.005
8.9	-0.609±0.006	36.3	-0.310±0.005	115.1	0.003±0.005
9.4	-0.601±0.005	37.6	-0.299±0.005	120.2	0.002±0.005
9.9	-0.597±0.005	38.9	-0.286±0.005	125.2	0.003±0.005
10.4	-0.589±0.005	41.4	-0.262±0.005	130.3	0.002±0.005
10.9	-0.577±0.005	44.0	-0.242±0.005	135.4	0.002±0.005
11.5	-0.575±0.005	46.5	-0.219±0.005	140.5	0.002±0.005

Table C.26 Kiel Probe Total Pressure Data at (x,z)=(-114 mm,0)

y, mm	CPT	y, mm	CPT	y, mm	CPT
0.8	-0.788±0.006	12.0	-0.568±0.005	49.0	-0.200±0.005
1.0	-0.781±0.006	12.5	-0.561±0.005	51.6	-0.178±0.005
1.3	-0.771±0.006	13.0	-0.555±0.005	54.1	-0.161±0.005
1.5	-0.762±0.006	13.5	-0.550±0.005	56.7	-0.140±0.005
1.8	-0.752±0.006	14.8	-0.533±0.005	59.2	-0.123±0.005
2.1	-0.746±0.006	16.0	-0.519±0.005	61.7	-0.105±0.005
2.3	-0.739±0.006	17.3	-0.504±0.005	64.3	-0.087±0.005
2.6	-0.732±0.006	18.6	-0.491±0.005	66.8	-0.074±0.005
2.8	-0.724±0.006	19.8	-0.476±0.005	69.4	-0.059±0.005
3.1	-0.719±0.006	21.1	-0.462±0.005	71.9	-0.045±0.005
3.3	-0.712±0.006	22.4	-0.449±0.005	74.4	-0.034±0.005
3.8	-0.701±0.006	23.6	-0.433±0.005	77.0	-0.025±0.005
4.3	-0.690±0.006	24.9	-0.420±0.005	79.5	-0.017±0.005
4.9	-0.680±0.006	26.2	-0.410±0.005	82.1	-0.011±0.005
5.4	-0.671±0.006	27.5	-0.396±0.005	84.6	-0.007±0.005
5.9	-0.660±0.006	28.7	-0.383±0.005	87.1	-0.003±0.005
6.4	-0.650±0.006	30.0	-0.371±0.005	89.7	-0.001±0.005
6.9	-0.642±0.006	31.3	-0.360±0.005	94.8	0.002±0.005
7.4	-0.633±0.006	32.5	-0.346±0.005	99.8	0.003±0.005
7.9	-0.627±0.006	33.8	-0.333±0.005	104.9	0.003±0.005
8.4	-0.618±0.006	35.1	-0.323±0.005	110.0	0.003±0.005
8.9	-0.610±0.006	36.3	-0.309±0.005	115.1	0.003±0.005
9.4	-0.604±0.006	37.6	-0.297±0.005	120.2	0.003±0.005
9.9	-0.594±0.005	38.9	-0.284±0.005	125.2	0.003±0.005
10.4	-0.589±0.005	41.4	-0.266±0.005	130.3	0.003±0.005
10.9	-0.581±0.005	44.0	-0.243±0.005	135.4	0.003±0.005
11.5	-0.575±0.005	46.5	-0.218±0.005	140.5	0.003±0.005

Table C.27 Kiel Probe Total Pressure Data at (x,z)=(-108 mm,0)

y, mm	CPT	y, mm	CPT	y, mm	CPT
0.8	-0.774±0.006	12.0	-0.565±0.005	49.0	-0.199±0.005
1.0	-0.768±0.006	12.5	-0.559±0.005	51.6	-0.178±0.005
1.3	-0.761±0.006	13.0	-0.553±0.005	54.1	-0.157±0.005
1.5	-0.753±0.006	13.5	-0.546±0.005	56.7	-0.139±0.005
1.8	-0.744±0.006	14.8	-0.532±0.005	59.2	-0.119±0.005
2.1	-0.737±0.006	16.0	-0.515±0.005	61.7	-0.106±0.005
2.3	-0.732±0.006	17.3	-0.500±0.005	64.3	-0.088±0.005
2.6	-0.724±0.006	18.6	-0.489±0.005	66.8	-0.073±0.005
2.8	-0.717±0.006	19.8	-0.475±0.005	69.4	-0.058±0.005
3.1	-0.713±0.006	21.1	-0.459±0.005	71.9	-0.047±0.005
3.3	-0.706±0.006	22.4	-0.446±0.005	74.4	-0.034±0.005
3.8	-0.697±0.006	23.6	-0.435±0.005	77.0	-0.025±0.005
4.3	-0.685±0.006	24.9	-0.418±0.005	79.5	-0.017±0.005
4.9	-0.674±0.006	26.2	-0.407±0.005	82.1	-0.011±0.005
5.4	-0.665±0.006	27.5	-0.393±0.005	84.6	-0.006±0.005
5.9	-0.655±0.006	28.7	-0.381±0.005	87.1	-0.003±0.005
6.4	-0.648±0.006	30.0	-0.371±0.005	89.7	-0.000±0.005
6.9	-0.640±0.006	31.3	-0.354±0.005	94.8	0.002±0.005
7.4	-0.631±0.006	32.5	-0.344±0.005	99.8	0.003±0.005
7.9	-0.623±0.006	33.8	-0.333±0.005	104.9	0.003±0.005
8.4	-0.614±0.006	35.1	-0.321±0.005	110.0	0.003±0.005
8.9	-0.607±0.005	36.3	-0.307±0.005	115.1	0.003±0.005
9.4	-0.597±0.005	37.6	-0.297±0.005	120.2	0.003±0.005
9.9	-0.592±0.005	38.9	-0.285±0.005	125.2	0.003±0.005
10.4	-0.586±0.005	41.4	-0.261±0.005	130.3	0.003±0.005
10.9	-0.578±0.005	44.0	-0.239±0.005	135.4	0.003±0.005
11.5	-0.571±0.005	46.5	-0.221±0.005	140.5	0.003±0.005

Table C.28 Kiel Probe Total Pressure Data at (x,z)=(-102 mm,0)

y, mm	CPT	y, mm	CPT	y, mm	CPT
0.8	-0.773±0.006	12.0	-0.565±0.005	49.0	-0.198±0.005
1.0	-0.765±0.006	12.5	-0.559±0.005	51.6	-0.176±0.005
1.3	-0.758±0.006	13.0	-0.553±0.005	54.1	-0.156±0.005
1.5	-0.750±0.006	13.5	-0.545±0.005	56.7	-0.139±0.005
1.8	-0.741±0.006	14.8	-0.531±0.005	59.2	-0.118±0.005
2.1	-0.736±0.006	16.0	-0.516±0.005	61.7	-0.103±0.005
2.3	-0.729±0.006	17.3	-0.501±0.005	64.3	-0.088±0.005
2.6	-0.725±0.006	18.6	-0.486±0.005	66.8	-0.072±0.005
2.8	-0.717±0.006	19.8	-0.473±0.005	69.4	-0.057±0.005
3.1	-0.710±0.006	21.1	-0.460±0.005	71.9	-0.044±0.005
3.3	-0.705±0.006	22.4	-0.445±0.005	74.4	-0.034±0.005
3.8	-0.694±0.006	23.6	-0.430±0.005	77.0	-0.025±0.005
4.3	-0.683±0.006	24.9	-0.417±0.005	79.5	-0.016±0.005
4.9	-0.671±0.006	26.2	-0.406±0.005	82.1	-0.011±0.005
5.4	-0.665±0.006	27.5	-0.394±0.005	84.6	-0.006±0.005
5.9	-0.654±0.006	28.7	-0.380±0.005	87.1	-0.003±0.005
6.4	-0.647±0.006	30.0	-0.370±0.005	89.7	-0.001±0.005
6.9	-0.638±0.006	31.3	-0.357±0.005	94.8	0.002±0.005
7.4	-0.631±0.006	32.5	-0.344±0.005	99.8	0.003±0.005
7.9	-0.619±0.006	33.8	-0.330±0.005	104.9	0.003±0.005
8.4	-0.614±0.006	35.1	-0.318±0.005	110.0	0.003±0.005
8.9	-0.608±0.005	36.3	-0.307±0.005	115.1	0.003±0.005
9.4	-0.601±0.005	37.6	-0.298±0.005	120.2	0.003±0.005
9.9	-0.590±0.005	38.9	-0.285±0.005	125.2	0.003±0.005
10.4	-0.586±0.005	41.4	-0.262±0.005	130.3	0.003±0.005
10.9	-0.578±0.005	44.0	-0.241±0.005	135.4	0.003±0.005
11.5	-0.570±0.005	46.5	-0.221±0.005	140.5	0.002±0.005

Table C.29 Kiel Probe Total Pressure Data at (x,z)=(-95 mm,0)

y, mm	CPT	y, mm	CPT	y, mm	CPT
0.8	-0.769±0.006	12.0	-0.564±0.005	49.0	-0.198±0.005
1.0	-0.763±0.006	12.5	-0.557±0.005	51.6	-0.176±0.005
1.3	-0.756±0.006	13.0	-0.553±0.005	54.1	-0.156±0.005
1.5	-0.747±0.006	13.5	-0.546±0.005	56.7	-0.137±0.005
1.8	-0.742±0.006	14.8	-0.532±0.005	59.2	-0.122±0.005
2.1	-0.734±0.006	16.0	-0.516±0.005	61.7	-0.104±0.005
2.3	-0.728±0.006	17.3	-0.501±0.005	64.3	-0.087±0.005
2.6	-0.722±0.006	18.6	-0.488±0.005	66.8	-0.072±0.005
2.8	-0.717±0.006	19.8	-0.471±0.005	69.4	-0.059±0.005
3.1	-0.711±0.006	21.1	-0.460±0.005	71.9	-0.045±0.005
3.3	-0.703±0.006	22.4	-0.447±0.005	74.4	-0.035±0.005
3.8	-0.693±0.006	23.6	-0.433±0.005	77.0	-0.025±0.005
4.3	-0.685±0.006	24.9	-0.420±0.005	79.5	-0.017±0.005
4.9	-0.674±0.006	26.2	-0.407±0.005	82.1	-0.011±0.005
5.4	-0.663±0.006	27.5	-0.393±0.005	84.6	-0.006±0.005
5.9	-0.655±0.006	28.7	-0.382±0.005	87.1	-0.003±0.005
6.4	-0.646±0.006	30.0	-0.367±0.005	89.7	-0.001±0.005
6.9	-0.641±0.006	31.3	-0.355±0.005	94.8	0.002±0.005
7.4	-0.630±0.006	32.5	-0.345±0.005	99.8	0.003±0.005
7.9	-0.621±0.006	33.8	-0.334±0.005	104.9	0.003±0.005
8.4	-0.615±0.006	35.1	-0.319±0.005	110.0	0.003±0.005
8.9	-0.607±0.006	36.3	-0.309±0.005	115.1	0.003±0.005
9.4	-0.600±0.005	37.6	-0.297±0.005	120.2	0.003±0.005
9.9	-0.594±0.005	38.9	-0.284±0.005	125.2	0.003±0.005
10.4	-0.584±0.005	41.4	-0.261±0.005	130.3	0.003±0.005
10.9	-0.578±0.005	44.0	-0.240±0.005	135.4	0.003±0.005
11.5	-0.570±0.005	46.5	-0.221±0.005	140.5	0.003±0.005

Table C.30 Kiel Probe Total Pressure Data at (x,z)=(-89 mm,0)

y, mm	CPT	y, mm	CPT	y, mm	CPT
0.8	-0.775±0.006	12.0	-0.572±0.005	49.0	-0.207±0.005
1.0	-0.767±0.006	12.5	-0.566±0.005	51.6	-0.184±0.005
1.3	-0.759±0.006	13.0	-0.562±0.005	54.1	-0.167±0.005
1.5	-0.751±0.006	13.5	-0.553±0.005	56.7	-0.143±0.005
1.8	-0.746±0.006	14.8	-0.539±0.005	59.2	-0.128±0.005
2.1	-0.739±0.006	16.0	-0.523±0.005	61.7	-0.109±0.005
2.3	-0.733±0.006	17.3	-0.509±0.005	64.3	-0.091±0.005
2.6	-0.728±0.006	18.6	-0.495±0.005	66.8	-0.078±0.005
2.8	-0.722±0.006	19.8	-0.482±0.005	69.4	-0.061±0.005
3.1	-0.715±0.006	21.1	-0.467±0.005	71.9	-0.048±0.005
3.3	-0.712±0.006	22.4	-0.455±0.005	74.4	-0.038±0.005
3.8	-0.700±0.006	23.6	-0.441±0.005	77.0	-0.027±0.005
4.3	-0.689±0.006	24.9	-0.427±0.005	79.5	-0.021±0.005
4.9	-0.679±0.006	26.2	-0.415±0.005	82.1	-0.013±0.005
5.4	-0.675±0.006	27.5	-0.401±0.005	84.6	-0.009±0.005
5.9	-0.662±0.006	28.7	-0.386±0.005	87.1	-0.005±0.005
6.4	-0.653±0.006	30.0	-0.379±0.005	89.7	-0.002±0.005
6.9	-0.644±0.006	31.3	-0.367±0.005	94.8	0.001±0.005
7.4	-0.639±0.006	32.5	-0.352±0.005	99.8	0.002±0.005
7.9	-0.629±0.006	33.8	-0.337±0.005	104.9	0.002±0.005
8.4	-0.624±0.006	35.1	-0.328±0.005	110.0	0.002±0.005
8.9	-0.614±0.006	36.3	-0.314±0.005	115.1	0.002±0.005
9.4	-0.607±0.006	37.6	-0.307±0.005	120.2	0.002±0.005
9.9	-0.602±0.006	38.9	-0.294±0.005	125.2	0.002±0.005
10.4	-0.592±0.005	41.4	-0.267±0.005	130.3	0.002±0.005
10.9	-0.587±0.005	44.0	-0.250±0.005	135.4	0.002±0.005
11.5	-0.580±0.005	46.5	-0.225±0.005	140.5	0.002±0.005

Table C.31 Kiel Probe Total Pressure Data at (x,z)=(-83 mm,0)

y, mm	CPT	y, mm	CPT	y, mm	CPT
0.8	-0.768±0.006	12.0	-0.576±0.005	49.0	-0.206±0.005
1.0	-0.762±0.006	12.5	-0.570±0.005	51.6	-0.186±0.005
1.3	-0.755±0.006	13.0	-0.563±0.005	54.1	-0.168±0.005
1.5	-0.749±0.006	13.5	-0.559±0.005	56.7	-0.147±0.005
1.8	-0.743±0.006	14.8	-0.540±0.005	59.2	-0.129±0.005
2.1	-0.737±0.006	16.0	-0.527±0.005	61.7	-0.111±0.005
2.3	-0.733±0.006	17.3	-0.512±0.005	64.3	-0.095±0.005
2.6	-0.727±0.006	18.6	-0.498±0.005	66.8	-0.079±0.005
2.8	-0.722±0.006	19.8	-0.485±0.005	69.4	-0.067±0.005
3.1	-0.716±0.006	21.1	-0.471±0.005	71.9	-0.052±0.005
3.3	-0.712±0.006	22.4	-0.458±0.005	74.4	-0.040±0.005
3.8	-0.701±0.006	23.6	-0.442±0.005	77.0	-0.030±0.005
4.3	-0.692±0.006	24.9	-0.430±0.005	79.5	-0.022±0.005
4.9	-0.681±0.006	26.2	-0.416±0.005	82.1	-0.015±0.005
5.4	-0.672±0.006	27.5	-0.406±0.005	84.6	-0.009±0.005
5.9	-0.663±0.006	28.7	-0.392±0.005	87.1	-0.005±0.005
6.4	-0.655±0.006	30.0	-0.381±0.005	89.7	-0.003±0.005
6.9	-0.649±0.006	31.3	-0.366±0.005	94.8	0.001±0.005
7.4	-0.640±0.006	32.5	-0.355±0.005	99.8	0.002±0.005
7.9	-0.631±0.006	33.8	-0.341±0.005	104.9	0.002±0.005
8.4	-0.624±0.005	35.1	-0.329±0.005	110.0	0.002±0.005
8.9	-0.617±0.005	36.3	-0.319±0.005	115.1	0.002±0.005
9.4	-0.608±0.005	37.6	-0.308±0.005	120.2	0.002±0.005
9.9	-0.605±0.005	38.9	-0.295±0.005	125.2	0.002±0.005
10.4	-0.597±0.005	41.4	-0.273±0.005	130.3	0.002±0.005
10.9	-0.591±0.005	44.0	-0.250±0.005	135.4	0.002±0.005
11.5	-0.584±0.005	46.5	-0.228±0.005	140.5	0.002±0.005

Table C.32 Kiel Probe Total Pressure Data at (x,z)=(-76 mm,0)

y, mm	CPT	y, mm	CPT	y, mm	CPT
0.8	-0.766±0.006	12.0	-0.580±0.005	49.0	-0.208±0.005
1.0	-0.760±0.006	12.5	-0.574±0.005	51.6	-0.187±0.005
1.3	-0.754±0.006	13.0	-0.565±0.005	54.1	-0.168±0.005
1.5	-0.749±0.006	13.5	-0.561±0.005	56.7	-0.149±0.005
1.8	-0.744±0.006	14.8	-0.543±0.005	59.2	-0.129±0.005
2.1	-0.737±0.006	16.0	-0.529±0.005	61.7	-0.112±0.005
2.3	-0.734±0.006	17.3	-0.514±0.005	64.3	-0.096±0.005
2.6	-0.727±0.006	18.6	-0.500±0.005	66.8	-0.079±0.005
2.8	-0.722±0.006	19.8	-0.487±0.005	69.4	-0.067±0.005
3.1	-0.718±0.006	21.1	-0.472±0.005	71.9	-0.052±0.005
3.3	-0.712±0.006	22.4	-0.457±0.005	74.4	-0.040±0.005
3.8	-0.704±0.006	23.6	-0.444±0.005	77.0	-0.031±0.005
4.3	-0.693±0.006	24.9	-0.433±0.005	79.5	-0.019±0.005
4.9	-0.684±0.006	26.2	-0.417±0.005	82.1	-0.013±0.005
5.4	-0.675±0.006	27.5	-0.405±0.005	84.6	-0.008±0.005
5.9	-0.667±0.006	28.7	-0.392±0.005	87.1	-0.004±0.005
6.4	-0.657±0.006	30.0	-0.378±0.005	89.7	-0.003±0.005
6.9	-0.651±0.006	31.3	-0.367±0.005	94.8	0.000±0.005
7.4	-0.643±0.006	32.5	-0.354±0.005	99.8	0.002±0.005
7.9	-0.637±0.006	33.8	-0.341±0.005	104.9	0.002±0.005
8.4	-0.626±0.006	35.1	-0.328±0.005	110.0	0.002±0.005
8.9	-0.622±0.005	36.3	-0.321±0.005	115.1	0.002±0.005
9.4	-0.611±0.005	37.6	-0.307±0.005	120.2	0.002±0.005
9.9	-0.606±0.005	38.9	-0.295±0.005	125.2	0.002±0.005
10.4	-0.600±0.005	41.4	-0.272±0.005	130.3	0.002±0.005
10.9	-0.594±0.005	44.0	-0.251±0.005	135.4	0.002±0.005
11.5	-0.584±0.005	46.5	-0.229±0.005	140.5	0.002±0.005

Table C.33 Kiel Probe Total Pressure Data at (x,z)=(-70 mm,0)

y, mm	CPT	y, mm	CPT	y, mm	CPT
0.8	-0.762±0.006	12.0	-0.583±0.005	49.0	-0.207±0.005
1.0	-0.756±0.006	12.5	-0.575±0.005	51.6	-0.187±0.005
1.3	-0.752±0.006	13.0	-0.569±0.005	54.1	-0.167±0.005
1.5	-0.746±0.006	13.5	-0.564±0.005	56.7	-0.148±0.005
1.8	-0.742±0.006	14.8	-0.546±0.005	59.2	-0.129±0.005
2.1	-0.735±0.006	16.0	-0.532±0.005	61.7	-0.111±0.005
2.3	-0.731±0.006	17.3	-0.518±0.005	64.3	-0.096±0.005
2.6	-0.725±0.006	18.6	-0.503±0.005	66.8	-0.079±0.005
2.8	-0.722±0.006	19.8	-0.487±0.005	69.4	-0.065±0.005
3.1	-0.719±0.006	21.1	-0.475±0.005	71.9	-0.052±0.005
3.3	-0.714±0.006	22.4	-0.460±0.005	74.4	-0.040±0.005
3.8	-0.703±0.006	23.6	-0.444±0.005	77.0	-0.030±0.005
4.3	-0.696±0.006	24.9	-0.432±0.005	79.5	-0.021±0.005
4.9	-0.688±0.006	26.2	-0.420±0.005	82.1	-0.014±0.005
5.4	-0.679±0.006	27.5	-0.405±0.005	84.6	-0.009±0.005
5.9	-0.670±0.006	28.7	-0.393±0.005	87.1	-0.005±0.005
6.4	-0.663±0.006	30.0	-0.380±0.005	89.7	-0.002±0.005
6.9	-0.652±0.006	31.3	-0.368±0.005	94.8	0.001±0.005
7.4	-0.646±0.006	32.5	-0.353±0.005	99.8	0.002±0.005
7.9	-0.640±0.006	33.8	-0.342±0.005	104.9	0.003±0.005
8.4	-0.630±0.005	35.1	-0.330±0.005	110.0	0.003±0.005
8.9	-0.624±0.005	36.3	-0.317±0.005	115.1	0.003±0.005
9.4	-0.617±0.005	37.6	-0.306±0.005	120.2	0.002±0.005
9.9	-0.610±0.005	38.9	-0.295±0.005	125.2	0.002±0.005
10.4	-0.604±0.005	41.4	-0.271±0.005	130.3	0.002±0.005
10.9	-0.593±0.005	44.0	-0.248±0.005	135.4	0.002±0.005
11.5	-0.589±0.005	46.5	-0.229±0.005	140.5	0.002±0.005

Table C.34 Kiel Probe Total Pressure Data at (x,z)=(-64 mm,0)

y, mm	CPT	y, mm	CPT	y, mm	CPT
0.8	-0.758±0.006	12.0	-0.584±0.005	49.0	-0.205±0.005
1.0	-0.754±0.006	12.5	-0.576±0.005	51.6	-0.184±0.005
1.3	-0.750±0.006	13.0	-0.571±0.005	54.1	-0.164±0.005
1.5	-0.745±0.006	13.5	-0.563±0.005	56.7	-0.145±0.005
1.8	-0.741±0.006	14.8	-0.547±0.005	59.2	-0.128±0.005
2.1	-0.736±0.006	16.0	-0.532±0.005	61.7	-0.111±0.005
2.3	-0.732±0.006	17.3	-0.519±0.005	64.3	-0.095±0.005
2.6	-0.729±0.006	18.6	-0.501±0.005	66.8	-0.079±0.005
2.8	-0.724±0.006	19.8	-0.487±0.005	69.4	-0.063±0.005
3.1	-0.721±0.006	21.1	-0.474±0.005	71.9	-0.050±0.005
3.3	-0.715±0.006	22.4	-0.462±0.005	74.4	-0.040±0.005
3.8	-0.708±0.006	23.6	-0.446±0.005	77.0	-0.029±0.005
4.3	-0.699±0.006	24.9	-0.432±0.005	79.5	-0.021±0.005
4.9	-0.690±0.006	26.2	-0.417±0.005	82.1	-0.014±0.005
5.4	-0.680±0.006	27.5	-0.403±0.005	84.6	-0.009±0.005
5.9	-0.675±0.006	28.7	-0.393±0.005	87.1	-0.004±0.005
6.4	-0.668±0.006	30.0	-0.380±0.005	89.7	-0.002±0.005
6.9	-0.657±0.006	31.3	-0.366±0.005	94.8	0.001±0.005
7.4	-0.647±0.006	32.5	-0.354±0.005	99.8	0.002±0.005
7.9	-0.643±0.006	33.8	-0.342±0.005	104.9	0.003±0.005
8.4	-0.635±0.005	35.1	-0.330±0.005	110.0	0.003±0.005
8.9	-0.627±0.005	36.3	-0.317±0.005	115.1	0.002±0.005
9.4	-0.619±0.005	37.6	-0.304±0.005	120.2	0.003±0.005
9.9	-0.614±0.005	38.9	-0.293±0.005	125.2	0.002±0.005
10.4	-0.607±0.005	41.4	-0.271±0.005	130.3	0.003±0.005
10.9	-0.599±0.005	44.0	-0.247±0.005	135.4	0.002±0.005
11.5	-0.590±0.005	46.5	-0.226±0.005	140.5	0.002±0.005

Table C.35 Kiel Probe Total Pressure Data at (x,z)=(-57 mm,0)

y, mm	CPT	y, mm	CPT	y, mm	CPT
0.8	-0.756±0.006	12.0	-0.584±0.005	49.0	-0.200±0.005
1.0	-0.751±0.006	12.5	-0.576±0.005	51.6	-0.181±0.005
1.3	-0.749±0.006	13.0	-0.571±0.005	54.1	-0.159±0.005
1.5	-0.744±0.006	13.5	-0.563±0.005	56.7	-0.138±0.005
1.8	-0.742±0.006	14.8	-0.548±0.005	59.2	-0.119±0.005
2.1	-0.737±0.006	16.0	-0.533±0.005	61.7	-0.102±0.005
2.3	-0.734±0.006	17.3	-0.516±0.005	64.3	-0.086±0.005
2.6	-0.729±0.006	18.6	-0.499±0.005	66.8	-0.071±0.005
2.8	-0.725±0.006	19.8	-0.486±0.005	69.4	-0.056±0.005
3.1	-0.721±0.006	21.1	-0.473±0.005	71.9	-0.046±0.005
3.3	-0.718±0.006	22.4	-0.458±0.005	74.4	-0.034±0.005
3.8	-0.707±0.006	23.6	-0.444±0.005	77.0	-0.024±0.005
4.3	-0.700±0.006	24.9	-0.430±0.005	79.5	-0.018±0.005
4.9	-0.691±0.006	26.2	-0.416±0.005	82.1	-0.012±0.005
5.4	-0.684±0.006	27.5	-0.401±0.005	84.6	-0.007±0.005
5.9	-0.676±0.006	28.7	-0.390±0.005	87.1	-0.004±0.005
6.4	-0.666±0.006	30.0	-0.377±0.005	89.7	-0.001±0.005
6.9	-0.659±0.006	31.3	-0.364±0.005	94.8	0.001±0.005
7.4	-0.651±0.006	32.5	-0.351±0.005	99.8	0.002±0.005
7.9	-0.644±0.006	33.8	-0.339±0.005	104.9	0.003±0.005
8.4	-0.635±0.005	35.1	-0.326±0.005	110.0	0.003±0.005
8.9	-0.629±0.005	36.3	-0.316±0.005	115.1	0.003±0.005
9.4	-0.620±0.005	37.6	-0.303±0.005	120.2	0.002±0.005
9.9	-0.615±0.005	38.9	-0.291±0.005	125.2	0.002±0.005
10.4	-0.607±0.005	41.4	-0.266±0.005	130.3	0.002±0.005
10.9	-0.601±0.005	44.0	-0.245±0.005	135.4	0.002±0.005
11.5	-0.593±0.005	46.5	-0.223±0.005	140.5	0.002±0.005

Table C.36 Kiel Probe Total Pressure Data at (x,z)=(-51 mm,0)

y, mm	CPT	y, mm	CPT	y, mm	CPT
0.8*	-0.747±0.006	12.0	-0.589±0.005	49.0	-0.194±0.005
1.0*	-0.748±0.006	12.5	-0.582±0.005	51.6	-0.174±0.005
1.3*	-0.747±0.006	13.0	-0.576±0.005	54.1	-0.154±0.005
1.5*	-0.749±0.006	13.5	-0.566±0.005	56.7	-0.135±0.005
1.8*	-0.749±0.006	14.8	-0.548±0.005	59.2	-0.114±0.005
2.1*	-0.750±0.006	16.0	-0.536±0.005	61.7	-0.099±0.005
2.3	-0.750±0.006	17.3	-0.518±0.005	64.3	-0.083±0.005
2.6	-0.751±0.006	18.6	-0.502±0.005	66.8	-0.069±0.005
2.8	-0.748±0.006	19.8	-0.489±0.005	69.4	-0.057±0.005
3.1	-0.744±0.006	21.1	-0.471±0.005	71.9	-0.044±0.005
3.3	-0.742±0.006	22.4	-0.457±0.005	74.4	-0.034±0.005
3.8	-0.732±0.006	23.6	-0.443±0.005	77.0	-0.025±0.005
4.3	-0.726±0.006	24.9	-0.429±0.005	79.5	-0.018±0.005
4.9	-0.718±0.006	26.2	-0.414±0.005	82.1	-0.012±0.005
5.4	-0.707±0.006	27.5	-0.401±0.005	84.6	-0.007±0.005
5.9	-0.698±0.006	28.7	-0.387±0.005	87.1	-0.003±0.005
6.4	-0.689±0.006	30.0	-0.373±0.005	89.7	-0.001±0.005
6.9	-0.679±0.006	31.3	-0.361±0.005	94.8	0.001±0.005
7.4	-0.671±0.006	32.5	-0.346±0.005	99.8	0.002±0.005
7.9	-0.663±0.006	33.8	-0.336±0.005	104.9	0.003±0.005
8.4	-0.654±0.006	35.1	-0.322±0.005	110.0	0.003±0.005
8.9	-0.639±0.005	36.3	-0.309±0.005	115.1	0.003±0.005
9.4	-0.632±0.005	37.6	-0.297±0.005	120.2	0.003±0.005
9.9	-0.622±0.005	38.9	-0.284±0.005	125.2	0.003±0.005
10.4	-0.616±0.005	41.4	-0.260±0.005	130.3	0.003±0.005
10.9	-0.606±0.005	44.0	-0.237±0.005	135.4	0.002±0.005
11.5	-0.597±0.005	46.5	-0.215±0.005	140.5	0.002±0.005

* => Reversed flow

Table C.37 Kiel Probe Total Pressure Data at (x,z)=(-44 mm,0)

y, mm	CPT	y, mm	CPT	y, mm	CPT
0.8*	-0.670±0.006	12.0	-0.603±0.005	49.0	-0.190±0.005
1.0*	-0.659±0.006	12.5	-0.589±0.005	51.6	-0.171±0.005
1.3*	-0.658±0.006	13.0	-0.583±0.005	54.1	-0.150±0.005
1.5*	-0.660±0.006	13.5	-0.574±0.005	56.7	-0.132±0.005
1.8*	-0.665±0.006	14.8	-0.553±0.005	59.2	-0.114±0.005
2.1*	-0.671±0.006	16.0	-0.535±0.005	61.7	-0.098±0.005
2.3*	-0.678±0.006	17.3	-0.517±0.005	64.3	-0.082±0.005
2.6*	-0.687±0.006	18.6	-0.502±0.005	66.8	-0.069±0.005
2.8*	-0.697±0.006	19.8	-0.484±0.005	69.4	-0.055±0.005
3.1*	-0.709±0.006	21.1	-0.467±0.005	71.9	-0.043±0.005
3.3*	-0.722±0.006	22.4	-0.453±0.005	74.4	-0.033±0.005
3.8*	-0.749±0.006	23.6	-0.439±0.005	77.0	-0.025±0.005
4.3*	-0.774±0.006	24.9	-0.420±0.005	79.5	-0.017±0.005
4.9*	-0.800±0.006	26.2	-0.410±0.005	82.1	-0.012±0.005
5.4	-0.822±0.006	27.5	-0.395±0.005	84.6	-0.007±0.005
5.9	-0.802±0.006	28.7	-0.380±0.005	87.1	-0.003±0.005
6.4	-0.788±0.006	30.0	-0.369±0.005	89.7	-0.001±0.005
6.9	-0.767±0.006	31.3	-0.355±0.005	94.8	0.002±0.005
7.4	-0.742±0.006	32.5	-0.340±0.005	99.8	0.002±0.005
7.9	-0.719±0.006	33.8	-0.330±0.005	104.9	0.003±0.005
8.4	-0.698±0.006	35.1	-0.317±0.005	110.0	0.003±0.005
8.9	-0.679±0.006	36.3	-0.305±0.005	115.1	0.003±0.005
9.4	-0.666±0.006	37.6	-0.293±0.005	120.2	0.003±0.005
9.9	-0.646±0.006	38.9	-0.280±0.005	125.2	0.003±0.005
10.4	-0.634±0.005	41.4	-0.256±0.005	130.3	0.003±0.005
10.9	-0.624±0.005	44.0	-0.235±0.005	135.4	0.002±0.005
11.5	-0.613±0.005	46.5	-0.212±0.005	140.5	0.002±0.005

* => Reversed flow

Table C.38 Kiel Probe Total Pressure Data at (x,z)=(-38 mm,0)

y, mm	CPT	y, mm	CPT	y, mm	CPT
0.8*	-0.524±0.006	12.0	-0.593±0.005	49.0	-0.187±0.005
1.0*	-0.520±0.006	12.5	-0.583±0.005	51.6	-0.166±0.005
1.3*	-0.528±0.006	13.0	-0.572±0.005	54.1	-0.147±0.005
1.5*	-0.540±0.006	13.5	-0.566±0.005	56.7	-0.130±0.005
1.8*	-0.556±0.006	14.8	-0.545±0.005	59.2	-0.110±0.005
2.1*	-0.576±0.006	16.0	-0.526±0.005	61.7	-0.095±0.005
2.3*	-0.596±0.006	17.3	-0.507±0.005	64.3	-0.081±0.005
2.6*	-0.616±0.006	18.6	-0.492±0.005	66.8	-0.067±0.005
2.8*	-0.636±0.006	19.8	-0.476±0.005	69.4	-0.053±0.005
3.1*	-0.657±0.006	21.1	-0.461±0.005	71.9	-0.043±0.005
3.3*	-0.675±0.006	22.4	-0.445±0.005	74.4	-0.033±0.005
3.8*	-0.714±0.006	23.6	-0.426±0.005	77.0	-0.024±0.005
4.3*	-0.744±0.006	24.9	-0.413±0.005	79.5	-0.016±0.005
4.9*	-0.773±0.006	26.2	-0.401±0.005	82.1	-0.011±0.005
5.4*	-0.795±0.006	27.5	-0.386±0.005	84.6	-0.006±0.005
5.9	-0.809±0.006	28.7	-0.373±0.005	87.1	-0.003±0.005
6.4	-0.787±0.006	30.0	-0.361±0.005	89.7	-0.001±0.005
6.9	-0.761±0.006	31.3	-0.345±0.005	94.8	0.002±0.005
7.4	-0.742±0.006	32.5	-0.332±0.005	99.8	0.003±0.005
7.9	-0.721±0.006	33.8	-0.322±0.005	104.9	0.003±0.005
8.4	-0.696±0.006	35.1	-0.310±0.005	110.0	0.003±0.005
8.9	-0.681±0.006	36.3	-0.298±0.005	115.1	0.003±0.005
9.4	-0.660±0.006	37.6	-0.284±0.005	120.2	0.003±0.005
9.9	-0.644±0.006	38.9	-0.273±0.005	125.2	0.003±0.005
10.4	-0.628±0.005	41.4	-0.250±0.005	130.3	0.003±0.005
10.9	-0.615±0.005	44.0	-0.227±0.005	135.4	0.003±0.005
11.5	-0.605±0.005	46.5	-0.207±0.005	140.5	0.003±0.005

* => Reversed flow

Table C.39 Kiel Probe Total Pressure Data at (x,z)=(-32 mm,0)

y, mm	CPT	y, mm	CPT	y, mm	CPT
0.8*	-0.470±0.006	12.0	-0.573±0.005	49.0	-0.180±0.005
1.0*	-0.474±0.006	12.5	-0.564±0.005	51.6	-0.162±0.005
1.3*	-0.485±0.006	13.0	-0.557±0.005	54.1	-0.142±0.005
1.5*	-0.498±0.006	13.5	-0.550±0.005	56.7	-0.126±0.005
1.8*	-0.512±0.006	14.8	-0.530±0.005	59.2	-0.108±0.005
2.1*	-0.527±0.006	16.0	-0.511±0.005	61.7	-0.093±0.005
2.3*	-0.542±0.006	17.3	-0.494±0.005	64.3	-0.078±0.005
2.6*	-0.558±0.006	18.6	-0.476±0.005	66.8	-0.064±0.005
2.8*	-0.575±0.006	19.8	-0.461±0.005	69.4	-0.051±0.005
3.1*	-0.589±0.006	21.1	-0.448±0.005	71.9	-0.040±0.005
3.3*	-0.603±0.006	22.4	-0.431±0.005	74.4	-0.031±0.005
3.8*	-0.627±0.006	23.6	-0.417±0.005	77.0	-0.023±0.005
4.3*	-0.647±0.006	24.9	-0.404±0.005	79.5	-0.016±0.005
4.9*	-0.664±0.006	26.2	-0.389±0.005	82.1	-0.010±0.005
5.4*	-0.676±0.006	27.5	-0.375±0.005	84.6	-0.006±0.005
5.9*	-0.687±0.006	28.7	-0.364±0.005	87.1	-0.003±0.005
6.4	-0.696±0.006	30.0	-0.349±0.005	89.7	-0.001±0.005
6.9	-0.686±0.006	31.3	-0.337±0.005	94.8	0.002±0.005
7.4	-0.678±0.006	32.5	-0.326±0.005	99.8	0.003±0.005
7.9	-0.666±0.006	33.8	-0.312±0.005	104.9	0.003±0.005
8.4	-0.654±0.006	35.1	-0.300±0.005	110.0	0.003±0.005
8.9	-0.640±0.006	36.3	-0.289±0.005	115.1	0.003±0.005
9.4	-0.630±0.006	37.6	-0.278±0.005	120.2	0.003±0.005
9.9	-0.619±0.005	38.9	-0.265±0.005	125.2	0.003±0.005
10.4	-0.606±0.005	41.4	-0.242±0.005	130.3	0.003±0.005
10.9	-0.596±0.005	44.0	-0.222±0.005	135.4	0.003±0.005
11.5	-0.588±0.005	46.5	-0.201±0.005	140.5	0.003±0.005

* => Reversed flow

Table C.40 Kiel Probe Total Pressure Data at (x,z)=(-25 mm,0)

y, mm	CPT	y, mm	CPT	y, mm	CPT
0.8*	-0.419±0.005	12.0	-0.564±0.005	49.0	-0.174±0.005
1.0*	-0.428±0.005	12.5	-0.556±0.005	51.6	-0.154±0.005
1.3*	-0.436±0.005	13.0	-0.550±0.005	54.1	-0.136±0.005
1.5*	-0.449±0.005	13.5	-0.544±0.005	56.7	-0.120±0.005
1.8*	-0.462±0.005	14.8	-0.520±0.005	59.2	-0.104±0.005
2.1*	-0.476±0.005	16.0	-0.504±0.005	61.7	-0.088±0.005
2.3*	-0.488±0.005	17.3	-0.484±0.005	64.3	-0.073±0.005
2.6*	-0.501±0.005	18.6	-0.468±0.005	66.8	-0.061±0.005
2.8*	-0.514±0.005	19.8	-0.449±0.005	69.4	-0.048±0.005
3.1*	-0.526±0.005	21.1	-0.435±0.005	71.9	-0.038±0.005
3.3*	-0.537±0.005	22.4	-0.421±0.005	74.4	-0.029±0.005
3.8*	-0.555±0.005	23.6	-0.406±0.005	77.0	-0.021±0.005
4.3*	-0.569±0.005	24.9	-0.393±0.005	79.5	-0.015±0.005
4.9*	-0.583±0.005	26.2	-0.379±0.005	82.1	-0.009±0.005
5.4*	-0.596±0.005	27.5	-0.365±0.005	84.6	-0.006±0.005
5.9*	-0.609±0.005	28.7	-0.353±0.005	87.1	-0.003±0.005
6.4*	-0.616±0.005	30.0	-0.338±0.005	89.7	-0.001±0.005
6.9*	-0.626±0.005	31.3	-0.325±0.005	94.8	0.002±0.005
7.4	-0.631±0.005	32.5	-0.312±0.005	99.8	0.003±0.005
7.9	-0.625±0.005	33.8	-0.301±0.005	104.9	0.003±0.005
8.4	-0.618±0.005	35.1	-0.289±0.005	110.0	0.003±0.005
8.9	-0.612±0.005	36.3	-0.277±0.005	115.1	0.003±0.005
9.4	-0.606±0.005	37.6	-0.266±0.005	120.2	0.003±0.005
9.9	-0.597±0.005	38.9	-0.255±0.005	125.2	0.003±0.005
10.4	-0.589±0.005	41.4	-0.234±0.005	130.3	0.003±0.005
10.9	-0.582±0.005	44.0	-0.213±0.005	135.4	0.003±0.005
11.5	-0.574±0.005	46.5	-0.191±0.005	140.5	0.003±0.005

* => Reversed flow

Table C.41 Kiel Probe Total Pressure Data at (x,z)=(-19 mm,0)

y, mm	CPT	y, mm	CPT	y, mm	CPT
0.8*	-0.363±0.005	12.0	-0.548±0.005	49.0	-0.163±0.005
1.0*	-0.371±0.005	12.5	-0.544±0.005	51.6	-0.145±0.005
1.3*	-0.383±0.005	13.0	-0.534±0.005	54.1	-0.129±0.005
1.5*	-0.393±0.005	13.5	-0.530±0.005	56.7	-0.111±0.005
1.8*	-0.406±0.005	14.8	-0.514±0.005	59.2	-0.096±0.005
2.1*	-0.418±0.005	16.0	-0.497±0.005	61.7	-0.081±0.005
2.3*	-0.427±0.005	17.3	-0.483±0.005	64.3	-0.068±0.005
2.6*	-0.438±0.005	18.6	-0.463±0.005	66.8	-0.055±0.005
2.8*	-0.449±0.005	19.8	-0.445±0.005	69.4	-0.045±0.005
3.1*	-0.458±0.005	21.1	-0.429±0.005	71.9	-0.035±0.005
3.3*	-0.467±0.005	22.4	-0.415±0.005	74.4	-0.026±0.005
3.8*	-0.484±0.005	23.6	-0.397±0.005	77.0	-0.019±0.005
4.3*	-0.499±0.005	24.9	-0.384±0.005	79.5	-0.013±0.005
4.9*	-0.514±0.005	26.2	-0.370±0.005	82.1	-0.009±0.005
5.4*	-0.526±0.005	27.5	-0.355±0.005	84.6	-0.005±0.005
5.9*	-0.539±0.005	28.7	-0.341±0.005	87.1	-0.002±0.005
6.4*	-0.551±0.005	30.0	-0.329±0.005	89.7	-0.001±0.005
6.9*	-0.561±0.005	31.3	-0.314±0.005	94.8	0.002±0.005
7.4*	-0.571±0.005	32.5	-0.304±0.005	99.8	0.002±0.005
7.9	-0.579±0.005	33.8	-0.289±0.005	104.9	0.003±0.005
8.4	-0.576±0.005	35.1	-0.279±0.005	110.0	0.003±0.005
8.9	-0.574±0.005	36.3	-0.267±0.005	115.1	0.003±0.005
9.4	-0.571±0.005	37.6	-0.257±0.005	120.2	0.003±0.005
9.9	-0.568±0.005	38.9	-0.245±0.005	125.2	0.003±0.005
10.4	-0.563±0.005	41.4	-0.224±0.005	130.3	0.003±0.005
10.9	-0.559±0.005	44.0	-0.202±0.005	135.4	0.003±0.005
11.5	-0.554±0.005	46.5	-0.181±0.005	140.5	0.003±0.005

* => Reversed flow

Table C.42 Kiel Probe Total Pressure Data at (x,z)=(-13 mm,0)

y, mm	CPT	y, mm	CPT	y, mm	CPT
0.8*	-0.311±0.005	12.0	-0.520±0.005	49.0	-0.161±0.005
1.0*	-0.320±0.005	12.5	-0.516±0.005	51.6	-0.140±0.005
1.3*	-0.327±0.005	13.0	-0.515±0.005	54.1	-0.120±0.005
1.5*	-0.334±0.005	13.5	-0.511±0.005	56.7	-0.103±0.005
1.8*	-0.344±0.005	14.8	-0.503±0.005	59.2	-0.090±0.005
2.1*	-0.352±0.005	16.0	-0.492±0.005	61.7	-0.074±0.004
2.3*	-0.360±0.005	17.3	-0.480±0.005	64.3	-0.060±0.004
2.6*	-0.370±0.005	18.6	-0.468±0.005	66.8	-0.049±0.004
2.8*	-0.378±0.005	19.8	-0.457±0.005	69.4	-0.039±0.004
3.1*	-0.386±0.005	21.1	-0.439±0.005	71.9	-0.030±0.004
3.3*	-0.395±0.005	22.4	-0.428±0.005	74.4	-0.021±0.004
3.8*	-0.412±0.005	23.6	-0.412±0.005	77.0	-0.016±0.005
4.3*	-0.428±0.005	24.9	-0.398±0.005	79.5	-0.010±0.005
4.9*	-0.444±0.005	26.2	-0.382±0.005	82.1	-0.007±0.005
5.4*	-0.460±0.005	27.5	-0.371±0.005	84.6	-0.004±0.005
5.9*	-0.476±0.005	28.7	-0.358±0.005	87.1	-0.002±0.005
6.4*	-0.490±0.005	30.0	-0.344±0.005	89.7	0.000±0.005
6.9*	-0.502±0.005	31.3	-0.328±0.005	94.8	0.002±0.005
7.4*	-0.513±0.005	32.5	-0.317±0.005	99.8	0.003±0.005
7.9	-0.521±0.005	33.8	-0.303±0.005	104.9	0.003±0.005
8.4	-0.521±0.005	35.1	-0.290±0.005	110.0	0.003±0.005
8.9	-0.524±0.005	36.3	-0.275±0.005	115.1	0.003±0.005
9.4	-0.525±0.005	37.6	-0.262±0.005	120.2	0.003±0.005
9.9	-0.523±0.005	38.9	-0.253±0.005	125.2	0.003±0.005
10.4	-0.524±0.005	41.4	-0.227±0.005	130.3	0.003±0.004
10.9	-0.522±0.005	44.0	-0.203±0.005	135.4	0.003±0.005
11.5	-0.519±0.005	46.5	-0.181±0.005	140.5	0.003±0.005

* => Reversed flow

APPENDIX D

Five-Hole Probe Data

In this appendix:

BETA $\equiv \beta$,

ALPHA $\equiv \alpha$,

CPT $\equiv C_{P,T}$,

CPS $\equiv C_{P,S}$,

SPEED $\equiv \bar{V}/\bar{V}_{*}$,

and U, V, and W are normalized with the speed at the wind tunnel throat. The estimated uncertainties are at the 5 percent significance level (95 percent confidence intervals or 19 to 1 odds).

Table D.1 Five-Hole Probe Data at (x,z)=(305 mm,-203 mm)

y, mm	BETA, deg	ALPHA, deg	CPT	CPS	SPEED	U	V	W
3.7	-2.6±0.3	0.4±0.6	-0.76±0.01	-1.17±0.02	0.642±0.007	0.641±0.007	0.005±0.007	0.030±0.004
4.7	-2.6±0.3	-0.3±0.5	-0.73±0.01	-1.18±0.02	0.671±0.007	0.671±0.007	-0.003±0.006	0.030±0.004
5.7	-2.4±0.3	-0.5±0.5	-0.69±0.01	-1.17±0.02	0.694±0.007	0.693±0.007	-0.006±0.006	0.029±0.004
6.7	-2.4±0.3	-0.6±0.5	-0.66±0.01	-1.17±0.02	0.714±0.007	0.713±0.007	-0.008±0.006	0.029±0.004
7.7	-2.2±0.3	-0.7±0.5	-0.64±0.01	-1.17±0.02	0.732±0.007	0.731±0.007	-0.009±0.006	0.028±0.004
8.7	-2.2±0.3	-0.7±0.4	-0.61±0.01	-1.17±0.02	0.746±0.007	0.745±0.007	-0.009±0.006	0.028±0.004
9.8	-2.1±0.3	-0.6±0.4	-0.60±0.01	-1.17±0.02	0.758±0.007	0.757±0.007	-0.008±0.006	0.027±0.004
10.8	-2.0±0.3	-0.6±0.4	-0.58±0.01	-1.18±0.02	0.772±0.007	0.772±0.007	-0.008±0.006	0.027±0.004
11.8	-2.0±0.3	-0.6±0.4	-0.57±0.01	-1.18±0.02	0.780±0.007	0.780±0.007	-0.008±0.006	0.027±0.004
12.8	-1.9±0.3	-0.6±0.4	-0.55±0.01	-1.17±0.02	0.789±0.007	0.788±0.007	-0.008±0.005	0.026±0.004
13.8	-1.9±0.3	-0.5±0.4	-0.54±0.01	-1.18±0.02	0.799±0.007	0.798±0.007	-0.007±0.005	0.027±0.004
16.4	-1.9±0.3	-0.4±0.4	-0.51±0.01	-1.18±0.02	0.818±0.006	0.817±0.006	-0.006±0.005	0.027±0.005
18.9	-2.0±0.3	-0.4±0.4	-0.48±0.01	-1.17±0.02	0.832±0.006	0.832±0.006	-0.005±0.005	0.029±0.005
21.4	-2.0±0.3	-0.3±0.3	-0.45±0.01	-1.17±0.02	0.849±0.006	0.849±0.006	-0.005±0.005	0.030±0.005
24.0	-2.1±0.3	-0.3±0.3	-0.43±0.01	-1.18±0.02	0.863±0.006	0.862±0.006	-0.005±0.005	0.032±0.005
26.5	-2.2±0.3	-0.3±0.3	-0.40±0.01	-1.17±0.02	0.878±0.006	0.878±0.006	-0.004±0.005	0.033±0.005
29.1	-2.2±0.3	-0.3±0.3	-0.38±0.01	-1.17±0.02	0.891±0.006	0.890±0.006	-0.004±0.005	0.034±0.005
31.6	-2.2±0.3	-0.3±0.3	-0.35±0.01	-1.17±0.02	0.904±0.006	0.904±0.006	-0.004±0.005	0.035±0.005
34.1	-2.3±0.3	-0.2±0.3	-0.33±0.01	-1.17±0.02	0.918±0.006	0.917±0.006	-0.004±0.005	0.037±0.005
36.7	-2.3±0.3	-0.2±0.3	-0.31±0.01	-1.17±0.02	0.930±0.006	0.930±0.006	-0.003±0.005	0.037±0.005
39.2	-2.3±0.3	-0.2±0.3	-0.28±0.01	-1.17±0.02	0.942±0.006	0.941±0.006	-0.003±0.005	0.038±0.005
44.3	-2.4±0.3	-0.2±0.3	-0.24±0.01	-1.17±0.02	0.966±0.006	0.965±0.006	-0.003±0.004	0.040±0.005
49.4	-2.4±0.3	-0.2±0.3	-0.19±0.01	-1.17±0.02	0.987±0.006	0.987±0.006	-0.003±0.004	0.041±0.005
54.5	-2.4±0.3	-0.2±0.2	-0.15±0.01	-1.17±0.02	1.008±0.006	1.007±0.006	-0.003±0.004	0.042±0.006
59.5	-2.4±0.3	-0.2±0.2	-0.11±0.01	-1.17±0.02	1.026±0.006	1.025±0.006	-0.003±0.004	0.043±0.006
64.6	-2.4±0.3	-0.2±0.2	-0.08±0.01	-1.17±0.02	1.042±0.006	1.041±0.006	-0.003±0.004	0.044±0.006
69.7	-2.4±0.3	-0.2±0.2	-0.05±0.01	-1.17±0.02	1.057±0.006	1.056±0.006	-0.003±0.004	0.045±0.006
74.8	-2.4±0.3	-0.2±0.2	-0.02±0.01	-1.17±0.02	1.068±0.006	1.068±0.006	-0.003±0.004	0.045±0.006
79.9	-2.4±0.3	-0.2±0.2	-0.01±0.01	-1.16±0.02	1.076±0.007	1.075±0.007	-0.003±0.004	0.045±0.006
84.9	-2.4±0.3	-0.2±0.2	0.00±0.01	-1.16±0.02	1.080±0.007	1.079±0.007	-0.004±0.004	0.045±0.006
90.0	-2.4±0.3	-0.2±0.2	0.01±0.01	-1.16±0.02	1.082±0.007	1.081±0.007	-0.004±0.004	0.045±0.006
100.2	-2.4±0.3	-0.3±0.2	0.01±0.01	-1.16±0.02	1.084±0.007	1.083±0.007	-0.006±0.004	0.045±0.006
110.3	-2.3±0.3	-0.5±0.2	0.01±0.01	-1.16±0.02	1.083±0.007	1.082±0.007	-0.009±0.004	0.043±0.006
120.5	-2.2±0.3	-0.6±0.2	0.01±0.01	-1.16±0.02	1.084±0.007	1.083±0.007	-0.011±0.004	0.043±0.006
130.7	-2.2±0.3	-0.7±0.2	0.01±0.01	-1.16±0.02	1.084±0.007	1.083±0.007	-0.013±0.004	0.043±0.006
140.8	-2.2±0.3	-0.7±0.2	0.01±0.01	-1.16±0.02	1.083±0.007	1.083±0.007	-0.014±0.004	0.041±0.006

Table D.2 Five-Hole Probe Data at (x,z)=(305 mm,-178 mm)

y, mm	BETA, deg	ALPHA, deg	CPT	CPS	SPEED	U	V	W
3.7	-1.9±0.3	0.4±0.6	-0.77±0.01	-1.17±0.02	0.629±0.007	0.628±0.007	0.004±0.007	0.020±0.003
4.7	-1.8±0.3	-0.3±0.6	-0.73±0.01	-1.17±0.02	0.660±0.007	0.660±0.007	-0.003±0.007	0.021±0.004
5.7	-1.8±0.3	-0.6±0.5	-0.70±0.01	-1.16±0.02	0.684±0.007	0.684±0.007	-0.007±0.006	0.022±0.004
6.7	-1.8±0.3	-0.7±0.5	-0.67±0.01	-1.16±0.02	0.703±0.007	0.703±0.007	-0.009±0.006	0.022±0.004
7.7	-1.6±0.3	-0.7±0.5	-0.64±0.01	-1.17±0.02	0.724±0.007	0.724±0.007	-0.009±0.006	0.021±0.004
8.7	-1.6±0.3	-0.7±0.5	-0.62±0.01	-1.17±0.02	0.738±0.007	0.738±0.007	-0.009±0.006	0.020±0.004
9.8	-1.5±0.3	-0.7±0.4	-0.60±0.01	-1.16±0.02	0.751±0.007	0.751±0.007	-0.009±0.006	0.020±0.004
10.8	-1.5±0.3	-0.6±0.4	-0.58±0.01	-1.17±0.02	0.763±0.007	0.763±0.007	-0.008±0.006	0.020±0.004
11.8	-1.5±0.3	-0.6±0.4	-0.57±0.01	-1.16±0.02	0.773±0.007	0.773±0.007	-0.008±0.006	0.020±0.004
12.8	-1.5±0.3	-0.5±0.4	-0.56±0.01	-1.17±0.02	0.781±0.007	0.781±0.007	-0.007±0.006	0.020±0.004
13.8	-1.5±0.3	-0.5±0.4	-0.54±0.01	-1.17±0.02	0.790±0.007	0.789±0.007	-0.006±0.005	0.021±0.004
16.4	-1.6±0.3	-0.4±0.4	-0.51±0.01	-1.16±0.02	0.808±0.007	0.807±0.007	-0.005±0.005	0.023±0.004
18.9	-1.7±0.3	-0.3±0.4	-0.49±0.01	-1.16±0.02	0.821±0.006	0.821±0.006	-0.004±0.005	0.025±0.005
21.4	-1.9±0.3	-0.2±0.4	-0.46±0.01	-1.16±0.02	0.838±0.006	0.837±0.006	-0.003±0.005	0.028±0.005
24.0	-2.0±0.3	-0.1±0.3	-0.44±0.01	-1.16±0.02	0.852±0.006	0.851±0.006	-0.002±0.005	0.030±0.005
26.5	-2.2±0.3	-0.1±0.3	-0.41±0.01	-1.16±0.02	0.865±0.006	0.864±0.006	-0.002±0.005	0.033±0.005
29.1	-2.3±0.3	-0.0±0.3	-0.39±0.01	-1.16±0.02	0.878±0.006	0.878±0.006	-0.001±0.005	0.035±0.005
31.6	-2.4±0.3	-0.0±0.3	-0.37±0.01	-1.16±0.02	0.891±0.006	0.890±0.006	-0.000±0.005	0.037±0.005
34.1	-2.4±0.3	0.0±0.3	-0.34±0.01	-1.16±0.02	0.906±0.006	0.905±0.006	0.000±0.005	0.038±0.005
36.7	-2.5±0.3	0.1±0.3	-0.32±0.01	-1.16±0.02	0.918±0.006	0.917±0.006	0.001±0.005	0.040±0.005
39.2	-2.6±0.3	0.0±0.3	-0.29±0.01	-1.16±0.02	0.929±0.006	0.928±0.006	0.001±0.005	0.042±0.005
44.3	-2.6±0.3	0.1±0.3	-0.25±0.01	-1.16±0.02	0.953±0.006	0.952±0.006	0.001±0.005	0.044±0.005
49.4	-2.7±0.3	0.1±0.3	-0.21±0.01	-1.16±0.02	0.975±0.006	0.973±0.006	0.001±0.004	0.046±0.005
54.5	-2.8±0.3	0.1±0.3	-0.17±0.01	-1.16±0.02	0.995±0.006	0.994±0.006	0.001±0.004	0.048±0.005
59.5	-2.8±0.3	0.0±0.2	-0.13±0.01	-1.15±0.02	1.014±0.006	1.013±0.006	0.001±0.004	0.049±0.006
64.6	-2.8±0.3	-0.0±0.2	-0.09±0.01	-1.15±0.02	1.032±0.006	1.031±0.006	-0.000±0.004	0.050±0.006
69.7	-2.8±0.3	-0.0±0.2	-0.06±0.01	-1.15±0.02	1.047±0.006	1.046±0.006	-0.001±0.004	0.051±0.006
74.8	-2.8±0.3	-0.1±0.2	-0.03±0.01	-1.15±0.02	1.060±0.006	1.058±0.006	-0.001±0.004	0.051±0.006
79.9	-2.8±0.3	-0.1±0.2	-0.01±0.01	-1.15±0.02	1.068±0.007	1.067±0.007	-0.002±0.004	0.051±0.006
84.9	-2.8±0.3	-0.1±0.2	-0.00±0.01	-1.15±0.02	1.074±0.007	1.072±0.007	-0.003±0.004	0.052±0.006
90.0	-2.7±0.3	-0.2±0.2	0.01±0.01	-1.15±0.02	1.076±0.007	1.075±0.007	-0.004±0.004	0.051±0.006
100.2	-2.7±0.3	-0.4±0.2	0.01±0.01	-1.15±0.02	1.078±0.007	1.077±0.007	-0.007±0.004	0.051±0.006
110.3	-2.7±0.3	-0.5±0.2	0.01±0.01	-1.15±0.02	1.078±0.007	1.076±0.007	-0.010±0.004	0.051±0.006
120.5	-2.7±0.3	-0.7±0.2	0.01±0.01	-1.15±0.02	1.077±0.007	1.076±0.007	-0.013±0.004	0.050±0.006
130.7	-2.5±0.3	-0.8±0.2	0.01±0.01	-1.15±0.02	1.078±0.007	1.077±0.007	-0.016±0.004	0.048±0.006
140.8	-2.4±0.3	-0.9±0.2	0.01±0.01	-1.15±0.02	1.078±0.007	1.077±0.007	-0.018±0.004	0.044±0.006

Table D.3 Five-Hole Probe Data at (x,z)=(305 mm,-152 mm)

y, mm	BETA, deg	ALPHA, deg	CPT	CPS	SPEED	U	V	W
3.7	-0.5±0.3	0.5±0.8	-0.83±0.01	-1.15±0.02	0.565±0.008	0.565±0.008	0.005±0.008	0.005±0.003
4.7	-0.6±0.3	-0.1±0.7	-0.80±0.01	-1.15±0.02	0.594±0.008	0.594±0.008	-0.001±0.007	0.006±0.003
5.7	-0.6±0.3	-0.3±0.6	-0.77±0.01	-1.15±0.02	0.621±0.007	0.621±0.007	-0.003±0.007	0.007±0.003
6.7	-0.6±0.3	-0.4±0.6	-0.74±0.01	-1.15±0.02	0.642±0.007	0.642±0.007	-0.005±0.007	0.007±0.004
7.7	-0.6±0.3	-0.3±0.6	-0.72±0.01	-1.15±0.02	0.659±0.007	0.659±0.007	-0.004±0.007	0.007±0.004
8.7	-0.6±0.3	-0.4±0.5	-0.69±0.01	-1.15±0.02	0.676±0.007	0.676±0.007	-0.004±0.006	0.007±0.004
9.8	-0.6±0.3	-0.3±0.5	-0.68±0.01	-1.15±0.02	0.689±0.007	0.689±0.007	-0.003±0.006	0.007±0.004
10.8	-0.6±0.3	-0.2±0.5	-0.66±0.01	-1.15±0.02	0.704±0.007	0.704±0.007	-0.002±0.006	0.008±0.004
11.8	-0.7±0.3	-0.1±0.5	-0.64±0.01	-1.15±0.02	0.715±0.007	0.714±0.007	-0.002±0.006	0.008±0.004
12.8	-0.8±0.3	-0.0±0.5	-0.62±0.01	-1.15±0.02	0.725±0.007	0.725±0.007	-0.000±0.006	0.010±0.004
13.8	-0.8±0.3	0.1±0.5	-0.61±0.01	-1.15±0.02	0.735±0.007	0.735±0.007	0.001±0.006	0.010±0.004
16.4	-1.1±0.3	0.2±0.4	-0.58±0.01	-1.15±0.02	0.753±0.007	0.753±0.007	0.003±0.006	0.014±0.004
18.9	-1.4±0.3	0.4±0.4	-0.56±0.01	-1.15±0.02	0.773±0.007	0.773±0.007	0.005±0.006	0.019±0.004
21.4	-1.7±0.3	0.5±0.4	-0.53±0.01	-1.15±0.02	0.787±0.007	0.786±0.007	0.006±0.005	0.024±0.004
24.0	-2.0±0.3	0.5±0.4	-0.50±0.01	-1.15±0.02	0.808±0.006	0.808±0.006	0.007±0.005	0.028±0.004
26.5	-2.3±0.3	0.6±0.4	-0.47±0.01	-1.15±0.02	0.823±0.006	0.822±0.006	0.008±0.005	0.033±0.005
29.1	-2.5±0.3	0.6±0.3	-0.44±0.01	-1.15±0.02	0.840±0.006	0.839±0.006	0.009±0.005	0.037±0.005
31.6	-2.6±0.3	0.6±0.3	-0.42±0.01	-1.15±0.02	0.858±0.006	0.857±0.006	0.009±0.005	0.040±0.005
34.1	-2.8±0.3	0.6±0.3	-0.39±0.01	-1.15±0.02	0.875±0.006	0.874±0.006	0.010±0.005	0.043±0.005
36.7	-2.9±0.3	0.6±0.3	-0.36±0.01	-1.15±0.02	0.890±0.006	0.889±0.006	0.010±0.005	0.046±0.005
39.2	-3.0±0.3	0.6±0.3	-0.33±0.01	-1.15±0.02	0.905±0.006	0.904±0.006	0.010±0.005	0.048±0.005
44.3	-3.1±0.3	0.6±0.3	-0.28±0.01	-1.15±0.02	0.932±0.006	0.930±0.006	0.009±0.005	0.051±0.005
49.4	-3.3±0.3	0.5±0.3	-0.23±0.01	-1.15±0.02	0.958±0.006	0.956±0.006	0.008±0.004	0.054±0.005
54.5	-3.4±0.3	0.4±0.3	-0.18±0.01	-1.14±0.02	0.980±0.006	0.978±0.006	0.007±0.004	0.058±0.005
59.5	-3.4±0.3	0.3±0.2	-0.14±0.01	-1.14±0.02	1.002±0.006	1.000±0.006	0.006±0.004	0.059±0.006
64.6	-3.4±0.3	0.3±0.2	-0.10±0.01	-1.14±0.02	1.020±0.006	1.018±0.006	0.004±0.004	0.060±0.006
69.7	-3.4±0.3	0.2±0.2	-0.06±0.01	-1.14±0.02	1.037±0.006	1.035±0.006	0.003±0.004	0.061±0.006
74.8	-3.4±0.3	0.1±0.2	-0.04±0.01	-1.14±0.02	1.050±0.006	1.048±0.006	0.001±0.004	0.062±0.006
79.9	-3.4±0.3	-0.0±0.2	-0.01±0.01	-1.14±0.02	1.060±0.006	1.058±0.006	-0.001±0.004	0.062±0.006
84.9	-3.3±0.3	-0.1±0.2	0.00±0.01	-1.14±0.02	1.066±0.006	1.065±0.006	-0.002±0.004	0.062±0.006
90.0	-3.3±0.3	-0.2±0.2	0.01±0.01	-1.14±0.02	1.070±0.006	1.068±0.006	-0.004±0.004	0.061±0.006
100.2	-3.3±0.3	-0.4±0.2	0.01±0.01	-1.14±0.02	1.071±0.006	1.069±0.006	-0.008±0.004	0.061±0.006
110.3	-3.1±0.3	-0.6±0.2	0.01±0.01	-1.14±0.02	1.071±0.006	1.069±0.006	-0.012±0.004	0.059±0.006
120.5	-3.0±0.3	-0.8±0.2	0.01±0.01	-1.14±0.02	1.071±0.006	1.070±0.006	-0.014±0.004	0.056±0.006
130.7	-2.9±0.3	-0.9±0.2	0.01±0.01	-1.14±0.02	1.071±0.006	1.069±0.006	-0.017±0.004	0.055±0.006
140.8	-2.8±0.3	-1.1±0.2	0.01±0.01	-1.14±0.02	1.072±0.006	1.070±0.006	-0.021±0.004	0.051±0.006

Table D.4 Five-Hole Probe Data at (x,z)=(305 mm,-140 mm)

y, mm	BETA, deg	ALPHA, deg	CPT	CPS	SPEED	U	V	W
3.7	1.1±0.3	0.7±0.9	-0.86±0.01	-1.15±0.02	0.534±0.008	0.533±0.008	0.007±0.008	-0.010±0.003
4.7	0.8±0.3	0.1±0.8	-0.83±0.01	-1.15±0.02	0.563±0.008	0.563±0.008	0.001±0.008	-0.008±0.003
5.7	0.5±0.3	-0.0±0.7	-0.81±0.01	-1.15±0.02	0.587±0.008	0.587±0.008	-0.000±0.007	-0.006±0.003
6.7	0.3±0.3	-0.1±0.7	-0.78±0.01	-1.15±0.02	0.607±0.007	0.607±0.007	-0.001±0.007	-0.004±0.003
7.7	0.2±0.3	0.0±0.6	-0.76±0.01	-1.16±0.02	0.629±0.007	0.629±0.007	0.000±0.007	-0.002±0.003
8.7	0.0±0.3	0.1±0.6	-0.74±0.01	-1.15±0.02	0.644±0.007	0.644±0.007	0.001±0.007	-0.000±0.004
9.8	0.0±0.3	0.2±0.6	-0.72±0.01	-1.15±0.02	0.658±0.007	0.658±0.007	0.002±0.007	-0.000±0.004
10.8	-0.2±0.3	0.3±0.6	-0.70±0.01	-1.15±0.02	0.669±0.007	0.669±0.007	0.004±0.006	0.002±0.004
11.8	-0.2±0.3	0.5±0.5	-0.69±0.01	-1.15±0.02	0.682±0.007	0.682±0.007	0.006±0.006	0.002±0.004
12.8	-0.3±0.3	0.5±0.5	-0.68±0.01	-1.16±0.02	0.693±0.007	0.693±0.007	0.006±0.006	0.004±0.004
13.8	-0.5±0.3	0.7±0.5	-0.67±0.01	-1.16±0.02	0.700±0.007	0.700±0.007	0.008±0.006	0.006±0.004
16.4	-0.8±0.3	0.9±0.5	-0.64±0.01	-1.16±0.02	0.721±0.007	0.721±0.007	0.011±0.006	0.010±0.004
18.9	-1.3±0.3	1.0±0.5	-0.61±0.01	-1.15±0.02	0.734±0.007	0.734±0.007	0.013±0.006	0.016±0.004
21.4	-1.7±0.3	1.2±0.4	-0.59±0.01	-1.15±0.02	0.753±0.007	0.753±0.007	0.015±0.006	0.023±0.004
24.0	-2.2±0.3	1.2±0.4	-0.56±0.01	-1.15±0.02	0.769±0.007	0.769±0.007	0.016±0.006	0.029±0.004
26.5	-2.6±0.3	1.2±0.4	-0.53±0.01	-1.15±0.02	0.787±0.007	0.786±0.007	0.017±0.005	0.036±0.004
29.1	-2.9±0.3	1.3±0.4	-0.50±0.01	-1.15±0.02	0.807±0.006	0.806±0.006	0.018±0.005	0.041±0.004
31.6	-3.2±0.3	1.2±0.4	-0.47±0.01	-1.15±0.02	0.826±0.006	0.825±0.006	0.017±0.005	0.047±0.005
34.1	-3.4±0.3	1.2±0.3	-0.43±0.01	-1.15±0.02	0.846±0.006	0.844±0.006	0.018±0.005	0.051±0.005
36.7	-3.6±0.3	1.2±0.3	-0.40±0.01	-1.15±0.02	0.865±0.006	0.864±0.006	0.017±0.005	0.055±0.005
39.2	-3.8±0.3	1.1±0.3	-0.37±0.01	-1.15±0.02	0.882±0.006	0.880±0.006	0.017±0.005	0.058±0.005
44.3	-4.0±0.3	1.0±0.3	-0.31±0.01	-1.14±0.02	0.914±0.006	0.912±0.006	0.015±0.005	0.063±0.005
49.4	-4.0±0.3	0.8±0.3	-0.25±0.01	-1.14±0.02	0.944±0.006	0.942±0.006	0.013±0.005	0.066±0.005
54.5	-4.1±0.3	0.6±0.3	-0.20±0.01	-1.14±0.02	0.970±0.006	0.968±0.006	0.011±0.004	0.069±0.005
59.5	-4.1±0.3	0.5±0.3	-0.15±0.01	-1.14±0.02	0.993±0.006	0.991±0.006	0.008±0.004	0.070±0.005
64.6	-4.1±0.3	0.3±0.2	-0.11±0.01	-1.14±0.02	1.015±0.006	1.013±0.006	0.006±0.004	0.072±0.006
69.7	-4.1±0.3	0.2±0.2	-0.07±0.01	-1.14±0.02	1.032±0.006	1.030±0.006	0.004±0.004	0.073±0.006
74.8	-4.0±0.3	0.1±0.2	-0.04±0.01	-1.14±0.02	1.047±0.006	1.044±0.006	0.002±0.004	0.073±0.006
79.9	-4.0±0.3	-0.0±0.2	-0.02±0.01	-1.14±0.02	1.057±0.006	1.055±0.006	-0.000±0.004	0.073±0.006
84.9	-3.9±0.3	-0.1±0.2	-0.00±0.01	-1.13±0.02	1.064±0.006	1.061±0.006	-0.002±0.004	0.073±0.006
90.0	-3.8±0.3	-0.2±0.2	0.01±0.01	-1.14±0.02	1.068±0.006	1.065±0.006	-0.005±0.004	0.072±0.006
100.2	-3.7±0.3	-0.4±0.2	0.01±0.01	-1.13±0.02	1.069±0.006	1.067±0.006	-0.008±0.004	0.070±0.006
110.3	-3.6±0.3	-0.7±0.2	0.01±0.01	-1.13±0.02	1.069±0.006	1.067±0.006	-0.012±0.004	0.067±0.006
120.5	-3.4±0.3	-0.9±0.2	0.01±0.01	-1.13±0.02	1.069±0.006	1.067±0.006	-0.016±0.004	0.064±0.006
130.7	-3.4±0.3	-1.0±0.2	0.01±0.01	-1.13±0.02	1.069±0.006	1.067±0.006	-0.019±0.004	0.063±0.006
140.8	-3.2±0.3	-1.2±0.2	0.01±0.01	-1.14±0.02	1.070±0.006	1.068±0.006	-0.023±0.004	0.060±0.006

Table D.5 Five-Hole Probe Data at (x,z)=(305 mm,-127 mm)

y, mm	BETA, deg	ALPHA, deg	CPT	CPS	SPEED	U	V	W
3.7	4.7±0.3	1.6±0.9	-0.86±0.01	-1.14±0.02	0.529±0.008	0.527±0.008	0.015±0.008	-0.044±0.003
4.7	4.3±0.3	1.1±0.8	-0.83±0.01	-1.14±0.02	0.555±0.008	0.553±0.008	0.011±0.008	-0.041±0.003
5.7	3.7±0.3	1.2±0.7	-0.81±0.01	-1.14±0.02	0.576±0.008	0.575±0.008	0.012±0.007	-0.037±0.003
6.7	3.4±0.3	1.4±0.7	-0.79±0.01	-1.14±0.02	0.593±0.008	0.592±0.008	0.014±0.007	-0.035±0.003
7.7	3.0±0.3	1.6±0.7	-0.77±0.01	-1.15±0.02	0.610±0.007	0.609±0.007	0.017±0.007	-0.032±0.003
8.7	2.6±0.3	1.9±0.6	-0.76±0.01	-1.14±0.02	0.619±0.007	0.618±0.007	0.020±0.007	-0.028±0.003
9.8	2.2±0.3	2.2±0.6	-0.75±0.01	-1.14±0.02	0.628±0.007	0.627±0.007	0.024±0.007	-0.024±0.003
10.8	1.8±0.3	2.4±0.6	-0.74±0.01	-1.14±0.02	0.638±0.007	0.637±0.007	0.026±0.007	-0.020±0.004
11.8	1.5±0.3	2.5±0.6	-0.73±0.01	-1.15±0.02	0.646±0.007	0.646±0.007	0.028±0.007	-0.017±0.004
12.8	1.1±0.3	2.7±0.6	-0.72±0.01	-1.15±0.02	0.652±0.007	0.651±0.007	0.031±0.007	-0.013±0.004
13.8	0.8±0.3	2.9±0.6	-0.71±0.01	-1.15±0.02	0.659±0.007	0.658±0.007	0.033±0.007	-0.009±0.004
16.4	-0.1±0.3	3.1±0.6	-0.70±0.01	-1.15±0.02	0.670±0.007	0.669±0.007	0.036±0.006	0.001±0.004
18.9	-1.0±0.3	3.1±0.5	-0.68±0.01	-1.15±0.02	0.685±0.007	0.684±0.007	0.038±0.006	0.012±0.004
21.4	-1.9±0.3	3.1±0.5	-0.66±0.01	-1.15±0.02	0.702±0.007	0.701±0.007	0.038±0.006	0.024±0.004
24.0	-2.8±0.3	2.9±0.5	-0.63±0.01	-1.15±0.02	0.717±0.007	0.715±0.007	0.036±0.006	0.034±0.004
26.5	-3.4±0.3	2.6±0.5	-0.61±0.01	-1.15±0.02	0.737±0.007	0.735±0.007	0.033±0.006	0.043±0.004
29.1	-3.9±0.3	2.3±0.4	-0.57±0.01	-1.15±0.02	0.759±0.007	0.756±0.007	0.030±0.006	0.051±0.004
31.6	-4.2±0.3	2.0±0.4	-0.53±0.01	-1.14±0.02	0.781±0.007	0.778±0.007	0.027±0.006	0.057±0.004
34.1	-4.5±0.3	1.8±0.4	-0.49±0.01	-1.14±0.02	0.807±0.006	0.804±0.006	0.025±0.005	0.063±0.004
36.7	-4.6±0.3	1.6±0.4	-0.45±0.01	-1.14±0.02	0.831±0.006	0.828±0.006	0.023±0.005	0.067±0.005
39.2	-4.8±0.3	1.4±0.3	-0.41±0.01	-1.14±0.02	0.854±0.006	0.851±0.006	0.021±0.005	0.071±0.005
44.3	-4.9±0.3	1.2±0.3	-0.34±0.01	-1.14±0.02	0.895±0.006	0.892±0.006	0.018±0.005	0.077±0.005
49.4	-4.9±0.3	0.9±0.3	-0.27±0.01	-1.14±0.02	0.929±0.006	0.925±0.006	0.015±0.005	0.080±0.005
54.5	-4.8±0.3	0.7±0.3	-0.22±0.01	-1.13±0.02	0.956±0.006	0.952±0.006	0.012±0.005	0.081±0.005
59.5	-4.8±0.3	0.5±0.3	-0.17±0.01	-1.13±0.02	0.982±0.006	0.978±0.006	0.008±0.004	0.082±0.005
64.6	-4.7±0.3	0.3±0.2	-0.12±0.01	-1.13±0.02	1.004±0.006	1.001±0.006	0.006±0.004	0.082±0.006
69.7	-4.6±0.3	0.2±0.2	-0.08±0.01	-1.13±0.02	1.023±0.006	1.020±0.006	0.003±0.004	0.083±0.006
74.8	-4.6±0.3	0.1±0.2	-0.05±0.01	-1.13±0.02	1.039±0.006	1.036±0.006	0.001±0.004	0.083±0.006
79.9	-4.5±0.3	-0.0±0.2	-0.02±0.01	-1.13±0.02	1.051±0.006	1.047±0.006	-0.001±0.004	0.082±0.006
84.9	-4.4±0.3	-0.2±0.2	-0.01±0.01	-1.13±0.02	1.059±0.006	1.056±0.006	-0.003±0.004	0.082±0.006
90.0	-4.3±0.3	-0.3±0.2	0.00±0.01	-1.13±0.02	1.063±0.006	1.060±0.006	-0.005±0.004	0.080±0.006
100.2	-4.1±0.3	-0.5±0.2	0.01±0.01	-1.13±0.02	1.066±0.006	1.063±0.006	-0.008±0.004	0.077±0.006
110.3	-4.0±0.3	-0.6±0.2	0.01±0.01	-1.12±0.02	1.065±0.006	1.063±0.006	-0.012±0.004	0.074±0.006
120.5	-3.8±0.3	-0.9±0.2	0.01±0.01	-1.13±0.02	1.065±0.006	1.063±0.006	-0.016±0.004	0.071±0.006
130.7	-3.7±0.3	-1.0±0.2	0.01±0.01	-1.13±0.02	1.066±0.006	1.063±0.006	-0.019±0.004	0.069±0.006
140.8	-3.6±0.3	-1.2±0.2	0.01±0.01	-1.13±0.02	1.066±0.006	1.063±0.006	-0.023±0.004	0.067±0.006

Table D.6 Five-Hole Probe Data at (x,z)=(305 mm,-121 mm)

y, mm	BETA, deg	ALPHA, deg	CPT	CPS	SPEED	U	V	W
3.7	7.0±0.3	2.1±0.8	-0.83±0.01	-1.14±0.02	0.560±0.008	0.556±0.008	0.021±0.008	-0.068±0.003
4.7	6.2±0.3	1.7±0.7	-0.80±0.01	-1.15±0.02	0.584±0.008	0.580±0.008	0.017±0.007	-0.063±0.003
5.7	5.7±0.3	1.7±0.7	-0.78±0.01	-1.15±0.02	0.603±0.007	0.600±0.007	0.018±0.007	-0.060±0.003
6.7	5.2±0.3	2.0±0.7	-0.77±0.01	-1.15±0.02	0.617±0.007	0.614±0.007	0.021±0.007	-0.056±0.003
7.7	4.7±0.3	2.3±0.6	-0.76±0.01	-1.15±0.02	0.627±0.007	0.624±0.007	0.025±0.007	-0.051±0.003
8.7	4.3±0.3	2.6±0.6	-0.75±0.01	-1.15±0.02	0.636±0.007	0.634±0.007	0.029±0.007	-0.047±0.004
9.8	3.6±0.3	2.9±0.6	-0.74±0.01	-1.15±0.02	0.640±0.007	0.638±0.007	0.032±0.007	-0.040±0.004
10.8	3.1±0.3	3.1±0.6	-0.74±0.01	-1.15±0.02	0.644±0.007	0.642±0.007	0.035±0.007	-0.035±0.004
11.8	2.6±0.3	3.3±0.6	-0.73±0.01	-1.16±0.02	0.650±0.007	0.648±0.007	0.038±0.007	-0.030±0.004
12.8	2.2±0.3	3.6±0.6	-0.73±0.01	-1.15±0.02	0.651±0.007	0.650±0.007	0.041±0.007	-0.024±0.004
13.8	1.6±0.3	3.8±0.6	-0.73±0.01	-1.16±0.02	0.655±0.007	0.653±0.007	0.043±0.007	-0.018±0.004
16.4	0.3±0.3	4.0±0.6	-0.72±0.01	-1.16±0.02	0.660±0.007	0.658±0.007	0.046±0.007	-0.004±0.004
18.9	-1.0±0.3	3.9±0.6	-0.71±0.01	-1.16±0.02	0.672±0.007	0.671±0.007	0.046±0.006	0.012±0.004
21.4	-2.3±0.3	3.7±0.5	-0.69±0.01	-1.16±0.02	0.681±0.007	0.679±0.007	0.044±0.006	0.027±0.004
24.0	-3.4±0.3	3.2±0.5	-0.67±0.01	-1.16±0.02	0.698±0.007	0.696±0.007	0.039±0.006	0.041±0.004
26.5	-4.1±0.3	2.9±0.5	-0.65±0.01	-1.16±0.02	0.717±0.007	0.715±0.007	0.036±0.006	0.051±0.004
29.1	-4.6±0.3	2.4±0.5	-0.61±0.01	-1.15±0.02	0.740±0.007	0.737±0.007	0.031±0.006	0.060±0.004
31.6	-5.0±0.3	2.0±0.4	-0.57±0.01	-1.16±0.02	0.768±0.007	0.765±0.007	0.027±0.006	0.067±0.004
34.1	-5.2±0.3	1.7±0.4	-0.52±0.01	-1.16±0.02	0.796±0.007	0.793±0.007	0.024±0.005	0.072±0.004
36.7	-5.3±0.3	1.5±0.4	-0.47±0.01	-1.15±0.02	0.822±0.006	0.818±0.006	0.022±0.005	0.076±0.005
39.2	-5.4±0.3	1.3±0.3	-0.43±0.01	-1.15±0.02	0.846±0.006	0.842±0.006	0.019±0.005	0.080±0.005
44.3	-5.5±0.3	1.0±0.3	-0.35±0.01	-1.15±0.02	0.894±0.006	0.889±0.006	0.016±0.005	0.085±0.005
49.4	-5.4±0.3	0.8±0.3	-0.28±0.01	-1.14±0.02	0.928±0.006	0.924±0.006	0.013±0.005	0.087±0.005
54.5	-5.3±0.3	0.6±0.3	-0.22±0.01	-1.13±0.02	0.956±0.006	0.952±0.006	0.010±0.005	0.088±0.005
59.5	-5.2±0.3	0.4±0.3	-0.17±0.01	-1.14±0.02	0.983±0.006	0.979±0.006	0.007±0.004	0.088±0.005
64.6	-5.0±0.3	0.2±0.2	-0.12±0.01	-1.13±0.02	1.005±0.006	1.001±0.006	0.004±0.004	0.088±0.006
69.7	-4.9±0.3	0.1±0.2	-0.08±0.01	-1.13±0.02	1.024±0.006	1.020±0.006	0.002±0.004	0.088±0.006
74.8	-4.9±0.3	-0.0±0.2	-0.05±0.01	-1.13±0.02	1.040±0.006	1.036±0.006	-0.000±0.004	0.088±0.006
79.9	-4.8±0.3	-0.1±0.2	-0.02±0.01	-1.13±0.02	1.051±0.006	1.048±0.006	-0.002±0.004	0.088±0.006
84.9	-4.7±0.3	-0.2±0.2	-0.01±0.01	-1.13±0.02	1.059±0.006	1.055±0.006	-0.004±0.004	0.086±0.006
90.0	-4.6±0.3	-0.3±0.2	0.00±0.01	-1.13±0.02	1.063±0.006	1.059±0.006	-0.006±0.004	0.085±0.006
100.2	-4.4±0.3	-0.5±0.2	0.01±0.01	-1.13±0.02	1.066±0.006	1.063±0.006	-0.009±0.004	0.081±0.006
110.3	-4.2±0.3	-0.7±0.2	0.01±0.01	-1.13±0.02	1.066±0.006	1.063±0.006	-0.013±0.004	0.078±0.006
120.5	-4.1±0.3	-0.9±0.2	0.01±0.01	-1.13±0.02	1.066±0.006	1.063±0.006	-0.017±0.004	0.076±0.006
130.7	-3.9±0.3	-1.1±0.2	0.01±0.01	-1.13±0.02	1.067±0.006	1.065±0.006	-0.020±0.004	0.072±0.006
140.8	-3.9±0.3	-1.3±0.2	0.01±0.01	-1.13±0.02	1.067±0.006	1.064±0.006	-0.024±0.004	0.072±0.006

Table D.7 Five-Hole Probe Data at (x,z)=(305 mm,-114 mm)

y, mm	BETA, deg	ALPHA, deg	CPT	CPS	SPEED	U	V	W
3.7	8.7±0.3	2.3±0.7	-0.77±0.01	-1.14±0.02	0.611±0.007	0.603±0.007	0.024±0.007	-0.092±0.004
4.7	8.1±0.3	1.8±0.6	-0.74±0.01	-1.14±0.02	0.633±0.007	0.626±0.007	0.020±0.007	-0.089±0.004
5.7	7.6±0.3	1.8±0.6	-0.73±0.01	-1.15±0.02	0.648±0.007	0.642±0.007	0.020±0.007	-0.085±0.004
6.7	7.0±0.3	1.9±0.6	-0.72±0.01	-1.15±0.02	0.656±0.007	0.651±0.007	0.022±0.007	-0.080±0.004
7.7	6.5±0.3	2.2±0.6	-0.71±0.01	-1.15±0.02	0.659±0.007	0.654±0.007	0.026±0.007	-0.075±0.004
8.7	5.9±0.3	2.5±0.6	-0.71±0.01	-1.15±0.02	0.661±0.007	0.657±0.007	0.028±0.007	-0.068±0.004
9.8	5.2±0.3	2.8±0.6	-0.71±0.01	-1.15±0.02	0.660±0.007	0.656±0.007	0.032±0.007	-0.060±0.004
10.8	4.7±0.3	3.0±0.6	-0.72±0.01	-1.15±0.02	0.657±0.007	0.654±0.007	0.034±0.007	-0.054±0.004
11.8	4.0±0.3	3.1±0.6	-0.72±0.01	-1.15±0.02	0.656±0.007	0.653±0.007	0.036±0.007	-0.046±0.004
12.8	3.5±0.3	3.3±0.6	-0.73±0.01	-1.15±0.02	0.652±0.007	0.650±0.007	0.038±0.007	-0.040±0.004
13.8	2.8±0.3	3.5±0.6	-0.73±0.01	-1.15±0.02	0.651±0.007	0.649±0.007	0.040±0.007	-0.031±0.004
16.4	1.0±0.3	3.6±0.6	-0.74±0.01	-1.16±0.02	0.649±0.007	0.648±0.007	0.040±0.007	-0.011±0.004
18.9	-0.9±0.3	3.4±0.6	-0.74±0.01	-1.16±0.02	0.651±0.007	0.650±0.007	0.039±0.007	0.010±0.004
21.4	-2.6±0.3	3.1±0.6	-0.73±0.01	-1.16±0.02	0.658±0.007	0.656±0.007	0.035±0.007	0.030±0.004
24.0	-4.0±0.3	2.6±0.6	-0.71±0.01	-1.16±0.02	0.673±0.007	0.670±0.007	0.031±0.006	0.047±0.004
26.5	-5.0±0.3	2.2±0.5	-0.67±0.01	-1.15±0.02	0.692±0.007	0.689±0.007	0.026±0.006	0.061±0.004
29.1	-5.7±0.3	1.8±0.5	-0.64±0.01	-1.15±0.02	0.716±0.007	0.712±0.007	0.022±0.006	0.071±0.004
31.6	-5.9±0.3	1.4±0.4	-0.59±0.01	-1.15±0.02	0.746±0.007	0.742±0.007	0.018±0.006	0.077±0.004
34.1	-6.2±0.3	1.2±0.4	-0.54±0.01	-1.14±0.02	0.776±0.007	0.772±0.007	0.016±0.006	0.083±0.004
36.7	-6.2±0.3	1.0±0.4	-0.49±0.01	-1.14±0.02	0.807±0.006	0.802±0.006	0.013±0.005	0.087±0.004
39.2	-6.2±0.3	0.9±0.4	-0.44±0.01	-1.14±0.02	0.836±0.006	0.831±0.006	0.013±0.005	0.090±0.005
44.3	-6.1±0.3	0.7±0.3	-0.35±0.01	-1.13±0.02	0.884±0.006	0.879±0.006	0.010±0.005	0.094±0.005
49.4	-6.0±0.3	0.5±0.3	-0.28±0.01	-1.13±0.02	0.922±0.006	0.917±0.006	0.009±0.005	0.096±0.005
54.5	-5.8±0.3	0.4±0.3	-0.22±0.01	-1.13±0.02	0.951±0.006	0.946±0.006	0.006±0.005	0.096±0.005
59.5	-5.6±0.3	0.2±0.3	-0.17±0.01	-1.13±0.02	0.977±0.006	0.972±0.006	0.004±0.004	0.095±0.005
64.6	-5.4±0.3	0.1±0.2	-0.12±0.01	-1.12±0.02	0.999±0.006	0.995±0.006	0.002±0.004	0.095±0.006
69.7	-5.3±0.3	-0.0±0.2	-0.08±0.01	-1.12±0.02	1.019±0.006	1.014±0.006	-0.000±0.004	0.094±0.006
74.8	-5.2±0.3	-0.1±0.2	-0.05±0.01	-1.12±0.02	1.033±0.006	1.028±0.006	-0.002±0.004	0.093±0.006
79.9	-5.1±0.3	-0.2±0.2	-0.02±0.01	-1.12±0.02	1.045±0.006	1.041±0.006	-0.004±0.004	0.093±0.006
84.9	-5.0±0.3	-0.3±0.2	-0.01±0.01	-1.12±0.02	1.053±0.006	1.049±0.006	-0.005±0.004	0.091±0.006
90.0	-4.8±0.3	-0.4±0.2	0.00±0.01	-1.12±0.02	1.057±0.006	1.053±0.006	-0.007±0.004	0.089±0.006
100.2	-4.6±0.3	-0.6±0.2	0.01±0.01	-1.11±0.02	1.059±0.006	1.056±0.006	-0.010±0.004	0.085±0.006
110.3	-4.5±0.3	-0.8±0.2	0.01±0.01	-1.11±0.02	1.059±0.006	1.056±0.006	-0.014±0.004	0.083±0.006
120.5	-4.3±0.3	-1.0±0.2	0.01±0.01	-1.11±0.02	1.059±0.006	1.056±0.006	-0.018±0.004	0.080±0.006
130.7	-4.2±0.3	-1.2±0.2	0.01±0.01	-1.11±0.02	1.060±0.006	1.057±0.006	-0.022±0.004	0.077±0.006
140.8	-4.1±0.3	-1.4±0.2	0.01±0.01	-1.11±0.02	1.060±0.006	1.057±0.006	-0.026±0.004	0.076±0.006

Table D.8 Five-Hole Probe Data at (x,z)=(305 mm,-108 mm)

y, mm	BETA, deg	ALPHA, deg	CPT	CPS	SPEED	U	V	W
3.7	9.0±0.3	1.8±0.6	-0.71±0.01	-1.15±0.02	0.663±0.007	0.654±0.007	0.021±0.007	-0.104±0.004
4.7	8.5±0.3	1.4±0.5	-0.69±0.01	-1.15±0.02	0.683±0.007	0.676±0.007	0.016±0.006	-0.101±0.004
5.7	7.9±0.3	1.3±0.5	-0.68±0.01	-1.16±0.02	0.694±0.007	0.687±0.007	0.015±0.006	-0.096±0.004
6.7	7.5±0.3	1.3±0.5	-0.67±0.01	-1.16±0.02	0.697±0.007	0.691±0.007	0.016±0.006	-0.091±0.004
7.7	6.9±0.3	1.4±0.5	-0.67±0.01	-1.16±0.02	0.695±0.007	0.689±0.007	0.016±0.006	-0.084±0.004
8.7	6.4±0.3	1.6±0.5	-0.68±0.01	-1.16±0.02	0.688±0.007	0.683±0.007	0.019±0.006	-0.077±0.004
9.8	5.8±0.3	1.6±0.5	-0.69±0.01	-1.16±0.02	0.683±0.007	0.679±0.007	0.019±0.006	-0.069±0.004
10.8	5.3±0.3	1.6±0.6	-0.71±0.01	-1.16±0.02	0.677±0.007	0.674±0.007	0.019±0.006	-0.062±0.004
11.8	4.6±0.3	1.7±0.6	-0.72±0.01	-1.16±0.02	0.669±0.007	0.667±0.007	0.020±0.007	-0.054±0.004
12.8	4.0±0.3	1.7±0.6	-0.72±0.01	-1.16±0.02	0.664±0.007	0.662±0.007	0.020±0.007	-0.046±0.004
13.8	3.2±0.3	1.7±0.6	-0.73±0.01	-1.17±0.02	0.658±0.007	0.657±0.007	0.019±0.007	-0.036±0.004
16.4	1.2±0.3	1.5±0.6	-0.75±0.01	-1.16±0.02	0.647±0.007	0.647±0.007	0.017±0.007	-0.013±0.004
18.9	-1.1±0.3	1.2±0.6	-0.75±0.01	-1.17±0.02	0.645±0.007	0.645±0.007	0.014±0.007	0.012±0.004
21.4	-3.1±0.3	0.9±0.6	-0.74±0.01	-1.17±0.02	0.652±0.007	0.651±0.007	0.010±0.007	0.035±0.004
24.0	-4.6±0.3	0.6±0.6	-0.72±0.01	-1.17±0.02	0.669±0.007	0.667±0.007	0.007±0.007	0.054±0.004
26.5	-5.8±0.3	0.3±0.5	-0.68±0.01	-1.16±0.02	0.689±0.007	0.686±0.007	0.003±0.006	0.070±0.004
29.1	-6.4±0.3	0.1±0.5	-0.64±0.01	-1.16±0.02	0.718±0.007	0.713±0.007	0.002±0.006	0.080±0.004
31.6	-6.7±0.3	0.1±0.5	-0.59±0.01	-1.15±0.02	0.748±0.007	0.743±0.007	0.002±0.006	0.087±0.004
34.1	-6.9±0.3	0.1±0.4	-0.54±0.01	-1.15±0.02	0.780±0.007	0.774±0.007	0.001±0.006	0.093±0.004
36.7	-6.9±0.3	0.1±0.4	-0.49±0.01	-1.15±0.02	0.815±0.007	0.809±0.007	0.001±0.005	0.098±0.005
39.2	-6.9±0.3	0.1±0.4	-0.43±0.01	-1.15±0.02	0.843±0.007	0.837±0.006	0.002±0.005	0.101±0.005
44.3	-6.8±0.3	0.2±0.3	-0.34±0.01	-1.14±0.02	0.891±0.006	0.885±0.006	0.002±0.005	0.105±0.005
49.4	-6.5±0.3	0.1±0.3	-0.27±0.01	-1.13±0.02	0.926±0.006	0.920±0.006	0.002±0.005	0.105±0.005
54.5	-6.3±0.3	0.1±0.3	-0.22±0.01	-1.13±0.02	0.956±0.006	0.950±0.006	0.001±0.005	0.104±0.005
59.5	-6.1±0.3	-0.0±0.3	-0.17±0.01	-1.13±0.02	0.981±0.006	0.976±0.006	-0.000±0.004	0.104±0.005
64.6	-5.9±0.3	-0.1±0.2	-0.12±0.01	-1.13±0.02	1.003±0.006	0.997±0.006	-0.001±0.004	0.103±0.006
69.7	-5.8±0.3	-0.2±0.2	-0.08±0.01	-1.13±0.02	1.021±0.007	1.016±0.006	-0.003±0.004	0.103±0.006
74.8	-5.7±0.3	-0.3±0.2	-0.05±0.01	-1.12±0.02	1.036±0.007	1.031±0.007	-0.005±0.004	0.102±0.006
79.9	-5.5±0.3	-0.3±0.2	-0.02±0.01	-1.12±0.02	1.049±0.007	1.044±0.007	-0.006±0.004	0.101±0.006
84.9	-5.4±0.3	-0.4±0.2	-0.01±0.01	-1.12±0.02	1.056±0.007	1.051±0.007	-0.007±0.004	0.100±0.006
90.0	-5.3±0.3	-0.5±0.2	0.00±0.01	-1.12±0.02	1.060±0.007	1.055±0.007	-0.009±0.004	0.098±0.006
100.2	-5.0±0.3	-0.7±0.2	0.01±0.01	-1.12±0.02	1.062±0.007	1.058±0.007	-0.013±0.004	0.093±0.006
110.3	-4.9±0.3	-0.9±0.2	0.01±0.01	-1.12±0.02	1.062±0.007	1.058±0.007	-0.017±0.004	0.091±0.006
120.5	-4.8±0.3	-1.1±0.2	0.01±0.01	-1.12±0.02	1.063±0.007	1.059±0.007	-0.020±0.004	0.088±0.006
130.7	-4.6±0.3	-1.3±0.2	0.01±0.01	-1.12±0.02	1.063±0.007	1.059±0.007	-0.025±0.004	0.085±0.006
140.8	-4.5±0.3	-1.5±0.2	0.01±0.01	-1.12±0.02	1.063±0.007	1.059±0.007	-0.028±0.004	0.083±0.006

Table D.9 Five-Hole Probe Data at (x,z)=(305 mm,-102 mm)

y, mm	BETA, deg	ALPHA, deg	CPT	CPS	SPEED	U	V	W
3.7	9.1±0.3	1.2±0.5	-0.66±0.01	-1.13±0.02	0.690±0.007	0.681±0.007	0.014±0.006	-0.109±0.004
4.7	8.5±0.3	0.6±0.5	-0.63±0.01	-1.14±0.02	0.713±0.007	0.705±0.007	0.008±0.006	-0.106±0.004
5.7	8.0±0.3	0.4±0.5	-0.62±0.01	-1.14±0.02	0.720±0.007	0.713±0.007	0.005±0.006	-0.100±0.004
6.7	7.6±0.3	0.3±0.5	-0.62±0.01	-1.14±0.02	0.723±0.007	0.717±0.007	0.004±0.006	-0.096±0.004
7.7	7.1±0.3	0.3±0.5	-0.62±0.01	-1.14±0.02	0.719±0.007	0.713±0.007	0.003±0.006	-0.089±0.004
8.7	6.7±0.3	0.1±0.5	-0.64±0.01	-1.15±0.02	0.714±0.007	0.709±0.007	0.002±0.006	-0.083±0.004
9.8	6.2±0.3	0.0±0.5	-0.65±0.01	-1.15±0.02	0.706±0.007	0.702±0.007	0.001±0.006	-0.076±0.004
10.8	5.7±0.3	-0.1±0.5	-0.66±0.01	-1.15±0.02	0.695±0.007	0.692±0.007	-0.001±0.006	-0.069±0.004
11.8	5.0±0.3	-0.2±0.5	-0.68±0.01	-1.15±0.02	0.688±0.007	0.685±0.007	-0.002±0.006	-0.060±0.004
12.8	4.3±0.3	-0.3±0.5	-0.69±0.01	-1.15±0.02	0.678±0.007	0.676±0.007	-0.003±0.006	-0.051±0.004
13.8	3.6±0.3	-0.5±0.6	-0.70±0.01	-1.15±0.02	0.670±0.007	0.669±0.007	-0.006±0.006	-0.043±0.004
16.4	1.8±0.3	-1.0±0.6	-0.71±0.01	-1.15±0.02	0.658±0.007	0.658±0.007	-0.011±0.007	-0.020±0.004
18.9	-0.5±0.3	-1.4±0.6	-0.72±0.01	-1.15±0.02	0.654±0.007	0.654±0.007	-0.015±0.007	0.005±0.004
21.4	-2.5±0.3	-1.6±0.6	-0.71±0.01	-1.14±0.02	0.661±0.007	0.660±0.007	-0.018±0.007	0.028±0.004
24.0	-4.1±0.3	-1.7±0.5	-0.69±0.01	-1.14±0.02	0.677±0.007	0.675±0.007	-0.020±0.006	0.048±0.004
26.5	-5.2±0.3	-1.6±0.5	-0.65±0.01	-1.14±0.02	0.699±0.007	0.696±0.007	-0.020±0.006	0.063±0.004
29.1	-6.0±0.3	-1.4±0.5	-0.61±0.01	-1.14±0.02	0.726±0.007	0.722±0.007	-0.018±0.006	0.075±0.004
31.6	-6.4±0.3	-1.3±0.4	-0.56±0.01	-1.13±0.02	0.757±0.007	0.752±0.007	-0.017±0.006	0.084±0.004
34.1	-6.6±0.3	-1.1±0.4	-0.51±0.01	-1.13±0.02	0.790±0.007	0.785±0.007	-0.015±0.005	0.091±0.004
36.7	-6.8±0.3	-0.9±0.4	-0.46±0.01	-1.13±0.02	0.820±0.007	0.814±0.007	-0.013±0.005	0.096±0.005
39.2	-6.8±0.3	-0.7±0.3	-0.41±0.01	-1.13±0.02	0.847±0.006	0.841±0.006	-0.010±0.005	0.100±0.005
44.3	-6.7±0.3	-0.4±0.3	-0.33±0.01	-1.12±0.02	0.891±0.006	0.885±0.006	-0.007±0.005	0.104±0.005
49.4	-6.5±0.3	-0.3±0.3	-0.26±0.01	-1.12±0.02	0.923±0.006	0.918±0.006	-0.005±0.005	0.104±0.005
54.5	-6.3±0.3	-0.2±0.3	-0.21±0.01	-1.11±0.02	0.950±0.006	0.944±0.006	-0.004±0.005	0.103±0.005
59.5	-6.1±0.3	-0.3±0.3	-0.16±0.01	-1.11±0.02	0.974±0.006	0.969±0.006	-0.005±0.004	0.103±0.005
64.6	-5.9±0.3	-0.3±0.3	-0.12±0.01	-1.11±0.02	0.995±0.006	0.990±0.006	-0.005±0.004	0.102±0.006
69.7	-5.7±0.3	-0.3±0.2	-0.08±0.01	-1.10±0.02	1.013±0.006	1.008±0.006	-0.006±0.004	0.101±0.006
74.8	-5.6±0.3	-0.4±0.2	-0.05±0.01	-1.11±0.02	1.029±0.006	1.024±0.006	-0.007±0.004	0.101±0.006
79.9	-5.5±0.3	-0.4±0.2	-0.02±0.01	-1.11±0.02	1.041±0.007	1.036±0.006	-0.008±0.004	0.099±0.006
84.9	-5.4±0.3	-0.5±0.2	-0.01±0.01	-1.10±0.02	1.048±0.007	1.043±0.007	-0.009±0.004	0.098±0.006
90.0	-5.2±0.3	-0.6±0.2	0.00±0.01	-1.10±0.02	1.052±0.007	1.047±0.007	-0.011±0.004	0.095±0.006
100.2	-5.0±0.3	-0.8±0.2	0.01±0.01	-1.10±0.02	1.053±0.007	1.049±0.007	-0.015±0.004	0.092±0.006
110.3	-4.8±0.3	-1.0±0.2	0.01±0.01	-1.10±0.02	1.054±0.007	1.050±0.007	-0.019±0.004	0.088±0.006
120.5	-4.7±0.3	-1.2±0.2	0.01±0.01	-1.10±0.02	1.054±0.007	1.050±0.007	-0.022±0.004	0.086±0.006
130.7	-4.5±0.3	-1.4±0.2	0.01±0.01	-1.10±0.02	1.054±0.007	1.051±0.007	-0.026±0.004	0.083±0.006
140.8	-4.4±0.3	-1.7±0.2	0.01±0.01	-1.10±0.02	1.055±0.007	1.051±0.007	-0.031±0.004	0.081±0.006

Table D.10 Five-Hole Probe Data at (x,z)=(305 mm,-95 mm)

y, mm	BETA, deg	ALPHA, deg	CPT	CPS	SPEED	U	V	W
3.7	7.9±0.3	0.8±0.5	-0.63±0.01	-1.12±0.02	0.706±0.007	0.699±0.007	0.009±0.006	-0.097±0.004
4.7	7.3±0.3	0.1±0.5	-0.60±0.01	-1.13±0.02	0.730±0.007	0.724±0.007	0.001±0.006	-0.093±0.004
5.7	6.8±0.3	-0.2±0.5	-0.59±0.01	-1.13±0.02	0.740±0.007	0.734±0.007	-0.002±0.006	-0.088±0.004
6.7	6.4±0.3	-0.4±0.5	-0.58±0.01	-1.14±0.02	0.743±0.007	0.738±0.007	-0.005±0.006	-0.082±0.004
7.7	5.9±0.3	-0.5±0.5	-0.59±0.01	-1.14±0.02	0.739±0.007	0.735±0.007	-0.007±0.006	-0.076±0.004
8.7	5.5±0.3	-0.7±0.5	-0.60±0.01	-1.14±0.02	0.733±0.007	0.730±0.007	-0.009±0.006	-0.070±0.004
9.8	5.1±0.3	-0.9±0.5	-0.61±0.01	-1.14±0.02	0.726±0.007	0.723±0.007	-0.012±0.006	-0.064±0.004
10.8	4.5±0.3	-1.1±0.5	-0.62±0.01	-1.14±0.02	0.718±0.007	0.716±0.007	-0.013±0.006	-0.057±0.004
11.8	4.0±0.3	-1.3±0.5	-0.64±0.01	-1.14±0.02	0.710±0.007	0.708±0.007	-0.016±0.006	-0.050±0.004
12.8	3.4±0.3	-1.5±0.5	-0.65±0.01	-1.14±0.02	0.701±0.007	0.700±0.007	-0.018±0.006	-0.042±0.004
13.8	2.8±0.3	-1.8±0.5	-0.65±0.01	-1.14±0.02	0.699±0.007	0.697±0.007	-0.022±0.006	-0.034±0.004
16.4	1.2±0.3	-2.4±0.5	-0.67±0.01	-1.14±0.02	0.687±0.007	0.687±0.007	-0.029±0.006	-0.014±0.004
18.9	-0.7±0.3	-2.7±0.5	-0.67±0.01	-1.14±0.02	0.685±0.007	0.684±0.007	-0.033±0.006	0.008±0.004
21.4	-2.4±0.3	-2.9±0.5	-0.65±0.01	-1.13±0.02	0.692±0.007	0.691±0.007	-0.035±0.006	0.029±0.004
24.0	-3.8±0.3	-3.0±0.5	-0.64±0.01	-1.14±0.02	0.708±0.007	0.705±0.007	-0.036±0.006	0.047±0.004
26.5	-5.0±0.3	-2.8±0.5	-0.61±0.01	-1.13±0.02	0.727±0.007	0.723±0.007	-0.035±0.006	0.063±0.004
29.1	-5.8±0.3	-2.4±0.4	-0.56±0.01	-1.13±0.02	0.755±0.007	0.751±0.007	-0.031±0.006	0.076±0.004
31.6	-6.4±0.3	-2.1±0.4	-0.52±0.01	-1.12±0.02	0.779±0.007	0.774±0.007	-0.029±0.006	0.086±0.004
34.1	-6.7±0.3	-1.8±0.4	-0.47±0.01	-1.13±0.02	0.811±0.007	0.805±0.007	-0.025±0.005	0.095±0.005
36.7	-6.9±0.3	-1.6±0.4	-0.42±0.01	-1.12±0.02	0.836±0.006	0.829±0.006	-0.023±0.005	0.101±0.005
39.2	-7.0±0.3	-1.3±0.3	-0.38±0.01	-1.12±0.02	0.860±0.006	0.853±0.006	-0.019±0.005	0.105±0.005
44.3	-7.0±0.3	-0.9±0.3	-0.31±0.01	-1.12±0.02	0.896±0.006	0.889±0.006	-0.014±0.005	0.109±0.005
49.4	-6.8±0.3	-0.6±0.3	-0.25±0.01	-1.11±0.02	0.927±0.006	0.921±0.006	-0.010±0.005	0.110±0.005
54.5	-6.7±0.3	-0.5±0.3	-0.21±0.01	-1.11±0.02	0.952±0.006	0.945±0.006	-0.009±0.005	0.110±0.005
59.5	-6.5±0.3	-0.5±0.3	-0.16±0.01	-1.11±0.02	0.975±0.006	0.969±0.006	-0.008±0.004	0.111±0.005
64.6	-6.3±0.3	-0.5±0.3	-0.12±0.01	-1.10±0.02	0.995±0.006	0.989±0.006	-0.008±0.004	0.110±0.006
69.7	-6.2±0.3	-0.5±0.2	-0.08±0.01	-1.11±0.02	1.014±0.006	1.008±0.006	-0.008±0.004	0.110±0.006
74.8	-6.1±0.3	-0.5±0.2	-0.04±0.01	-1.10±0.02	1.028±0.006	1.022±0.006	-0.009±0.004	0.109±0.006
79.9	-6.0±0.3	-0.6±0.2	-0.02±0.01	-1.10±0.02	1.039±0.006	1.033±0.006	-0.010±0.004	0.108±0.006
84.9	-5.8±0.3	-0.6±0.2	-0.01±0.01	-1.10±0.02	1.046±0.006	1.041±0.006	-0.011±0.004	0.106±0.006
90.0	-5.7±0.3	-0.7±0.2	0.00±0.01	-1.10±0.02	1.049±0.006	1.044±0.006	-0.013±0.004	0.104±0.006
100.2	-5.5±0.3	-0.9±0.2	0.01±0.01	-1.10±0.02	1.053±0.006	1.048±0.006	-0.017±0.004	0.100±0.006
110.3	-5.3±0.3	-1.1±0.2	0.01±0.01	-1.10±0.02	1.052±0.006	1.047±0.006	-0.020±0.004	0.096±0.006
120.5	-5.1±0.3	-1.3±0.2	0.01±0.01	-1.10±0.02	1.052±0.006	1.048±0.006	-0.024±0.004	0.094±0.006
130.7	-5.0±0.3	-1.5±0.2	0.01±0.01	-1.10±0.02	1.053±0.006	1.049±0.007	-0.028±0.004	0.092±0.006
140.8	-4.9±0.3	-1.8±0.2	0.01±0.01	-1.10±0.02	1.053±0.007	1.049±0.007	-0.033±0.004	0.089±0.006

Table D.11 Five-Hole Probe Data at (x,z)=(305 mm,-89 mm)

y, mm	BETA, deg	ALPHA, deg	CPT	CPS	SPEED	U	V	W
3.7	7.1±0.3	0.6±0.5	-0.61±0.01	-1.12±0.02	0.714±0.007	0.708±0.007	0.008±0.006	-0.088±0.004
4.7	6.4±0.3	-0.1±0.5	-0.58±0.01	-1.13±0.02	0.742±0.007	0.737±0.007	-0.001±0.006	-0.083±0.004
5.7	5.9±0.3	-0.4±0.4	-0.56±0.01	-1.13±0.02	0.754±0.007	0.750±0.007	-0.006±0.006	-0.077±0.004
6.7	5.4±0.3	-0.6±0.4	-0.55±0.01	-1.13±0.02	0.758±0.007	0.755±0.007	-0.008±0.006	-0.072±0.004
7.7	5.0±0.3	-0.8±0.4	-0.55±0.01	-1.13±0.02	0.759±0.007	0.757±0.007	-0.011±0.006	-0.066±0.004
8.7	4.6±0.3	-1.1±0.4	-0.56±0.01	-1.13±0.02	0.755±0.007	0.753±0.007	-0.014±0.006	-0.060±0.004
9.8	4.1±0.3	-1.2±0.4	-0.57±0.01	-1.13±0.02	0.752±0.007	0.750±0.007	-0.016±0.006	-0.054±0.004
10.8	3.6±0.3	-1.5±0.4	-0.58±0.01	-1.13±0.02	0.745±0.007	0.744±0.007	-0.019±0.006	-0.047±0.004
11.8	3.1±0.3	-1.7±0.5	-0.59±0.01	-1.13±0.02	0.741±0.007	0.739±0.007	-0.022±0.006	-0.040±0.004
12.8	2.6±0.3	-2.0±0.5	-0.59±0.01	-1.13±0.02	0.735±0.007	0.734±0.007	-0.025±0.006	-0.033±0.004
13.8	2.1±0.3	-2.2±0.5	-0.60±0.01	-1.14±0.02	0.731±0.007	0.730±0.007	-0.028±0.006	-0.027±0.004
16.4	0.7±0.3	-2.7±0.5	-0.61±0.01	-1.14±0.02	0.726±0.007	0.725±0.007	-0.034±0.006	-0.009±0.004
18.9	-0.7±0.3	-3.0±0.5	-0.61±0.01	-1.14±0.02	0.729±0.007	0.728±0.007	-0.039±0.006	0.009±0.004
21.4	-2.1±0.3	-3.3±0.5	-0.59±0.01	-1.13±0.02	0.734±0.007	0.732±0.007	-0.042±0.006	0.027±0.004
24.0	-3.4±0.3	-3.2±0.4	-0.57±0.01	-1.13±0.02	0.748±0.007	0.745±0.007	-0.042±0.006	0.044±0.004
26.5	-4.4±0.3	-3.1±0.4	-0.54±0.01	-1.13±0.02	0.767±0.007	0.764±0.007	-0.041±0.006	0.059±0.004
29.1	-5.2±0.3	-2.9±0.4	-0.50±0.01	-1.13±0.02	0.788±0.007	0.784±0.007	-0.039±0.005	0.071±0.004
31.6	-5.7±0.3	-2.5±0.4	-0.47±0.01	-1.13±0.02	0.811±0.007	0.806±0.007	-0.036±0.005	0.081±0.004
34.1	-6.1±0.3	-2.2±0.4	-0.43±0.01	-1.12±0.02	0.834±0.006	0.828±0.006	-0.032±0.005	0.089±0.005
36.7	-6.4±0.3	-1.9±0.3	-0.39±0.01	-1.12±0.02	0.853±0.006	0.848±0.006	-0.028±0.005	0.095±0.005
39.2	-6.6±0.3	-1.7±0.3	-0.36±0.01	-1.12±0.02	0.872±0.006	0.866±0.006	-0.025±0.005	0.100±0.005
44.3	-6.6±0.3	-1.2±0.3	-0.30±0.01	-1.12±0.02	0.905±0.006	0.899±0.006	-0.019±0.005	0.105±0.005
49.4	-6.6±0.3	-0.9±0.3	-0.25±0.01	-1.11±0.02	0.931±0.006	0.925±0.006	-0.015±0.005	0.106±0.005
54.5	-6.5±0.3	-0.8±0.3	-0.20±0.01	-1.11±0.02	0.957±0.006	0.950±0.006	-0.013±0.005	0.108±0.005
59.5	-6.4±0.3	-0.7±0.3	-0.15±0.01	-1.11±0.02	0.977±0.006	0.971±0.006	-0.012±0.004	0.109±0.005
64.6	-6.3±0.3	-0.6±0.3	-0.11±0.01	-1.10±0.02	0.998±0.006	0.992±0.006	-0.011±0.004	0.109±0.006
69.7	-6.1±0.3	-0.6±0.2	-0.07±0.01	-1.10±0.02	1.015±0.006	1.009±0.006	-0.011±0.004	0.108±0.006
74.8	-6.0±0.3	-0.7±0.2	-0.04±0.01	-1.10±0.02	1.029±0.006	1.023±0.006	-0.012±0.004	0.108±0.006
79.9	-5.9±0.3	-0.7±0.2	-0.02±0.01	-1.10±0.02	1.039±0.006	1.034±0.006	-0.013±0.004	0.107±0.006
84.9	-5.8±0.3	-0.8±0.2	-0.00±0.01	-1.10±0.02	1.046±0.007	1.040±0.007	-0.014±0.004	0.106±0.006
90.0	-5.7±0.3	-0.8±0.2	0.00±0.01	-1.10±0.02	1.050±0.007	1.044±0.007	-0.015±0.004	0.104±0.006
100.2	-5.4±0.3	-1.0±0.2	0.01±0.01	-1.10±0.02	1.051±0.007	1.046±0.007	-0.019±0.004	0.099±0.006
110.3	-5.2±0.3	-1.2±0.2	0.01±0.01	-1.10±0.02	1.052±0.007	1.047±0.007	-0.022±0.004	0.096±0.006
120.5	-5.1±0.3	-1.4±0.2	0.01±0.01	-1.10±0.02	1.053±0.007	1.048±0.007	-0.025±0.004	0.093±0.006
130.7	-5.0±0.3	-1.6±0.2	0.01±0.01	-1.10±0.02	1.053±0.007	1.048±0.007	-0.030±0.004	0.092±0.006
140.8	-4.8±0.3	-1.9±0.2	0.01±0.01	-1.10±0.02	1.053±0.007	1.048±0.007	-0.034±0.004	0.089±0.006

Table D.12 Five-Hole Probe Data at (x,z)=(305 mm,-83 mm)

y, mm	BETA, deg	ALPHA, deg	CPT	CPS	SPEED	U	V	W
3.7	6.2±0.3	0.6±0.5	-0.60±0.01	-1.12±0.02	0.721±0.007	0.717±0.007	0.008±0.006	-0.078±0.004
4.7	5.4±0.3	-0.1±0.4	-0.56±0.01	-1.12±0.02	0.749±0.007	0.746±0.007	-0.001±0.006	-0.071±0.004
5.7	4.8±0.3	-0.4±0.4	-0.54±0.01	-1.12±0.02	0.764±0.007	0.762±0.007	-0.006±0.006	-0.064±0.004
6.7	4.3±0.3	-0.6±0.4	-0.53±0.01	-1.12±0.02	0.772±0.007	0.770±0.007	-0.008±0.006	-0.058±0.004
7.7	3.8±0.3	-0.8±0.4	-0.53±0.01	-1.13±0.02	0.774±0.007	0.772±0.007	-0.011±0.006	-0.052±0.004
8.7	3.4±0.3	-0.9±0.4	-0.53±0.01	-1.13±0.02	0.774±0.007	0.773±0.007	-0.013±0.006	-0.046±0.004
9.8	3.0±0.3	-1.2±0.4	-0.53±0.01	-1.13±0.02	0.770±0.007	0.769±0.007	-0.015±0.006	-0.040±0.004
10.8	2.5±0.3	-1.3±0.4	-0.54±0.01	-1.13±0.02	0.768±0.007	0.767±0.007	-0.017±0.006	-0.033±0.004
11.8	2.1±0.3	-1.6±0.4	-0.55±0.01	-1.13±0.02	0.765±0.007	0.764±0.007	-0.021±0.006	-0.027±0.004
12.8	1.6±0.3	-1.7±0.4	-0.55±0.01	-1.13±0.02	0.763±0.007	0.762±0.007	-0.023±0.006	-0.021±0.004
13.8	1.2±0.3	-2.0±0.4	-0.55±0.01	-1.13±0.02	0.759±0.007	0.758±0.007	-0.026±0.006	-0.015±0.004
16.4	-0.0±0.3	-2.4±0.4	-0.55±0.01	-1.13±0.02	0.759±0.007	0.758±0.007	-0.032±0.006	0.000±0.004
18.9	-1.2±0.3	-2.7±0.4	-0.54±0.01	-1.13±0.02	0.765±0.007	0.764±0.007	-0.036±0.006	0.016±0.004
21.4	-2.3±0.3	-2.9±0.4	-0.53±0.01	-1.13±0.02	0.773±0.007	0.771±0.007	-0.039±0.006	0.030±0.004
24.0	-3.2±0.3	-2.9±0.4	-0.51±0.01	-1.12±0.02	0.787±0.007	0.784±0.007	-0.040±0.006	0.044±0.004
26.5	-4.1±0.3	-2.8±0.4	-0.48±0.01	-1.12±0.02	0.802±0.007	0.799±0.007	-0.040±0.005	0.057±0.004
29.1	-4.8±0.3	-2.7±0.4	-0.45±0.01	-1.12±0.02	0.820±0.007	0.816±0.007	-0.038±0.005	0.069±0.005
31.6	-5.4±0.3	-2.5±0.4	-0.42±0.01	-1.12±0.02	0.835±0.007	0.831±0.007	-0.036±0.005	0.078±0.005
34.1	-5.8±0.3	-2.2±0.3	-0.39±0.01	-1.11±0.02	0.853±0.006	0.848±0.006	-0.033±0.005	0.086±0.005
36.7	-6.1±0.3	-2.0±0.3	-0.36±0.01	-1.12±0.02	0.869±0.006	0.864±0.006	-0.030±0.005	0.092±0.005
39.2	-6.3±0.3	-1.8±0.3	-0.33±0.01	-1.12±0.02	0.886±0.006	0.880±0.006	-0.027±0.005	0.097±0.005
44.3	-6.4±0.3	-1.4±0.3	-0.28±0.01	-1.11±0.02	0.911±0.006	0.905±0.006	-0.022±0.005	0.102±0.005
49.4	-6.5±0.3	-1.1±0.3	-0.23±0.01	-1.11±0.02	0.934±0.006	0.928±0.006	-0.018±0.005	0.105±0.005
54.5	-6.5±0.3	-1.0±0.3	-0.19±0.01	-1.10±0.02	0.958±0.006	0.952±0.006	-0.016±0.005	0.108±0.005
59.5	-6.4±0.3	-0.9±0.3	-0.14±0.01	-1.10±0.02	0.979±0.006	0.973±0.006	-0.015±0.004	0.109±0.005
64.6	-6.3±0.3	-0.8±0.3	-0.10±0.01	-1.10±0.02	0.998±0.006	0.992±0.006	-0.014±0.004	0.110±0.006
69.7	-6.3±0.3	-0.8±0.2	-0.07±0.01	-1.10±0.02	1.016±0.006	1.010±0.006	-0.014±0.004	0.111±0.006
74.8	-6.2±0.3	-0.8±0.2	-0.04±0.01	-1.10±0.02	1.028±0.007	1.022±0.006	-0.015±0.004	0.110±0.006
79.9	-6.1±0.3	-0.9±0.2	-0.02±0.01	-1.10±0.02	1.038±0.007	1.032±0.007	-0.015±0.004	0.110±0.006
84.9	-5.9±0.3	-0.9±0.2	-0.00±0.01	-1.09±0.02	1.044±0.007	1.039±0.007	-0.017±0.004	0.108±0.006
90.0	-5.9±0.3	-1.0±0.2	0.00±0.01	-1.09±0.02	1.048±0.007	1.042±0.007	-0.018±0.004	0.107±0.006
100.2	-5.6±0.3	-1.1±0.2	0.01±0.01	-1.09±0.02	1.049±0.007	1.044±0.007	-0.021±0.004	0.102±0.006
110.3	-5.4±0.3	-1.3±0.2	0.01±0.01	-1.09±0.02	1.049±0.007	1.044±0.007	-0.024±0.004	0.098±0.006
120.5	-5.3±0.3	-1.5±0.2	0.01±0.01	-1.09±0.02	1.050±0.007	1.045±0.007	-0.027±0.004	0.096±0.006
130.7	-5.2±0.3	-1.7±0.2	0.01±0.01	-1.10±0.02	1.051±0.007	1.046±0.007	-0.031±0.004	0.095±0.006
140.8	-5.0±0.3	-1.9±0.2	0.01±0.01	-1.10±0.02	1.051±0.007	1.047±0.007	-0.035±0.004	0.092±0.006

Table D.13 Five-Hole Probe Data at (x,z)=(305 mm,-76 mm)

y, mm	BETA, deg	ALPHA, deg	CPT	CPS	SPEED	U	V	W
3.7	5.0±0.3	0.9±0.5	-0.58±0.01	-1.10±0.02	0.722±0.007	0.719±0.007	0.011±0.006	-0.063±0.004
4.7	4.3±0.3	0.1±0.4	-0.54±0.01	-1.10±0.02	0.752±0.007	0.750±0.007	0.002±0.006	-0.056±0.004
5.7	3.6±0.3	-0.2±0.4	-0.51±0.01	-1.10±0.02	0.768±0.007	0.766±0.007	-0.002±0.006	-0.048±0.004
6.7	3.0±0.3	-0.4±0.4	-0.50±0.01	-1.10±0.02	0.776±0.007	0.775±0.007	-0.005±0.006	-0.041±0.004
7.7	2.5±0.3	-0.6±0.4	-0.50±0.01	-1.11±0.02	0.781±0.007	0.780±0.007	-0.008±0.006	-0.034±0.004
8.7	2.1±0.3	-0.7±0.4	-0.50±0.01	-1.11±0.02	0.781±0.007	0.780±0.007	-0.009±0.006	-0.028±0.004
9.8	1.6±0.3	-0.8±0.4	-0.50±0.01	-1.11±0.02	0.780±0.007	0.780±0.007	-0.011±0.006	-0.022±0.004
10.8	1.2±0.3	-1.0±0.4	-0.50±0.01	-1.11±0.02	0.778±0.007	0.777±0.007	-0.013±0.006	-0.016±0.004
11.8	0.7±0.3	-1.2±0.4	-0.50±0.01	-1.11±0.02	0.776±0.007	0.776±0.007	-0.016±0.006	-0.010±0.004
12.8	0.3±0.3	-1.3±0.4	-0.51±0.01	-1.11±0.02	0.775±0.007	0.775±0.007	-0.018±0.006	-0.004±0.004
13.8	-0.1±0.3	-1.5±0.4	-0.51±0.01	-1.11±0.02	0.776±0.007	0.776±0.007	-0.020±0.006	0.001±0.004
16.4	-1.1±0.3	-1.9±0.4	-0.50±0.01	-1.11±0.02	0.780±0.007	0.780±0.007	-0.025±0.006	0.015±0.004
18.9	-2.1±0.3	-2.1±0.4	-0.49±0.01	-1.11±0.02	0.786±0.007	0.785±0.007	-0.029±0.006	0.028±0.004
21.4	-2.9±0.3	-2.3±0.4	-0.47±0.01	-1.11±0.02	0.794±0.007	0.792±0.007	-0.032±0.005	0.040±0.004
24.0	-3.7±0.3	-2.4±0.4	-0.45±0.01	-1.10±0.02	0.805±0.007	0.803±0.007	-0.034±0.005	0.052±0.004
26.5	-4.4±0.3	-2.4±0.4	-0.43±0.01	-1.10±0.02	0.819±0.007	0.816±0.007	-0.035±0.005	0.062±0.005
29.1	-5.0±0.3	-2.3±0.4	-0.41±0.01	-1.10±0.02	0.833±0.007	0.829±0.007	-0.034±0.005	0.072±0.005
31.6	-5.5±0.3	-2.2±0.3	-0.39±0.01	-1.10±0.02	0.847±0.006	0.843±0.006	-0.032±0.005	0.081±0.005
34.1	-5.9±0.3	-2.1±0.3	-0.36±0.01	-1.10±0.02	0.860±0.006	0.855±0.006	-0.031±0.005	0.088±0.005
36.7	-6.2±0.3	-1.9±0.3	-0.34±0.01	-1.10±0.02	0.872±0.006	0.867±0.006	-0.028±0.005	0.094±0.005
39.2	-6.4±0.3	-1.8±0.3	-0.31±0.01	-1.09±0.02	0.885±0.006	0.879±0.006	-0.027±0.005	0.098±0.005
44.3	-6.6±0.3	-1.5±0.3	-0.27±0.01	-1.10±0.02	0.910±0.006	0.904±0.006	-0.023±0.005	0.105±0.005
49.4	-6.8±0.3	-1.2±0.3	-0.22±0.01	-1.09±0.02	0.933±0.006	0.926±0.006	-0.020±0.005	0.110±0.005
54.5	-6.8±0.3	-1.1±0.3	-0.18±0.01	-1.09±0.02	0.954±0.006	0.947±0.006	-0.019±0.005	0.113±0.005
59.5	-6.8±0.3	-1.0±0.3	-0.13±0.01	-1.09±0.02	0.975±0.006	0.968±0.006	-0.018±0.004	0.116±0.005
64.6	-6.8±0.3	-1.0±0.3	-0.09±0.01	-1.08±0.02	0.992±0.006	0.985±0.006	-0.017±0.004	0.117±0.005
69.7	-6.8±0.3	-1.0±0.2	-0.06±0.01	-1.08±0.02	1.008±0.006	1.001±0.006	-0.017±0.004	0.118±0.006
74.8	-6.7±0.3	-1.0±0.2	-0.04±0.01	-1.08±0.02	1.022±0.006	1.015±0.006	-0.018±0.004	0.119±0.006
79.9	-6.6±0.3	-1.0±0.2	-0.01±0.01	-1.08±0.02	1.030±0.006	1.023±0.006	-0.018±0.004	0.118±0.006
84.9	-6.5±0.3	-1.1±0.2	-0.00±0.01	-1.08±0.02	1.036±0.006	1.029±0.006	-0.019±0.004	0.117±0.006
90.0	-6.4±0.3	-1.1±0.2	0.00±0.01	-1.08±0.02	1.039±0.007	1.032±0.006	-0.020±0.004	0.115±0.006
100.2	-6.1±0.3	-1.3±0.2	0.01±0.01	-1.08±0.02	1.041±0.007	1.035±0.007	-0.023±0.004	0.111±0.006
110.3	-5.9±0.3	-1.4±0.2	0.01±0.01	-1.07±0.02	1.040±0.007	1.035±0.007	-0.026±0.004	0.107±0.006
120.5	-5.8±0.3	-1.6±0.2	0.01±0.01	-1.08±0.02	1.041±0.007	1.035±0.007	-0.029±0.004	0.105±0.006
130.7	-5.7±0.3	-1.8±0.2	0.01±0.01	-1.08±0.02	1.041±0.007	1.035±0.007	-0.032±0.004	0.104±0.006
140.8	-5.6±0.3	-2.0±0.2	0.01±0.01	-1.08±0.02	1.042±0.007	1.037±0.007	-0.036±0.004	0.102±0.006

Table D.14 Five-Hole Probe Data at (x,z)=(305 mm,-70 mm)

y, mm	BETA, deg	ALPHA, deg	CPT	CPS	SPEED	U	V	W
3.7	4.7±0.3	0.9±0.5	-0.56±0.01	-1.09±0.02	0.730±0.007	0.728±0.007	0.011±0.006	-0.060±0.004
4.7	3.9±0.3	0.2±0.4	-0.52±0.01	-1.09±0.02	0.758±0.007	0.757±0.007	0.003±0.006	-0.052±0.004
5.7	3.3±0.3	-0.1±0.4	-0.49±0.01	-1.09±0.02	0.775±0.007	0.773±0.007	-0.001±0.006	-0.044±0.004
6.7	2.6±0.3	-0.2±0.4	-0.48±0.01	-1.10±0.02	0.785±0.007	0.785±0.007	-0.003±0.006	-0.036±0.004
7.7	2.1±0.3	-0.4±0.4	-0.48±0.01	-1.10±0.02	0.790±0.007	0.790±0.007	-0.005±0.005	-0.029±0.004
8.7	1.6±0.3	-0.4±0.4	-0.47±0.01	-1.10±0.02	0.791±0.007	0.790±0.007	-0.006±0.005	-0.022±0.004
9.8	1.1±0.3	-0.6±0.4	-0.47±0.01	-1.10±0.02	0.791±0.007	0.791±0.007	-0.008±0.005	-0.016±0.004
10.8	0.6±0.3	-0.7±0.4	-0.48±0.01	-1.10±0.02	0.789±0.007	0.788±0.007	-0.009±0.006	-0.009±0.004
11.8	0.2±0.3	-0.8±0.4	-0.48±0.01	-1.10±0.02	0.786±0.007	0.786±0.007	-0.011±0.006	-0.003±0.004
12.8	-0.2±0.3	-1.0±0.4	-0.48±0.01	-1.10±0.02	0.787±0.007	0.787±0.007	-0.013±0.006	0.003±0.004
13.8	-0.6±0.3	-1.1±0.4	-0.48±0.01	-1.10±0.02	0.786±0.007	0.786±0.007	-0.015±0.006	0.008±0.004
16.4	-1.5±0.3	-1.4±0.4	-0.47±0.01	-1.10±0.02	0.790±0.007	0.789±0.007	-0.019±0.005	0.020±0.004
18.9	-2.3±0.3	-1.6±0.4	-0.46±0.01	-1.10±0.02	0.797±0.007	0.796±0.007	-0.023±0.005	0.032±0.004
21.4	-3.0±0.3	-1.8±0.4	-0.45±0.01	-1.10±0.02	0.807±0.007	0.806±0.007	-0.026±0.005	0.042±0.004
24.0	-3.7±0.3	-1.9±0.4	-0.43±0.01	-1.09±0.02	0.817±0.007	0.815±0.007	-0.027±0.005	0.052±0.005
26.5	-4.3±0.3	-1.9±0.4	-0.41±0.01	-1.09±0.02	0.829±0.007	0.826±0.007	-0.028±0.005	0.062±0.005
29.1	-4.7±0.3	-1.9±0.4	-0.39±0.01	-1.09±0.02	0.840±0.006	0.837±0.006	-0.028±0.005	0.069±0.005
31.6	-5.1±0.3	-1.9±0.3	-0.36±0.01	-1.09±0.02	0.853±0.006	0.849±0.006	-0.027±0.005	0.076±0.005
34.1	-5.5±0.3	-1.8±0.3	-0.34±0.01	-1.09±0.02	0.866±0.006	0.862±0.006	-0.027±0.005	0.083±0.005
36.7	-5.7±0.3	-1.7±0.3	-0.32±0.01	-1.09±0.02	0.877±0.006	0.873±0.006	-0.026±0.005	0.088±0.005
39.2	-6.0±0.3	-1.6±0.3	-0.30±0.01	-1.09±0.02	0.888±0.006	0.883±0.006	-0.025±0.005	0.093±0.005
44.3	-6.3±0.3	-1.4±0.3	-0.25±0.01	-1.09±0.02	0.912±0.006	0.907±0.006	-0.022±0.005	0.100±0.005
49.4	-6.4±0.3	-1.3±0.3	-0.21±0.01	-1.09±0.02	0.935±0.006	0.929±0.006	-0.021±0.005	0.105±0.005
54.5	-6.5±0.3	-1.2±0.3	-0.17±0.01	-1.08±0.02	0.955±0.006	0.948±0.006	-0.020±0.005	0.109±0.005
59.5	-6.6±0.3	-1.2±0.3	-0.13±0.01	-1.08±0.02	0.974±0.006	0.968±0.006	-0.020±0.004	0.112±0.005
64.6	-6.6±0.3	-1.2±0.3	-0.09±0.01	-1.07±0.02	0.992±0.006	0.986±0.006	-0.020±0.004	0.113±0.005
69.7	-6.5±0.3	-1.1±0.2	-0.06±0.01	-1.07±0.02	1.007±0.006	1.000±0.006	-0.020±0.004	0.115±0.006
74.8	-6.5±0.3	-1.2±0.2	-0.03±0.01	-1.07±0.02	1.020±0.006	1.013±0.006	-0.021±0.004	0.115±0.006
79.9	-6.4±0.3	-1.2±0.2	-0.01±0.01	-1.07±0.02	1.027±0.006	1.021±0.006	-0.021±0.004	0.114±0.006
84.9	-6.3±0.3	-1.2±0.2	-0.00±0.01	-1.07±0.02	1.032±0.006	1.026±0.006	-0.021±0.004	0.113±0.006
90.0	-6.2±0.3	-1.2±0.2	0.00±0.01	-1.07±0.02	1.034±0.006	1.028±0.006	-0.022±0.004	0.111±0.006
100.2	-6.0±0.3	-1.3±0.2	0.01±0.01	-1.07±0.02	1.036±0.006	1.031±0.006	-0.024±0.004	0.108±0.006
110.3	-5.8±0.3	-1.5±0.2	0.01±0.01	-1.07±0.02	1.036±0.006	1.030±0.006	-0.027±0.004	0.104±0.006
120.5	-5.6±0.3	-1.7±0.2	0.01±0.01	-1.07±0.02	1.038±0.006	1.032±0.006	-0.031±0.004	0.102±0.006
130.7	-5.6±0.3	-1.9±0.2	0.01±0.01	-1.07±0.02	1.038±0.006	1.032±0.007	-0.034±0.004	0.101±0.006
140.8	-5.5±0.3	-2.1±0.2	0.01±0.01	-1.07±0.02	1.040±0.007	1.034±0.007	-0.038±0.004	0.099±0.006

Table D.15 Five-Hole Probe Data at (x,z)=(305 mm,-64 mm)

y, mm	BETA, deg	ALPHA, deg	CPT	CPS	SPEED	U	V	W
3.7	4.4±0.3	1.1±0.5	-0.53±0.01	-1.08±0.02	0.741±0.007	0.739±0.007	0.014±0.006	-0.057±0.004
4.7	3.6±0.3	0.4±0.4	-0.49±0.01	-1.08±0.02	0.770±0.007	0.769±0.007	0.005±0.006	-0.048±0.004
5.7	2.8±0.3	0.1±0.4	-0.47±0.01	-1.08±0.02	0.786±0.007	0.785±0.007	0.001±0.006	-0.039±0.004
6.7	2.1±0.3	-0.1±0.4	-0.45±0.01	-1.08±0.02	0.793±0.007	0.793±0.007	-0.001±0.006	-0.029±0.004
7.7	1.5±0.3	-0.1±0.4	-0.45±0.01	-1.09±0.02	0.796±0.007	0.796±0.007	-0.002±0.005	-0.022±0.004
8.7	1.1±0.3	-0.3±0.4	-0.45±0.01	-1.09±0.02	0.799±0.007	0.799±0.007	-0.004±0.005	-0.015±0.004
9.8	0.5±0.3	-0.3±0.4	-0.45±0.01	-1.09±0.02	0.798±0.007	0.798±0.007	-0.005±0.005	-0.008±0.004
10.8	0.1±0.3	-0.5±0.4	-0.45±0.01	-1.09±0.02	0.795±0.007	0.795±0.007	-0.006±0.005	-0.001±0.004
11.8	-0.4±0.3	-0.6±0.4	-0.46±0.01	-1.09±0.02	0.795±0.007	0.795±0.007	-0.008±0.005	0.005±0.004
12.8	-0.8±0.3	-0.7±0.4	-0.46±0.01	-1.09±0.02	0.793±0.007	0.793±0.007	-0.010±0.005	0.011±0.004
13.8	-1.2±0.3	-0.8±0.4	-0.46±0.01	-1.09±0.02	0.793±0.007	0.793±0.007	-0.011±0.005	0.016±0.004
16.4	-2.0±0.3	-1.1±0.4	-0.45±0.01	-1.09±0.02	0.798±0.007	0.797±0.007	-0.015±0.005	0.028±0.004
18.9	-2.8±0.3	-1.3±0.4	-0.44±0.01	-1.09±0.02	0.805±0.007	0.803±0.007	-0.018±0.005	0.039±0.004
21.4	-3.4±0.3	-1.4±0.4	-0.43±0.01	-1.09±0.02	0.814±0.007	0.813±0.007	-0.020±0.005	0.049±0.005
24.0	-4.0±0.3	-1.6±0.4	-0.41±0.01	-1.09±0.02	0.824±0.007	0.822±0.007	-0.023±0.005	0.057±0.005
26.5	-4.5±0.3	-1.6±0.4	-0.39±0.01	-1.09±0.02	0.835±0.007	0.832±0.007	-0.023±0.005	0.065±0.005
29.1	-4.9±0.3	-1.6±0.4	-0.37±0.01	-1.08±0.02	0.845±0.007	0.842±0.007	-0.024±0.005	0.072±0.005
31.6	-5.3±0.3	-1.6±0.3	-0.35±0.01	-1.08±0.02	0.857±0.006	0.853±0.006	-0.024±0.005	0.079±0.005
34.1	-5.5±0.3	-1.6±0.3	-0.33±0.01	-1.08±0.02	0.868±0.006	0.864±0.006	-0.024±0.005	0.084±0.005
36.7	-5.8±0.3	-1.5±0.3	-0.31±0.01	-1.08±0.02	0.880±0.006	0.875±0.006	-0.024±0.005	0.089±0.005
39.2	-6.0±0.3	-1.5±0.3	-0.29±0.01	-1.08±0.02	0.892±0.006	0.886±0.006	-0.023±0.005	0.094±0.005
44.3	-6.3±0.3	-1.4±0.3	-0.24±0.01	-1.08±0.02	0.913±0.006	0.907±0.006	-0.023±0.005	0.101±0.005
49.4	-6.6±0.3	-1.4±0.3	-0.20±0.01	-1.08±0.02	0.936±0.006	0.929±0.006	-0.022±0.005	0.107±0.005
54.5	-6.7±0.3	-1.4±0.3	-0.16±0.01	-1.08±0.02	0.957±0.006	0.950±0.006	-0.022±0.005	0.112±0.005
59.5	-6.8±0.3	-1.3±0.3	-0.12±0.01	-1.07±0.02	0.975±0.006	0.968±0.006	-0.022±0.004	0.115±0.005
64.6	-6.8±0.3	-1.3±0.3	-0.08±0.01	-1.07±0.02	0.993±0.006	0.986±0.006	-0.023±0.004	0.117±0.005
69.7	-6.7±0.3	-1.3±0.2	-0.05±0.01	-1.07±0.02	1.007±0.006	1.000±0.006	-0.023±0.004	0.118±0.006
74.8	-6.7±0.3	-1.3±0.2	-0.03±0.01	-1.07±0.02	1.019±0.006	1.012±0.006	-0.024±0.004	0.119±0.006
79.9	-6.6±0.3	-1.3±0.2	-0.01±0.01	-1.06±0.02	1.027±0.007	1.020±0.006	-0.024±0.004	0.117±0.006
84.9	-6.5±0.3	-1.4±0.2	-0.00±0.01	-1.06±0.02	1.030±0.007	1.023±0.007	-0.024±0.004	0.116±0.006
90.0	-6.4±0.3	-1.4±0.2	0.01±0.01	-1.06±0.02	1.033±0.007	1.026±0.007	-0.025±0.004	0.115±0.006
100.2	-6.2±0.3	-1.5±0.2	0.01±0.01	-1.06±0.02	1.033±0.007	1.027±0.007	-0.027±0.004	0.111±0.006
110.3	-6.0±0.3	-1.6±0.2	0.01±0.01	-1.06±0.02	1.034±0.007	1.028±0.007	-0.029±0.004	0.108±0.006
120.5	-5.8±0.3	-1.8±0.2	0.01±0.01	-1.06±0.02	1.035±0.007	1.029±0.007	-0.032±0.004	0.105±0.006
130.7	-5.8±0.3	-2.0±0.2	0.01±0.01	-1.06±0.02	1.036±0.007	1.030±0.007	-0.036±0.004	0.105±0.006
140.8	-5.7±0.3	-2.2±0.2	0.01±0.01	-1.07±0.02	1.037±0.007	1.031±0.007	-0.039±0.004	0.103±0.006

Table D.16 Five-Hole Probe Data at (x,z)=(305 mm,-57 mm)

y, mm	BETA, deg	ALPHA, deg	CPT	CPS	SPEED	U	V	W
3.7	4.5±0.3	1.2±0.4	-0.49±0.01	-1.06±0.02	0.753±0.007	0.751±0.007	0.015±0.006	-0.059±0.004
4.7	3.5±0.3	0.5±0.4	-0.45±0.01	-1.06±0.02	0.779±0.007	0.777±0.007	0.007±0.006	-0.048±0.004
5.7	2.8±0.3	0.2±0.4	-0.43±0.01	-1.06±0.02	0.793±0.007	0.792±0.007	0.003±0.005	-0.038±0.004
6.7	2.1±0.3	0.1±0.4	-0.42±0.01	-1.06±0.02	0.799±0.007	0.798±0.007	0.001±0.005	-0.029±0.004
7.7	1.5±0.3	-0.0±0.4	-0.42±0.01	-1.06±0.02	0.800±0.007	0.799±0.007	-0.001±0.005	-0.021±0.004
8.7	0.9±0.3	-0.1±0.4	-0.43±0.01	-1.06±0.02	0.799±0.007	0.798±0.007	-0.002±0.005	-0.013±0.004
9.8	0.4±0.3	-0.2±0.4	-0.43±0.01	-1.06±0.02	0.794±0.007	0.794±0.007	-0.003±0.005	-0.006±0.004
10.8	-0.0±0.3	-0.3±0.4	-0.43±0.01	-1.06±0.02	0.795±0.007	0.795±0.007	-0.005±0.005	0.000±0.004
11.8	-0.5±0.3	-0.5±0.4	-0.43±0.01	-1.06±0.02	0.794±0.007	0.794±0.007	-0.007±0.005	0.007±0.004
12.8	-1.0±0.3	-0.6±0.4	-0.43±0.01	-1.06±0.02	0.794±0.007	0.793±0.007	-0.008±0.005	0.013±0.004
13.8	-1.4±0.3	-0.7±0.4	-0.44±0.01	-1.07±0.02	0.795±0.007	0.794±0.007	-0.009±0.005	0.019±0.004
16.4	-2.2±0.3	-0.9±0.4	-0.43±0.01	-1.06±0.02	0.796±0.007	0.795±0.007	-0.013±0.005	0.030±0.004
18.9	-2.9±0.3	-1.1±0.4	-0.41±0.01	-1.06±0.02	0.805±0.007	0.804±0.007	-0.015±0.005	0.041±0.004
21.4	-3.4±0.3	-1.3±0.4	-0.40±0.01	-1.06±0.02	0.813±0.007	0.811±0.007	-0.018±0.005	0.049±0.004
24.0	-4.0±0.3	-1.3±0.4	-0.38±0.01	-1.06±0.02	0.824±0.007	0.822±0.007	-0.019±0.005	0.057±0.005
26.5	-4.3±0.3	-1.4±0.4	-0.37±0.01	-1.06±0.02	0.833±0.007	0.830±0.007	-0.021±0.005	0.063±0.005
29.1	-4.7±0.3	-1.4±0.4	-0.35±0.01	-1.06±0.02	0.843±0.006	0.840±0.006	-0.021±0.005	0.070±0.005
31.6	-5.1±0.3	-1.5±0.3	-0.33±0.01	-1.06±0.02	0.854±0.006	0.850±0.006	-0.022±0.005	0.076±0.005
34.1	-5.4±0.3	-1.5±0.3	-0.31±0.01	-1.06±0.02	0.865±0.006	0.861±0.006	-0.022±0.005	0.081±0.005
36.7	-5.6±0.3	-1.5±0.3	-0.29±0.01	-1.05±0.02	0.875±0.006	0.871±0.006	-0.022±0.005	0.086±0.005
39.2	-5.9±0.3	-1.5±0.3	-0.27±0.01	-1.06±0.02	0.885±0.006	0.880±0.006	-0.023±0.005	0.090±0.005
44.3	-6.2±0.3	-1.5±0.3	-0.23±0.01	-1.05±0.02	0.909±0.006	0.903±0.006	-0.023±0.005	0.098±0.005
49.4	-6.4±0.3	-1.5±0.3	-0.19±0.01	-1.05±0.02	0.929±0.006	0.923±0.006	-0.024±0.005	0.104±0.005
54.5	-6.6±0.3	-1.5±0.3	-0.15±0.01	-1.05±0.02	0.950±0.006	0.943±0.006	-0.024±0.005	0.109±0.005
59.5	-6.7±0.3	-1.5±0.3	-0.11±0.01	-1.04±0.02	0.967±0.006	0.960±0.006	-0.025±0.004	0.113±0.005
64.6	-6.7±0.3	-1.5±0.3	-0.08±0.01	-1.05±0.02	0.985±0.006	0.978±0.006	-0.026±0.004	0.115±0.005
69.7	-6.7±0.3	-1.5±0.3	-0.05±0.01	-1.04±0.02	0.998±0.006	0.991±0.006	-0.026±0.004	0.116±0.006
74.8	-6.6±0.3	-1.6±0.2	-0.02±0.01	-1.04±0.02	1.008±0.006	1.001±0.006	-0.028±0.004	0.116±0.006
79.9	-6.5±0.3	-1.6±0.2	-0.01±0.01	-1.04±0.02	1.014±0.006	1.007±0.006	-0.028±0.004	0.115±0.006
84.9	-6.4±0.3	-1.6±0.2	-0.00±0.01	-1.04±0.02	1.019±0.006	1.013±0.006	-0.028±0.004	0.114±0.006
90.0	-6.3±0.3	-1.6±0.2	0.00±0.01	-1.04±0.02	1.022±0.006	1.015±0.006	-0.029±0.004	0.113±0.006
100.2	-6.1±0.3	-1.7±0.2	0.01±0.01	-1.04±0.02	1.023±0.006	1.017±0.006	-0.030±0.004	0.110±0.006
110.3	-6.0±0.3	-1.8±0.2	0.01±0.01	-1.04±0.02	1.023±0.006	1.017±0.006	-0.031±0.004	0.106±0.006
120.5	-5.9±0.3	-1.9±0.2	0.01±0.01	-1.04±0.02	1.024±0.006	1.019±0.006	-0.033±0.004	0.105±0.006
130.7	-5.9±0.3	-2.0±0.2	0.01±0.01	-1.04±0.02	1.026±0.006	1.020±0.006	-0.036±0.004	0.105±0.006
140.8	-5.8±0.3	-2.2±0.2	0.01±0.01	-1.05±0.02	1.026±0.006	1.020±0.006	-0.040±0.004	0.104±0.006

Table D.17 Five-Hole Probe Data at (x,z)=(305 mm,-51 mm)

y, mm	BETA, deg	ALPHA, deg	CPT	CPS	SPEED	U	V	W
3.7	3.3±0.3	1.1±0.4	-0.45±0.01	-1.05±0.02	0.771±0.007	0.770±0.007	0.015±0.006	-0.045±0.004
4.7	2.4±0.3	0.5±0.4	-0.42±0.01	-1.05±0.02	0.796±0.007	0.795±0.007	0.006±0.005	-0.033±0.004
5.7	1.7±0.3	0.2±0.4	-0.40±0.01	-1.06±0.02	0.808±0.007	0.808±0.007	0.003±0.005	-0.023±0.004
6.7	1.0±0.3	0.0±0.4	-0.40±0.01	-1.05±0.02	0.811±0.007	0.811±0.007	0.000±0.005	-0.014±0.004
7.7	0.4±0.3	-0.1±0.4	-0.40±0.01	-1.05±0.02	0.811±0.007	0.811±0.007	-0.001±0.005	-0.006±0.004
8.7	-0.1±0.3	-0.2±0.4	-0.40±0.01	-1.05±0.02	0.810±0.007	0.810±0.007	-0.003±0.005	0.002±0.004
9.8	-0.6±0.3	-0.3±0.4	-0.40±0.01	-1.06±0.02	0.807±0.007	0.807±0.007	-0.005±0.005	0.008±0.004
10.8	-1.1±0.3	-0.4±0.4	-0.40±0.01	-1.06±0.02	0.807±0.007	0.807±0.007	-0.006±0.005	0.015±0.004
11.8	-1.5±0.3	-0.6±0.4	-0.41±0.01	-1.06±0.02	0.807±0.007	0.807±0.007	-0.008±0.005	0.021±0.004
12.8	-1.9±0.3	-0.7±0.4	-0.41±0.01	-1.06±0.02	0.806±0.007	0.805±0.007	-0.009±0.005	0.026±0.004
13.8	-2.2±0.3	-0.7±0.4	-0.41±0.01	-1.06±0.02	0.807±0.007	0.806±0.007	-0.010±0.005	0.031±0.004
16.4	-3.0±0.3	-0.9±0.4	-0.40±0.01	-1.06±0.02	0.808±0.007	0.807±0.007	-0.013±0.005	0.043±0.004
18.9	-3.7±0.3	-1.1±0.4	-0.39±0.01	-1.06±0.02	0.814±0.007	0.812±0.007	-0.016±0.005	0.052±0.005
21.4	-4.2±0.3	-1.2±0.4	-0.38±0.01	-1.06±0.02	0.823±0.007	0.821±0.007	-0.017±0.005	0.060±0.005
24.0	-4.7±0.3	-1.3±0.4	-0.37±0.01	-1.06±0.02	0.831±0.007	0.828±0.007	-0.019±0.005	0.068±0.005
26.5	-5.1±0.3	-1.4±0.4	-0.35±0.01	-1.06±0.02	0.839±0.006	0.836±0.006	-0.020±0.005	0.074±0.005
29.1	-5.4±0.3	-1.5±0.3	-0.34±0.01	-1.06±0.02	0.850±0.006	0.846±0.006	-0.022±0.005	0.080±0.005
31.6	-5.8±0.3	-1.5±0.3	-0.31±0.01	-1.05±0.02	0.860±0.006	0.856±0.006	-0.023±0.005	0.086±0.005
34.1	-6.0±0.3	-1.6±0.3	-0.30±0.01	-1.06±0.02	0.871±0.006	0.866±0.006	-0.024±0.005	0.092±0.005
36.7	-6.3±0.3	-1.6±0.3	-0.27±0.01	-1.05±0.02	0.882±0.006	0.876±0.006	-0.024±0.005	0.097±0.005
39.2	-6.5±0.3	-1.6±0.3	-0.26±0.01	-1.05±0.02	0.892±0.006	0.886±0.006	-0.025±0.005	0.101±0.005
44.3	-6.9±0.3	-1.7±0.3	-0.22±0.01	-1.05±0.02	0.913±0.006	0.906±0.006	-0.026±0.005	0.109±0.005
49.4	-7.1±0.3	-1.7±0.3	-0.17±0.01	-1.05±0.02	0.934±0.006	0.926±0.006	-0.027±0.005	0.115±0.005
54.5	-7.2±0.3	-1.7±0.3	-0.13±0.01	-1.05±0.02	0.955±0.006	0.946±0.006	-0.029±0.005	0.120±0.005
59.5	-7.3±0.3	-1.8±0.3	-0.09±0.01	-1.04±0.02	0.971±0.006	0.963±0.006	-0.029±0.004	0.123±0.005
64.6	-7.3±0.3	-1.8±0.3	-0.06±0.01	-1.04±0.02	0.987±0.006	0.978±0.006	-0.030±0.004	0.125±0.005
69.7	-7.2±0.3	-1.8±0.3	-0.04±0.01	-1.04±0.02	0.999±0.006	0.991±0.006	-0.031±0.004	0.126±0.006
74.8	-7.2±0.3	-1.8±0.2	-0.02±0.01	-1.04±0.02	1.008±0.006	1.000±0.006	-0.032±0.004	0.126±0.006
79.9	-7.1±0.3	-1.8±0.2	-0.00±0.01	-1.03±0.02	1.013±0.006	1.005±0.006	-0.032±0.004	0.125±0.006
84.9	-6.9±0.3	-1.8±0.2	0.00±0.01	-1.03±0.02	1.017±0.006	1.009±0.006	-0.032±0.004	0.123±0.006
90.0	-6.8±0.3	-1.8±0.2	0.01±0.01	-1.03±0.02	1.018±0.006	1.010±0.006	-0.032±0.004	0.121±0.006
100.2	-6.6±0.3	-1.9±0.2	0.01±0.01	-1.03±0.02	1.018±0.006	1.011±0.006	-0.033±0.004	0.117±0.006
110.3	-6.5±0.3	-1.9±0.2	0.01±0.01	-1.03±0.02	1.018±0.006	1.011±0.006	-0.034±0.004	0.115±0.006
120.5	-6.4±0.3	-2.0±0.2	0.01±0.01	-1.03±0.02	1.019±0.006	1.012±0.006	-0.035±0.004	0.113±0.006
130.7	-6.4±0.3	-2.1±0.2	0.01±0.01	-1.03±0.02	1.021±0.006	1.014±0.006	-0.037±0.004	0.114±0.006
140.8	-6.4±0.3	-2.3±0.2	0.01±0.01	-1.04±0.02	1.022±0.006	1.015±0.006	-0.040±0.004	0.115±0.006

Table D.18 Five-Hole Probe Data at (x,z)=(305 mm,-44 mm)

y, mm	BETA, deg	ALPHA, deg	CPT	CPS	SPEED	U	V	W
3.7	3.3±0.3	0.9±0.4	-0.42±0.01	-1.02±0.02	0.778±0.007	0.777±0.007	0.013±0.006	-0.044±0.004
4.7	2.2±0.3	0.3±0.4	-0.38±0.01	-1.03±0.02	0.802±0.007	0.802±0.007	0.004±0.005	-0.031±0.004
5.7	1.5±0.3	0.0±0.4	-0.37±0.01	-1.03±0.02	0.813±0.007	0.812±0.007	0.000±0.005	-0.022±0.004
6.7	0.9±0.3	-0.2±0.4	-0.37±0.01	-1.03±0.02	0.814±0.007	0.814±0.007	-0.002±0.005	-0.013±0.004
7.7	0.4±0.3	-0.3±0.4	-0.37±0.01	-1.03±0.02	0.816±0.007	0.816±0.007	-0.004±0.005	-0.005±0.005
8.7	-0.2±0.3	-0.4±0.4	-0.37±0.01	-1.03±0.02	0.815±0.007	0.814±0.007	-0.006±0.005	0.002±0.004
9.8	-0.6±0.3	-0.5±0.4	-0.38±0.01	-1.04±0.02	0.813±0.007	0.813±0.007	-0.008±0.005	0.008±0.004
10.8	-1.0±0.3	-0.6±0.4	-0.38±0.01	-1.04±0.02	0.812±0.007	0.812±0.007	-0.009±0.005	0.015±0.004
11.8	-1.5±0.3	-0.7±0.4	-0.38±0.01	-1.04±0.02	0.811±0.007	0.811±0.007	-0.010±0.005	0.021±0.004
12.8	-1.8±0.3	-0.8±0.4	-0.38±0.01	-1.03±0.02	0.809±0.007	0.808±0.007	-0.012±0.005	0.026±0.004
13.8	-2.1±0.3	-0.9±0.4	-0.38±0.01	-1.03±0.02	0.810±0.007	0.809±0.007	-0.013±0.005	0.030±0.004
16.4	-2.9±0.3	-1.1±0.4	-0.37±0.01	-1.03±0.02	0.814±0.007	0.812±0.007	-0.015±0.005	0.041±0.004
18.9	-3.5±0.3	-1.2±0.4	-0.36±0.01	-1.03±0.02	0.817±0.007	0.815±0.007	-0.017±0.005	0.050±0.005
21.4	-4.0±0.3	-1.3±0.4	-0.35±0.01	-1.03±0.02	0.824±0.007	0.822±0.007	-0.019±0.005	0.057±0.005
24.0	-4.4±0.3	-1.5±0.4	-0.34±0.01	-1.03±0.02	0.832±0.007	0.829±0.007	-0.021±0.005	0.065±0.005
26.5	-4.9±0.3	-1.5±0.4	-0.32±0.01	-1.03±0.02	0.840±0.007	0.837±0.007	-0.023±0.005	0.071±0.005
29.1	-5.2±0.3	-1.6±0.3	-0.31±0.01	-1.03±0.02	0.852±0.006	0.848±0.006	-0.024±0.005	0.077±0.005
31.6	-5.5±0.3	-1.7±0.3	-0.29±0.01	-1.02±0.02	0.859±0.006	0.854±0.006	-0.025±0.005	0.083±0.005
34.1	-5.8±0.3	-1.7±0.3	-0.27±0.01	-1.02±0.02	0.870±0.006	0.865±0.006	-0.026±0.005	0.088±0.005
36.7	-6.1±0.3	-1.8±0.3	-0.25±0.01	-1.02±0.02	0.878±0.006	0.873±0.006	-0.028±0.005	0.093±0.005
39.2	-6.2±0.3	-1.8±0.3	-0.23±0.01	-1.03±0.02	0.891±0.006	0.886±0.006	-0.028±0.005	0.097±0.005
44.3	-6.6±0.3	-1.9±0.3	-0.19±0.01	-1.02±0.02	0.912±0.006	0.906±0.006	-0.030±0.005	0.104±0.005
49.4	-6.8±0.3	-2.0±0.3	-0.15±0.01	-1.02±0.02	0.932±0.006	0.924±0.006	-0.032±0.005	0.110±0.005
54.5	-7.0±0.3	-2.0±0.3	-0.11±0.01	-1.02±0.02	0.949±0.006	0.942±0.006	-0.034±0.005	0.115±0.005
59.5	-7.0±0.3	-2.1±0.3	-0.08±0.01	-1.01±0.02	0.965±0.006	0.958±0.006	-0.035±0.005	0.118±0.005
64.6	-7.0±0.3	-2.1±0.3	-0.05±0.01	-1.01±0.02	0.980±0.006	0.971±0.006	-0.036±0.004	0.120±0.005
69.7	-7.0±0.3	-2.1±0.3	-0.03±0.01	-1.01±0.02	0.990±0.006	0.982±0.006	-0.037±0.004	0.120±0.005
74.8	-6.9±0.3	-2.1±0.3	-0.01±0.01	-1.01±0.02	0.997±0.006	0.990±0.006	-0.037±0.004	0.119±0.006
79.9	-6.8±0.3	-2.1±0.3	-0.00±0.01	-1.01±0.02	1.003±0.006	0.995±0.006	-0.037±0.004	0.118±0.006
84.9	-6.6±0.3	-2.1±0.3	0.00±0.01	-1.00±0.02	1.004±0.006	0.996±0.006	-0.037±0.004	0.116±0.006
90.0	-6.5±0.3	-2.1±0.2	0.01±0.01	-1.00±0.02	1.005±0.006	0.998±0.006	-0.037±0.004	0.114±0.006
100.2	-6.3±0.3	-2.0±0.2	0.01±0.01	-1.00±0.02	1.005±0.006	0.999±0.006	-0.036±0.004	0.111±0.006
110.3	-6.1±0.3	-2.0±0.2	0.01±0.01	-1.00±0.02	1.006±0.006	0.999±0.006	-0.035±0.004	0.107±0.006
120.5	-6.1±0.3	-2.1±0.2	0.01±0.01	-1.01±0.02	1.007±0.006	1.001±0.006	-0.036±0.004	0.107±0.006
130.7	-6.2±0.3	-2.2±0.2	0.01±0.01	-1.01±0.02	1.008±0.006	1.001±0.006	-0.038±0.004	0.109±0.006
140.8	-6.3±0.3	-2.3±0.2	0.01±0.01	-1.01±0.02	1.010±0.006	1.003±0.006	-0.041±0.004	0.110±0.006

Table D.19 Five-Hole Probe Data at (x,z)=(305 mm,-38 mm)

y, mm	BETA, deg	ALPHA, deg	CPT	CPS	SPEED	U	V	W
3.7	2.3±0.3	0.8±0.4	-0.41±0.01	-1.01±0.02	0.774±0.007	0.773±0.007	0.011±0.006	-0.032±0.004
4.7	1.4±0.3	0.1±0.4	-0.38±0.01	-1.01±0.02	0.796±0.007	0.796±0.007	0.001±0.005	-0.020±0.004
5.7	0.7±0.3	-0.3±0.4	-0.36±0.01	-1.01±0.02	0.806±0.007	0.806±0.007	-0.004±0.005	-0.010±0.004
6.7	0.1±0.3	-0.5±0.4	-0.35±0.01	-1.01±0.02	0.814±0.007	0.814±0.007	-0.007±0.005	-0.002±0.004
7.7	-0.4±0.3	-0.7±0.4	-0.35±0.01	-1.01±0.02	0.818±0.007	0.818±0.007	-0.009±0.005	0.005±0.005
8.7	-0.8±0.3	-0.8±0.4	-0.35±0.01	-1.02±0.02	0.818±0.007	0.818±0.007	-0.012±0.005	0.011±0.005
9.8	-1.2±0.3	-0.9±0.4	-0.35±0.01	-1.02±0.02	0.819±0.007	0.819±0.007	-0.013±0.005	0.017±0.005
10.8	-1.5±0.3	-1.0±0.4	-0.34±0.01	-1.01±0.02	0.819±0.007	0.819±0.007	-0.015±0.005	0.022±0.005
11.8	-1.9±0.3	-1.1±0.4	-0.34±0.01	-1.02±0.02	0.820±0.007	0.819±0.007	-0.016±0.005	0.027±0.005
12.8	-2.2±0.3	-1.2±0.4	-0.34±0.01	-1.02±0.02	0.819±0.007	0.818±0.007	-0.017±0.005	0.032±0.005
13.8	-2.5±0.3	-1.3±0.4	-0.35±0.01	-1.02±0.02	0.820±0.007	0.819±0.007	-0.018±0.005	0.036±0.005
16.4	-3.2±0.3	-1.4±0.4	-0.34±0.01	-1.02±0.02	0.824±0.007	0.822±0.007	-0.020±0.005	0.046±0.005
18.9	-3.8±0.3	-1.5±0.4	-0.33±0.01	-1.02±0.02	0.827±0.007	0.825±0.007	-0.022±0.005	0.055±0.005
21.4	-4.3±0.3	-1.6±0.4	-0.32±0.01	-1.02±0.02	0.833±0.006	0.831±0.007	-0.023±0.005	0.063±0.005
24.0	-4.9±0.3	-1.7±0.4	-0.31±0.01	-1.02±0.02	0.841±0.006	0.838±0.006	-0.025±0.005	0.071±0.005
26.5	-5.2±0.3	-1.8±0.3	-0.30±0.01	-1.01±0.02	0.847±0.006	0.844±0.006	-0.026±0.005	0.077±0.005
29.1	-5.6±0.3	-1.9±0.3	-0.28±0.01	-1.01±0.02	0.855±0.006	0.851±0.006	-0.029±0.005	0.083±0.005
31.6	-5.9±0.3	-2.0±0.3	-0.26±0.01	-1.01±0.02	0.864±0.006	0.859±0.006	-0.030±0.005	0.089±0.005
34.1	-6.1±0.3	-2.1±0.3	-0.25±0.01	-1.01±0.02	0.875±0.006	0.869±0.006	-0.031±0.005	0.093±0.005
36.7	-6.4±0.3	-2.2±0.3	-0.23±0.01	-1.01±0.02	0.884±0.006	0.878±0.006	-0.033±0.005	0.098±0.005
39.2	-6.6±0.3	-2.2±0.3	-0.21±0.01	-1.01±0.02	0.894±0.006	0.887±0.006	-0.034±0.005	0.102±0.005
44.3	-6.9±0.3	-2.3±0.3	-0.17±0.01	-1.00±0.02	0.911±0.006	0.904±0.006	-0.036±0.005	0.109±0.005
49.4	-7.1±0.3	-2.4±0.3	-0.14±0.01	-1.00±0.02	0.931±0.006	0.923±0.006	-0.038±0.005	0.115±0.005
54.5	-7.2±0.3	-2.4±0.3	-0.10±0.01	-1.00±0.02	0.947±0.006	0.939±0.006	-0.040±0.005	0.119±0.005
59.5	-7.3±0.3	-2.5±0.3	-0.07±0.01	-1.00±0.02	0.963±0.006	0.955±0.006	-0.041±0.005	0.122±0.005
64.6	-7.3±0.3	-2.5±0.3	-0.04±0.01	-0.99±0.02	0.974±0.006	0.966±0.006	-0.042±0.004	0.123±0.005
69.7	-7.2±0.3	-2.5±0.3	-0.02±0.01	-0.99±0.02	0.985±0.006	0.976±0.006	-0.043±0.004	0.123±0.005
74.8	-7.1±0.3	-2.5±0.3	-0.01±0.01	-0.99±0.02	0.991±0.006	0.982±0.006	-0.043±0.004	0.122±0.005
79.9	-6.9±0.3	-2.5±0.3	0.00±0.01	-0.99±0.02	0.994±0.006	0.986±0.006	-0.043±0.004	0.120±0.005
84.9	-6.8±0.3	-2.4±0.3	0.01±0.01	-0.98±0.02	0.995±0.006	0.987±0.006	-0.042±0.004	0.118±0.005
90.0	-6.7±0.3	-2.3±0.3	0.01±0.01	-0.98±0.02	0.996±0.006	0.988±0.006	-0.040±0.004	0.115±0.006
100.2	-6.5±0.3	-2.2±0.3	0.01±0.01	-0.98±0.02	0.996±0.006	0.989±0.006	-0.037±0.004	0.112±0.006
110.3	-6.4±0.3	-2.1±0.3	0.01±0.01	-0.99±0.02	0.997±0.006	0.990±0.006	-0.036±0.004	0.110±0.006
120.5	-6.4±0.3	-2.1±0.3	0.01±0.01	-0.99±0.02	0.998±0.006	0.991±0.006	-0.036±0.004	0.111±0.006
130.7	-6.5±0.3	-2.1±0.3	0.01±0.01	-0.99±0.02	0.999±0.006	0.992±0.006	-0.037±0.004	0.114±0.006
140.8	-6.7±0.3	-2.3±0.3	0.01±0.01	-1.00±0.02	1.001±0.006	0.994±0.006	-0.039±0.004	0.117±0.006

Table D.20 Five-Hole Probe Data at (x,z)=(305 mm,-32 mm)

y, mm	BETA, deg	ALPHA, deg	CPT	CPS	SPEED	U	V	W
3.7	0.8±0.3	0.6±0.5	-0.43±0.01	-0.98±0.02	0.742±0.007	0.742±0.007	0.008±0.006	-0.011±0.004
4.7	-0.0±0.3	-0.3±0.4	-0.40±0.01	-0.98±0.02	0.762±0.007	0.762±0.007	-0.004±0.006	0.000±0.004
5.7	-0.6±0.3	-0.7±0.4	-0.38±0.01	-0.98±0.02	0.775±0.007	0.775±0.007	-0.010±0.006	0.008±0.004
6.7	-1.0±0.3	-1.1±0.4	-0.37±0.01	-0.98±0.02	0.784±0.007	0.783±0.007	-0.015±0.006	0.014±0.004
7.7	-1.4±0.3	-1.3±0.4	-0.36±0.01	-0.99±0.02	0.793±0.007	0.792±0.007	-0.018±0.005	0.019±0.004
8.7	-1.7±0.3	-1.5±0.4	-0.35±0.01	-0.99±0.02	0.801±0.007	0.800±0.007	-0.021±0.005	0.024±0.004
9.8	-2.0±0.3	-1.6±0.4	-0.34±0.01	-0.99±0.02	0.805±0.007	0.805±0.007	-0.023±0.005	0.029±0.004
10.8	-2.3±0.3	-1.8±0.4	-0.33±0.01	-0.99±0.02	0.810±0.007	0.809±0.007	-0.025±0.005	0.032±0.004
11.8	-2.6±0.3	-1.8±0.4	-0.32±0.01	-0.98±0.02	0.815±0.007	0.814±0.007	-0.026±0.005	0.037±0.005
12.8	-2.8±0.3	-1.9±0.4	-0.31±0.01	-0.98±0.02	0.819±0.007	0.818±0.007	-0.028±0.005	0.040±0.005
13.8	-3.1±0.3	-2.0±0.4	-0.31±0.01	-0.99±0.02	0.823±0.007	0.822±0.007	-0.029±0.005	0.045±0.005
16.4	-3.7±0.3	-2.0±0.4	-0.30±0.01	-0.99±0.02	0.832±0.006	0.829±0.007	-0.030±0.005	0.053±0.005
18.9	-4.3±0.3	-2.1±0.4	-0.29±0.01	-0.98±0.02	0.836±0.006	0.833±0.007	-0.031±0.005	0.063±0.005
21.4	-4.8±0.3	-2.2±0.4	-0.28±0.01	-0.99±0.02	0.841±0.006	0.837±0.006	-0.032±0.005	0.071±0.005
24.0	-5.3±0.3	-2.3±0.3	-0.27±0.01	-0.99±0.02	0.849±0.006	0.845±0.006	-0.033±0.005	0.078±0.005
26.5	-5.7±0.3	-2.4±0.3	-0.26±0.01	-0.99±0.02	0.854±0.006	0.849±0.006	-0.035±0.005	0.085±0.005
29.1	-6.1±0.3	-2.5±0.3	-0.24±0.01	-0.98±0.02	0.861±0.006	0.855±0.006	-0.037±0.005	0.091±0.005
31.6	-6.3±0.3	-2.6±0.3	-0.23±0.01	-0.98±0.02	0.869±0.006	0.863±0.006	-0.039±0.005	0.095±0.005
34.1	-6.6±0.3	-2.6±0.3	-0.21±0.01	-0.98±0.02	0.878±0.006	0.871±0.006	-0.040±0.005	0.101±0.005
36.7	-6.8±0.3	-2.7±0.3	-0.20±0.01	-0.98±0.02	0.886±0.006	0.878±0.006	-0.042±0.005	0.105±0.005
39.2	-7.0±0.3	-2.8±0.3	-0.18±0.01	-0.98±0.02	0.894±0.006	0.886±0.006	-0.044±0.005	0.108±0.005
44.3	-7.3±0.3	-2.9±0.3	-0.14±0.01	-0.98±0.02	0.912±0.006	0.903±0.006	-0.045±0.005	0.115±0.005
49.4	-7.4±0.3	-3.0±0.3	-0.11±0.01	-0.97±0.02	0.928±0.006	0.919±0.006	-0.048±0.005	0.120±0.005
54.5	-7.5±0.3	-3.0±0.3	-0.08±0.01	-0.97±0.02	0.942±0.006	0.932±0.006	-0.049±0.005	0.123±0.005
59.5	-7.6±0.3	-3.0±0.3	-0.05±0.01	-0.96±0.02	0.954±0.006	0.945±0.006	-0.050±0.005	0.126±0.005
64.6	-7.6±0.3	-3.0±0.3	-0.03±0.01	-0.96±0.02	0.964±0.006	0.955±0.006	-0.051±0.005	0.127±0.005
69.7	-7.5±0.3	-3.0±0.3	-0.01±0.01	-0.96±0.02	0.972±0.006	0.963±0.006	-0.050±0.004	0.126±0.005
74.8	-7.3±0.3	-2.9±0.3	-0.00±0.01	-0.95±0.02	0.976±0.006	0.967±0.006	-0.049±0.004	0.124±0.005
79.9	-7.1±0.3	-2.7±0.3	0.00±0.01	-0.95±0.02	0.977±0.006	0.969±0.006	-0.046±0.004	0.121±0.005
84.9	-7.0±0.3	-2.6±0.3	0.00±0.01	-0.95±0.02	0.978±0.006	0.970±0.006	-0.044±0.004	0.118±0.005
90.0	-6.9±0.3	-2.5±0.3	0.00±0.01	-0.95±0.02	0.977±0.006	0.969±0.006	-0.042±0.004	0.117±0.005
100.2	-6.8±0.3	-2.3±0.3	-0.01±0.01	-0.95±0.02	0.974±0.006	0.967±0.006	-0.038±0.004	0.116±0.005
110.3	-6.9±0.3	-2.1±0.3	-0.02±0.01	-0.96±0.02	0.970±0.006	0.962±0.006	-0.036±0.004	0.116±0.005
120.5	-6.9±0.3	-2.1±0.3	-0.02±0.01	-0.96±0.02	0.967±0.006	0.960±0.006	-0.035±0.004	0.117±0.005
130.7	-7.1±0.3	-2.0±0.3	-0.03±0.01	-0.96±0.02	0.968±0.006	0.960±0.006	-0.034±0.004	0.119±0.005
140.8	-7.3±0.3	-2.1±0.3	-0.03±0.01	-0.97±0.02	0.971±0.006	0.962±0.006	-0.036±0.004	0.124±0.005

Table D.21 Five-Hole Probe Data at (x,z)=(305 mm,-25 mm)

y, mm	BETA, deg	ALPHA, deg	CPT	CPS	SPEED	U	V	W
3.7	-0.5±0.3	0.1±0.5	-0.49±0.01	-0.96±0.02	0.681±0.007	0.681±0.007	0.001±0.006	0.006±0.004
4.7	-1.1±0.3	-0.9±0.5	-0.48±0.01	-0.97±0.02	0.700±0.007	0.700±0.007	-0.011±0.006	0.013±0.004
5.7	-1.4±0.3	-1.5±0.5	-0.46±0.01	-0.96±0.02	0.707±0.007	0.707±0.007	-0.018±0.006	0.017±0.004
6.7	-1.6±0.3	-1.9±0.5	-0.45±0.01	-0.97±0.02	0.719±0.007	0.719±0.007	-0.023±0.006	0.021±0.004
7.7	-1.9±0.3	-2.3±0.5	-0.44±0.01	-0.97±0.02	0.724±0.007	0.723±0.007	-0.028±0.006	0.024±0.004
8.7	-2.1±0.3	-2.5±0.5	-0.43±0.01	-0.97±0.02	0.734±0.007	0.733±0.007	-0.032±0.006	0.027±0.004
9.8	-2.4±0.3	-2.6±0.4	-0.41±0.01	-0.97±0.02	0.747±0.007	0.745±0.007	-0.034±0.006	0.031±0.004
10.8	-2.6±0.3	-2.8±0.4	-0.40±0.01	-0.97±0.02	0.758±0.007	0.756±0.007	-0.037±0.006	0.034±0.004
11.8	-2.9±0.3	-2.9±0.4	-0.37±0.01	-0.97±0.02	0.769±0.007	0.767±0.007	-0.038±0.006	0.038±0.004
12.8	-3.1±0.3	-2.9±0.4	-0.36±0.01	-0.97±0.02	0.782±0.007	0.780±0.007	-0.040±0.006	0.042±0.004
13.8	-3.3±0.3	-3.0±0.4	-0.34±0.01	-0.97±0.02	0.793±0.007	0.790±0.007	-0.041±0.005	0.046±0.004
16.4	-3.9±0.3	-3.0±0.4	-0.30±0.01	-0.97±0.02	0.818±0.007	0.815±0.007	-0.043±0.005	0.056±0.005
18.9	-4.5±0.3	-3.0±0.4	-0.27±0.01	-0.97±0.02	0.838±0.006	0.834±0.007	-0.044±0.005	0.065±0.005
21.4	-4.9±0.3	-3.1±0.3	-0.25±0.01	-0.97±0.02	0.850±0.006	0.846±0.006	-0.046±0.005	0.073±0.005
24.0	-5.4±0.3	-3.2±0.3	-0.23±0.01	-0.96±0.02	0.859±0.006	0.853±0.006	-0.047±0.005	0.080±0.005
26.5	-5.7±0.3	-3.3±0.3	-0.21±0.01	-0.96±0.02	0.866±0.006	0.861±0.006	-0.049±0.005	0.086±0.005
29.1	-6.0±0.3	-3.3±0.3	-0.20±0.01	-0.96±0.02	0.872±0.006	0.865±0.006	-0.050±0.005	0.092±0.005
31.6	-6.3±0.3	-3.4±0.3	-0.19±0.01	-0.96±0.02	0.880±0.006	0.873±0.006	-0.052±0.005	0.096±0.005
34.1	-6.5±0.3	-3.5±0.3	-0.18±0.01	-0.96±0.02	0.885±0.006	0.878±0.006	-0.054±0.005	0.100±0.005
36.7	-6.7±0.3	-3.6±0.3	-0.16±0.01	-0.96±0.02	0.893±0.006	0.885±0.006	-0.055±0.005	0.104±0.005
39.2	-6.8±0.3	-3.6±0.3	-0.15±0.01	-0.96±0.02	0.899±0.006	0.891±0.006	-0.057±0.005	0.107±0.005
44.3	-7.1±0.3	-3.7±0.3	-0.12±0.01	-0.95±0.02	0.914±0.006	0.905±0.006	-0.059±0.005	0.112±0.005
49.4	-7.3±0.3	-3.7±0.3	-0.09±0.01	-0.95±0.02	0.928±0.006	0.918±0.006	-0.060±0.005	0.117±0.005
54.5	-7.4±0.3	-3.7±0.3	-0.06±0.01	-0.94±0.02	0.940±0.006	0.931±0.006	-0.060±0.005	0.120±0.005
59.5	-7.4±0.3	-3.7±0.3	-0.04±0.01	-0.94±0.02	0.949±0.006	0.940±0.006	-0.060±0.005	0.122±0.005
64.6	-7.4±0.3	-3.5±0.3	-0.02±0.01	-0.94±0.02	0.957±0.006	0.948±0.006	-0.059±0.005	0.123±0.005
69.7	-7.3±0.3	-3.4±0.3	-0.01±0.01	-0.94±0.02	0.961±0.006	0.952±0.006	-0.057±0.005	0.122±0.005
74.8	-7.2±0.3	-3.2±0.3	-0.02±0.01	-0.94±0.02	0.959±0.006	0.950±0.006	-0.054±0.005	0.119±0.005
79.9	-7.0±0.3	-3.1±0.3	-0.03±0.01	-0.94±0.02	0.951±0.006	0.942±0.006	-0.051±0.005	0.115±0.005
84.9	-6.9±0.3	-2.9±0.3	-0.06±0.01	-0.94±0.02	0.937±0.006	0.929±0.006	-0.047±0.005	0.112±0.005
90.0	-6.9±0.3	-2.7±0.3	-0.08±0.01	-0.94±0.02	0.925±0.006	0.917±0.006	-0.044±0.005	0.111±0.005
100.2	-6.9±0.3	-2.5±0.3	-0.12±0.01	-0.94±0.02	0.909±0.006	0.902±0.006	-0.040±0.005	0.109±0.005
110.3	-7.0±0.3	-2.4±0.3	-0.15±0.01	-0.95±0.02	0.894±0.006	0.886±0.006	-0.037±0.005	0.108±0.005
120.5	-7.0±0.3	-2.3±0.3	-0.17±0.01	-0.95±0.02	0.886±0.006	0.879±0.006	-0.036±0.005	0.109±0.005
130.7	-7.2±0.3	-2.3±0.3	-0.17±0.01	-0.95±0.02	0.885±0.006	0.877±0.006	-0.035±0.005	0.111±0.005
140.8	-7.5±0.3	-2.3±0.3	-0.16±0.01	-0.95±0.02	0.892±0.006	0.884±0.006	-0.036±0.005	0.117±0.005

Table D.22 Five-Hole Probe Data at (x,z)=(305 mm,-19 mm)

y, mm	BETA, deg	ALPHA, deg	CPT	CPS	SPEED	U	V	W
3.7	-2.6±0.3	-0.3±0.7	-0.58±0.01	-0.94±0.02	0.605±0.008	0.605±0.008	-0.003±0.007	0.027±0.003
4.7	-2.7±0.3	-1.5±0.7	-0.57±0.01	-0.95±0.02	0.617±0.007	0.616±0.007	-0.016±0.007	0.029±0.003
5.7	-2.6±0.3	-2.2±0.6	-0.56±0.01	-0.95±0.02	0.622±0.007	0.621±0.007	-0.024±0.007	0.028±0.003
6.7	-2.5±0.3	-2.9±0.6	-0.56±0.01	-0.95±0.02	0.624±0.007	0.623±0.007	-0.031±0.007	0.027±0.003
7.7	-2.4±0.3	-3.4±0.6	-0.56±0.01	-0.95±0.02	0.627±0.007	0.625±0.007	-0.037±0.007	0.026±0.003
8.7	-2.4±0.3	-3.8±0.6	-0.55±0.01	-0.96±0.02	0.635±0.007	0.633±0.007	-0.042±0.007	0.027±0.004
9.8	-2.5±0.3	-4.1±0.6	-0.54±0.01	-0.95±0.02	0.645±0.007	0.643±0.007	-0.047±0.007	0.028±0.004
10.8	-2.8±0.3	-4.4±0.6	-0.52±0.01	-0.95±0.02	0.655±0.007	0.652±0.007	-0.050±0.007	0.031±0.004
11.8	-3.0±0.3	-4.5±0.6	-0.50±0.01	-0.95±0.02	0.672±0.007	0.669±0.007	-0.052±0.006	0.036±0.004
12.8	-3.4±0.3	-4.6±0.5	-0.48±0.01	-0.95±0.02	0.689±0.007	0.685±0.007	-0.055±0.006	0.040±0.004
13.8	-3.7±0.3	-4.6±0.5	-0.46±0.01	-0.95±0.02	0.705±0.007	0.702±0.007	-0.057±0.006	0.046±0.004
16.4	-4.5±0.3	-4.6±0.4	-0.39±0.01	-0.95±0.02	0.752±0.007	0.748±0.007	-0.060±0.006	0.059±0.004
18.9	-5.2±0.3	-4.5±0.4	-0.32±0.01	-0.95±0.02	0.794±0.007	0.789±0.007	-0.062±0.005	0.071±0.004
21.4	-5.6±0.3	-4.5±0.4	-0.26±0.01	-0.94±0.02	0.825±0.007	0.819±0.007	-0.065±0.005	0.081±0.005
24.0	-6.0±0.3	-4.6±0.4	-0.22±0.01	-0.94±0.02	0.848±0.006	0.841±0.007	-0.067±0.005	0.089±0.005
26.5	-6.3±0.3	-4.6±0.3	-0.19±0.01	-0.94±0.02	0.866±0.006	0.858±0.007	-0.069±0.005	0.094±0.005
29.1	-6.5±0.3	-4.7±0.3	-0.17±0.01	-0.94±0.02	0.874±0.006	0.866±0.007	-0.071±0.005	0.099±0.005
31.6	-6.6±0.3	-4.8±0.3	-0.16±0.01	-0.94±0.02	0.883±0.006	0.874±0.006	-0.073±0.005	0.102±0.005
34.1	-6.8±0.3	-4.8±0.3	-0.14±0.01	-0.93±0.02	0.889±0.006	0.880±0.006	-0.074±0.005	0.105±0.005
36.7	-6.9±0.3	-4.8±0.3	-0.13±0.01	-0.93±0.02	0.896±0.006	0.886±0.006	-0.075±0.005	0.108±0.005
39.2	-7.1±0.3	-4.8±0.3	-0.11±0.01	-0.92±0.02	0.900±0.006	0.890±0.006	-0.075±0.005	0.110±0.005
44.3	-7.3±0.3	-4.8±0.3	-0.09±0.01	-0.92±0.02	0.913±0.006	0.902±0.006	-0.075±0.005	0.115±0.005
49.4	-7.4±0.3	-4.7±0.3	-0.07±0.01	-0.92±0.02	0.921±0.006	0.911±0.006	-0.074±0.005	0.119±0.005
54.5	-7.5±0.3	-4.5±0.3	-0.05±0.01	-0.91±0.02	0.927±0.006	0.916±0.006	-0.072±0.005	0.121±0.005
59.5	-7.6±0.3	-4.3±0.3	-0.05±0.01	-0.91±0.02	0.929±0.006	0.918±0.006	-0.069±0.005	0.123±0.005
64.6	-7.7±0.3	-4.1±0.3	-0.07±0.01	-0.91±0.02	0.921±0.006	0.910±0.006	-0.066±0.005	0.123±0.005
69.7	-7.6±0.3	-3.9±0.3	-0.10±0.01	-0.92±0.02	0.904±0.006	0.894±0.006	-0.062±0.005	0.120±0.005
74.8	-7.5±0.3	-3.8±0.3	-0.15±0.01	-0.92±0.02	0.875±0.006	0.865±0.006	-0.057±0.005	0.114±0.005
79.9	-7.3±0.3	-3.6±0.4	-0.22±0.01	-0.91±0.02	0.833±0.007	0.825±0.007	-0.052±0.005	0.106±0.005
84.9	-7.1±0.3	-3.3±0.4	-0.28±0.01	-0.92±0.02	0.804±0.007	0.796±0.007	-0.046±0.005	0.100±0.004
90.0	-7.1±0.3	-3.1±0.4	-0.32±0.01	-0.93±0.02	0.781±0.007	0.774±0.007	-0.043±0.006	0.096±0.004
100.2	-7.3±0.3	-3.0±0.4	-0.35±0.01	-0.93±0.02	0.759±0.007	0.752±0.007	-0.039±0.006	0.096±0.004
110.3	-7.3±0.3	-3.0±0.5	-0.38±0.01	-0.93±0.02	0.744±0.007	0.737±0.007	-0.039±0.006	0.094±0.004
120.5	-7.3±0.3	-3.2±0.5	-0.39±0.01	-0.93±0.02	0.738±0.007	0.731±0.007	-0.041±0.006	0.093±0.004
130.7	-7.3±0.3	-3.4±0.5	-0.38±0.01	-0.94±0.02	0.746±0.007	0.738±0.007	-0.043±0.006	0.094±0.004
140.8	-7.6±0.3	-3.6±0.4	-0.35±0.01	-0.94±0.02	0.770±0.007	0.762±0.007	-0.048±0.006	0.101±0.004

Table D.23 Five-Hole Probe Data at (x,z)=(127 mm,-203 mm)

y, mm	BETA, deg	ALPHA, deg	CPT	CPS	SPEED	U	V	W
3.7	-0.2±0.3	0.9±0.4	-0.70±0.01	-1.31±0.02	0.781±0.007	0.781±0.007	0.012±0.006	0.003±0.004
4.7	0.1±0.3	0.3±0.4	-0.67±0.01	-1.32±0.02	0.807±0.007	0.807±0.007	0.005±0.005	-0.001±0.004
5.7	0.3±0.3	0.1±0.4	-0.64±0.01	-1.32±0.02	0.825±0.007	0.825±0.007	0.001±0.005	-0.004±0.005
6.7	0.3±0.3	-0.0±0.4	-0.62±0.01	-1.33±0.02	0.842±0.006	0.842±0.006	-0.000±0.005	-0.005±0.005
7.7	0.4±0.3	-0.1±0.3	-0.60±0.01	-1.32±0.02	0.852±0.006	0.852±0.006	-0.001±0.005	-0.005±0.005
8.7	0.3±0.3	-0.1±0.3	-0.59±0.01	-1.33±0.02	0.863±0.006	0.863±0.006	-0.002±0.005	-0.004±0.005
9.8	0.2±0.3	-0.1±0.3	-0.57±0.01	-1.33±0.02	0.872±0.006	0.872±0.006	-0.002±0.005	-0.004±0.005
10.8	0.1±0.3	-0.1±0.3	-0.55±0.01	-1.32±0.02	0.877±0.006	0.877±0.006	-0.002±0.005	-0.002±0.005
11.8	0.1±0.3	-0.1±0.3	-0.54±0.01	-1.32±0.02	0.885±0.006	0.885±0.006	-0.002±0.005	-0.001±0.005
12.8	-0.0±0.3	-0.1±0.3	-0.53±0.01	-1.33±0.02	0.892±0.006	0.892±0.006	-0.001±0.005	0.000±0.005
13.8	-0.1±0.3	-0.2±0.3	-0.52±0.01	-1.33±0.02	0.899±0.006	0.899±0.006	-0.003±0.005	0.002±0.005
16.4	-0.3±0.3	-0.1±0.3	-0.49±0.01	-1.33±0.02	0.915±0.006	0.915±0.006	-0.001±0.005	0.005±0.005
18.9	-0.4±0.3	-0.0±0.3	-0.46±0.01	-1.33±0.02	0.930±0.006	0.930±0.006	-0.001±0.005	0.007±0.005
21.4	-0.6±0.3	0.0±0.3	-0.44±0.01	-1.32±0.02	0.942±0.006	0.942±0.006	0.001±0.005	0.010±0.005
24.0	-0.7±0.3	0.1±0.3	-0.41±0.01	-1.33±0.02	0.955±0.006	0.955±0.006	0.001±0.005	0.012±0.005
26.5	-0.8±0.3	0.1±0.3	-0.39±0.01	-1.33±0.02	0.970±0.006	0.969±0.006	0.001±0.004	0.013±0.005
29.1	-0.9±0.3	0.1±0.3	-0.36±0.01	-1.33±0.02	0.982±0.006	0.982±0.006	0.002±0.004	0.015±0.005
31.6	-0.9±0.3	0.1±0.3	-0.34±0.01	-1.32±0.02	0.994±0.006	0.994±0.006	0.002±0.004	0.016±0.005
34.1	-1.0±0.3	0.1±0.2	-0.31±0.01	-1.33±0.02	1.007±0.006	1.007±0.006	0.002±0.004	0.018±0.006
36.7	-1.0±0.3	0.1±0.2	-0.29±0.01	-1.32±0.02	1.018±0.006	1.018±0.006	0.002±0.004	0.019±0.006
39.2	-1.1±0.3	0.1±0.2	-0.26±0.01	-1.32±0.02	1.029±0.006	1.028±0.006	0.002±0.004	0.019±0.006
44.3	-1.2±0.3	0.2±0.2	-0.22±0.01	-1.33±0.02	1.050±0.007	1.050±0.007	0.003±0.004	0.021±0.006
49.4	-1.3±0.3	0.1±0.2	-0.18±0.01	-1.32±0.02	1.071±0.007	1.071±0.007	0.002±0.004	0.024±0.006
54.5	-1.3±0.3	0.1±0.2	-0.14±0.01	-1.32±0.02	1.089±0.007	1.089±0.007	0.002±0.004	0.024±0.006
59.5	-1.3±0.3	0.1±0.2	-0.10±0.01	-1.32±0.02	1.106±0.007	1.105±0.007	0.003±0.004	0.026±0.006
64.6	-1.3±0.3	0.1±0.2	-0.07±0.01	-1.32±0.02	1.120±0.007	1.120±0.007	0.003±0.004	0.026±0.006
69.7	-1.3±0.3	0.1±0.2	-0.04±0.01	-1.32±0.02	1.131±0.007	1.131±0.007	0.003±0.004	0.026±0.006
74.8	-1.4±0.3	0.2±0.2	-0.02±0.01	-1.31±0.02	1.140±0.007	1.139±0.007	0.003±0.004	0.027±0.006
79.9	-1.4±0.3	0.1±0.2	-0.00±0.01	-1.31±0.02	1.146±0.007	1.145±0.007	0.003±0.004	0.027±0.006
84.9	-1.4±0.3	0.1±0.2	0.00±0.01	-1.32±0.02	1.149±0.007	1.149±0.007	0.002±0.004	0.028±0.006
90.0	-1.3±0.3	0.1±0.2	0.01±0.01	-1.31±0.02	1.151±0.007	1.150±0.007	0.002±0.004	0.027±0.006
100.2	-1.3±0.3	0.0±0.2	0.01±0.01	-1.31±0.02	1.151±0.007	1.150±0.007	0.000±0.004	0.027±0.006
110.3	-1.3±0.3	-0.1±0.2	0.01±0.01	-1.31±0.02	1.150±0.007	1.150±0.007	-0.001±0.004	0.026±0.006
120.5	-1.2±0.3	-0.2±0.2	0.01±0:01	-1.31±0.02	1.150±0.007	1.149±0.007	-0.004±0.004	0.025±0.006
130.7	-1.2±0.3	-0.3±0.2	0.01±0.01	-1.31±0.02	1.148±0.007	1.148±0.007	-0.006±0.004	0.025±0.006
140.8	-1.1±0.3	-0.4±0.2	0.01±0.01	-1.31±0.02	1.148±0.007	1.147±0.007	-0.008±0.004	0.022±0.006

Table D.24 Five-Hole Probe Data at (x,z)=(127 mm,-178 mm)

y, mm	BETA, deg	ALPHA, deg	CPT	CPS	SPEED	U	V	W
3.7	-0.1±0.3	0.8±0.4	-0.73±0.01	-1.35±0.02	0.791±0.007	0.791±0.007	0.011±0.005	0.001±0.004
4.7	0.3±0.3	0.3±0.4	-0.68±0.01	-1.35±0.02	0.815±0.007	0.815±0.007	0.005±0.005	-0.005±0.005
5.7	0.6±0.3	0.1±0.4	-0.66±0.01	-1.36±0.02	0.836±0.006	0.836±0.006	0.002±0.005	-0.008±0.005
6.7	0.6±0.3	0.1±0.3	-0.63±0.01	-1.36±0.02	0.851±0.006	0.851±0.006	0.001±0.005	-0.009±0.005
7.7	0.6±0.3	0.1±0.3	-0.62±0.01	-1.36±0.02	0.861±0.006	0.861±0.006	0.001±0.005	-0.009±0.005
8.7	0.5±0.3	0.1±0.3	-0.60±0.01	-1.36±0.02	0.872±0.006	0.872±0.006	0.001±0.005	-0.007±0.005
9.8	0.4±0.3	0.1±0.3	-0.59±0.01	-1.36±0.02	0.878±0.006	0.878±0.006	0.001±0.005	-0.006±0.005
10.8	0.2±0.3	0.1±0.3	-0.57±0.01	-1.36±0.02	0.888±0.006	0.888±0.006	0.002±0.005	-0.004±0.005
11.8	0.1±0.3	0.1±0.3	-0.56±0.01	-1.36±0.02	0.896±0.006	0.896±0.006	0.002±0.005	-0.001±0.005
12.8	-0.1±0.3	0.2±0.3	-0.55±0.01	-1.36±0.02	0.904±0.006	0.904±0.006	0.002±0.005	0.001±0.005
13.8	-0.2±0.3	0.2±0.3	-0.53±0.01	-1.36±0.02	0.911±0.006	0.911±0.006	0.003±0.005	0.004±0.005
16.4	-0.5±0.3	0.2±0.3	-0.50±0.01	-1.36±0.02	0.927±0.006	0.927±0.006	0.003±0.005	0.008±0.005
18.9	-0.7±0.3	0.2±0.3	-0.47±0.01	-1.36±0.02	0.943±0.006	0.943±0.006	0.004±0.005	0.012±0.005
21.4	-0.9±0.3	0.3±0.3	-0.44±0.01	-1.36±0.02	0.961±0.006	0.961±0.006	0.004±0.005	0.015±0.005
24.0	-1.1±0.3	0.3±0.3	-0.41±0.01	-1.36±0.02	0.974±0.006	0.974±0.006	0.005±0.004	0.019±0.005
26.5	-1.2±0.3	0.3±0.3	-0.38±0.01	-1.36±0.02	0.988±0.006	0.988±0.006	0.005±0.004	0.021±0.005
29.1	-1.3±0.3	0.3±0.2	-0.36±0.01	-1.36±0.02	1.000±0.006	1.000±0.006	0.006±0.004	0.023±0.006
31.6	-1.5±0.3	0.4±0.2	-0.33±0.01	-1.36±0.02	1.013±0.006	1.013±0.006	0.006±0.004	0.026±0.006
34.1	-1.5±0.3	0.4±0.2	-0.31±0.01	-1.36±0.02	1.024±0.006	1.024±0.006	0.007±0.004	0.027±0.006
36.7	-1.6±0.3	0.4±0.2	-0.29±0.01	-1.36±0.02	1.036±0.006	1.036±0.006	0.007±0.004	0.030±0.006
39.2	-1.7±0.3	0.4±0.2	-0.26±0.01	-1.36±0.02	1.047±0.006	1.047±0.006	0.007±0.004	0.031±0.006
44.3	-1.8±0.3	0.4±0.2	-0.22±0.01	-1.36±0.02	1.066±0.007	1.066±0.007	0.007±0.004	0.034±0.006
49.4	-1.9±0.3	0.4±0.2	-0.18±0.01	-1.36±0.02	1.087±0.007	1.086±0.007	0.007±0.004	0.036±0.006
54.5	-2.0±0.3	0.4±0.2	-0.14±0.01	-1.36±0.02	1.105±0.007	1.104±0.007	0.007±0.004	0.038±0.006
59.5	-2.0±0.3	0.3±0.2	-0.10±0.01	-1.36±0.02	1.121±0.007	1.121±0.007	0.007±0.004	0.040±0.006
64.6	-2.0±0.3	0.3±0.2	-0.07±0.01	-1.36±0.02	1.136±0.007	1.135±0.007	0.006±0.004	0.040±0.006
69.7	-2.1±0.3	0.3±0.2	-0.04±0.01	-1.35±0.02	1.147±0.007	1.147±0.007	0.006±0.004	0.041±0.006
74.8	-2.0±0.3	0.2±0.2	-0.02±0.01	-1.36±0.02	1.157±0.007	1.156±0.007	0.004±0.004	0.041±0.006
79.9	-2.0±0.3	0.1±0.2	-0.00±0.01	-1.36±0.02	1.164±0.007	1.163±0.007	0.003±0.004	0.040±0.006
84.9	-2.0±0.3	0.1±0.2	0.01±0.01	-1.35±0.02	1.166±0.007	1.166±0.007	0.002±0.004	0.041±0.006
90.0	-2.0±0.3	0.0±0.2	0.01±0.01	-1.35±0.02	1.168±0.007	1.167±0.007	0.000±0.004	0.041±0.006
100.2	-2.0±0.3	-0.1±0.2	0.01±0.01	-1.35±0.02	1.167±0.007	1.167±0.007	-0.002±0.004	0.040±0.006
110.3	-1.9±0.3	-0.2±0.2	0.01±0.01	-1.35±0.02	1.166±0.007	1.166±0.007	-0.004±0.004	0.038±0.006
120.5	-1.8±0.3	-0.3±0.2	0.01±0.01	-1.35±0.02	1.166±0.007	1.165±0.007	-0.006±0.004	0.038±0.006
130.7	-1.7±0.3	-0.4±0.2	0.01±0.01	-1.34±0.02	1.165±0.007	1.164±0.007	-0.007±0.004	0.035±0.006
140.8	-1.6±0.3	-0.4±0.2	0.01±0.01	-1.34±0.02	1.164±0.007	1.163±0.007	-0.009±0.004	0.032±0.006

Table D.25 Five-Hole Probe Data at (x,z)=(127 mm,-152 mm)

y, mm	BETA, deg	ALPHA, deg	CPT	CPS	SPEED	U	V	W
3.7	1.7±0.3	1.1±0.4	-0.74±0.01	-1.40±0.02	0.809±0.007	0.809±0.007	0.015±0.005	-0.024±0.004
4.7	2.3±0.3	0.7±0.4	-0.71±0.01	-1.40±0.02	0.832±0.007	0.831±0.007	0.010±0.005	-0.033±0.005
5.7	2.5±0.3	0.6±0.3	-0.68±0.01	-1.40±0.02	0.850±0.006	0.849±0.006	0.008±0.005	-0.037±0.005
6.7	2.4±0.3	0.6±0.3	-0.66±0.01	-1.40±0.02	0.860±0.006	0.859±0.006	0.009±0.005	-0.035±0.005
7.7	2.1±0.3	0.7±0.3	-0.65±0.01	-1.40±0.02	0.868±0.006	0.868±0.006	0.010±0.005	-0.031±0.005
8.7	1.8±0.3	0.7±0.3	-0.64±0.01	-1.40±0.02	0.876±0.006	0.876±0.006	0.011±0.005	-0.027±0.005
9.8	1.4±0.3	0.8±0.3	-0.63±0.01	-1.40±0.02	0.881±0.006	0.881±0.006	0.012±0.005	-0.021±0.005
10.8	1.0±0.3	0.8±0.3	-0.62±0.01	-1.40±0.02	0.886±0.006	0.886±0.006	0.013±0.005	-0.015±0.005
11.8	0.5±0.3	0.9±0.3	-0.61±0.01	-1.40±0.02	0.891±0.006	0.891±0.006	0.014±0.005	-0.008±0.005
12.8	0.1±0.3	1.0±0.3	-0.60±0.01	-1.40±0.02	0.897±0.006	0.897±0.006	0.016±0.005	-0.002±0.005
13.8	-0.3±0.3	1.1±0.3	-0.59±0.01	-1.40±0.02	0.902±0.006	0.902±0.006	0.018±0.005	0.005±0.005
16.4	-1.0±0.3	1.3±0.3	-0.56±0.01	-1.40±0.02	0.919±0.006	0.919±0.006	0.021±0.005	0.016±0.005
18.9	-1.7±0.3	1.5±0.3	-0.53±0.01	-1.40±0.02	0.936±0.006	0.935±0.006	0.024±0.005	0.027±0.005
21.4	-2.1±0.3	1.5±0.3	-0.49±0.01	-1.40±0.02	0.951±0.006	0.950±0.006	0.025±0.005	0.035±0.005
24.0	-2.5±0.3	1.6±0.3	-0.47±0.01	-1.40±0.02	0.966±0.006	0.965±0.006	0.027±0.005	0.041±0.005
26.5	-2.7±0.3	1.6±0.3	-0.44±0.01	-1.40±0.02	0.982±0.006	0.980±0.006	0.027±0.004	0.047±0.005
29.1	-3.0±0.3	1.5±0.3	-0.41±0.01	-1.40±0.02	0.996±0.006	0.994±0.006	0.027±0.004	0.051±0.005
31.6	-3.1±0.3	1.5±0.2	-0.38±0.01	-1.40±0.02	1.010±0.006	1.008±0.006	0.026±0.004	0.054±0.006
34.1	-3.2±0.3	1.4±0.2	-0.35±0.01	-1.40±0.02	1.023±0.006	1.021±0.006	0.025±0.004	0.057±0.006
36.7	-3.3±0.3	1.3±0.2	-0.33±0.01	-1.40±0.02	1.036±0.006	1.034±0.006	0.023±0.004	0.059±0.006
39.2	-3.4±0.3	1.2±0.2	-0.30±0.01	-1.40±0.02	1.048±0.007	1.046±0.007	0.022±0.004	0.061±0.006
44.3	-3.4±0.3	1.1±0.2	-0.25±0.01	-1.40±0.02	1.071±0.007	1.069±0.007	0.020±0.004	0.063±0.006
49.4	-3.4±0.3	0.9±0.2	-0.20±0.01	-1.40±0.02	1.092±0.007	1.090±0.007	0.017±0.004	0.065±0.006
54.5	-3.5±0.3	0.7±0.2	-0.16±0.01	-1.40±0.02	1.113±0.007	1.111±0.007	0.014±0.004	0.067±0.006
59.5	-3.5±0.3	0.6±0.2	-0.12±0.01	-1.40±0.02	1.130±0.007	1.128±0.007	0.012±0.004	0.068±0.006
64.6	-3.5±0.3	0.5±0.2	-0.08±0.01	-1.40±0.02	1.146±0.007	1.144±0.007	0.010±0.004	0.069±0.006
69.7	-3.5±0.3	0.4±0.2	-0.05±0.01	-1.39±0.02	1.159±0.007	1.157±0.007	0.008±0.004	0.070±0.006
74.8	-3.4±0.3	0.3±0.2	-0.02±0.01	-1.40±0.02	1.171±0.007	1.169±0.007	0.007±0.004	0.070±0.006
79.9	-3.4±0.3	0.3±0.2	-0.01±0.01	-1.39±0.02	1.178±0.007	1.176±0.007	0.005±0.004	0.070±0.007
84.9	-3.3±0.3	0.2±0.2	0.00±0.01	-1.40±0.02	1.183±0.007	1.181±0.007	0.003±0.004	0.068±0.007
90.0	-3.3±0.3	0.1±0.2	0.01±0.01	-1.39±0.02	1.185±0.007	1.183±0.007	0.001±0.004	0.067±0.007
100.2	-3.1±0.3	-0.1±0.2	0.01±0.01	-1.39±0.02	1.185±0.007	1.183±0.007	-0.002±0.004	0.064±0.007
110.3	-3.0±0.3	-0.2±0.2	0.01±0.01	-1.39±0.02	1.184±0.007	1.183±0.007	-0.004±0.004	0.061±0.007
120.5	-2.8±0.3	-0.3±0.2	0.01±0.01	-1.39±0.02	1.183±0.007	1.182±0.007	-0.007±0.004	0.058±0.007
130.7	-2.7±0.3	-0.5±0.2	0.01±0.01	-1.38±0.02	1.181±0.007	1.180±0.007	-0.010±0.004	0.056±0.007
140.8	-2.6±0.3	-0.6±0.2	0.01±0.01	-1.38±0.02	1.180±0.007	1.179±0.007	-0.012±0.004	0.054±0.007

Table D.26 Five-Hole Probe Data at (x,z)=(127 mm,-140 mm)

y, mm	BETA, deg	ALPHA, deg	CPT	CPS	SPEED	U	V	W
3.7	2.3±0.3	1.5±0.4	-0.74±0.01	-1.42±0.02	0.825±0.007	0.824±0.007	0.022±0.005	-0.033±0.005
4.7	2.9±0.3	1.3±0.4	-0.71±0.01	-1.43±0.02	0.847±0.006	0.845±0.006	0.019±0.005	-0.042±0.005
5.7	3.1±0.3	1.3±0.3	-0.70±0.01	-1.43±0.02	0.856±0.006	0.854±0.006	0.019±0.005	-0.046±0.005
6.7	3.0±0.3	1.4±0.3	-0.68±0.01	-1.43±0.02	0.862±0.006	0.861±0.006	0.021±0.005	-0.046±0.005
7.7	2.8±0.3	1.7±0.3	-0.68±0.01	-1.43±0.02	0.869±0.006	0.868±0.006	0.025±0.005	-0.043±0.005
8.7	2.4±0.3	1.8±0.3	-0.67±0.01	-1.43±0.02	0.875±0.006	0.873±0.006	0.027±0.005	-0.037±0.005
9.8	1.9±0.3	1.9±0.3	-0.67±0.01	-1.43±0.02	0.877±0.006	0.876±0.006	0.030±0.005	-0.029±0.005
10.8	1.3±0.3	2.2±0.3	-0.66±0.01	-1.44±0.02	0.884±0.006	0.883±0.006	0.034±0.005	-0.021±0.005
11.8	0.8±0.3	2.4±0.3	-0.65±0.01	-1.44±0.02	0.889±0.006	0.888±0.006	0.037±0.005	-0.012±0.005
12.8	0.2±0.3	2.5±0.3	-0.64±0.01	-1.44±0.02	0.894±0.006	0.893±0.006	0.039±0.005	-0.002±0.005
13.8	-0.4±0.3	2.6±0.3	-0.63±0.01	-1.44±0.02	0.900±0.006	0.899±0.006	0.040±0.005	0.006±0.005
16.4	-1.7±0.3	2.8±0.3	-0.59±0.01	-1.44±0.02	0.919±0.006	0.917±0.006	0.044±0.005	0.027±0.005
18.9	-2.8±0.3	2.7±0.3	-0.56±0.01	-1.44±0.02	0.937±0.006	0.935±0.006	0.044±0.005	0.045±0.005
21.4	-3.5±0.3	2.6±0.3	-0.53±0.01	-1.43±0.02	0.954±0.006	0.951±0.006	0.043±0.005	0.058±0.005
24.0	-4.1±0.3	2.4±0.3	-0.49±0.01	-1.43±0.02	0.971±0.006	0.967±0.006	0.040±0.005	0.069±0.005
26.5	-4.5±0.3	2.3±0.3	-0.45±0.01	-1.43±0.02	0.989±0.006	0.985±0.006	0.039±0.004	0.077±0.005
29.1	-4.7±0.3	2.1±0.3	-0.42±0.01	-1.43±0.02	1.003±0.006	0.999±0.006	0.036±0.004	0.082±0.006
31.6	-4.9±0.3	1.9±0.2	-0.39±0.01	-1.43±0.02	1.019±0.006	1.014±0.006	0.033±0.004	0.087±0.006
34.1	-5.0±0.3	1.7±0.2	-0.36±0.01	-1.43±0.02	1.031±0.006	1.027±0.006	0.030±0.004	0.090±0.006
36.7	-5.0±0.3	1.5±0.2	-0.34±0.01	-1.43±0.02	1.045±0.006	1.040±0.006	0.027±0.004	0.092±0.006
39.2	-5.0±0.3	1.4±0.2	-0.31±0.01	-1.43±0.02	1.056±0.007	1.052±0.007	0.025±0.004	0.093±0.006
44.3	-5.0±0.3	1.1±0.2	-0.26±0.01	-1.43±0.02	1.079±0.007	1.075±0.007	0.021±0.004	0.095±0.006
49.4	-5.0±0.3	0.9±0.2	-0.21±0.01	-1.42±0.02	1.101±0.007	1.096±0.007	0.018±0.004	0.095±0.006
54.5	-4.9±0.3	0.8±0.2	-0.17±0.01	-1.42±0.02	1.121±0.007	1.116±0.007	0.015±0.004	0.095±0.006
59.5	-4.9±0.3	0.6±0.2	-0.13±0.01	-1.42±0.02	1.139±0.007	1.135±0.007	0.012±0.004	0.096±0.006
64.6	-4.7±0.3	0.5±0.2	-0.09±0.01	-1.43±0.02	1.156±0.007	1.152±0.007	0.010±0.004	0.096±0.006
69.7	-4.7±0.3	0.4±0.2	-0.06±0.01	-1.42±0.02	1.169±0.007	1.166±0.007	0.007±0.004	0.095±0.006
74.8	-4.6±0.3	0.3±0.2	-0.03±0.01	-1.42±0.02	1.180±0.007	1.176±0.007	0.005±0.004	0.095±0.007
79.9	-4.6±0.3	0.2±0.2	-0.01±0.01	-1.42±0.02	1.188±0.007	1.184±0.007	0.003±0.004	0.095±0.007
84.9	-4.5±0.3	0.1±0.2	0.00±0.01	-1.42±0.02	1.194±0.007	1.190±0.007	0.002±0.004	0.094±0.007
90.0	-4.4±0.3	0.0±0.2	0.01±0.01	-1.42±0.02	1.195±0.007	1.192±0.007	0.000±0.004	0.092±0.007
100.2	-4.2±0.3	-0.1±0.2	0.01±0.01	-1.42±0.02	1.197±0.007	1.194±0.007	-0.002±0.004	0.088±0.007
110.3	-4.1±0.3	-0.2±0.2	0.01±0.01	-1.42±0.02	1.196±0.007	1.193±0.007	-0.005±0.004	0.085±0.007
120.5	-4.0±0.3	-0.3±0.2	0.01±0.01	-1.42±0.02	1.196±0.007	1.193±0.007	-0.007±0.004	0.083±0.007
130.7	-3.8±0.3	-0.5±0.2	0.01±0.01	-1.42±0.02	1.195±0.007	1.192±0.007	-0.009±0.004	0.079±0.007
140.8	-3.7±0.3	-0.6±0.2	0.01±0.01	-1.41±0.02	1.192±0.007	1.190±0.007	-0.012±0.004	0.078±0.007

Table D.27 Five-Hole Probe Data at (x,z)=(127 mm,-127 mm)

y, mm	BETA, deg	ALPHA, deg	CPT	CPS	SPEED	U	V	W
3.7	7.8±0.3	3.9±0.4	-0.74±0.01	-1.46±0.02	0.848±0.006	0.839±0.006	0.057±0.005	-0.114±0.005
4.7	8.0±0.3	4.3±0.4	-0.73±0.01	-1.47±0.02	0.859±0.006	0.848±0.006	0.064±0.005	-0.118±0.005
5.7	7.7±0.3	4.8±0.3	-0.74±0.01	-1.49±0.02	0.864±0.006	0.853±0.006	0.071±0.005	-0.115±0.005
6.7	7.1±0.3	5.1±0.3	-0.75±0.01	-1.49±0.02	0.863±0.006	0.853±0.006	0.077±0.005	-0.107±0.005
7.7	6.5±0.3	5.7±0.3	-0.76±0.01	-1.51±0.02	0.867±0.006	0.857±0.006	0.086±0.005	-0.097±0.005
8.7	5.3±0.3	5.9±0.3	-0.77±0.01	-1.52±0.02	0.866±0.006	0.857±0.007	0.089±0.005	-0.079±0.005
9.8	4.0±0.3	6.2±0.4	-0.77±0.01	-1.52±0.02	0.864±0.006	0.857±0.007	0.093±0.005	-0.060±0.005
10.8	2.4±0.3	6.2±0.4	-0.78±0.01	-1.52±0.02	0.864±0.006	0.858±0.007	0.093±0.005	-0.036±0.005
11.8	0.8±0.3	6.0±0.3	-0.77±0.01	-1.53±0.02	0.869±0.006	0.864±0.007	0.091±0.005	-0.012±0.005
12.8	-0.8±0.3	5.9±0.3	-0.77±0.01	-1.54±0.02	0.874±0.006	0.870±0.007	0.089±0.005	0.012±0.005
13.8	-2.2±0.3	5.7±0.3	-0.75±0.01	-1.52±0.02	0.879±0.006	0.874±0.006	0.088±0.005	0.034±0.005
16.4	-4.8±0.3	4.8±0.3	-0.70±0.01	-1.51±0.02	0.903±0.006	0.897±0.006	0.075±0.005	0.075±0.005
18.9	-6.2±0.3	3.8±0.3	-0.64±0.01	-1.51±0.02	0.930±0.006	0.923±0.006	0.061±0.005	0.100±0.005
21.4	-6.8±0.3	3.0±0.3	-0.58±0.01	-1.49±0.02	0.955±0.006	0.947±0.006	0.050±0.005	0.112±0.005
24.0	-6.9±0.3	2.4±0.3	-0.53±0.01	-1.49±0.02	0.981±0.006	0.973±0.006	0.042±0.005	0.118±0.005
26.5	-6.9±0.3	2.1±0.3	-0.47±0.01	-1.47±0.02	1.000±0.006	0.992±0.006	0.036±0.004	0.120±0.006
29.1	-6.9±0.3	1.8±0.2	-0.43±0.01	-1.48±0.02	1.021±0.006	1.013±0.006	0.031±0.004	0.122±0.006
31.6	-6.8±0.3	1.5±0.2	-0.40±0.01	-1.47±0.02	1.036±0.006	1.029±0.006	0.028±0.004	0.122±0.006
34.1	-6.7±0.3	1.4±0.2	-0.37±0.01	-1.47±0.02	1.049±0.007	1.041±0.006	0.025±0.004	0.122±0.006
36.7	-6.6±0.3	1.2±0.2	-0.34±0.01	-1.46±0.02	1.061±0.007	1.054±0.007	0.022±0.004	0.121±0.006
39.2	-6.4±0.3	1.1±0.2	-0.31±0.01	-1.47±0.02	1.075±0.007	1.068±0.007	0.020±0.004	0.120±0.006
44.3	-6.2±0.3	0.8±0.2	-0.26±0.01	-1.46±0.02	1.099±0.007	1.092±0.007	0.016±0.004	0.119±0.006
49.4	-6.1±0.3	0.7±0.2	-0.21±0.01	-1.46±0.02	1.119±0.007	1.113±0.007	0.013±0.004	0.118±0.006
54.5	-5.9±0.3	0.5±0.2	-0.16±0.01	-1.46±0.02	1.139±0.007	1.133±0.007	0.011±0.004	0.117±0.006
59.5	-5.7±0.3	0.4±0.2	-0.12±0.01	-1.46±0.02	1.157±0.007	1.151±0.007	0.008±0.004	0.115±0.006
64.6	-5.7±0.3	0.3±0.2	-0.09±0.01	-1.46±0.02	1.172±0.007	1.166±0.007	0.006±0.004	0.116±0.006
69.7	-5.5±0.3	0.2±0.2	-0.06±0.01	-1.46±0.02	1.186±0.007	1.180±0.007	0.004±0.004	0.115±0.007
74.8	-5.4±0.3	0.1±0.2	-0.03±0.01	-1.46±0.02	1.197±0.007	1.192±0.007	0.003±0.004	0.114±0.007
79.9	-5.3±0.3	0.0±0.2	-0.01±0.01	-1.46±0.02	1.205±0.007	1.199±0.007	0.001±0.004	0.112±0.007
84.9	-5.2±0.3	-0.0±0.2	-0.00±0.01	-1.46±0.02	1.209±0.007	1.204±0.007	-0.000±0.004	0.110±0.007
90.0	-5.2±0.3	-0.1±0.2	0.01±0.01	-1.46±0.02	1.211±0.007	1.206±0.007	-0.002±0.004	0.109±0.007
100.2	-4.9±0.3	-0.3±0.2	0.01±0.01	-1.46±0.02	1.213±0.007	1.208±0.007	-0.006±0.004	0.104±0.007
110.3	-4.8±0.3	-0.5±0.2	0.01±0.01	-1.46±0.02	1.212±0.007	1.208±0.007	-0.010±0.004	0.101±0.007
120.5	-4.6±0.3	-0.6±0.2	0.01±0.01	-1.45±0.02	1.211±0.007	1.207±0.007	-0.012±0.004	0.097±0.007
130.7	-4.5±0.3	-0.7±0.2	0.01±0.01	-1.45±0.02	1.210±0.007	1.206±0.007	-0.014±0.004	0.096±0.007
140.8	-4.5±0.3	-1.1±0.2	0.01±0.01	-1.43±0.02	1.202±0.007	1.198±0.007	-0.022±0.004	0.094±0.007

Table D.28 Five-Hole Probe Data at (x,z)=(127 mm,-114 mm)

y, mm	BETA, deg	ALPHA, deg	CPT	CPS	SPEED	U	V	W
3.7	11.3±0.3	2.4±0.3	-0.61±0.01	-1.50±0.02	0.942±0.006	0.924±0.006	0.038±0.005	-0.184±0.005
4.7	10.8±0.3	1.8±0.3	-0.65±0.01	-1.51±0.02	0.930±0.006	0.913±0.006	0.028±0.005	-0.174±0.005
5.7	9.9±0.3	1.4±0.3	-0.69±0.01	-1.52±0.02	0.912±0.006	0.898±0.006	0.023±0.005	-0.158±0.005
6.7	9.0±0.3	1.2±0.3	-0.73±0.01	-1.53±0.02	0.895±0.006	0.883±0.006	0.019±0.005	-0.140±0.005
7.7	7.8±0.3	0.6±0.3	-0.77±0.01	-1.54±0.02	0.878±0.006	0.870±0.006	0.009±0.005	-0.119±0.005
8.7	6.3±0.3	0.3±0.3	-0.80±0.01	-1.55±0.02	0.866±0.006	0.860±0.006	0.004±0.005	-0.095±0.005
9.8	4.3±0.3	-0.1±0.3	-0.82±0.01	-1.55±0.02	0.852±0.006	0.850±0.006	-0.001±0.005	-0.064±0.005
10.8	2.2±0.3	-0.5±0.3	-0.84±0.01	-1.56±0.02	0.849±0.006	0.848±0.006	-0.008±0.005	-0.033±0.005
11.8	-0.2±0.3	-1.3±0.3	-0.84±0.01	-1.56±0.02	0.849±0.006	0.848±0.006	-0.020±0.005	0.004±0.005
12.8	-2.3±0.3	-1.8±0.3	-0.83±0.01	-1.55±0.02	0.853±0.006	0.852±0.006	-0.027±0.005	0.035±0.005
13.8	-4.3±0.3	-2.1±0.3	-0.80±0.01	-1.54±0.02	0.863±0.006	0.860±0.006	-0.032±0.005	0.065±0.005
16.4	-7.6±0.3	-2.0±0.3	-0.72±0.01	-1.53±0.02	0.899±0.006	0.891±0.006	-0.032±0.005	0.119±0.005
18.9	-8.9±0.3	-1.4±0.3	-0.64±0.01	-1.52±0.02	0.937±0.006	0.925±0.006	-0.023±0.005	0.145±0.005
21.4	-9.2±0.3	-1.0±0.3	-0.56±0.01	-1.50±0.02	0.968±0.006	0.955±0.006	-0.017±0.004	0.155±0.005
24.0	-9.1±0.3	-0.7±0.3	-0.50±0.01	-1.49±0.02	0.997±0.006	0.985±0.006	-0.012±0.004	0.158±0.006
26.5	-9.0±0.3	-0.4±0.2	-0.45±0.01	-1.48±0.02	1.015±0.006	1.003±0.006	-0.007±0.004	0.159±0.006
29.1	-8.8±0.3	-0.2±0.2	-0.41±0.01	-1.48±0.02	1.034±0.006	1.022±0.006	-0.004±0.004	0.158±0.006
31.6	-8.6±0.3	-0.1±0.2	-0.38±0.01	-1.48±0.02	1.048±0.006	1.037±0.006	-0.003±0.004	0.157±0.006
34.1	-8.4±0.3	-0.1±0.2	-0.35±0.01	-1.48±0.02	1.063±0.007	1.052±0.006	-0.001±0.004	0.156±0.006
36.7	-8.2±0.3	0.0±0.2	-0.32±0.01	-1.48±0.02	1.075±0.007	1.064±0.007	0.000±0.004	0.153±0.006
39.2	-8.1±0.3	0.0±0.2	-0.29±0.01	-1.47±0.02	1.084±0.007	1.073±0.007	0.001±0.004	0.152±0.006
44.3	-7.7±0.3	0.1±0.2	-0.24±0.01	-1.47±0.02	1.108±0.007	1.098±0.007	0.001±0.004	0.149±0.006
49.4	-7.5±0.3	0.0±0.2	-0.20±0.01	-1.47±0.02	1.128±0.007	1.118±0.007	0.000±0.004	0.148±0.006
54.5	-7.4±0.3	-0.0±0.2	-0.16±0.01	-1.47±0.02	1.147±0.007	1.138±0.007	-0.000±0.004	0.147±0.006
59.5	-7.2±0.3	-0.1±0.2	-0.12±0.01	-1.47±0.02	1.164±0.007	1.155±0.007	-0.001±0.004	0.146±0.006
64.6	-7.1±0.3	-0.2±0.2	-0.08±0.01	-1.47±0.02	1.179±0.007	1.170±0.007	-0.003±0.004	0.145±0.007
69.7	-7.0±0.3	-0.2±0.2	-0.05±0.01	-1.47±0.02	1.192±0.007	1.183±0.007	-0.005±0.004	0.145±0.007
74.8	-6.9±0.3	-0.3±0.2	-0.03±0.01	-1.47±0.02	1.202±0.007	1.194±0.007	-0.006±0.004	0.144±0.007
79.9	-6.8±0.3	-0.4±0.2	-0.01±0.01	-1.47±0.02	1.209±0.007	1.200±0.007	-0.009±0.004	0.142±0.007
84.9	-6.6±0.3	-0.5±0.2	0.00±0.01	-1.47±0.02	1.214±0.007	1.206±0.007	-0.010±0.004	0.141±0.007
90.0	-6.5±0.3	-0.6±0.2	0.01±0.01	-1.47±0.02	1.216±0.007	1.208±0.007	-0.013±0.004	0.138±0.007
100.2	-6.3±0.3	-0.8±0.2	0.01±0.01	-1.47±0.02	1.216±0.007	1.209±0.007	-0.017±0.004	0.133±0.007
110.3	-6.1±0.3	-0.9±0.2	0.01±0.01	-1.47±0.02	1.216±0.007	1.209±0.007	-0.020±0.004	0.129±0.007
120.5	-5.9±0.3	-1.1±0.2	0.01±0.01	-1.47±0.02	1.215±0.007	1.208±0.007	-0.023±0.004	0.125±0.007
130.7	-5.8±0.3	-1.2±0.2	0.01±0.01	-1.46±0.02	1.213±0.007	1.206±0.007	-0.026±0.004	0.123±0.007
140.8	-5.7±0.3	-1.4±0.2	0.01±0.01	-1.45±0.02	1.210±0.007	1.204±0.007	-0.030±0.004	0.120±0.007

Table D.29 Five-Hole Probe Data at (x,z)=(127 mm,-108 mm)

y, mm	BETA, deg	ALPHA, deg	CPT	CPS	SPEED	U	V	W
3.7	9.2±0.3	1.2±0.3	-0.55±0.01	-1.51±0.02	0.981±0.006	0.969±0.006	0.020±0.004	-0.157±0.005
4.7	8.4±0.3	0.3±0.3	-0.59±0.01	-1.52±0.02	0.967±0.006	0.956±0.006	0.006±0.005	-0.140±0.005
5.7	7.3±0.3	-0.4±0.3	-0.63±0.01	-1.53±0.02	0.949±0.006	0.941±0.006	-0.006±0.005	-0.121±0.005
6.7	6.2±0.3	-1.0±0.3	-0.66±0.01	-1.53±0.02	0.934±0.006	0.928±0.006	-0.017±0.005	-0.101±0.005
7.7	5.0±0.3	-1.8±0.3	-0.69±0.01	-1.54±0.02	0.920±0.006	0.916±0.006	-0.029±0.005	-0.080±0.005
8.7	3.6±0.3	-2.5±0.3	-0.71±0.01	-1.54±0.02	0.912±0.006	0.909±0.006	-0.039±0.005	-0.057±0.005
9.8	2.1±0.3	-3.0±0.3	-0.72±0.01	-1.54±0.02	0.904±0.006	0.902±0.006	-0.047±0.005	-0.033±0.005
10.8	0.5±0.3	-3.5±0.3	-0.74±0.01	-1.55±0.02	0.902±0.006	0.900±0.006	-0.055±0.005	-0.008±0.005
11.8	-1.2±0.3	-4.1±0.3	-0.73±0.01	-1.54±0.02	0.901±0.006	0.898±0.006	-0.064±0.005	0.019±0.005
12.8	-2.7±0.3	-4.2±0.3	-0.71±0.01	-1.53±0.02	0.907±0.006	0.904±0.006	-0.067±0.005	0.043±0.005
13.8	-4.1±0.3	-4.1±0.3	-0.70±0.01	-1.54±0.02	0.915±0.006	0.910±0.006	-0.065±0.005	0.066±0.005
16.4	-6.6±0.3	-3.8±0.3	-0.63±0.01	-1.52±0.02	0.945±0.006	0.937±0.006	-0.063±0.005	0.108±0.005
18.9	-8.1±0.3	-3.3±0.3	-0.57±0.01	-1.52±0.02	0.974±0.006	0.963±0.006	-0.056±0.004	0.136±0.005
21.4	-8.6±0.3	-2.5±0.3	-0.51±0.01	-1.52±0.02	1.001±0.006	0.989±0.006	-0.043±0.004	0.149±0.006
24.0	-8.9±0.3	-1.9±0.2	-0.46±0.01	-1.51±0.02	1.025±0.006	1.012±0.006	-0.033±0.004	0.158±0.006
26.5	-8.9±0.3	-1.4±0.2	-0.42±0.01	-1.50±0.02	1.041±0.006	1.028±0.006	-0.026±0.004	0.161±0.006
29.1	-8.9±0.3	-1.0±0.2	-0.39±0.01	-1.51±0.02	1.057±0.007	1.044±0.006	-0.018±0.004	0.163±0.006
31.6	-8.8±0.3	-0.8±0.2	-0.36±0.01	-1.50±0.02	1.069±0.007	1.056±0.007	-0.014±0.004	0.163±0.006
34.1	-8.6±0.3	-0.5±0.2	-0.33±0.01	-1.50±0.02	1.081±0.007	1.069±0.007	-0.010±0.004	0.162±0.006
36.7	-8.5±0.3	-0.3±0.2	-0.31±0.01	-1.50±0.02	1.094±0.007	1.082±0.007	-0.006±0.004	0.162±0.006
39.2	-8.4±0.3	-0.3±0.2	-0.28±0.01	-1.50±0.02	1.105±0.007	1.093±0.007	-0.005±0.004	0.162±0.006
44.3	-8.2±0.3	-0.1±0.2	-0.23±0.01	-1.51±0.02	1.128±0.007	1.116±0.007	-0.002±0.004	0.161±0.006
49.4	-8.0±0.3	-0.1±0.2	-0.19±0.01	-1.51±0.02	1.147±0.007	1.136±0.007	-0.001±0.004	0.160±0.006
54.5	-7.9±0.3	-0.1±0.2	-0.15±0.01	-1.50±0.02	1.164±0.007	1.153±0.007	-0.001±0.004	0.160±0.006
59.5	-7.7±0.3	-0.1±0.2	-0.11±0.01	-1.50±0.02	1.182±0.007	1.171±0.007	-0.002±0.004	0.158±0.007
64.6	-7.6±0.3	-0.1±0.2	-0.07±0.01	-1.51±0.02	1.197±0.007	1.187±0.007	-0.003±0.004	0.158±0.007
69.7	-7.4±0.3	-0.2±0.2	-0.05±0.01	-1.51±0.02	1.209±0.007	1.199±0.007	-0.004±0.004	0.156±0.007
74.8	-7.3±0.3	-0.3±0.2	-0.02±0.01	-1.51±0.02	1.219±0.007	1.209±0.007	-0.006±0.004	0.154±0.007
79.9	-7.2±0.3	-0.4±0.2	-0.01±0.01	-1.51±0.02	1.226±0.007	1.216±0.007	-0.008±0.004	0.153±0.007
84.9	-7.0±0.3	-0.4±0.2	0.00±0.01	-1.51±0.02	1.231±0.007	1.222±0.007	-0.009±0.004	0.150±0.007
90.0	-6.9±0.3	-0.5±0.2	0.01±0.01	-1.51±0.02	1.233±0.007	1.224±0.007	-0.011±0.004	0.148±0.007
100.2	-6.6±0.3	-0.6±0.2	0.01±0.01	-1.51±0.02	1.235±0.007	1.227±0.007	-0.013±0.004	0.142±0.007
110.3	-6.4±0.3	-0.8±0.2	0.01±0.01	-1.51±0.02	1.234±0.007	1.226±0.007	-0.017±0.004	0.138±0.007
120.5	-6.3±0.3	-0.9±0.2	0.01±0.01	-1.51±0.02	1.232±0.007	1.224±0.007	-0.020±0.004	0.135±0.007
130.7	-6.2±0.3	-1.0±0.2	0.01±0.01	-1.50±0.02	1.231±0.007	1.223±0.007	-0.022±0.004	0.133±0.007
140.8	-6.0±0.3	-1.2±0.2	0.01±0.01	-1.50±0.02	1.228±0.007	1.221±0.007	-0.025±0.004	0.129±0.007

Table D.30 Five-Hole Probe Data at (x,z)=(127 mm,-102 mm)

y, mm	BETA, deg	ALPHA, deg	CPT	CPS	SPEED	U	V	W
3.7	6.1±0.3	0.9±0.2	-0.50±0.01	-1.51±0.02	1.009±0.006	1.003±0.006	0.016±0.004	-0.107±0.006
4.7	5.0±0.3	0.0±0.3	-0.53±0.01	-1.52±0.02	0.996±0.006	0.992±0.006	0.001±0.004	-0.087±0.006
5.7	3.9±0.3	-0.6±0.3	-0.56±0.01	-1.52±0.02	0.981±0.006	0.979±0.006	-0.010±0.004	-0.066±0.005
6.7	2.7±0.3	-1.3±0.3	-0.58±0.01	-1.52±0.02	0.971±0.006	0.970±0.006	-0.022±0.004	-0.045±0.005
7.7	1.5±0.3	-1.8±0.3	-0.60±0.01	-1.53±0.02	0.965±0.006	0.964±0.006	-0.031±0.004	-0.026±0.005
8.7	0.4±0.3	-2.4±0.3	-0.61±0.01	-1.52±0.02	0.956±0.006	0.955±0.006	-0.039±0.005	-0.006±0.005
9.8	-0.7±0.3	-2.8±0.3	-0.61±0.01	-1.52±0.02	0.955±0.006	0.953±0.006	-0.047±0.005	0.012±0.005
10.8	-1.7±0.3	-3.1±0.3	-0.61±0.01	-1.52±0.02	0.956±0.006	0.954±0.006	-0.052±0.005	0.028±0.005
11.8	-2.8±0.3	-3.5±0.3	-0.61±0.01	-1.53±0.02	0.958±0.006	0.955±0.006	-0.058±0.005	0.046±0.005
12.8	-3.7±0.3	-3.6±0.3	-0.60±0.01	-1.52±0.02	0.963±0.006	0.959±0.006	-0.060±0.005	0.062±0.005
13.8	-4.7±0.3	-3.6±0.3	-0.59±0.01	-1.53±0.02	0.970±0.006	0.965±0.006	-0.061±0.004	0.079±0.005
16.4	-6.3±0.3	-3.5±0.3	-0.54±0.01	-1.52±0.02	0.987±0.006	0.980±0.006	-0.060±0.004	0.109±0.005
18.9	-7.5±0.3	-3.0±0.2	-0.50±0.01	-1.52±0.02	1.008±0.006	0.998±0.006	-0.052±0.004	0.131±0.006
21.4	-8.1±0.3	-2.5±0.2	-0.46±0.01	-1.52±0.02	1.027±0.006	1.016±0.006	-0.045±0.004	0.145±0.006
24.0	-8.6±0.3	-2.1±0.2	-0.43±0.01	-1.52±0.02	1.043±0.006	1.030±0.006	-0.037±0.004	0.156±0.006
26.5	-8.8±0.3	-1.7±0.2	-0.40±0.01	-1.52±0.02	1.057±0.006	1.044±0.006	-0.030±0.004	0.162±0.006
29.1	-9.0±0.3	-1.4±0.2	-0.37±0.01	-1.51±0.02	1.071±0.007	1.057±0.007	-0.025±0.004	0.167±0.006
31.6	-9.0±0.3	-1.1±0.2	-0.35±0.01	-1.51±0.02	1.081±0.007	1.067±0.007	-0.020±0.004	0.169±0.006
34.1	-9.0±0.3	-0.8±0.2	-0.32±0.01	-1.51±0.02	1.095±0.007	1.081±0.007	-0.016±0.004	0.171±0.006
36.7	-9.0±0.3	-0.6±0.2	-0.29±0.01	-1.52±0.02	1.106±0.007	1.093±0.007	-0.012±0.004	0.173±0.006
39.2	-8.9±0.3	-0.5±0.2	-0.27±0.01	-1.51±0.02	1.117±0.007	1.103±0.007	-0.010±0.004	0.174±0.006
44.3	-8.8±0.3	-0.4±0.2	-0.22±0.01	-1.51±0.02	1.138±0.007	1.124±0.007	-0.007±0.004	0.175±0.006
49.4	-8.7±0.3	-0.3±0.2	-0.18±0.01	-1.52±0.02	1.158±0.007	1.145±0.007	-0.005±0.004	0.176±0.006
54.5	-8.6±0.3	-0.2±0.2	-0.14±0.01	-1.52±0.02	1.174±0.007	1.161±0.007	-0.005±0.004	0.176±0.006
59.5	-8.5±0.3	-0.3±0.2	-0.10±0.01	-1.52±0.02	1.191±0.007	1.178±0.007	-0.005±0.004	0.175±0.007
64.6	-8.3±0.3	-0.3±0.2	-0.07±0.01	-1.52±0.02	1.204±0.007	1.191±0.007	-0.006±0.004	0.174±0.007
69.7	-8.2±0.3	-0.3±0.2	-0.04±0.01	-1.52±0.02	1.217±0.007	1.205±0.007	-0.007±0.004	0.173±0.007
74.8	-8.1±0.3	-0.4±0.2	-0.02±0.01	-1.53±0.02	1.227±0.007	1.215±0.007	-0.009±0.004	0.172±0.007
79.9	-7.9±0.3	-0.5±0.2	-0.01±0.01	-1.53±0.02	1.233±0.007	1.221±0.007	-0.010±0.004	0.170±0.007
84.9	-7.8±0.3	-0.5±0.2	0.00±0.01	-1.53±0.02	1.237±0.007	1.225±0.007	-0.011±0.004	0.168±0.007
90.0	-7.7±0.3	-0.6±0.2	0.01±0.01	-1.53±0.02	1.239±0.007	1.228±0.007	-0.013±0.003	0.166±0.007
100.2	-7.4±0.3	-0.7±0.2	0.01±0.01	-1.53±0.02	1.240±0.007	1.230±0.007	-0.015±0.003	0.160±0.007
110.3	-7.2±0.3	-0.9±0.2	0.01±0.01	-1.53±0.02	1.240±0.007	1.230±0.007	-0.019±0.003	0.155±0.007
120.5	-7.0±0.3	-1.0±0.2	0.01±0.01	-1.52±0.02	1.238±0.007	1.229±0.007	-0.021±0.004	0.151±0.007
130.7	-6.9±0.3	-1.1±0.2	0.01±0.01	-1.52±0.02	1.237±0.007	1.227±0.007	-0.024±0.004	0.149±0.007
140.8	-6.8±0.3	-1.2±0.2	0.01±0.01	-1.51±0.02	1.235±0.007	1.226±0.007	-0.025±0.004	0.146±0.007

Table D.31 Five-Hole Probe Data at (x,z)=(127 mm,-95 mm)

y, mm	BETA, deg	ALPHA, deg	CPT	CPS	SPEED	U	V	W
3.7	3.4±0.3	1.0±0.2	-0.45±0.01	-1.50±0.02	1.026±0.006	1.024±0.006	0.019±0.004	-0.060±0.006
4.7	2.2±0.3	0.4±0.2	-0.48±0.01	-1.51±0.02	1.016±0.006	1.016±0.006	0.006±0.004	-0.040±0.006
5.7	1.0±0.3	-0.2±0.2	-0.50±0.01	-1.52±0.02	1.007±0.006	1.007±0.006	-0.004±0.004	-0.018±0.006
6.7	-0.2±0.3	-0.7±0.2	-0.52±0.01	-1.52±0.02	0.998±0.006	0.998±0.006	-0.013±0.004	0.004±0.006
7.7	-1.2±0.3	-1.2±0.3	-0.53±0.01	-1.52±0.02	0.994±0.006	0.994±0.006	-0.020±0.004	0.021±0.005
8.7	-2.2±0.3	-1.6±0.3	-0.54±0.01	-1.52±0.02	0.991±0.006	0.990±0.006	-0.028±0.004	0.037±0.005
9.8	-3.0±0.3	-1.9±0.3	-0.54±0.01	-1.52±0.02	0.991±0.006	0.989±0.006	-0.032±0.004	0.051±0.005
10.8	-3.8±0.3	-2.1±0.3	-0.53±0.01	-1.52±0.02	0.994±0.006	0.991±0.006	-0.037±0.004	0.065±0.005
11.8	-4.5±0.3	-2.3±0.3	-0.53±0.01	-1.52±0.02	0.996±0.006	0.992±0.006	-0.040±0.004	0.079±0.005
12.8	-5.1±0.3	-2.4±0.2	-0.52±0.01	-1.52±0.02	1.001±0.006	0.996±0.006	-0.042±0.004	0.090±0.006
13.8	-5.8±0.3	-2.5±0.2	-0.51±0.01	-1.52±0.02	1.006±0.006	0.999±0.006	-0.044±0.004	0.101±0.006
16.4	-7.0±0.3	-2.5±0.2	-0.48±0.01	-1.52±0.02	1.019±0.006	1.011±0.006	-0.045±0.004	0.124±0.006
18.9	-7.8±0.3	-2.3±0.2	-0.45±0.01	-1.52±0.02	1.034±0.006	1.023±0.006	-0.042±0.004	0.141±0.006
21.4	-8.5±0.3	-2.1±0.2	-0.42±0.01	-1.52±0.02	1.047±0.006	1.035±0.006	-0.037±0.004	0.154±0.006
24.0	-9.0±0.3	-1.8±0.2	-0.40±0.01	-1.52±0.02	1.061±0.006	1.047±0.006	-0.033±0.004	0.165±0.006
26.5	-9.2±0.3	-1.6±0.2	-0.37±0.01	-1.52±0.02	1.073±0.007	1.059±0.007	-0.029±0.004	0.172±0.006
29.1	-9.4±0.3	-1.3±0.2	-0.35±0.01	-1.52±0.02	1.084±0.007	1.069±0.007	-0.025±0.004	0.177±0.006
31.6	-9.6±0.3	-1.1±0.2	-0.32±0.01	-1.53±0.02	1.097±0.007	1.082±0.007	-0.021±0.004	0.182±0.006
34.1	-9.6±0.3	-1.0±0.2	-0.30±0.01	-1.53±0.02	1.108±0.007	1.092±0.007	-0.018±0.004	0.186±0.006
36.7	-9.7±0.3	-0.8±0.2	-0.28±0.01	-1.53±0.02	1.118±0.007	1.102±0.007	-0.016±0.004	0.188±0.006
39.2	-9.7±0.3	-0.7±0.2	-0.25±0.01	-1.53±0.02	1.130±0.007	1.114±0.007	-0.013±0.004	0.191±0.006
44.3	-9.7±0.3	-0.5±0.2	-0.21±0.01	-1.53±0.02	1.149±0.007	1.133±0.007	-0.010±0.004	0.193±0.006
49.4	-9.6±0.3	-0.5±0.2	-0.17±0.01	-1.53±0.02	1.167±0.007	1.151±0.007	-0.009±0.004	0.195±0.006
54.5	-9.5±0.3	-0.4±0.2	-0.13±0.01	-1.53±0.02	1.185±0.007	1.168±0.007	-0.008±0.004	0.196±0.007
59.5	-9.5±0.3	-0.4±0.2	-0.09±0.01	-1.53±0.02	1.200±0.007	1.184±0.007	-0.009±0.004	0.197±0.007
64.6	-9.3±0.3	-0.5±0.2	-0.06±0.01	-1.54±0.02	1.214±0.007	1.198±0.007	-0.009±0.004	0.197±0.007
69.7	-9.2±0.3	-0.5±0.2	-0.04±0.01	-1.54±0.02	1.225±0.007	1.209±0.007	-0.011±0.004	0.196±0.007
74.8	-9.1±0.3	-0.6±0.2	-0.02±0.01	-1.54±0.02	1.234±0.007	1.218±0.007	-0.012±0.004	0.194±0.007
79.9	-8.9±0.3	-0.6±0.2	-0.00±0.01	-1.54±0.02	1.240±0.007	1.225±0.007	-0.013±0.003	0.192±0.007
84.9	-8.8±0.3	-0.7±0.2	0.01±0.01	-1.54±0.02	1.244±0.007	1.229±0.007	-0.015±0.003	0.190±0.007
90.0	-8.6±0.3	-0.7±0.2	0.01±0.01	-1.54±0.02	1.246±0.007	1.231±0.007	-0.016±0.003	0.187±0.007
100.2	-8.4±0.3	-0.9±0.2	0.01±0.01	-1.54±0.02	1.246±0.007	1.233±0.007	-0.018±0.003	0.182±0.007
110.3	-8.2±0.3	-1.0±0.2	0.01±0.01	-1.54±0.02	1.246±0.007	1.233±0.007	-0.021±0.003	0.177±0.007
120.5	-8.0±0.3	-1.1±0.2	0.01±0.01	-1.54±0.02	1.244±0.007	1.232±0.007	-0.024±0.003	0.173±0.007
130.7	-7.9±0.3	-1.2±0.2	0.01±0.01	-1.53±0.02	1.242±0.007	1.230±0.007	-0.026±0.003	0.170±0.007
140.8	-7.8±0.3	-1.3±0.2	0.01±0.01	-1.53±0.02	1.240±0.007	1.228±0.007	-0.028±0.003	0.167±0.007

Table D.32 Five-Hole Probe Data at (x,z)=(127 mm,-89 mm)

y, mm	BETA, deg	ALPHA, deg	CPT	CPS	SPEED	U	V	W
3.7	1.3±0.3	1.3±0.2	-0.42±0.01	-1.51±0.02	1.044±0.006	1.044±0.006	0.023±0.004	-0.023±0.006
4.7	0.0±0.3	0.6±0.2	-0.44±0.01	-1.52±0.02	1.039±0.006	1.039±0.006	0.011±0.004	-0.001±0.006
5.7	-1.2±0.3	0.2±0.2	-0.47±0.01	-1.53±0.02	1.032±0.006	1.032±0.006	0.003±0.004	0.021±0.006
6.7	-2.3±0.3	-0.2±0.2	-0.48±0.01	-1.53±0.02	1.024±0.006	1.023±0.006	-0.004±0.004	0.041±0.006
7.7	-3.2±0.3	-0.5±0.2	-0.49±0.01	-1.53±0.02	1.023±0.006	1.022±0.006	-0.010±0.004	0.058±0.006
8.7	-4.1±0.3	-0.9±0.2	-0.49±0.01	-1.53±0.02	1.022±0.006	1.019±0.006	-0.015±0.004	0.073±0.006
9.8	-4.8±0.3	-1.1±0.2	-0.49±0.01	-1.53±0.02	1.023±0.006	1.019±0.006	-0.020±0.004	0.085±0.006
10.8	-5.4±0.3	-1.3±0.2	-0.48±0.01	-1.53±0.02	1.025±0.006	1.020±0.006	-0.023±0.004	0.096±0.006
11.8	-5.9±0.3	-1.5±0.2	-0.48±0.01	-1.53±0.02	1.028±0.006	1.022±0.006	-0.026±0.004	0.106±0.006
12.8	-6.4±0.3	-1.6±0.2	-0.47±0.01	-1.53±0.02	1.030±0.006	1.023±0.006	-0.029±0.004	0.116±0.006
13.8	-6.8±0.3	-1.7±0.2	-0.46±0.01	-1.53±0.02	1.034±0.006	1.026±0.006	-0.030±0.004	0.123±0.006
16.4	-7.7±0.3	-1.8±0.2	-0.44±0.01	-1.54±0.02	1.046±0.006	1.036±0.006	-0.033±0.004	0.140±0.006
18.9	-8.4±0.3	-1.7±0.2	-0.42±0.01	-1.54±0.02	1.056±0.006	1.044±0.006	-0.032±0.004	0.155±0.006
21.4	-9.0±0.3	-1.7±0.2	-0.39±0.01	-1.53±0.02	1.068±0.007	1.054±0.007	-0.031±0.004	0.166±0.006
24.0	-9.4±0.3	-1.6±0.2	-0.37±0.01	-1.54±0.02	1.080±0.007	1.065±0.007	-0.029±0.004	0.176±0.006
26.5	-9.7±0.3	-1.4±0.2	-0.35±0.01	-1.54±0.02	1.091±0.007	1.075±0.007	-0.027±0.004	0.184±0.006
29.1	-9.9±0.3	-1.3±0.2	-0.33±0.01	-1.54±0.02	1.102±0.007	1.085±0.007	-0.024±0.004	0.190±0.006
31.6	-10.1±0.3	-1.1±0.2	-0.30±0.01	-1.54±0.02	1.112±0.007	1.095±0.007	-0.022±0.004	0.195±0.006
34.1	-10.2±0.3	-1.0±0.2	-0.28±0.01	-1.54±0.02	1.122±0.007	1.104±0.007	-0.020±0.004	0.199±0.006
36.7	-10.3±0.3	-0.9±0.2	-0.26±0.01	-1.55±0.02	1.135±0.007	1.116±0.007	-0.018±0.004	0.203±0.006
39.2	-10.4±0.3	-0.8±0.2	-0.24±0.01	-1.54±0.02	1.144±0.007	1.125±0.007	-0.017±0.004	0.206±0.006
44.3	-10.4±0.3	-0.7±0.2	-0.20±0.01	-1.55±0.02	1.163±0.007	1.144±0.007	-0.014±0.004	0.210±0.006
49.4	-10.4±0.3	-0.6±0.2	-0.16±0.01	-1.55±0.02	1.180±0.007	1.160±0.007	-0.013±0.004	0.214±0.007
54.5	-10.4±0.3	-0.6±0.2	-0.12±0.01	-1.55±0.02	1.196±0.007	1.176±0.007	-0.013±0.004	0.215±0.007
59.5	-10.3±0.3	-0.6±0.2	-0.09±0.01	-1.55±0.02	1.211±0.007	1.191±0.007	-0.013±0.004	0.217±0.007
64.6	-10.2±0.3	-0.6±0.2	-0.06±0.01	-1.56±0.02	1.225±0.007	1.205±0.007	-0.013±0.004	0.217±0.007
69.7	-10.0±0.3	-0.7±0.2	-0.03±0.01	-1.56±0.02	1.235±0.007	1.216±0.007	-0.015±0.004	0.216±0.007
74.8	-9.9±0.3	-0.8±0.2	-0.02±0.01	-1.56±0.02	1.243±0.007	1.224±0.007	-0.016±0.003	0.214±0.007
79.9	-9.8±0.3	-0.8±0.2	-0.00±0.01	-1.56±0.02	1.248±0.007	1.230±0.007	-0.017±0.003	0.212±0.007
84.9	-9.7±0.3	-0.9±0.2	0.00±0.01	-1.56±0.02	1.252±0.007	1.234±0.007	-0.019±0.003	0.210±0.007
90.0	-9.5±0.3	-0.9±0.2	0.01±0.01	-1.56±0.02	1.253±0.007	1.236±0.007	-0.020±0.003	0.208±0.007
100.2	-9.3±0.3	-1.0±0.2	0.01±0.01	-1.56±0.02	1.255±0.007	1.239±0.007	-0.022±0.003	0.202±0.007
110.3	-9.0±0.3	-1.1±0.2	0.01±0.01	-1.56±0.02	1.255±0.007	1.239±0.007	-0.024±0.003	0.197±0.007
120.5	-8.9±0.3	-1.2±0.2	0.01±0.01	-1.56±0.02	1.253±0.007	1.238±0.007	-0.026±0.003	0.193±0.007
130.7	-8.8±0.3	-1.3±0.2	0.01±0.01	-1.56±0.02	1.252±0.007	1.237±0.007	-0.027±0.003	0.190±0.007
140.8	-8.7±0.3	-1.4±0.2	0.01±0.01	-1.55±0.02	1.249±0.007	1.234±0.007	-0.030±0.003	0.188±0.007

Table D.33 Five-Hole Probe Data at (x,z)=(127 mm,-83 mm)

y, mm	BETA, deg	ALPHA, deg	CPT	CPS	SPEED	U	V	W
3.7	-0.3±0.3	1.4±0.2	-0.40±0.01	-1.53±0.02	1.063±0.007	1.063±0.007	0.026±0.004	0.005±0.006
4.7	-1.4±0.3	0.8±0.2	-0.42±0.01	-1.53±0.02	1.056±0.006	1.056±0.006	0.015±0.004	0.027±0.006
5.7	-2.7±0.3	0.4±0.2	-0.43±0.01	-1.54±0.02	1.051±0.006	1.050±0.006	0.007±0.004	0.049±0.006
6.7	-3.7±0.3	0.0±0.2	-0.44±0.01	-1.54±0.02	1.046±0.006	1.044±0.006	0.000±0.004	0.068±0.006
7.7	-4.6±0.3	-0.3±0.2	-0.45±0.01	-1.54±0.02	1.045±0.006	1.042±0.006	-0.006±0.004	0.085±0.006
8.7	-5.4±0.3	-0.5±0.2	-0.45±0.01	-1.54±0.02	1.046±0.006	1.041±0.006	-0.010±0.004	0.098±0.006
9.8	-6.0±0.3	-0.8±0.2	-0.45±0.01	-1.55±0.02	1.047±0.006	1.041±0.006	-0.014±0.004	0.110±0.006
10.8	-6.5±0.3	-0.9±0.2	-0.44±0.01	-1.54±0.02	1.049±0.006	1.042±0.006	-0.017±0.004	0.118±0.006
11.8	-7.0±0.3	-1.1±0.2	-0.44±0.01	-1.55±0.02	1.051±0.006	1.043±0.006	-0.020±0.004	0.127±0.006
12.8	-7.3±0.3	-1.2±0.2	-0.43±0.01	-1.55±0.02	1.055±0.006	1.046±0.006	-0.022±0.004	0.134±0.006
13.8	-7.7±0.3	-1.3±0.2	-0.43±0.01	-1.55±0.02	1.059±0.006	1.049±0.006	-0.024±0.004	0.141±0.006
16.4	-8.4±0.3	-1.5±0.2	-0.41±0.01	-1.55±0.02	1.068±0.007	1.057±0.007	-0.027±0.004	0.155±0.006
18.9	-9.0±0.3	-1.5±0.2	-0.39±0.01	-1.55±0.02	1.077±0.007	1.063±0.007	-0.028±0.004	0.168±0.006
21.4	-9.4±0.3	-1.5±0.2	-0.37±0.01	-1.55±0.02	1.088±0.007	1.073±0.007	-0.027±0.004	0.178±0.006
24.0	-9.8±0.3	-1.4±0.2	-0.35±0.01	-1.55±0.02	1.098±0.007	1.081±0.007	-0.027±0.004	0.186±0.006
26.5	-10.0±0.3	-1.4±0.2	-0.33±0.01	-1.56±0.02	1.109±0.007	1.091±0.007	-0.026±0.004	0.193±0.006
29.1	-10.3±0.3	-1.3±0.2	-0.30±0.01	-1.56±0.02	1.119±0.007	1.101±0.007	-0.025±0.004	0.199±0.006
31.6	-10.4±0.3	-1.3±0.2	-0.28±0.01	-1.56±0.02	1.129±0.007	1.110±0.007	-0.024±0.004	0.205±0.006
34.1	-10.6±0.3	-1.2±0.2	-0.26±0.01	-1.56±0.02	1.140±0.007	1.120±0.007	-0.023±0.004	0.210±0.006
36.7	-10.7±0.3	-1.1±0.2	-0.24±0.01	-1.56±0.02	1.149±0.007	1.129±0.007	-0.021±0.004	0.213±0.006
39.2	-10.8±0.3	-1.1±0.2	-0.22±0.01	-1.56±0.02	1.158±0.007	1.137±0.007	-0.021±0.004	0.217±0.006
44.3	-10.9±0.3	-1.0±0.2	-0.18±0.01	-1.57±0.02	1.177±0.007	1.155±0.007	-0.019±0.004	0.223±0.007
49.4	-10.9±0.3	-0.9±0.2	-0.14±0.01	-1.57±0.02	1.194±0.007	1.172±0.007	-0.019±0.004	0.227±0.007
54.5	-10.9±0.3	-0.9±0.2	-0.11±0.01	-1.57±0.02	1.207±0.007	1.185±0.007	-0.018±0.004	0.229±0.007
59.5	-10.9±0.3	-0.9±0.2	-0.08±0.01	-1.58±0.02	1.223±0.007	1.201±0.007	-0.018±0.004	0.231±0.007
64.6	-10.8±0.3	-0.9±0.2	-0.05±0.01	-1.58±0.02	1.234±0.007	1.212±0.007	-0.020±0.004	0.231±0.007
69.7	-10.7±0.3	-1.0±0.2	-0.03±0.01	-1.58±0.02	1.244±0.007	1.223±0.007	-0.021±0.003	0.231±0.007
74.8	-10.6±0.3	-1.0±0.2	-0.01±0.01	-1.58±0.02	1.252±0.007	1.230±0.007	-0.022±0.003	0.229±0.007
79.9	-10.4±0.3	-1.1±0.2	0.00±0.01	-1.58±0.02	1.257±0.007	1.236±0.007	-0.023±0.003	0.227±0.007
84.9	-10.3±0.3	-1.1±0.2	0.00±0.01	-1.58±0.02	1.260±0.007	1.240±0.007	-0.024±0.003	0.225±0.007
90.0	-10.1±0.3	-1.2±0.2	0.01±0.01	-1.58±0.02	1.262±0.007	1.242±0.007	-0.026±0.003	0.222±0.007
100.2	-9.9±0.3	-1.2±0.2	0.01±0.01	-1.58±0.02	1.263±0.007	1.244±0.007	-0.027±0.003	0.216±0.007
110.3	-9.7±0.3	-1.3±0.2	0.01±0.01	-1.58±0.02	1.263±0.007	1.245±0.007	-0.027±0.003	0.212±0.007
120.5	-9.5±0.3	-1.3±0.2	0.01±0.01	-1.58±0.02	1.262±0.007	1.244±0.007	-0.028±0.003	0.208±0.007
130.7	-9.4±0.3	-1.4±0.2	0.01±0.01	-1.58±0.02	1.260±0.007	1.243±0.007	-0.030±0.003	0.205±0.007
140.8	-9.3±0.3	-1.5±0.2	0.01±0.01	-1.57±0.02	1.257±0.007	1.240±0.007	-0.032±0.003	0.204±0.007

Table D.34 Five-Hole Probe Data at (x,z)=(127 mm,-76 mm)

y, mm	BETA, deg	ALPHA, deg	CPT	CPS	SPEED	U	V	W
3.7	-2.2±0.3	1.5±0.2	-0.37±0.01	-1.53±0.02	1.079±0.007	1.078±0.007	0.027±0.004	0.042±0.006
4.7	-3.4±0.3	0.8±0.2	-0.38±0.01	-1.53±0.02	1.072±0.007	1.070±0.007	0.015±0.004	0.064±0.006
5.7	-4.5±0.3	0.4±0.2	-0.40±0.01	-1.54±0.02	1.068±0.007	1.064±0.007	0.007±0.004	0.084±0.006
6.7	-5.6±0.3	-0.0±0.2	-0.41±0.01	-1.54±0.02	1.064±0.007	1.059±0.006	-0.001±0.004	0.103±0.006
7.7	-6.4±0.3	-0.4±0.2	-0.41±0.01	-1.54±0.02	1.061±0.007	1.054±0.006	-0.007±0.004	0.118±0.006
8.7	-7.0±0.3	-0.6±0.2	-0.41±0.01	-1.54±0.02	1.063±0.007	1.055±0.006	-0.011±0.004	0.130±0.006
9.8	-7.5±0.3	-0.9±0.2	-0.41±0.01	-1.54±0.02	1.064±0.007	1.054±0.006	-0.016±0.004	0.139±0.006
10.8	-8.0±0.3	-1.0±0.2	-0.41±0.01	-1.54±0.02	1.063±0.007	1.053±0.006	-0.019±0.004	0.148±0.006
11.8	-8.4±0.3	-1.1±0.2	-0.41±0.01	-1.54±0.02	1.067±0.007	1.055±0.007	-0.021±0.004	0.155±0.006
12.8	-8.7±0.3	-1.3±0.2	-0.40±0.01	-1.54±0.02	1.068±0.007	1.056±0.007	-0.024±0.004	0.162±0.006
13.8	-9.0±0.3	-1.4±0.2	-0.39±0.01	-1.54±0.02	1.071±0.007	1.058±0.007	-0.026±0.004	0.168±0.006
16.4	-9.6±0.3	-1.5±0.2	-0.38±0.01	-1.55±0.02	1.081±0.007	1.066±0.007	-0.028±0.004	0.180±0.006
18.9	-10.1±0.3	-1.6±0.2	-0.36±0.01	-1.55±0.02	1.090±0.007	1.073±0.007	-0.031±0.004	0.191±0.006
21.4	-10.5±0.3	-1.6±0.2	-0.34±0.01	-1.55±0.02	1.099±0.007	1.080±0.007	-0.031±0.004	0.200±0.006
24.0	-10.8±0.3	-1.7±0.2	-0.32±0.01	-1.55±0.02	1.109±0.007	1.089±0.007	-0.031±0.004	0.208±0.006
26.5	-11.0±0.3	-1.6±0.2	-0.30±0.01	-1.55±0.02	1.120±0.007	1.099±0.007	-0.030±0.004	0.214±0.006
29.1	-11.3±0.3	-1.6±0.2	-0.28±0.01	-1.55±0.02	1.129±0.007	1.107±0.007	-0.030±0.004	0.220±0.006
31.6	-11.5±0.3	-1.5±0.2	-0.26±0.01	-1.55±0.02	1.139±0.007	1.116±0.007	-0.030±0.004	0.226±0.006
34.1	-11.6±0.3	-1.5±0.2	-0.24±0.01	-1.56±0.02	1.149±0.007	1.125±0.007	-0.029±0.004	0.231±0.006
36.7	-11.7±0.3	-1.4±0.2	-0.22±0.01	-1.56±0.02	1.157±0.007	1.133±0.007	-0.029±0.004	0.234±0.006
39.2	-11.8±0.3	-1.4±0.2	-0.20±0.01	-1.56±0.02	1.166±0.007	1.141±0.007	-0.028±0.004	0.239±0.006
44.3	-11.9±0.3	-1.3±0.2	-0.16±0.01	-1.56±0.02	1.183±0.007	1.157±0.007	-0.027±0.004	0.245±0.007
49.4	-12.0±0.3	-1.3±0.2	-0.13±0.01	-1.57±0.02	1.200±0.007	1.173±0.007	-0.026±0.004	0.250±0.007
54.5	-12.0±0.3	-1.3±0.2	-0.10±0.01	-1.57±0.02	1.213±0.007	1.187±0.007	-0.026±0.004	0.253±0.007
59.5	-12.0±0.3	-1.3±0.2	-0.07±0.01	-1.58±0.02	1.226±0.007	1.199±0.007	-0.026±0.004	0.255±0.007
64.6	-11.9±0.3	-1.3±0.2	-0.04±0.01	-1.57±0.02	1.238±0.007	1.211±0.007	-0.027±0.004	0.256±0.007
69.7	-11.8±0.3	-1.3±0.2	-0.02±0.01	-1.58±0.02	1.246±0.007	1.219±0.007	-0.028±0.003	0.256±0.007
74.8	-11.7±0.3	-1.4±0.2	-0.01±0.01	-1.58±0.02	1.252±0.007	1.226±0.007	-0.029±0.003	0.254±0.007
79.9	-11.5±0.3	-1.4±0.2	0.00±0.01	-1.58±0.02	1.257±0.007	1.231±0.007	-0.030±0.003	0.252±0.007
84.9	-11.4±0.3	-1.4±0.2	0.01±0.01	-1.58±0.02	1.260±0.007	1.234±0.007	-0.031±0.003	0.249±0.007
90.0	-11.2±0.3	-1.5±0.2	0.01±0.01	-1.58±0.02	1.261±0.007	1.237±0.007	-0.032±0.003	0.245±0.007
100.2	-11.0±0.3	-1.4±0.2	0.01±0.01	-1.58±0.02	1.263±0.007	1.239±0.007	-0.031±0.003	0.240±0.007
110.3	-10.8±0.3	-1.4±0.2	0.01±0.01	-1.58±0.02	1.262±0.007	1.240±0.007	-0.030±0.003	0.236±0.007
120.5	-10.6±0.3	-1.4±0.2	0.01±0.01	-1.58±0.02	1.261±0.007	1.239±0.007	-0.031±0.003	0.233±0.007
130.7	-10.6±0.3	-1.5±0.2	0.01±0.01	-1.58±0.02	1.260±0.007	1.238±0.007	-0.033±0.003	0.232±0.007
140.8	-10.5±0.3	-1.6±0.2	0.01±0.01	-1.57±0.02	1.256±0.007	1.235±0.007	-0.035±0.003	0.229±0.007

Table D.35 Five-Hole Probe Data at (x,z)=(127 mm,-70 mm)

y, mm	BETA, deg	ALPHA, deg	CPT	CPS	SPEED	U	V	W
3.7	-4.1±0.3	1.1±0.2	-0.33±0.01	-1.53±0.02	1.098±0.007	1.095±0.007	0.021±0.004	0.078±0.006
4.7	-5.1±0.3	0.3±0.2	-0.35±0.01	-1.54±0.02	1.093±0.007	1.088±0.007	0.005±0.004	0.098±0.006
5.7	-6.1±0.3	-0.3±0.2	-0.36±0.01	-1.54±0.02	1.088±0.007	1.082±0.007	-0.005±0.004	0.115±0.006
6.7	-6.9±0.3	-0.8±0.2	-0.37±0.01	-1.55±0.02	1.084±0.007	1.076±0.007	-0.014±0.004	0.131±0.006
7.7	-7.6±0.3	-1.1±0.2	-0.37±0.01	-1.55±0.02	1.085±0.007	1.075±0.007	-0.021±0.004	0.143±0.006
8.7	-8.1±0.3	-1.4±0.2	-0.37±0.01	-1.55±0.02	1.084±0.007	1.073±0.007	-0.026±0.004	0.153±0.006
9.8	-8.6±0.3	-1.6±0.2	-0.37±0.01	-1.55±0.02	1.086±0.007	1.073±0.007	-0.030±0.004	0.162±0.006
10.8	-8.9±0.3	-1.8±0.2	-0.37±0.01	-1.55±0.02	1.089±0.007	1.075±0.007	-0.034±0.004	0.169±0.006
11.8	-9.3±0.3	-1.9±0.2	-0.36±0.01	-1.55±0.02	1.091±0.007	1.076±0.007	-0.036±0.004	0.176±0.006
12.8	-9.5±0.3	-2.0±0.2	-0.36±0.01	-1.55±0.02	1.093±0.007	1.077±0.007	-0.038±0.004	0.181±0.006
13.8	-9.7±0.3	-2.1±0.2	-0.36±0.01	-1.56±0.02	1.097±0.007	1.080±0.007	-0.040±0.004	0.185±0.006
16.4	-10.2±0.3	-2.2±0.2	-0.34±0.01	-1.56±0.02	1.105±0.007	1.087±0.007	-0.043±0.004	0.196±0.006
18.9	-10.6±0.3	-2.3±0.2	-0.32±0.01	-1.56±0.02	1.113±0.007	1.093±0.007	-0.043±0.004	0.205±0.006
21.4	-11.0±0.3	-2.2±0.2	-0.30±0.01	-1.56±0.02	1.122±0.007	1.101±0.007	-0.043±0.004	0.215±0.006
24.0	-11.3±0.3	-2.3±0.2	-0.29±0.01	-1.57±0.02	1.131±0.007	1.108±0.007	-0.044±0.004	0.221±0.006
26.5	-11.5±0.3	-2.2±0.2	-0.27±0.01	-1.57±0.02	1.140±0.007	1.116±0.007	-0.044±0.004	0.228±0.006
29.1	-11.8±0.3	-2.2±0.2	-0.25±0.01	-1.58±0.02	1.150±0.007	1.125±0.007	-0.043±0.004	0.234±0.006
31.6	-11.9±0.3	-2.1±0.2	-0.23±0.01	-1.57±0.02	1.158±0.007	1.132±0.007	-0.042±0.004	0.239±0.006
34.1	-12.1±0.3	-2.1±0.2	-0.22±0.01	-1.58±0.02	1.167±0.007	1.140±0.007	-0.042±0.004	0.244±0.006
36.7	-12.2±0.3	-2.1±0.2	-0.20±0.01	-1.58±0.02	1.175±0.007	1.147±0.007	-0.041±0.004	0.249±0.006
39.2	-12.3±0.3	-2.0±0.2	-0.18±0.01	-1.58±0.02	1.183±0.007	1.155±0.007	-0.041±0.004	0.253±0.007
44.3	-12.4±0.3	-2.0±0.2	-0.15±0.01	-1.59±0.02	1.200±0.007	1.171±0.007	-0.040±0.004	0.258±0.007
49.4	-12.5±0.3	-1.9±0.2	-0.12±0.01	-1.59±0.02	1.214±0.007	1.184±0.007	-0.039±0.004	0.263±0.007
54.5	-12.6±0.3	-1.9±0.2	-0.09±0.01	-1.59±0.02	1.226±0.007	1.196±0.007	-0.039±0.004	0.267±0.007
59.5	-12.6±0.3	-1.8±0.2	-0.06±0.01	-1.59±0.02	1.238±0.007	1.208±0.007	-0.038±0.004	0.270±0.007
64.6	-12.5±0.3	-1.8±0.2	-0.04±0.01	-1.60±0.02	1.250±0.007	1.220±0.007	-0.038±0.003	0.271±0.007
69.7	-12.4±0.3	-1.8±0.2	-0.02±0.01	-1.60±0.02	1.257±0.007	1.227±0.007	-0.038±0.003	0.271±0.007
74.8	-12.3±0.3	-1.8±0.2	-0.01±0.01	-1.60±0.02	1.265±0.007	1.235±0.007	-0.038±0.003	0.270±0.007
79.9	-12.2±0.3	-1.8±0.2	0.00±0.01	-1.60±0.02	1.268±0.007	1.239±0.007	-0.038±0.003	0.268±0.007
84.9	-12.0±0.3	-1.8±0.2	0.01±0.01	-1.61±0.02	1.270±0.007	1.242±0.007	-0.038±0.003	0.264±0.007
90.0	-11.8±0.3	-1.7±0.2	0.01±0.01	-1.61±0.02	1.272±0.007	1.244±0.007	-0.037±0.003	0.261±0.007
100.2	-11.6±0.3	-1.6±0.2	0.01±0.01	-1.61±0.02	1.273±0.007	1.246±0.007	-0.034±0.003	0.255±0.007
110.3	-11.5±0.3	-1.5±0.2	0.01±0.01	-1.61±0.02	1.273±0.007	1.247±0.007	-0.033±0.003	0.253±0.007
120.5	-11.4±0.3	-1.5±0.2	0.01±0.01	-1.61±0.02	1.272±0.007	1.246±0.007	-0.033±0.003	0.250±0.007
130.7	-11.4±0.3	-1.6±0.2	0.01±0.01	-1.60±0.02	1.269±0.007	1.244±0.007	-0.035±0.003	0.250±0.007
140.8	-11.3±0.3	-1.7±0.2	0.01±0.01	-1.59±0.02	1.265±0.007	1.240±0.007	-0.038±0.003	0.248±0.007

Table D.36 Five-Hole Probe Data at (x,z)=(127 mm,-64 mm)

y, mm	BETA, deg	ALPHA, deg	CPT	CPS	SPEED	U	V	W
3.7	-7.1±0.3	-0.5±0.2	-0.28±0.01	-1.50±0.02	1.106±0.007	1.097±0.007	-0.010±0.004	0.136±0.006
4.7	-7.5±0.3	-1.8±0.2	-0.28±0.01	-1.50±0.02	1.105±0.007	1.095±0.007	-0.035±0.004	0.144±0.006
5.7	-8.0±0.3	-2.7±0.2	-0.29±0.01	-1.50±0.02	1.103±0.007	1.091±0.007	-0.051±0.004	0.153±0.006
6.7	-8.4±0.3	-3.2±0.2	-0.29±0.01	-1.50±0.02	1.102±0.007	1.088±0.007	-0.061±0.004	0.161±0.006
7.7	-8.7±0.3	-3.6±0.2	-0.29±0.01	-1.51±0.02	1.102±0.007	1.088±0.007	-0.068±0.004	0.167±0.006
8.7	-9.0±0.3	-3.8±0.2	-0.29±0.01	-1.51±0.02	1.104±0.007	1.088±0.007	-0.073±0.004	0.173±0.006
9.8	-9.3±0.3	-4.0±0.2	-0.29±0.01	-1.51±0.02	1.104±0.007	1.087±0.007	-0.076±0.004	0.178±0.006
10.8	-9.5±0.3	-4.1±0.2	-0.29±0.01	-1.51±0.02	1.105±0.007	1.087±0.007	-0.078±0.004	0.182±0.006
11.8	-9.7±0.3	-4.2±0.2	-0.29±0.01	-1.51±0.02	1.107±0.007	1.088±0.007	-0.079±0.004	0.186±0.006
12.8	-9.9±0.3	-4.1±0.2	-0.28±0.01	-1.52±0.02	1.110±0.007	1.091±0.007	-0.079±0.004	0.191±0.006
13.8	-10.1±0.3	-4.2±0.2	-0.28±0.01	-1.52±0.02	1.112±0.007	1.092±0.007	-0.080±0.004	0.194±0.006
16.4	-10.5±0.3	-4.1±0.2	-0.27±0.01	-1.52±0.02	1.117±0.007	1.096±0.007	-0.078±0.004	0.203±0.006
18.9	-10.9±0.3	-4.0±0.2	-0.26±0.01	-1.53±0.02	1.126±0.007	1.103±0.007	-0.077±0.004	0.211±0.006
21.4	-11.2±0.3	-3.9±0.2	-0.25±0.01	-1.52±0.02	1.131±0.007	1.107±0.007	-0.076±0.004	0.219±0.006
24.0	-11.5±0.3	-3.9±0.2	-0.23±0.01	-1.53±0.02	1.140±0.007	1.114±0.007	-0.075±0.004	0.227±0.006
26.5	-11.8±0.3	-3.8±0.2	-0.21±0.01	-1.53±0.02	1.148±0.007	1.122±0.007	-0.074±0.004	0.234±0.006
29.1	-12.0±0.3	-3.7±0.2	-0.20±0.01	-1.53±0.02	1.155±0.007	1.128±0.007	-0.074±0.004	0.240±0.006
31.6	-12.2±0.3	-3.7±0.2	-0.19±0.01	-1.54±0.02	1.163±0.007	1.134±0.007	-0.074±0.004	0.245±0.006
34.1	-12.4±0.3	-3.7±0.2	-0.17±0.01	-1.54±0.02	1.170±0.007	1.141±0.007	-0.073±0.004	0.250±0.006
36.7	-12.5±0.3	-3.6±0.2	-0.16±0.01	-1.55±0.02	1.179±0.007	1.149±0.007	-0.072±0.004	0.255±0.007
39.2	-12.6±0.3	-3.5±0.2	-0.14±0.01	-1.55±0.02	1.187±0.007	1.156±0.007	-0.071±0.004	0.259±0.007
44.3	-12.8±0.3	-3.4±0.2	-0.11±0.01	-1.55±0.02	1.200±0.007	1.169±0.007	-0.069±0.004	0.265±0.007
49.4	-12.9±0.3	-3.2±0.2	-0.09±0.01	-1.56±0.02	1.213±0.007	1.180±0.007	-0.066±0.004	0.270±0.007
54.5	-13.0±0.3	-3.1±0.2	-0.07±0.01	-1.57±0.02	1.225±0.007	1.192±0.007	-0.064±0.004	0.275±0.007
59.5	-13.0±0.3	-2.9±0.2	-0.04±0.01	-1.57±0.02	1.235±0.007	1.202±0.007	-0.061±0.004	0.278±0.007
64.6	-13.0±0.3	-2.7±0.2	-0.03±0.01	-1.58±0.02	1.245±0.007	1.211±0.007	-0.058±0.004	0.280±0.007
69.7	-13.0±0.3	-2.6±0.2	-0.01±0.01	-1.58±0.02	1.253±0.007	1.220±0.007	-0.055±0.004	0.281±0.007
74.8	-12.9±0.3	-2.4±0.2	-0.00±0.01	-1.59±0.02	1.259±0.007	1.226±0.007	-0.051±0.003	0.281±0.007
79.9	-12.8±0.3	-2.2±0.2	0.00±0.01	-1.59±0.02	1.264±0.007	1.231±0.007	-0.048±0.003	0.280±0.007
84.9	-12.7±0.3	-2.1±0.2	0.01±0.01	-1.60±0.02	1.266±0.007	1.235±0.007	-0.045±0.003	0.278±0.007
90.0	-12.5±0.3	-1.9±0.2	0.01±0.01	-1.60±0.02	1.269±0.007	1.238±0.007	-0.042±0.003	0.275±0.007
100.2	-12.4±0.3	-1.7±0.2	0.01±0.01	-1.61±0.02	1.271±0.007	1.241±0.007	-0.036±0.003	0.273±0.007
110.3	-12.4±0.3	-1.5±0.2	0.01±0.01	-1.60±0.02	1.271±0.007	1.240±0.007	-0.033±0.003	0.274±0.007
120.5	-12.4±0.3	-1.5±0.2	0.01±0.01	-1.60±0.02	1.270±0.007	1.240±0.007	-0.032±0.003	0.273±0.007
130.7	-12.4±0.3	-1.5±0.2	0.01±0.01	-1.60±0.02	1.268±0.007	1.238±0.007	-0.033±0.003	0.273±0.007
140.8	-12.4±0.3	-1.7±0.2	0.01±0.01	-1.59±0.02	1.265±0.007	1.235±0.007	-0.037±0.003	0.272±0.007

Table D.37 Five-Hole Probe Data at (x,z)=(-203 mm,0)

y, mm	ALPHA, deg	CPT	CPS	SPEED	U	V
3.7	0.9±0.8	-0.72±0.01	-1.04±0.02	0.564±0.008	0.563±0.008	0.009±0.008
4.7	0.3±0.7	-0.70±0.01	-1.04±0.02	0.588±0.008	0.588±0.008	0.003±0.008
5.7	0.1±0.7	-0.67±0.01	-1.04±0.02	0.610±0.008	0.610±0.008	0.001±0.007
6.7	-0.1±0.7	-0.65±0.01	-1.04±0.02	0.626±0.008	0.626±0.008	-0.001±0.007
7.7	-0.2±0.6	-0.63±0.01	-1.05±0.02	0.645±0.007	0.645±0.007	-0.002±0.007
8.7	-0.2±0.6	-0.61±0.01	-1.04±0.02	0.657±0.007	0.657±0.007	-0.003±0.007
9.8	-0.2±0.6	-0.60±0.01	-1.05±0.02	0.670±0.007	0.670±0.007	-0.003±0.007
10.8	-0.2±0.6	-0.58±0.01	-1.04±0.02	0.678±0.007	0.678±0.007	-0.002±0.007
11.8	-0.2±0.5	-0.57±0.01	-1.05±0.02	0.691±0.007	0.691±0.007	-0.003±0.006
12.8	-0.2±0.5	-0.55±0.01	-1.05±0.02	0.702±0.007	0.702±0.007	-0.003±0.006
13.8	-0.2±0.5	-0.55±0.01	-1.05±0.02	0.708±0.007	0.708±0.007	-0.003±0.006
16.4	-0.1±0.5	-0.52±0.01	-1.05±0.02	0.731±0.007	0.731±0.007	-0.001±0.006
18.9	-0.1±0.5	-0.49±0.01	-1.05±0.02	0.752±0.007	0.752±0.007	-0.001±0.006
21.4	-0.0±0.4	-0.46±0.01	-1.05±0.02	0.770±0.007	0.770±0.007	-0.001±0.006
24.0	0.1±0.4	-0.43±0.01	-1.05±0.02	0.786±0.007	0.786±0.007	0.001±0.006
26.5	0.2±0.4	-0.40±0.01	-1.04±0.02	0.803±0.007	0.803±0.007	0.002±0.006
29.1	0.2±0.4	-0.38±0.01	-1.05±0.02	0.821±0.007	0.821±0.007	0.003±0.005
31.6	0.2±0.4	-0.35±0.01	-1.05±0.02	0.836±0.007	0.836±0.007	0.003±0.005
34.1	0.2±0.4	-0.33±0.01	-1.06±0.02	0.853±0.007	0.853±0.007	0.004±0.005
36.7	0.3±0.3	-0.30±0.01	-1.04±0.02	0.864±0.007	0.864±0.007	0.005±0.005
39.2	0.4±0.3	-0.28±0.01	-1.04±0.02	0.875±0.007	0.875±0.007	0.006±0.005
44.3	0.4±0.3	-0.23±0.01	-1.05±0.02	0.904±0.007	0.904±0.007	0.007±0.005
49.4	0.5±0.3	-0.19±0.01	-1.04±0.02	0.926±0.006	0.926±0.006	0.008±0.005
54.5	0.6±0.3	-0.16±0.01	-1.05±0.02	0.947±0.006	0.947±0.006	0.009±0.005
59.5	0.7±0.3	-0.11±0.01	-1.05±0.02	0.968±0.007	0.968±0.007	0.011±0.005
64.6	0.7±0.3	-0.07±0.01	-1.05±0.02	0.986±0.007	0.986±0.007	0.012±0.005
69.7	0.8±0.3	-0.05±0.01	-1.05±0.02	1.001±0.007	1.001±0.007	0.014±0.004
74.8	0.9±0.2	-0.02±0.01	-1.05±0.02	1.011±0.007	1.011±0.007	0.016±0.004
79.9	1.0±0.2	-0.01±0.01	-1.05±0.02	1.020±0.007	1.020±0.007	0.017±0.004
84.9	1.0±0.2	0.00±0.01	-1.05±0.02	1.026±0.007	1.026±0.007	0.017±0.004
90.0	1.0±0.2	0.01±0.01	-1.05±0.02	1.028±0.007	1.028±0.007	0.019±0.004
100.2	1.1±0.2	0.01±0.01	-1.05±0.02	1.030±0.007	1.030±0.007	0.019±0.004
110.3	1.1±0.2	0.01±0.01	-1.05±0.02	1.030±0.007	1.030±0.007	0.021±0.004
120.5	1.2±0.2	0.01±0.01	-1.06±0.02	1.032±0.007	1.031±0.007	0.022±0.004
130.7	1.3±0.2	0.01±0.01	-1.06±0.02	1.034±0.007	1.034±0.007	0.023±0.004
140.8	1.3±0.2	0.01±0.01	-1.06±0.02	1.035±0.007	1.035±0.007	0.023±0.004

Table D.38 Five-Hole Probe Data at (x,z)=(-178 mm,0)

y, mm	ALPHA, deg	CPT	CPS	SPEED	U	V
3.7	1.0±0.9	-0.71±0.01	-0.99±0.02	0.526±0.008	0.526±0.008	0.009±0.008
4.7	0.2±0.8	-0.69±0.01	-0.99±0.02	0.553±0.008	0.553±0.008	0.002±0.008
5.7	-0.1±0.8	-0.67±0.01	-1.00±0.02	0.578±0.008	0.578±0.008	-0.001±0.008
6.7	-0.3±0.7	-0.65±0.01	-1.00±0.02	0.594±0.008	0.594±0.008	-0.003±0.007
7.7	-0.3±0.7	-0.63±0.01	-1.00±0.02	0.612±0.008	0.612±0.008	-0.003±0.007
8.7	-0.3±0.7	-0.61±0.01	-1.00±0.02	0.622±0.007	0.622±0.007	-0.004±0.007
9.8	-0.4±0.6	-0.60±0.01	-1.00±0.02	0.636±0.007	0.636±0.007	-0.004±0.007
10.8	-0.3±0.6	-0.59±0.01	-1.00±0.02	0.647±0.007	0.647±0.007	-0.004±0.007
11.8	-0.4±0.6	-0.57±0.01	-1.00±0.02	0.659±0.007	0.659±0.007	-0.004±0.007
12.8	-0.3±0.6	-0.55±0.01	-1.01±0.02	0.672±0.007	0.672±0.007	-0.003±0.007
13.8	-0.3±0.5	-0.54±0.01	-1.00±0.02	0.679±0.007	0.679±0.007	-0.003±0.006
16.4	-0.2±0.5	-0.51±0.01	-1.01±0.02	0.704±0.007	0.704±0.007	-0.002±0.006
18.9	-0.1±0.5	-0.48±0.01	-1.01±0.02	0.724±0.007	0.724±0.007	-0.002±0.006
21.4	-0.0±0.5	-0.45±0.01	-1.00±0.02	0.742±0.007	0.742±0.007	-0.000±0.006
24.0	0.0±0.4	-0.42±0.01	-1.01±0.02	0.763±0.007	0.763±0.007	0.000±0.006
26.5	0.1±0.4	-0.40±0.01	-1.00±0.02	0.778±0.007	0.778±0.007	0.001±0.006
29.1	0.1±0.4	-0.38±0.01	-1.01±0.02	0.795±0.007	0.795±0.007	0.002±0.006
31.6	0.2±0.4	-0.35±0.01	-1.00±0.02	0.808±0.007	0.808±0.007	0.003±0.005
34.1	0.3±0.4	-0.33±0.01	-1.01±0.02	0.823±0.007	0.823±0.007	0.004±0.005
36.7	0.3±0.4	-0.30±0.01	-1.00±0.02	0.836±0.007	0.836±0.007	0.005±0.005
39.2	0.4±0.4	-0.28±0.01	-1.00±0.02	0.848±0.007	0.848±0.007	0.006±0.005
44.3	0.5±0.3	-0.24±0.01	-1.00±0.02	0.875±0.006	0.875±0.006	0.008±0.005
49.4	0.6±0.3	-0.19±0.01	-1.01±0.02	0.903±0.006	0.903±0.006	0.009±0.005
54.5	0.7±0.3	-0.15±0.01	-1.01±0.02	0.923±0.006	0.923±0.006	0.011±0.005
59.5	0.7±0.3	-0.11±0.01	-1.00±0.02	0.944±0.006	0.944±0.006	0.012±0.005
64.6	0.8±0.3	-0.08±0.01	-1.01±0.02	0.962±0.006	0.962±0.006	0.013±0.005
69.7	0.9±0.3	-0.05±0.01	-1.01±0.02	0.978±0.006	0.977±0.006	0.015±0.005
74.8	1.0±0.3	-0.03±0.01	-1.01±0.02	0.990±0.006	0.990±0.006	0.017±0.004
79.9	1.0±0.3	-0.01±0.01	-1.01±0.02	1.001±0.006	1.000±0.006	0.018±0.004
84.9	1.1±0.3	0.00±0.01	-1.01±0.02	1.005±0.006	1.005±0.006	0.019±0.004
90.0	1.2±0.2	0.01±0.01	-1.01±0.02	1.008±0.006	1.008±0.006	0.021±0.004
100.2	1.2±0.2	0.01±0.01	-1.01±0.02	1.010±0.006	1.009±0.006	0.021±0.004
110.3	1.3±0.2	0.01±0.01	-1.01±0.02	1.010±0.006	1.010±0.006	0.023±0.004
120.5	1.4±0.2	0.01±0.01	-1.01±0.02	1.012±0.006	1.012±0.006	0.024±0.004
130.7	1.5±0.2	0.01±0.01	-1.02±0.02	1.015±0.006	1.014±0.006	0.026±0.004
140.8	1.5±0.2	0.01±0.01	-1.02±0.02	1.016±0.006	1.016±0.006	0.027±0.004

Table D.39 Five-Hole Probe Data at (x,z)=(-152 mm,0)

y, mm	ALPHA, deg	CPT	CPS	SPEED	U	V
3.7	0.6±1.0	-0.72±0.01	-0.98±0.02	0.506±0.009	0.506±0.009	0.005±0.009
4.7	-0.0±0.9	-0.69±0.01	-0.98±0.02	0.532±0.008	0.532±0.008	-0.000±0.008
5.7	-0.3±0.8	-0.67±0.01	-0.98±0.02	0.554±0.008	0.554±0.008	-0.002±0.008
6.7	-0.4±0.8	-0.65±0.01	-0.98±0.02	0.568±0.008	0.568±0.008	-0.004±0.008
7.7	-0.4±0.7	-0.64±0.01	-0.98±0.02	0.583±0.008	0.583±0.008	-0.004±0.008
8.7	-0.4±0.7	-0.62±0.01	-0.98±0.02	0.600±0.008	0.600±0.008	-0.004±0.007
9.8	-0.3±0.7	-0.60±0.01	-0.98±0.02	0.614±0.008	0.614±0.008	-0.004±0.007
10.8	-0.4±0.6	-0.59±0.01	-0.98±0.02	0.626±0.007	0.626±0.007	-0.004±0.007
11.8	-0.4±0.6	-0.58±0.01	-0.98±0.02	0.636±0.007	0.636±0.007	-0.004±0.007
12.8	-0.3±0.6	-0.56±0.01	-0.98±0.02	0.647±0.007	0.647±0.007	-0.004±0.007
13.8	-0.3±0.6	-0.55±0.01	-0.98±0.02	0.659±0.007	0.659±0.007	-0.003±0.007
16.4	-0.2±0.5	-0.52±0.01	-0.98±0.02	0.682±0.007	0.682±0.007	-0.002±0.006
18.9	-0.1±0.5	-0.49±0.01	-0.98±0.02	0.700±0.007	0.700±0.007	-0.001±0.006
21.4	-0.0±0.5	-0.46±0.01	-0.99±0.02	0.724±0.007	0.724±0.007	-0.000±0.006
24.0	0.1±0.5	-0.43±0.01	-0.98±0.02	0.741±0.007	0.741±0.007	0.001±0.006
26.5	0.1±0.4	-0.41±0.01	-0.99±0.02	0.762±0.007	0.762±0.007	0.002±0.006
29.1	0.2±0.4	-0.38±0.01	-0.98±0.02	0.777±0.007	0.777±0.007	0.003±0.006
31.6	0.3±0.4	-0.36±0.01	-0.98±0.02	0.791±0.007	0.791±0.007	0.003±0.006
34.1	0.3±0.4	-0.33±0.01	-0.98±0.02	0.807±0.007	0.807±0.007	0.005±0.005
36.7	0.3±0.4	-0.31±0.01	-0.99±0.02	0.824±0.007	0.824±0.007	0.005±0.005
39.2	0.4±0.4	-0.29±0.01	-0.98±0.02	0.835±0.007	0.835±0.007	0.006±0.005
44.3	0.5±0.3	-0.24±0.01	-0.98±0.02	0.862±0.006	0.862±0.006	0.008±0.005
49.4	0.6±0.3	-0.19±0.01	-0.98±0.02	0.889±0.006	0.889±0.006	0.009±0.005
54.5	0.7±0.3	-0.16±0.01	-0.99±0.02	0.912±0.006	0.912±0.006	0.010±0.005
59.5	0.7±0.3	-0.12±0.01	-0.98±0.02	0.930±0.006	0.930±0.006	0.012±0.005
64.6	0.8±0.3	-0.08±0.01	-0.99±0.02	0.950±0.006	0.950±0.006	0.014±0.005
69.7	0.9±0.3	-0.05±0.01	-0.98±0.02	0.965±0.006	0.965±0.006	0.015±0.005
74.8	1.0±0.3	-0.03±0.01	-0.99±0.02	0.978±0.006	0.978±0.006	0.017±0.005
79.9	1.1±0.3	-0.01±0.01	-0.99±0.02	0.987±0.006	0.987±0.006	0.018±0.004
84.9	1.2±0.3	-0.00±0.01	-0.99±0.02	0.994±0.006	0.993±0.006	0.020±0.004
90.0	1.2±0.3	0.01±0.01	-0.99±0.02	0.997±0.006	0.996±0.006	0.021±0.004
100.2	1.3±0.3	0.01±0.01	-0.99±0.02	0.998±0.006	0.997±0.006	0.022±0.004
110.3	1.4±0.3	0.01±0.01	-0.99±0.02	0.998±0.006	0.998±0.006	0.025±0.004
120.5	1.5±0.3	0.01±0.01	-0.99±0.02	1.001±0.006	1.000±0.006	0.027±0.004
130.7	1.6±0.3	0.01±0.01	-1.00±0.02	1.003±0.006	1.003±0.006	0.028±0.004
140.8	1.7±0.3	0.01±0.01	-1.00±0.02	1.005±0.006	1.004±0.006	0.030±0.004

Table D.40 Five-Hole Probe Data at (x,z)=(-127 mm,0)

y, mm	ALPHA, deg	CPT	CPS	SPEED	U	V
3.7	0.1±1.2	-0.72±0.01	-0.93±0.02	0.466±0.009	0.466±0.009	0.001±0.009
4.7	-0.3±1.0	-0.69±0.01	-0.93±0.02	0.495±0.009	0.495±0.009	-0.003±0.009
5.7	-0.5±1.0	-0.67±0.01	-0.93±0.02	0.516±0.009	0.516±0.009	-0.005±0.009
6.7	-0.5±0.9	-0.65±0.01	-0.94±0.02	0.539±0.008	0.539±0.008	-0.005±0.008
7.7	-0.6±0.8	-0.63±0.01	-0.93±0.02	0.548±0.008	0.548±0.008	-0.005±0.008
8.7	-0.5±0.8	-0.62±0.01	-0.94±0.02	0.567±0.008	0.567±0.008	-0.005±0.008
9.8	-0.5±0.8	-0.60±0.01	-0.94±0.02	0.580±0.008	0.580±0.008	-0.005±0.008
10.8	-0.4±0.7	-0.59±0.01	-0.94±0.02	0.592±0.008	0.592±0.008	-0.004±0.007
11.8	-0.4±0.7	-0.57±0.01	-0.94±0.02	0.603±0.008	0.603±0.008	-0.004±0.007
12.8	-0.4±0.7	-0.56±0.01	-0.93±0.02	0.611±0.008	0.611±0.008	-0.004±0.007
13.8	-0.3±0.6	-0.55±0.01	-0.94±0.02	0.626±0.007	0.626±0.007	-0.004±0.007
16.4	-0.1±0.6	-0.51±0.01	-0.94±0.02	0.650±0.007	0.650±0.007	-0.002±0.007
18.9	-0.1±0.6	-0.49±0.01	-0.93±0.02	0.670±0.007	0.670±0.007	-0.002±0.007
21.4	-0.0±0.5	-0.46±0.01	-0.94±0.02	0.691±0.007	0.691±0.007	-0.000±0.006
24.0	0.0±0.5	-0.43±0.01	-0.93±0.02	0.710±0.007	0.710±0.007	0.000±0.006
26.5	0.1±0.5	-0.40±0.01	-0.94±0.02	0.733±0.007	0.733±0.007	0.002±0.006
29.1	0.2±0.5	-0.38±0.01	-0.94±0.02	0.749±0.007	0.749±0.007	0.003±0.006
31.6	0.3±0.4	-0.36±0.01	-0.94±0.02	0.764±0.007	0.764±0.007	0.003±0.006
34.1	0.3±0.4	-0.33±0.01	-0.93±0.02	0.778±0.007	0.778±0.007	0.004±0.006
36.7	0.3±0.4	-0.31±0.01	-0.94±0.02	0.794±0.007	0.794±0.007	0.005±0.006
39.2	0.4±0.4	-0.29±0.01	-0.94±0.02	0.810±0.007	0.810±0.007	0.006±0.005
44.3	0.5±0.4	-0.24±0.01	-0.94±0.02	0.837±0.007	0.837±0.007	0.007±0.005
49.4	0.5±0.3	-0.20±0.01	-0.94±0.02	0.862±0.006	0.862±0.006	0.008±0.005
54.5	0.6±0.3	-0.16±0.01	-0.94±0.02	0.882±0.006	0.882±0.006	0.010±0.005
59.5	0.7±0.3	-0.12±0.01	-0.93±0.02	0.904±0.006	0.904±0.006	0.011±0.005
64.6	0.8±0.3	-0.09±0.01	-0.94±0.02	0.922±0.006	0.922±0.006	0.012±0.005
69.7	0.9±0.3	-0.06±0.01	-0.94±0.02	0.936±0.006	0.936±0.006	0.014±0.005
74.8	1.0±0.3	-0.03±0.01	-0.94±0.02	0.951±0.006	0.951±0.006	0.016±0.005
79.9	1.0±0.3	-0.01±0.01	-0.93±0.02	0.960±0.006	0.960±0.006	0.017±0.005
84.9	1.1±0.3	-0.00±0.01	-0.94±0.02	0.967±0.006	0.967±0.006	0.019±0.005
90.0	1.2±0.3	0.00±0.01	-0.94±0.02	0.970±0.006	0.970±0.006	0.020±0.005
100.2	1.3±0.3	0.01±0.01	-0.93±0.02	0.971±0.006	0.971±0.006	0.022±0.005
110.3	1.5±0.3	0.01±0.01	-0.93±0.02	0.971±0.006	0.971±0.006	0.026±0.005
120.5	1.7±0.3	0.01±0.01	-0.94±0.02	0.972±0.006	0.972±0.006	0.029±0.005
130.7	1.8±0.3	0.01±0.01	-0.94±0.02	0.975±0.006	0.975±0.006	0.031±0.005
140.8	2.0±0.3	0.01±0.01	-0.95±0.02	0.977±0.006	0.977±0.006	0.035±0.005

Table D.41 Five-Hole Probe Data at (x,z)=(-102 mm,0)

y, mm	ALPHA, deg	CPT	CPS	SPEED	U	V
3.7	0.5±1.6	-0.72±0.01	-0.88±0.02	0.398±0.011	0.398±0.011	0.003±0.011
4.7	-0.1±1.4	-0.69±0.01	-0.87±0.02	0.428±0.010	0.428±0.010	-0.001±0.010
5.7	-0.3±1.2	-0.67±0.01	-0.88±0.02	0.452±0.010	0.452±0.010	-0.002±0.010
6.7	-0.3±1.1	-0.65±0.01	-0.87±0.02	0.472±0.009	0.472±0.009	-0.003±0.009
7.7	-0.4±1.1	-0.64±0.01	-0.88±0.02	0.490±0.009	0.490±0.009	-0.003±0.009
8.7	-0.4±1.0	-0.62±0.01	-0.87±0.02	0.505±0.009	0.505±0.009	-0.003±0.009
9.8	-0.4±0.9	-0.61±0.01	-0.88±0.02	0.521±0.008	0.521±0.009	-0.003±0.008
10.8	-0.2±0.9	-0.59±0.01	-0.88±0.02	0.538±0.008	0.538±0.008	-0.002±0.008
11.8	-0.2±0.8	-0.58±0.01	-0.88±0.02	0.548±0.008	0.548±0.008	-0.002±0.008
12.8	-0.2±0.8	-0.57±0.01	-0.88±0.02	0.561±0.008	0.561±0.008	-0.002±0.008
13.8	-0.2±0.8	-0.55±0.01	-0.88±0.02	0.572±0.008	0.572±0.008	-0.002±0.008
16.4	-0.1±0.7	-0.52±0.01	-0.88±0.02	0.598±0.008	0.598±0.008	-0.001±0.007
18.9	0.0±0.7	-0.49±0.01	-0.88±0.02	0.622±0.007	0.622±0.007	0.000±0.007
21.4	0.1±0.6	-0.47±0.01	-0.88±0.02	0.644±0.007	0.644±0.007	0.001±0.007
24.0	0.2±0.6	-0.44±0.01	-0.88±0.02	0.665±0.007	0.665±0.007	0.002±0.007
26.5	0.1±0.5	-0.41±0.01	-0.88±0.02	0.682±0.007	0.682±0.007	0.002±0.006
29.1	0.2±0.5	-0.39±0.01	-0.88±0.02	0.702±0.007	0.702±0.007	0.002±0.006
31.6	0.2±0.5	-0.36±0.01	-0.88±0.02	0.719±0.007	0.719±0.007	0.003±0.006
34.1	0.2±0.5	-0.34±0.01	-0.88±0.02	0.735±0.007	0.735±0.007	0.002±0.006
36.7	0.3±0.4	-0.31±0.01	-0.88±0.02	0.752±0.007	0.752±0.007	0.004±0.006
39.2	0.2±0.4	-0.30±0.01	-0.88±0.02	0.767±0.007	0.767±0.007	0.003±0.006
44.3	0.3±0.4	-0.25±0.01	-0.88±0.02	0.796±0.007	0.796±0.007	0.004±0.006
49.4	0.3±0.4	-0.21±0.01	-0.88±0.02	0.821±0.007	0.821±0.007	0.004±0.005
54.5	0.3±0.4	-0.16±0.01	-0.87±0.02	0.843±0.007	0.843±0.007	0.004±0.005
59.5	0.3±0.3	-0.13±0.01	-0.87±0.02	0.862±0.006	0.862±0.006	0.005±0.005
64.6	0.4±0.3	-0.09±0.01	-0.87±0.02	0.882±0.006	0.882±0.006	0.006±0.005
69.7	0.5±0.3	-0.06±0.01	-0.87±0.02	0.897±0.006	0.897±0.006	0.008±0.005
74.8	0.6±0.3	-0.04±0.01	-0.87±0.02	0.911±0.006	0.911±0.006	0.010±0.005
79.9	0.7±0.3	-0.02±0.01	-0.87±0.02	0.921±0.006	0.921±0.006	0.012±0.005
84.9	0.8±0.3	-0.00±0.01	-0.86±0.02	0.927±0.006	0.927±0.006	0.014±0.005
90.0	0.9±0.3	0.00±0.01	-0.86±0.02	0.929±0.006	0.929±0.006	0.015±0.005
100.2	1.2±0.3	0.01±0.01	-0.86±0.02	0.930±0.006	0.930±0.006	0.019±0.005
110.3	1.4±0.3	0.01±0.01	-0.86±0.02	0.929±0.006	0.929±0.006	0.023±0.005
120.5	1.7±0.3	0.01±0.01	-0.86±0.02	0.930±0.006	0.929±0.006	0.027±0.005
130.7	2.0±0.3	0.01±0.01	-0.86±0.02	0.933±0.006	0.932±0.006	0.033±0.005
140.8	2.3±0.3	0.01±0.01	-0.87±0.02	0.935±0.006	0.934±0.006	0.038±0.005

-3.5

Table D.42 Five-Hole Probe Data at (x,z)=(-89 mm,0)

y, mm	ALPHA, deg	CPT	CPS	SPEED	U	V
3.7	0.3±1.9	-0.71±0.01	-0.85±0.01	0.365±0.012	0.364±0.012	0.002±0.012
4.7	-0.3±1.7	-0.69±0.01	-0.84±0.01	0.389±0.011	0.389±0.011	-0.002±0.011
5.7	-0.4±1.4	-0.67±0.01	-0.85±0.01	0.419±0.010	0.419±0.010	-0.003±0.011
6.7	-0.4±1.3	-0.65±0.01	-0.85±0.01	0.437±0.010	0.437±0.010	-0.003±0.010
7.7	-0.5±1.2	-0.64±0.01	-0.84±0.01	0.456±0.010	0.456±0.010	-0.004±0.010
8.7	-0.4±1.1	-0.62±0.01	-0.84±0.01	0.471±0.009	0.471±0.009	-0.004±0.009
9.8	-0.3±1.0	-0.60±0.01	-0.85±0.01	0.491±0.009	0.491±0.009	-0.003±0.009
10.8	-0.3±1.0	-0.59±0.01	-0.85±0.01	0.505±0.009	0.504±0.009	-0.003±0.009
11.8	-0.3±0.9	-0.58±0.01	-0.85±0.01	0.520±0.009	0.520±0.009	-0.002±0.008
12.8	-0.2±0.9	-0.57±0.01	-0.85±0.01	0.530±0.008	0.530±0.008	-0.002±0.008
13.8	-0.1±0.9	-0.55±0.01	-0.85±0.01	0.543±0.008	0.543±0.008	-0.001±0.008
16.4	-0.1±0.8	-0.53±0.01	-0.85±0.01	0.570±0.008	0.570±0.008	-0.001±0.008
18.9	0.0±0.7	-0.50±0.01	-0.85±0.01	0.594±0.008	0.594±0.008	0.000±0.007
21.4	0.1±0.7	-0.47±0.01	-0.85±0.01	0.615±0.008	0.615±0.008	0.001±0.007
24.0	-0.0±0.6	-0.44±0.01	-0.85±0.01	0.639±0.007	0.639±0.007	-0.000±0.007
26.5	-0.0±0.6	-0.41±0.01	-0.85±0.01	0.658±0.007	0.658±0.007	-0.000±0.007
29.1	-0.0±0.6	-0.39±0.01	-0.85±0.01	0.675±0.007	0.675±0.007	-0.000±0.007
31.6	-0.0±0.5	-0.37±0.01	-0.85±0.01	0.696±0.007	0.696±0.007	-0.000±0.006
34.1	-0.0±0.5	-0.34±0.01	-0.85±0.01	0.710±0.007	0.710±0.007	-0.000±0.006
36.7	-0.0±0.5	-0.32±0.01	-0.84±0.01	0.726±0.007	0.726±0.007	-0.000±0.006
39.2	-0.0±0.5	-0.29±0.01	-0.84±0.01	0.741±0.007	0.741±0.007	-0.001±0.006
44.3	-0.1±0.4	-0.25±0.01	-0.84±0.01	0.769±0.007	0.769±0.007	-0.001±0.006
49.4	-0.1±0.4	-0.21±0.01	-0.84±0.01	0.795±0.007	0.795±0.007	-0.002±0.006
54.5	-0.1±0.4	-0.16±0.01	-0.83±0.01	0.816±0.007	0.816±0.007	-0.002±0.005
59.5	-0.1±0.4	-0.13±0.01	-0.83±0.01	0.838±0.007	0.838±0.007	-0.001±0.005
64.6	0.0±0.3	-0.09±0.01	-0.83±0.01	0.856±0.006	0.856±0.006	0.000±0.005
69.7	0.1±0.3	-0.06±0.01	-0.82±0.01	0.871±0.006	0.871±0.006	0.001±0.005
74.8	0.2±0.3	-0.04±0.01	-0.82±0.01	0.885±0.006	0.885±0.006	0.004±0.005
79.9	0.4±0.3	-0.02±0.01	-0.81±0.01	0.892±0.006	0.892±0.006	0.006±0.005
84.9	0.5±0.3	-0.00±0.01	-0.81±0.01	0.898±0.006	0.898±0.006	0.008±0.005
90.0	0.6±0.3	0.00±0.01	-0.81±0.01	0.900±0.006	0.900±0.006	0.010±0.005
100.2	0.9±0.3	0.01±0.01	-0.80±0.01	0.900±0.006	0.900±0.006	0.014±0.005
110.3	1.2±0.3	0.01±0.01	-0.80±0.01	0.898±0.006	0.898±0.006	0.019±0.005
120.5	1.6±0.3	0.01±0.01	-0.80±0.01	0.898±0.006	0.898±0.006	0.026±0.005
130.7	2.0±0.3	0.01±0.01	-0.80±0.01	0.901±0.006	0.900±0.006	0.032±0.005
140.8	2.5±0.3	0.01±0.01	-0.81±0.01	0.903±0.006	0.902±0.006	0.039±0.005

-3"

Table D.43 Five-Hole Probe Data at (x,z)=(-76 mm,0)

y, mm	ALPHA, deg	CPT	CPS	SPEED	U	V
3.7	0.1±2.7	-0.72±0.01	-0.81±0.01	0.304±0.014	0.304±0.014	0.000±0.014
4.7	-0.4±2.2	-0.70±0.01	-0.82±0.01	0.339±0.012	0.339±0.012	-0.002±0.013
5.7	-0.5±1.9	-0.68±0.01	-0.81±0.01	0.363±0.012	0.363±0.012	-0.003±0.012
6.7	-0.5±1.7	-0.66±0.01	-0.81±0.01	0.385±0.011	0.385±0.011	-0.003±0.011
7.7	-0.4±1.5	-0.65±0.01	-0.81±0.01	0.410±0.010	0.410±0.010	-0.003±0.011
8.7	-0.3±1.4	-0.63±0.01	-0.81±0.01	0.430±0.010	0.430±0.010	-0.002±0.010
9.8	-0.3±1.3	-0.62±0.01	-0.81±0.01	0.445±0.010	0.445±0.010	-0.003±0.010
10.8	-0.1±1.2	-0.60±0.01	-0.82±0.01	0.464±0.009	0.464±0.009	-0.001±0.009
11.8	-0.0±1.1	-0.59±0.01	-0.81±0.01	0.476±0.009	0.476±0.009	-0.000±0.009
12.8	-0.1±1.0	-0.57±0.01	-0.81±0.01	0.489±0.009	0.489±0.009	-0.001±0.009
13.8	-0.1±1.0	-0.56±0.01	-0.81±0.01	0.504±0.009	0.504±0.009	-0.001±0.009
16.4	-0.1±0.9	-0.53±0.01	-0.82±0.01	0.535±0.008	0.535±0.008	-0.000±0.008
18.9	-0.1±0.8	-0.50±0.01	-0.82±0.01	0.562±0.008	0.562±0.008	-0.001±0.008
21.4	-0.2±0.7	-0.47±0.01	-0.81±0.01	0.585±0.008	0.585±0.008	-0.002±0.007
24.0	-0.2±0.7	-0.44±0.01	-0.81±0.01	0.607±0.008	0.607±0.008	-0.003±0.007
26.5	-0.3±0.6	-0.42±0.01	-0.81±0.01	0.627±0.007	0.627±0.007	-0.004±0.007
29.1	-0.5±0.6	-0.39±0.01	-0.81±0.01	0.647±0.007	0.647±0.007	-0.005±0.007
31.6	-0.6±0.6	-0.37±0.01	-0.81±0.01	0.664±0.007	0.664±0.007	-0.007±0.007
34.1	-0.6±0.5	-0.34±0.01	-0.81±0.01	0.683±0.007	0.683±0.007	-0.007±0.006
36.7	-0.7±0.5	-0.32±0.01	-0.80±0.01	0.696±0.007	0.696±0.007	-0.009±0.006
39.2	-0.8±0.5	-0.30±0.01	-0.80±0.01	0.712±0.007	0.712±0.007	-0.010±0.006
44.3	-0.8±0.5	-0.25±0.01	-0.80±0.01	0.738±0.007	0.738±0.007	-0.011±0.006
49.4	-0.9±0.4	-0.21±0.01	-0.80±0.01	0.765±0.007	0.765±0.007	-0.012±0.006
54.5	-0.9±0.4	-0.17±0.01	-0.79±0.01	0.787±0.007	0.786±0.007	-0.013±0.006
59.5	-0.9±0.4	-0.13±0.01	-0.78±0.01	0.806±0.007	0.806±0.007	-0.012±0.005
64.6	-0.8±0.4	-0.10±0.01	-0.78±0.01	0.825±0.007	0.825±0.007	-0.011±0.005
69.7	-0.6±0.4	-0.07±0.01	-0.77±0.01	0.839±0.007	0.839±0.007	-0.009±0.005
74.8	-0.5±0.3	-0.04±0.01	-0.76±0.01	0.850±0.006	0.850±0.006	-0.007±0.005
79.9	-0.3±0.3	-0.02±0.01	-0.76±0.01	0.858±0.006	0.858±0.006	-0.005±0.005
84.9	-0.1±0.3	-0.01±0.01	-0.75±0.01	0.863±0.006	0.863±0.006	-0.002±0.005
90.0	0.0±0.3	0.00±0.01	-0.74±0.01	0.864±0.006	0.864±0.006	0.000±0.005
100.2	0.4±0.3	0.01±0.01	-0.74±0.01	0.861±0.006	0.861±0.006	0.006±0.005
110.3	0.8±0.3	0.01±0.01	-0.73±0.01	0.859±0.006	0.858±0.006	0.013±0.005
120.5	1.4±0.3	0.01±0.01	-0.73±0.01	0.857±0.006	0.857±0.006	0.020±0.005
130.7	1.9±0.3	0.01±0.01	-0.73±0.01	0.860±0.006	0.859±0.006	0.029±0.005
140.8	2.5±0.3	0.01±0.01	-0.74±0.01	0.863±0.006	0.863±0.006	0.038±0.005

Table D.44 Five-Hole Probe Data at (x,z)=(-70 mm,0)

y, mm	ALPHA, deg	CPT	CPS	SPEED	U	V
3.7	-0.3±3.5	-0.72±0.01	-0.79±0.01	0.268±0.016	0.268±0.016	-0.001±0.016
4.7	-0.6±2.7	-0.70±0.01	-0.80±0.01	0.306±0.014	0.306±0.014	-0.003±0.014
5.7	-0.7±2.4	-0.68±0.01	-0.79±0.01	0.327±0.013	0.327±0.013	-0.004±0.013
6.7	-0.5±1.9	-0.66±0.01	-0.79±0.01	0.360±0.012	0.360±0.012	-0.003±0.012
7.7	-0.3±1.7	-0.65±0.01	-0.80±0.01	0.382±0.011	0.382±0.011	-0.002±0.012
8.7	-0.3±1.5	-0.63±0.01	-0.79±0.01	0.405±0.011	0.405±0.011	-0.002±0.011
9.8	-0.1±1.4	-0.62±0.01	-0.79±0.01	0.423±0.010	0.423±0.010	-0.001±0.010
10.8	-0.2±1.3	-0.60±0.01	-0.79±0.01	0.437±0.010	0.437±0.010	-0.001±0.010
11.8	-0.1±1.2	-0.59±0.01	-0.80±0.01	0.456±0.009	0.456±0.009	-0.001±0.010
12.8	-0.1±1.1	-0.58±0.01	-0.80±0.01	0.470±0.009	0.470±0.009	-0.001±0.009
13.8	-0.1±1.1	-0.56±0.01	-0.80±0.01	0.485±0.009	0.485±0.009	-0.001±0.009
16.4	-0.2±1.0	-0.53±0.01	-0.80±0.01	0.514±0.009	0.514±0.009	-0.002±0.009
18.9	-0.3±0.8	-0.50±0.01	-0.80±0.01	0.545±0.008	0.545±0.008	-0.003±0.008
21.4	-0.4±0.8	-0.48±0.01	-0.80±0.01	0.566±0.008	0.566±0.008	-0.004±0.008
24.0	-0.6±0.7	-0.45±0.01	-0.80±0.01	0.592±0.008	0.592±0.008	-0.006±0.007
26.5	-0.8±0.7	-0.42±0.01	-0.79±0.01	0.611±0.008	0.611±0.008	-0.009±0.007
29.1	-0.9±0.6	-0.40±0.01	-0.79±0.01	0.629±0.007	0.629±0.007	-0.010±0.007
31.6	-1.1±0.6	-0.37±0.01	-0.79±0.01	0.648±0.007	0.648±0.007	-0.013±0.007
34.1	-1.2±0.6	-0.34±0.01	-0.79±0.01	0.664±0.007	0.664±0.007	-0.013±0.007
36.7	-1.3±0.5	-0.32±0.01	-0.78±0.01	0.680±0.007	0.680±0.007	-0.015±0.006
39.2	-1.4±0.5	-0.30±0.01	-0.78±0.01	0.698±0.007	0.698±0.007	-0.017±0.006
44.3	-1.5±0.5	-0.25±0.01	-0.77±0.01	0.721±0.007	0.721±0.007	-0.019±0.006
49.4	-1.6±0.5	-0.21±0.01	-0.76±0.01	0.746±0.007	0.746±0.007	-0.020±0.006
54.5	-1.5±0.4	-0.17±0.01	-0.76±0.01	0.770±0.007	0.770±0.007	-0.021±0.006
59.5	-1.5±0.4	-0.13±0.01	-0.75±0.01	0.789±0.007	0.789±0.007	-0.021±0.006
64.6	-1.4±0.4	-0.10±0.01	-0.75±0.01	0.805±0.007	0.805±0.007	-0.020±0.005
69.7	-1.2±0.4	-0.07±0.01	-0.74±0.01	0.821±0.007	0.820±0.007	-0.017±0.005
74.8	-1.0±0.4	-0.04±0.01	-0.73±0.01	0.831±0.007	0.831±0.007	-0.015±0.005
79.9	-0.8±0.4	-0.02±0.01	-0.72±0.01	0.837±0.007	0.837±0.007	-0.012±0.005
84.9	-0.6±0.4	-0.01±0.01	-0.71±0.01	0.841±0.007	0.840±0.007	-0.009±0.005
90.0	-0.4±0.4	0.00±0.01	-0.71±0.01	0.841±0.007	0.841±0.007	-0.006±0.005
100.2	-0.0±0.4	0.01±0.01	-0.69±0.01	0.837±0.007	0.837±0.007	-0.000±0.005
110.3	0.5±0.4	0.01±0.01	-0.69±0.01	0.833±0.007	0.833±0.007	0.007±0.005
120.5	1.1±0.4	0.01±0.01	-0.69±0.01	0.832±0.007	0.832±0.007	0.017±0.005
130.7	1.8±0.4	0.01±0.01	-0.69±0.01	0.834±0.007	0.834±0.007	0.026±0.005
140.8	2.5±0.4	0.01±0.01	-0.69±0.01	0.838±0.007	0.837±0.007	0.037±0.005

-2.5

Table D.45 Five-Hole Probe Data at (x,z)=(-64 mm,0)

y, mm	ALPHA, deg	CPT	CPS	SPEED	U	V
3.7	-0.4±4.9	-0.72±0.01	-0.77±0.01	0.227±0.019	0.227±0.019	-0.001±0.019
4.7	-0.7±3.6	-0.71±0.01	-0.78±0.01	0.266±0.016	0.266±0.016	-0.003±0.017
5.7	-0.6±2.8	-0.69±0.01	-0.78±0.01	0.298±0.014	0.298±0.014	-0.003±0.015
6.7	-0.5±2.3	-0.67±0.01	-0.78±0.01	0.329±0.013	0.329±0.013	-0.003±0.013
7.7	-0.3±2.0	-0.65±0.01	-0.77±0.01	0.351±0.012	0.351±0.012	-0.002±0.013
8.7	-0.3±1.8	-0.64±0.01	-0.78±0.01	0.372±0.011	0.372±0.011	-0.002±0.012
9.8	-0.0±1.6	-0.62±0.01	-0.78±0.01	0.395±0.011	0.395±0.011	-0.000±0.011
10.8	0.0±1.5	-0.61±0.01	-0.78±0.01	0.416±0.010	0.416±0.010	0.000±0.011
11.8	-0.0±1.4	-0.60±0.01	-0.78±0.01	0.425±0.010	0.425±0.010	-0.000±0.010
12.8	0.0±1.3	-0.58±0.01	-0.78±0.01	0.445±0.010	0.445±0.010	0.000±0.010
13.8	0.0±1.2	-0.57±0.01	-0.78±0.01	0.463±0.009	0.463±0.009	0.000±0.009
16.4	-0.3±1.0	-0.54±0.01	-0.78±0.01	0.496±0.009	0.496±0.009	-0.002±0.009
18.9	-0.6±0.9	-0.51±0.01	-0.78±0.01	0.524±0.008	0.524±0.008	-0.006±0.008
21.4	-0.8±0.8	-0.47±0.01	-0.77±0.01	0.547±0.008	0.547±0.008	-0.008±0.008
24.0	-1.2±0.8	-0.45±0.01	-0.78±0.01	0.572±0.008	0.572±0.008	-0.012±0.008
26.5	-1.5±0.7	-0.42±0.01	-0.77±0.01	0.593±0.008	0.593±0.008	-0.015±0.007
29.1	-1.6±0.7	-0.40±0.01	-0.77±0.01	0.614±0.008	0.613±0.008	-0.017±0.007
31.6	-1.8±0.6	-0.37±0.01	-0.77±0.01	0.632±0.007	0.632±0.007	-0.020±0.007
34.1	-2.0±0.6	-0.35±0.01	-0.76±0.01	0.647±0.007	0.646±0.007	-0.022±0.007
36.7	-2.1±0.6	-0.32±0.01	-0.76±0.01	0.662±0.007	0.661±0.007	-0.024±0.007
39.2	-2.2±0.5	-0.29±0.01	-0.75±0.01	0.678±0.007	0.677±0.007	-0.026±0.006
44.3	-2.3±0.5	-0.25±0.01	-0.74±0.01	0.701±0.007	0.701±0.007	-0.028±0.006
49.4	-2.4±0.5	-0.21±0.01	-0.74±0.01	0.726±0.007	0.725±0.007	-0.030±0.006
54.5	-2.4±0.5	-0.17±0.01	-0.73±0.01	0.747±0.007	0.746±0.007	-0.031±0.006
59.5	-2.3±0.4	-0.13±0.01	-0.72±0.01	0.767±0.007	0.766±0.007	-0.031±0.006
64.6	-2.2±0.4	-0.10±0.01	-0.71±0.01	0.783±0.007	0.783±0.007	-0.029±0.006
69.7	-1.9±0.4	-0.07±0.01	-0.70±0.01	0.796±0.007	0.795±0.007	-0.027±0.006
74.8	-1.7±0.4	-0.04±0.01	-0.69±0.01	0.807±0.007	0.807±0.007	-0.024±0.005
79.9	-1.4±0.4	-0.02±0.01	-0.68±0.01	0.812±0.007	0.812±0.007	-0.020±0.005
84.9	-1.2±0.4	-0.01±0.01	-0.67±0.01	0.814±0.007	0.814±0.007	-0.017±0.005
90.0	-0.9±0.4	-0.00±0.01	-0.66±0.01	0.814±0.007	0.814±0.007	-0.013±0.005
100.2	-0.4±0.4	0.01±0.01	-0.65±0.01	0.809±0.007	0.809±0.007	-0.005±0.005
110.3	0.3±0.4	0.01±0.01	-0.64±0.01	0.804±0.007	0.804±0.007	0.004±0.005
120.5	1.0±0.4	0.01±0.01	-0.64±0.01	0.802±0.007	0.802±0.007	0.014±0.005
130.7	1.7±0.4	0.01±0.01	-0.64±0.01	0.803±0.007	0.803±0.007	0.024±0.005
140.8	2.5±0.4	0.01±0.01	-0.64±0.01	0.806±0.007	0.805±0.007	0.035±0.005

Table D.46 Five-Hole Probe Data at (x,z)=(-57 mm,0)

y, mm	ALPHA, deg	CPT	CPS	SPEED	U	V
3.7	4.2±***	-0.74±0.01	-0.77±0.01	0.159±0.027	0.159±0.027	0.012±0.028
4.7	2.4±6.0	-0.73±0.01	-0.77±0.01	0.206±0.021	0.206±0.021	0.009±0.022
5.7	0.8±4.4	-0.71±0.01	-0.77±0.01	0.241±0.017	0.241±0.017	0.003±0.018
6.7	0.5±3.2	-0.68±0.01	-0.76±0.01	0.281±0.015	0.281±0.015	0.002±0.016
7.7	0.7±2.7	-0.67±0.01	-0.76±0.01	0.307±0.014	0.307±0.014	0.004±0.014
8.7	0.8±2.3	-0.65±0.01	-0.76±0.01	0.330±0.013	0.330±0.013	0.004±0.013
9.8	1.2±1.9	-0.64±0.01	-0.77±0.01	0.363±0.012	0.363±0.012	0.008±0.012
10.8	1.0±1.7	-0.62±0.01	-0.77±0.01	0.382±0.011	0.382±0.011	0.007±0.012
11.8	1.1±1.6	-0.60±0.01	-0.76±0.01	0.402±0.011	0.402±0.011	0.007±0.011
12.8	0.6±1.4	-0.59±0.01	-0.77±0.01	0.425±0.010	0.425±0.010	0.004±0.010
13.8	0.2±1.3	-0.57±0.01	-0.77±0.01	0.439±0.010	0.439±0.010	0.002±0.010
16.4	-0.4±1.1	-0.54±0.01	-0.76±0.01	0.475±0.009	0.475±0.009	-0.003±0.009
18.9	-1.1±1.0	-0.51±0.01	-0.76±0.01	0.508±0.009	0.508±0.009	-0.010±0.009
21.4	-1.7±0.9	-0.48±0.01	-0.76±0.01	0.530±0.008	0.530±0.008	-0.016±0.008
24.0	-2.0±0.8	-0.45±0.01	-0.76±0.01	0.555±0.008	0.555±0.008	-0.020±0.008
26.5	-2.4±0.8	-0.43±0.01	-0.76±0.01	0.578±0.008	0.577±0.008	-0.024±0.008
29.1	-2.6±0.7	-0.40±0.01	-0.76±0.01	0.596±0.008	0.595±0.008	-0.027±0.007
31.6	-2.9±0.7	-0.37±0.01	-0.75±0.01	0.612±0.008	0.611±0.008	-0.031±0.007
34.1	-3.0±0.6	-0.34±0.01	-0.74±0.01	0.629±0.007	0.628±0.007	-0.033±0.007
36.7	-3.2±0.6	-0.32±0.01	-0.73±0.01	0.643±0.007	0.642±0.007	-0.035±0.007
39.2	-3.2±0.6	-0.30±0.01	-0.73±0.01	0.658±0.007	0.657±0.007	-0.037±0.007
44.3	-3.3±0.5	-0.25±0.01	-0.72±0.01	0.684±0.007	0.682±0.007	-0.039±0.006
49.4	-3.4±0.5	-0.21±0.01	-0.71±0.01	0.705±0.007	0.704±0.007	-0.041±0.006
54.5	-3.3±0.5	-0.17±0.01	-0.69±0.01	0.725±0.007	0.724±0.007	-0.042±0.006
59.5	-3.2±0.5	-0.13±0.01	-0.68±0.01	0.744±0.007	0.743±0.007	-0.042±0.006
64.6	-3.3±0.4	-0.10±0.01	-0.67±0.01	0.757±0.007	0.756±0.007	-0.043±0.006
69.7	-3.5±0.4	-0.06±0.01	-0.65±0.01	0.769±0.007	0.767±0.007	-0.047±0.006
74.8	-3.4±0.4	-0.04±0.01	-0.65±0.01	0.781±0.007	0.779±0.007	-0.047±0.006
79.9	-3.0±0.4	-0.02±0.01	-0.64±0.01	0.787±0.007	0.786±0.007	-0.041±0.006
84.9	-2.7±0.4	-0.01±0.01	-0.63±0.01	0.789±0.007	0.788±0.007	-0.037±0.006
90.0	-2.1±0.4	-0.00±0.01	-0.62±0.01	0.788±0.007	0.788±0.007	-0.029±0.006
100.2	-1.1±0.4	0.01±0.01	-0.61±0.01	0.781±0.007	0.781±0.007	-0.015±0.006
110.3	0.0±0.4	0.00±0.01	-0.60±0.01	0.775±0.007	0.775±0.007	0.000±0.006
120.5	0.9±0.4	0.01±0.01	-0.59±0.01	0.771±0.007	0.771±0.007	0.012±0.006
130.7	1.7±0.4	0.01±0.01	-0.59±0.01	0.770±0.007	0.770±0.007	0.023±0.006
140.8	2.5±0.4	0.01±0.01	-0.59±0.01	0.771±0.007	0.771±0.007	0.034±0.006

Table D.47 Five-Hole Probe Data at (x,z)=(-51 mm,0)

y, mm	ALPHA, deg	CPT	CPS	SPEED	U	V
3.7	44.7±***	-0.74±0.10	-0.75±0.11	0.127±0.038	0.090±0.067	0.089±0.021
4.7	31.0±***	-0.77±0.03	-0.79±0.04	0.156±0.029	0.134±0.043	0.080±0.025
5.7	21.0±9.1	-0.76±0.02	-0.79±0.02	0.184±0.023	0.172±0.029	0.066±0.023
6.7	12.8±5.8	-0.73±0.01	-0.78±0.02	0.218±0.019	0.213±0.021	0.048±0.020
7.7	9.8±4.0	-0.71±0.01	-0.77±0.01	0.257±0.016	0.253±0.017	0.044±0.017
8.7	7.7±3.0	-0.70±0.01	-0.79±0.01	0.295±0.014	0.293±0.015	0.040±0.015
9.8	6.9±2.5	-0.67±0.01	-0.77±0.01	0.324±0.013	0.321±0.013	0.039±0.014
10.8	5.4±2.0	-0.64±0.01	-0.77±0.01	0.355±0.012	0.353±0.012	0.033±0.013
11.8	3.6±1.7	-0.63±0.01	-0.77±0.01	0.383±0.011	0.383±0.011	0.024±0.012
12.8	1.9±1.5	-0.60±0.01	-0.77±0.01	0.405±0.011	0.405±0.011	0.014±0.011
13.8	1.0±1.4	-0.58±0.01	-0.76±0.01	0.424±0.010	0.424±0.010	0.007±0.010
16.4	-0.9±1.2	-0.55±0.01	-0.76±0.01	0.459±0.009	0.459±0.009	-0.008±0.010
18.9	-2.1±1.1	-0.52±0.01	-0.75±0.01	0.488±0.009	0.488±0.009	-0.018±0.009
21.4	-2.8±0.9	-0.48±0.01	-0.75±0.01	0.515±0.009	0.515±0.009	-0.025±0.008
24.0	-3.4±0.9	-0.45±0.01	-0.74±0.01	0.537±0.008	0.536±0.008	-0.032±0.008
26.5	-3.8±0.8	-0.42±0.01	-0.73±0.01	0.557±0.008	0.556±0.008	-0.037±0.008
29.1	-4.1±0.8	-0.40±0.01	-0.73±0.01	0.574±0.008	0.573±0.008	-0.041±0.008
31.6	-4.3±0.7	-0.37±0.01	-0.72±0.01	0.593±0.008	0.591±0.008	-0.044±0.007
34.1	-4.5±0.7	-0.34±0.01	-0.71±0.01	0.606±0.008	0.604±0.008	-0.048±0.007
36.7	-4.8±0.7	-0.32±0.01	-0.70±0.01	0.619±0.007	0.617±0.008	-0.052±0.007
39.2	-5.1±0.6	-0.29±0.01	-0.69±0.01	0.631±0.007	0.629±0.008	-0.056±0.007
44.3	-5.9±0.6	-0.25±0.01	-0.68±0.01	0.653±0.007	0.650±0.007	-0.068±0.007
49.4	-6.7±0.6	-0.20±0.01	-0.65±0.01	0.670±0.007	0.666±0.007	-0.079±0.006
54.5	-7.5±0.5	-0.16±0.01	-0.64±0.01	0.689±0.007	0.684±0.007	-0.090±0.006
59.5	-7.8±0.5	-0.12±0.01	-0.62±0.01	0.711±0.007	0.705±0.007	-0.097±0.006
64.6	-7.1±0.5	-0.09±0.01	-0.62±0.01	0.732±0.007	0.727±0.007	-0.090±0.006
69.7	-6.2±0.5	-0.06±0.01	-0.61±0.01	0.743±0.007	0.738±0.007	-0.080±0.006
74.8	-5.3±0.5	-0.04±0.01	-0.60±0.01	0.751±0.007	0.747±0.007	-0.070±0.006
79.9	-4.5±0.4	-0.02±0.01	-0.59±0.01	0.756±0.007	0.753±0.007	-0.060±0.006
84.9	-3.6±0.4	-0.01±0.01	-0.58±0.01	0.757±0.007	0.755±0.007	-0.047±0.006
90.0	-2.6±0.4	0.00±0.01	-0.57±0.01	0.755±0.007	0.754±0.007	-0.034±0.006
100.2	-0.9±0.5	0.01±0.01	-0.55±0.01	0.744±0.007	0.744±0.007	-0.011±0.006
110.3	0.0±0.5	0.01±0.01	-0.54±0.01	0.737±0.007	0.737±0.007	0.001±0.006
120.5	0.9±0.5	0.01±0.01	-0.53±0.01	0.731±0.007	0.731±0.007	0.011±0.006
130.7	1.7±0.5	0.01±0.01	-0.52±0.01	0.727±0.007	0.727±0.007	0.022±0.006
140.8	2.4±0.5	0.01±0.01	-0.52±0.01	0.724±0.007	0.724±0.007	0.031±0.006

Table D.48 Five-Hole Probe Data at (x,z)=(-44 mm,0)

y, mm	ALPHA, deg	CPT	CPS	SPEED	U	V
3.7	130.6±***	-0.61±0.12	-0.66±0.13	0.201±0.024	-0.131±0.044	0.153±0.012
4.7	55.1±***	-0.76±0.18	-0.78±0.19	0.124±0.042	0.071±0.077	0.101±0.014
5.7	36.1±***	-0.84±0.05	-0.86±0.06	0.146±0.031	0.118±0.050	0.086±0.024
6.7	20.7±9.2	-0.84±0.02	-0.87±0.02	0.182±0.024	0.170±0.029	0.064±0.023
7.7	9.5±5.8	-0.81±0.01	-0.86±0.02	0.214±0.020	0.211±0.021	0.035±0.021
8.7	5.8±3.9	-0.78±0.01	-0.84±0.01	0.255±0.016	0.254±0.017	0.026±0.017
9.8	3.3±2.8	-0.73±0.01	-0.82±0.01	0.299±0.014	0.299±0.014	0.017±0.015
10.8	1.1±2.1	-0.69±0.01	-0.81±0.01	0.344±0.012	0.344±0.012	0.007±0.013
11.8	0.0±1.8	-0.65±0.01	-0.79±0.01	0.378±0.011	0.378±0.011	0.000±0.012
12.8	-1.8±1.6	-0.62±0.01	-0.78±0.01	0.400±0.011	0.400±0.011	-0.013±0.011
13.8	-3.1±1.4	-0.59±0.01	-0.76±0.01	0.417±0.010	0.417±0.010	-0.022±0.010
16.4	-4.8±1.3	-0.54±0.01	-0.74±0.01	0.447±0.010	0.446±0.010	-0.038±0.010
18.9	-5.9±1.2	-0.51±0.01	-0.73±0.01	0.470±0.009	0.467±0.009	-0.048±0.009
21.4	-6.8±1.1	-0.47±0.01	-0.71±0.01	0.491±0.009	0.487±0.009	-0.058±0.009
24.0	-7.6±1.0	-0.44±0.01	-0.70±0.01	0.507±0.009	0.502±0.009	-0.067±0.008
26.5	-8.2±0.9	-0.41±0.01	-0.69±0.01	0.526±0.008	0.520±0.009	-0.075±0.008
29.1	-8.6±0.9	-0.39±0.01	-0.68±0.01	0.540±0.008	0.534±0.009	-0.081±0.008
31.6	-8.9±0.8	-0.36±0.01	-0.66±0.01	0.554±0.008	0.547±0.009	-0.086±0.008
34.1	-9.3±0.8	-0.33±0.01	-0.65±0.01	0.566±0.008	0.558±0.008	-0.091±0.008
36.7	-9.4±0.8	-0.31±0.01	-0.64±0.01	0.579±0.008	0.571±0.008	-0.094±0.007
39.2	-9.5±0.7	-0.28±0.01	-0.63±0.01	0.592±0.008	0.584±0.008	-0.098±0.007
44.3	-9.7±0.7	-0.24±0.01	-0.62±0.01	0.615±0.008	0.606±0.008	-0.104±0.007
49.4	-9.8±0.6	-0.20±0.01	-0.60±0.01	0.639±0.007	0.630±0.008	-0.108±0.007
54.5	-9.5±0.6	-0.15±0.01	-0.59±0.01	0.664±0.007	0.655±0.008	-0.110±0.006
59.5	-8.7±0.6	-0.12±0.01	-0.58±0.01	0.682±0.007	0.675±0.007	-0.103±0.006
64.6	-7.5±0.5	-0.08±0.01	-0.57±0.01	0.697±0.007	0.691±0.007	-0.091±0.006
69.7	-6.6±0.5	-0.06±0.01	-0.56±0.01	0.706±0.007	0.702±0.007	-0.081±0.006
74.8	-5.6±0.5	-0.04±0.01	-0.55±0.01	0.714±0.007	0.710±0.007	-0.070±0.006
79.9	-4.6±0.5	-0.02±0.01	-0.53±0.01	0.716±0.007	0.714±0.007	-0.057±0.006
84.9	-3.5±0.5	-0.01±0.01	-0.52±0.01	0.716±0.007	0.714±0.007	-0.044±0.006
90.0	-2.3±0.5	0.00±0.01	-0.50±0.01	0.709±0.007	0.709±0.007	-0.028±0.006
100.2	-0.8±0.5	0.00±0.01	-0.48±0.01	0.697±0.007	0.697±0.007	-0.010±0.006
110.3	0.2±0.5	0.01±0.01	-0.47±0.01	0.688±0.007	0.688±0.007	0.002±0.006
120.5	1.0±0.5	0.01±0.01	-0.46±0.01	0.679±0.007	0.679±0.007	0.011±0.006
130.7	1.6±0.5	0.01±0.01	-0.45±0.01	0.676±0.007	0.676±0.007	0.019±0.006
140.8	2.2±0.6	0.01±0.01	-0.45±0.01	0.676±0.007	0.675±0.007	0.026±0.006

Table D.49 Five-Hole Probe Data at (x,z)=(-38 mm,0)

y, mm	ALPHA, deg	CPT	CPS	SPEED	U	V
3.7	176.4±2.4	-0.73±0.01	-0.83±0.01	0.322±0.013	-0.321±0.013	0.020±0.014
4.7	179.0±4.2	-0.82±0.01	-0.88±0.02	0.244±0.017	-0.244±0.017	0.004±0.018
5.7	-172.7±7.0	-0.90±0.01	-0.94±0.02	0.191±0.022	-0.189±0.023	-0.024±0.022
6.7	-131.4±***	-0.90±0.10	-0.91±0.11	0.109±0.046	-0.072±0.075	-0.082±0.015
8.7	-40.0±8.8	-0.73±0.06	-0.77±0.06	0.202±0.024	0.155±0.037	-0.130±0.012
9.8	-25.0±4.5	-0.73±0.02	-0.80±0.02	0.263±0.017	0.238±0.022	-0.111±0.014
10.8	-18.8±2.9	-0.69±0.01	-0.79±0.02	0.312±0.014	0.296±0.017	-0.101±0.013
11.8	-14.5±2.2	-0.66±0.01	-0.78±0.02	0.351±0.012	0.340±0.014	-0.088±0.012
12.8	-13.0±1.9	-0.62±0.01	-0.76±0.02	0.376±0.012	0.367±0.013	-0.085±0.011
13.8	-12.8±1.8	-0.59±0.01	-0.75±0.02	0.388±0.011	0.379±0.012	-0.086±0.011
16.4	-12.2±1.5	-0.54±0.01	-0.72±0.02	0.422±0.010	0.412±0.011	-0.089±0.010
18.9	-12.8±1.4	-0.50±0.01	-0.70±0.02	0.441±0.010	0.430±0.011	-0.098±0.010
21.4	-13.0±1.3	-0.47±0.01	-0.69±0.02	0.463±0.010	0.451±0.011	-0.104±0.009
24.0	-13.2±1.2	-0.44±0.01	-0.67±0.02	0.480±0.009	0.467±0.010	-0.110±0.009
26.5	-13.3±1.1	-0.41±0.01	-0.66±0.01	0.496±0.009	0.482±0.010	-0.114±0.009
29.1	-13.3±1.0	-0.38±0.01	-0.65±0.01	0.512±0.009	0.498±0.010	-0.118±0.008
31.6	-13.5±1.0	-0.36±0.01	-0.63±0.01	0.522±0.009	0.508±0.010	-0.122±0.008
34.1	-13.3±0.9	-0.32±0.01	-0.61±0.01	0.537±0.008	0.523±0.009	-0.124±0.008
36.7	-13.1±0.9	-0.30±0.01	-0.61±0.01	0.554±0.008	0.540±0.009	-0.125±0.008
39.2	-13.0±0.8	-0.28±0.01	-0.60±0.01	0.567±0.008	0.553±0.009	-0.128±0.008
44.3	-12.6±0.8	-0.23±0.01	-0.58±0.01	0.591±0.008	0.576±0.009	-0.129±0.007
49.4	-12.0±0.7	-0.19±0.01	-0.57±0.01	0.617±0.008	0.603±0.008	-0.128±0.007
54.5	-10.9±0.7	-0.15±0.01	-0.56±0.01	0.639±0.007	0.627±0.008	-0.121±0.007
59.5	-9.5±0.6	-0.12±0.01	-0.54±0.01	0.653±0.007	0.644±0.008	-0.107±0.007
64.6	-8.2±0.6	-0.09±0.01	-0.53±0.01	0.663±0.007	0.656±0.008	-0.095±0.007
69.7	-7.2±0.6	-0.06±0.01	-0.51±0.01	0.672±0.007	0.667±0.007	-0.084±0.007
74.8	-6.1±0.6	-0.04±0.01	-0.49±0.01	0.676±0.007	0.672±0.007	-0.072±0.006
79.9	-4.8±0.6	-0.02±0.01	-0.48±0.01	0.678±0.007	0.676±0.007	-0.057±0.006
84.9	-3.6±0.6	-0.01±0.01	-0.46±0.01	0.674±0.007	0.673±0.007	-0.043±0.007
90.0	-2.4±0.6	-0.00±0.01	-0.45±0.01	0.667±0.007	0.667±0.007	-0.028±0.007
100.2	-0.7±0.6	0.00±0.01	-0.42±0.01	0.654±0.007	0.654±0.007	-0.008±0.007
110.3	0.4±0.6	0.01±0.01	-0.41±0.01	0.644±0.007	0.644±0.007	0.005±0.007
120.5	1.1±0.6	0.01±0.01	-0.40±0.01	0.635±0.007	0.635±0.007	0.012±0.007
130.7	1.8±0.6	0.01±0.01	-0.40±0.01	0.633±0.007	0.633±0.007	0.019±0.007
140.8	2.5±0.6	0.01±0.01	-0.40±0.01	0.638±0.007	0.637±0.007	0.028±0.007

Table D.50 Five-Hole Probe Data at (x,z)=(-32 mm,0)

y, mm	ALPHA, deg	CPT	CPS	SPEED	U	V
3.7	-171.9±2.1	-0.63±0.01	-0.75±0.01	0.348±0.012	-0.345±0.013	-0.049±0.012
4.7	-161.8±3.2	-0.68±0.01	-0.77±0.02	0.296±0.015	-0.281±0.017	-0.093±0.013
5.7	-149.2±5.2	-0.70±0.03	-0.76±0.03	0.249±0.018	-0.214±0.026	-0.128±0.013
6.7	-132.1±8.9	-0.62±0.09	-0.66±0.10	0.206±0.024	-0.138±0.039	-0.153±0.009
7.7	-102.0±***	-0.30±0.68	-0.32±0.64	0.138±0.217	-0.029±0.066	-0.135±0.207
9.8	-48.9±9.6	-0.52±0.10	-0.56±0.10	0.199±0.025	0.131±0.041	-0.150±0.009
10.8	-36.3±5.9	-0.58±0.04	-0.63±0.05	0.242±0.019	0.195±0.029	-0.143±0.012
11.8	-26.5±3.8	-0.60±0.02	-0.68±0.03	0.288±0.016	0.258±0.021	-0.129±0.013
12.8	-23.2±3.0	-0.58±0.02	-0.67±0.02	0.315±0.014	0.290±0.018	-0.124±0.012
13.8	-21.4±2.6	-0.56±0.01	-0.67±0.02	0.336±0.013	0.313±0.017	-0.123±0.012
16.4	-19.6±2.1	-0.52±0.01	-0.66±0.02	0.376±0.012	0.354±0.014	-0.126±0.011
18.9	-18.7±1.7	-0.49±0.01	-0.65±0.02	0.408±0.011	0.386±0.013	-0.131±0.010
21.4	-18.6±1.6	-0.45±0.01	-0.63±0.02	0.430±0.010	0.407±0.012	-0.137±0.009
24.0	-18.5±1.4	-0.42±0.01	-0.62±0.02	0.448±0.010	0.425±0.012	-0.142±0.009
26.5	-18.1±1.3	-0.39±0.01	-0.61±0.02	0.465±0.010	0.442±0.011	-0.145±0.009
29.1	-17.6±1.2	-0.36±0.01	-0.60±0.02	0.484±0.009	0.461±0.011	-0.146±0.009
31.6	-17.4±1.2	-0.34±0.01	-0.58±0.02	0.495±0.009	0.472±0.011	-0.148±0.008
34.1	-17.1±1.1	-0.31±0.01	-0.57±0.02	0.508±0.009	0.485±0.010	-0.149±0.008
36.7	-16.5±1.0	-0.29±0.01	-0.56±0.02	0.521±0.009	0.499±0.010	-0.148±0.008
39.2	-16.0±1.0	-0.27±0.01	-0.56±0.02	0.534±0.009	0.513±0.010	-0.147±0.008
44.3	-15.0±0.9	-0.22±0.01	-0.53±0.02	0.556±0.008	0.537±0.009	-0.144±0.008
49.4	-13.8±0.8	-0.18±0.01	-0.52±0.01	0.577±0.008	0.561±0.009	-0.137±0.007
54.5	-12.5±0.8	-0.15±0.01	-0.50±0.01	0.591±0.008	0.577±0.009	-0.128±0.007
59.5	-10.6±0.7	-0.11±0.01	-0.48±0.01	0.606±0.008	0.596±0.008	-0.111±0.007
64.6	-8.9±0.7	-0.08±0.01	-0.46±0.01	0.614±0.008	0.607±0.008	-0.095±0.007
69.7	-7.6±0.7	-0.06±0.01	-0.44±0.01	0.619±0.008	0.614±0.008	-0.082±0.007
74.8	-6.3±0.7	-0.03±0.01	-0.42±0.01	0.623±0.007	0.619±0.008	-0.068±0.007
79.9	-4.9±0.7	-0.02±0.01	-0.40±0.01	0.622±0.007	0.619±0.008	-0.053±0.007
84.9	-3.5±0.7	-0.01±0.01	-0.38±0.01	0.614±0.008	0.613±0.008	-0.038±0.007
90.0	-2.3±0.7	0.00±0.01	-0.37±0.01	0.606±0.008	0.605±0.008	-0.024±0.007
100.2	-0.9±0.7	0.00±0.01	-0.35±0.01	0.599±0.008	0.599±0.008	-0.009±0.007
110.3	0.3±0.7	0.01±0.01	-0.34±0.01	0.592±0.008	0.592±0.008	0.003±0.007
120.5	1.1±0.7	0.00±0.01	-0.34±0.01	0.583±0.008	0.583±0.008	0.011±0.008
130.7	2.0±0.7	0.01±0.01	-0.34±0.01	0.584±0.008	0.583±0.008	0.021±0.008
140.8	3.0±0.7	0.00±0.01	-0.34±0.01	0.587±0.008	0.586±0.008	0.031±0.008

Table D.51 Five-Hole Probe Data at (x,z)=(-25 mm,0)

y, mm	ALPHA, deg	CPT	CPS	SPEED	U	V
3.7	-167.3±2.0	-0.56±0.01	-0.69±0.01	0.362±0.012	-0.353±0.013	-0.079±0.012
4.7	-157.9±2.9	-0.59±0.01	-0.69±0.02	0.320±0.014	-0.297±0.017	-0.120±0.012
5.7	-147.7±4.1	-0.58±0.03	-0.66±0.04	0.285±0.016	-0.241±0.023	-0.153±0.011
6.7	-133.8±6.4	-0.49±0.08	-0.55±0.09	0.242±0.020	-0.167±0.033	-0.174±0.008
7.7	-113.5±****	-0.23±0.19	-0.26±0.20	0.185±0.031	-0.074±0.045	-0.170±0.016
10.8	-67.4±****	-0.25±0.19	-0.27±0.20	0.152±0.037	0.059±0.054	-0.141±0.019
11.8	-50.0±9.3	-0.40±0.10	-0.44±0.11	0.203±0.025	0.130±0.040	-0.155±0.008
12.8	-41.7±6.6	-0.45±0.06	-0.50±0.07	0.233±0.020	0.174±0.032	-0.155±0.010
13.8	-35.6±4.9	-0.47±0.04	-0.54±0.05	0.264±0.018	0.215±0.026	-0.154±0.011
16.4	-29.3±3.2	-0.46±0.02	-0.56±0.03	0.317±0.014	0.277±0.020	-0.155±0.011
18.9	-26.8±2.5	-0.44±0.02	-0.56±0.03	0.354±0.013	0.316±0.017	-0.160±0.010
21.4	-25.5±2.1	-0.41±0.02	-0.56±0.02	0.383±0.012	0.345±0.016	-0.165±0.010
24.0	-24.8±1.9	-0.38±0.02	-0.55±0.02	0.403±0.011	0.366±0.015	-0.169±0.009
26.5	-24.0±1.7	-0.36±0.02	-0.53±0.02	0.421±0.011	0.385±0.014	-0.171±0.009
29.1	-23.0±1.6	-0.33±0.01	-0.52±0.02	0.437±0.010	0.402±0.013	-0.171±0.009
31.6	-22.0±1.5	-0.31±0.01	-0.52±0.02	0.452±0.010	0.419±0.013	-0.169±0.009
34.1	-21.3±1.4	-0.29±0.01	-0.50±0.02	0.462±0.010	0.430±0.012	-0.168±0.009
36.7	-20.2±1.3	-0.27±0.01	-0.50±0.02	0.474±0.009	0.445±0.012	-0.164±0.008
39.2	-19.3±1.2	-0.25±0.01	-0.48±0.02	0.481±0.009	0.455±0.011	-0.159±0.008
44.3	-16.9±1.1	-0.22±0.01	-0.47±0.02	0.499±0.009	0.478±0.010	-0.145±0.008
49.4	-14.8±1.1	-0.18±0.01	-0.44±0.01	0.511±0.009	0.494±0.010	-0.131±0.008
54.5	-12.7±1.0	-0.14±0.01	-0.42±0.01	0.525±0.008	0.512±0.009	-0.116±0.008
59.5	-10.7±0.9	-0.11±0.01	-0.40±0.01	0.536±0.008	0.526±0.009	-0.100±0.008
64.6	-8.8±0.9	-0.08±0.01	-0.38±0.01	0.542±0.008	0.535±0.009	-0.083±0.008
69.7	-7.2±0.9	-0.06±0.01	-0.35±0.01	0.544±0.008	0.539±0.008	-0.068±0.008
74.8	-5.6±0.9	-0.03±0.01	-0.33±0.01	0.544±0.008	0.541±0.008	-0.053±0.008
79.9	-4.1±0.9	-0.02±0.01	-0.31±0.01	0.539±0.008	0.538±0.008	-0.039±0.008
84.9	-2.6±0.9	-0.01±0.01	-0.29±0.01	0.530±0.008	0.529±0.008	-0.024±0.008
90.0	-1.5±0.9	-0.00±0.01	-0.27±0.01	0.519±0.008	0.519±0.008	-0.014±0.008
100.2	-0.5±1.0	0.00±0.01	-0.25±0.01	0.504±0.009	0.504±0.009	-0.005±0.009
110.3	0.3±1.0	0.00±0.01	-0.24±0.01	0.491±0.009	0.491±0.009	0.003±0.009
120.5	1.0±1.1	0.00±0.01	-0.23±0.01	0.486±0.009	0.486±0.009	0.009±0.009
130.7	1.8±1.1	0.00±0.01	-0.23±0.01	0.488±0.009	0.488±0.009	0.015±0.009
140.8	2.3±1.0	0.00±0.01	-0.24±0.01	0.491±0.009	0.490±0.009	0.020±0.009

The vita has been removed from the scanned document